NATIONAL AERONAUTICS AND SPACE ADMINISTRATION

Technical Memorandum 33-467

Proceedings of the Third Annual Conference on Effects of Lithium Doping on Silicon Solar Cells

Held at the Jet Propulsion Laboratory
Pasadena, California
April 27 and 28, 1970

Edited by
P A Berman and J Weingart

JET PROPULSION LABORATORY
CALIFORNIA INSTITUTE OF TECHNOLOGY
PASADENA, CALIFORNIA

April 1, 1971

PREFACE

The purpose of this conference was to provide a forum for an in-depth review and discussion of the results of investigations being carried out by various organizations under NASA/JPL sponsorship as part of the Solar Cell Research and Development Program Participating organizations included cell manufacturers and university and industrial research laboratories Because of the relevance of this program to activities outside JPL, members of the aerospace industry involved in the space effort were invited to attend the conference in addition to representatives of NASA, JPL and JPL contractor organizations It is gratifying that in these times of severely curtailed travel budgets a significant cross-section of the aerospace community participated in the conference, as attested by the list of attendees

To accommodate all of the participants and provide ample time for informal discussions and interactions, as well as for formal presentations the conference was extended to two days A significant portion of the conference was devoted to an open forum during which technical, as well as broader philosophical issues, were explored

The conference co-chairmen wish to thank all those who participated in the conference, and in particular NASA Headquarters and JPL personnel for their support of this program

P Berman and J Weingart
Co-Chairmen

LIST OF ATTENDEES

ABBOTT, D
The Boeing Co , Seattle, Wash

BASS R
Northrop Corporate Laboratories, Hawthorne, Calif

BALLARD, R
Space & Missile Sys Org El Segundo Calif

BERRY E R
Aerospace Corp Los Angeles Calif

BRIGGS D C
Philco-Ford Corp Palo Alto, Calif

BRODERSEN R W
Massachusetts Institute of Technology
Cambridge, Mass

CARTER, J
TRW Systems Redondo Beach Calif

COHN, E
NASA Headquarters, Washington, D C

COLEMAN, W
North American Rockwell, Downey, Calif

COMPTON, W D
University of Illinois, Urbana, Ill

CORELLI, J
Rensselaer Polytechnic, Troy, N Y

CURTIS, O L
Northrop Corporate Laboratories, Hawthorne
Calif

DAYTON R
Lockheed-Georgia Co Marietta, Ga

DEWYS, E C
University of Denver Denver Colo

DOWNING R G
TRW Systems, Redondo Beach Calif

DRESSELHAUS M S
Massachusetts Institute of Technology,
Cambridge, Mass

FRIEDLANDER, S
EOS, Pasadena, Calif

FAITH, T
RCA Astro Electronics Div Highstown, N J

GIVEN, R
Lockheed Missiles and Space Co San Jose,
Calif

ILES, P A
Centralab, Division of Globe Union

JOHNSON E
University of Illinois, Urbana, Ill

KIRKPATRICK A
Ion Physics Corp , Burlington, Mass

LEE, T
Aerospace Corp , Los Angeles, Calif

LOFERSKI, J
Brown University, Providence, RI

LUFT, W
TRW Systems, Redondo Beach, Calif

MAULDIN, W
Space & Missile Sys Org , El Segundo,
Calif

MONTGOMERY, R
Penn State College, Pa

MORTKA, T
Rensselaer Polytechnic, Troy, N Y

NABER, J
Gulf General Atomic, San Diego Calif

NEWMAN P
NASA-Goddard, Greenbelt, Md

PASSENHEIM, B
Gulf General Atomic, San Diego Calif

PAYNE, P
Heliotek, Div of Textron, Inc , Sylmar, Calif

POLLARD H E
Philco-Ford, Palo Alto, Calif

RALPH, E L
Heliotek, Div of Textron, Inc , Sylmar, Calif

REYNARD, D L
Philco-Ford, Palo Alto, Calif

SARGENT, G
University of Kentucky, Lexington, Ky

SCHEIN, L
University of Illinois, Urbana, Ill

SO, S
Penn State College, Pa

SOSIN, A
University of Utah

STANNARD, J
Naval Research Laboratory, Washington, D C

STATLER, R
Naval Research Laboratory, Washington, D C

STOFEL, E
Aerospace Corp , Los Angeles, Calif

STREETMAN, B
University of Illinois, Urbana, Ill

THOMPSON, L
University of Utah

VEDAM, K
Penn State College, Pa

WHIFFEN, C
Lockheed-Georgia Co Marietta, Ga

PRECEDING PAGE BLANK NOT FILMED

CONTENTS

SUMMARY OF PROCEEDINGS

P Berman and J Weingart

The P/N junction diffusion technique strongly affects the number of dislocations and the amount of stress in Li-doped cells Improvements in diffusion techniques have resulted in lower dislocations and stresses Additional work is indicated to further improve the cell efficiencies

The use of evaporated lithium as a diffusion source has resulted in cells with efficiencies equal to those of cells fabricated with the standard paint-on Li source technique The yield distribution of the evaporated Li cells, however, is not as high Since the evaporation technique is more amenable to high volume production and should, if properly controlled, give more reproducible results than the paint-on technique, further investigations are warranted

The use of low-temperature long-time lithium diffusion schedules has yielded very high efficiency cells that exhibit recovered powers which are more than 20% higher than state-of-the-art N/P cells, as measured in a solar simulator after exposure to 3×10^{15} 1-MeV electrons/cm^2 This improvement in radiation resistance is in excess of that achieved when N/P solar cells replaced P/N cells Furthermore, all indications are that there is an even greater advantage when irradiation is by protons and neutrons (whereas the advantage of N/P over P/N non-Li cells becomes smaller for these heavier particles)

The results of measurements of carrier removal diffusion length, and other such physical properties are often very strongly affected by the amount of Li-doping The behavior of lightly Li-doped Si can be significantly different than that of heavily Li-doped Si, possibly due to a masking effect or competing mechanisms Therefore, great care must be exercised in extrapolating the results of one level of Li-doping to those of different levels of Li-doping

Some phenomena associated with light Li doping of float-zone Si, which have not been observed in heavily Li-doped float-zone material are as follows

(1) A minimum in carrier removal rate as a function of reciprocal bombardment temperature for 1 MeV electron radiation

(2) A spread of energy level over a wide range observed in measurements of carrier density as a function of reciprocal temperature after 1 MeV electron irradiation

(3) A slow change in carrier density and mobility at room temperature after 1 MeV electron irradiation

(4) No room temperature increase in donor concentration after irradiation by 1 MeV electrons

(5) Recovery time can be slower than that of heavily Li-doped crucible Si after electron irradiation

Some correlations between lightly and heavily Li-doped float-zones Si are as follows

(1) Formation of a defect center with an energy level 0 17 eV below the conduction band and of a center with a deeper-lying level

(2) The deeper level concentration increases with increasing Li concentration while the 0 17 eV level remains constant, indicating that the deeper level is associated with Li while the 0 17 eV level is not

(3) Damage constant immediately after 30 MeV electron irradiation of lightly Li-doped samples approximates that of non-Li-doped Si but increases with increasing Li concentration indicating that initial defects which contain Li are very effective recombination centers

(4) Damage constant immediately after neutron irradiation appears to be independent of Li concentration, indicating that Li does not increase the effectiveness of recombination centers associated with cluster defects

All analyses of annealing properties indicate an activation energy consistent with that of diffusion of lithium in both oxygen-rich (crucible) and oxygen-lean (float zone) Si This is true for both solar cells and bulk silicon, and for irradiation by electrons and neutrons This is one of the strongest points of agreement among all investigators During storage at room temperature and above, lithium appears to associate with all radiation-induced defects and significantly reduce their effectiveness as recombination centers The experimental work associated with identifying the nature, behavior, and role in the damage production and annealing mechanisms is summarized in Table 1

Table 1 Summary of experimental work

Energy relative to band edge	Identification	Participation in minority carrier recombination	Thermal annealing behavior	Dependence on oxygen	Dependence on lithium	Dependence on other impurities or defects	Electron irradiation parameters	Material characteristics	Correlation with cell behavior	Experimental techniques	Comments	References
E_c 0.08	?	No	Remains after 60 h at 300 K	Appears in QC material (only?)	$[Li] \sim 2 \times 10^{15}$ 2×10^{16}	?	1 MeV 80 250 K	QC	?	Hall		RCA
E_c 0.1	Li O V(?)	No		Seen only in FZ material	Seen only in high resistivity Si $[Li] \leq 2 \times 10^{14}$ $\rho \sim 10$ 20 Ω cm		1 MeV 80 250 K	FZ		Hall		RCA
E_c 0.13	May be real	?	?	QC (third quarterly report) FZ (letter)	Appears to require Li	?	1 MeV 80 250 K	QC FZ		Hall		RCA
E_c 0.13	Donor	?	Remains after room temp annealing $T_A > 300$ K		$[Li] \sim 1 \times 10^{14}$			FZ				NRL
E_c 0.17	Recombination center	Yes	Anneals at ≈400 C $T_A \propto f[Li]$	Only studied in FZ	Found in Li diff FZ Si	Only studied for $R_1 \gg 1$	30 MeV 77 300 K	FZ 10^4 Ω cm starting material		Lifetime	Becomes trapping center at high fluence	GA
E_c 0.17	V O (A center)	Yes	$T_A \approx 325$ C	Yes	Appears in non Li Si	Other impurities lower introduction rate	1 30 MeV T 300 K $0.04 \leq \eta \leq 0.15$ cm^{-1}	0.5 Ω cm CG (non Li)	Yes	ESR		GA
E_c 0.17	V O	Yes	$T_A \approx 20$ C T_A f[Li]	Yes	Yes η T_A decrease as [Li] increases			50 Ω cm n Si $[Li] \approx 10^{16}$ FZ		ESR	η 0.15 cm^{-1} $[Li] \sim 10^{16}$ η 0.025 cm^{-1} $[Li] \sim 4 \times 10^{17}$	GA
E_c 0.17	V O	Not measured	$\eta \propto f[O]$ for $10^{15} \leq [O] \approx 10^{17}$				1 MeV 300 K $\phi \sim 10^{14}$ 10^{15}	Li diff Hall bars Li doped QC solar cells		Hall capacitance $\epsilon(\omega)$		TRW
E_c 0.17	Vacancy complex	Important in electron irradiated n Si	Dose dependent sharp anneal ~230 C for low doses	Slight inverse dependence			10 MeV $\phi \approx 10^{13}$			τ vs $1/T^2$ τ vs Δn		Northrop
$E_v + 0.4 \leq E \leq E_c$ 0.4	Recombination center	Yes	$T_A \approx 450$ K in 10^4 Ω cm FZ n Si				30 MeV	10 150 10^4 Ω cm n Si P Si		τ vs 1/T		GA
$E_v + 0.35 \leq E \leq E_c$ 0.35	Recombination center may contain Li	Yes	$T_A \approx 320$ K $dn/dt \propto f([O])$	Seen in FZ possibly in CG	Yes η T_A are $F([Li])$		30 MeV T 77 300 K	10^4 Ω cm FZ 50 Ω cm CG both Li diff	Yes	τ vs 1/T	$R_1 > 1$ ($n_\phi < [Li]$)	GA
E_c 0.4	Li complex prob Li V	Dominates in one experimental sample	Anneals in ~1/2 h at $T_A \approx 250$ C		Only observed in Li diff material	?	Co^{60} (γ) 10^{16} γ's/cm^2	T I Lopex P doped (130 Ω cm) 12 Ω cm after Li diff		τ vs 1/T		Northrop
E_c 0.4	Li V (?)	Not measured	Not measured	Not found in CG material			1 MeV T 26 C $\phi \sim 10^{14}$ 10^{15}	Li diff Hall samples and FZ solar cells		Hall capacitance	η k[Li] cm^{-1} in FZ	TRW
E_c 0.4	V V in n Si	Appears to be	$T_A \approx 500$ K	η decreases as [O] increases			1 30 MeV 300 K	0.1 Ω cm QC 0.2 Ω cm FZ		ESR	Phosphorus doped	GA
			$T_A \approx 300$ K if Li present	η decreases as [Li] increases			30 MeV 300 K	0.5 Ω cm η Si $[Li] \approx 3 \times 10^{16}$				

Notes: ϕ in e/cm^2; All densities in number/cm^3; R_1 [Li]/[ϕ]; R_2 [O]/[Li]; R_3 [O]/[ϕ]; T_A Annealing temperature; η(cm^{-1}) Introduction rate; V Vacancy; O Oxygen

PROGRESS REPORT ON LITHIUM-DIFFUSED SILICON SOLAR CELLS

P A Iles
Centralab Semiconductor Division
Globe-Union Inc El Monte, Calif

I INTRODUCTION

This talk outlines the progress made in the performance and understanding of lithium cells in the past year The possibility of their use in some space missions is examined

II SURVEY OF 1969 TALK

A year ago the work could be summarized as follows

(1) Cell performance had improved, with increased control within the groups of cells shipped

(2) Detailed measurements had led to a better understanding of the lithium distributions within the cells as a result of the different lithium diffusion schedules used

(3) Uniform lithium concentrations had proved difficult to achieve because of the fall-off in lithium level near the two major cell surfaces

(4) Tests had shown that the lithium concentration near the PN junction could be reduced

(5) Crucible grown silicon was used more, because of its greater initial output and its postirradiation stability The slower recovery rate was considered adequate for missions where the particle fluence was not high particularly for missions where cell temperatures were high (above 50°C), providing faster recovery

(6) Following a given lithium schedule, cells made from non-CG silicon had given consistently lower I_{sc} and V_{oc}, and they tended to redegrade Some good cells had been made from Lopex silicon

III SURVEY OF WORK TO DATE

A Boron Diffusion Methods

The lower I_{sc} and V_{oc} values found for non-CG silicon were partly the result of the method used to diffuse boron into the cells The use of sources other than boron trichloride gave better performance for non-CG silicon, although overall, the consistency was not as good as that obtained from BCl_3 The BCl_3 method used to date had some advantages, providing cells of good output, especially for CG silicon in relatively large numbers The gas etching in the process allowed a wide range of surface finish to be used, and the compound formed at the surface gettered harmful impurities The surface layer remaining had low reflectivity either alone or when combined with silicon monoxide or other coatings The disadvantages were that gas etching complicated the formation of structures needing an N+ or oxygen layer near the PN junction Also, the surface compound was thermally mismatched to silicon and on cooling caused severe stresses in the silicon, leading to high dislocation densities or to warping of thin slices

B Other Boron Methods

The use of boron tribromide overcame most of the disadvantages of BCl_3 However, the consistency of cell output from nominally similar runs is not yet satisfactory

The older BCl_3 method was evaluated in more detail to see whether its disadvantages could be reduced The usual procedure is to preheat the silicon at around 1050°C for 10 min in inert gas flow, to introduce BCl_3 for 10 min ("tack-on") and then to stop BCl_3 flow and indiffuse boron for 10 min from the surface compounds formed This surface compound was found to build up linearly with tack-on time at around 1 5 mg/min Measurements showed that sufficient boron was available if the tack-on time was reduced drastically Thus, by reducing the thickness of the compound layer, stresses were reduced, and also I_{sc} and V_{oc} for non-CG silicon increased, while CG silicon maintained its good output Because this modified BCl_3 process involved only one parameter change, it was useful to have continuity with the older method to allow better understanding of the detailed effects of boron diffusion on lithium cell properties, before and after irradiation Figure 1 shows the increase of etch-pit density as the BCl_3 tack-on time was increased

C Cell Properties After Different Boron Methods

Figure 2 shows I_{sc}, I_{450}, and V_{oc}[1] for three forms of silicon for various boron diffusion conditions after a redistribution lithium schedule In general, V_{oc} behavior is more consistent, i e , small variation with boron conditions for CG silicon, and decreased for non-CG silicon at longer BCl_3 tack-on times The I_{sc} values depend also on the diffused layer properties and on coating variations

Figure 3 shows the same variations, this time following a drive-in lithium schedule The differences are more pronounced and more consistent

JPL shipment C-9 was intended to compare directly the effects of long tack-on time BCl_3 versus BBr_3 using float-zone (FZ) silicon and redistributed lithium

Figure 4 shows the cumulative yield for C-9, but did not show the differences seen in other tests The reason was partly because the BCl_3 did not decrease the FZ silicon I-V parameters as much as usual

JPL shipment C-10 used three forms of silicon growth (CG, Lopex, and FZ), two BCl_3 tack-on times (2 and 8 min), and a drive-in lithium diffusion Figure 5 shows the I-V variations in the groups The sequence repeats that found in smaller tests The 2-min tack-on samples gave fairly good cells for all groups Figure 6 is a log-log plot of capacitance-reverse bias voltage for C-10 for the same lithium schedule The slopes of these curves are lower in the sequence CG-Lopex-FZ, and show much more lithium near the PN junction for non-CG silicon The capacitance values did not show marked or consistent dependence on the BCl_3 tack-on time

Other ingots have also given cells of good performance with reduced BCl_3 tack-on times Figure 7 shows typical yield curves The FZ ingots show wider variations for a given lithium diffusion, the CG ingots are more consistent Figure 8 is a log-log plot of C-V for the ingots shown in Fig 7 Here the sequence of slope and capacitance follows that shown in Fig 6 for the drive-in lithium diffusion, for the redistribution cycle, the CG capacitance is not changed much, but FZ silicon showed severe depletion of lithium near the PN junction

D Conclusions on Boron Methods

Tests will continue to evaluate the best non-BCl_3 methods, expecially BBr_3 Further tests using modified BCl_3 will also be conducted the goal being the consistency of good output cells for all forms of silicon and the ease of scaling-up for pilot production quantities

IV LITHIUM STUDIES

This year's work has used two sources lithium-aluminum hydride in ether painted-on, and lithium metal evaporated in vacuum Both methods have given good results, however, to date, evaporation has not been as consistent, especially for higher temperature lithium cycles However, work will continue on both sources because evaporation appears more suited to quantity production

A Lithium Diffusion Schedules

Earlier, the trend was towards redistribution cycles to lower the lithium concentration and gradient In the present work, more attention was concentrated on single drive-in cycles using lower diffusion temperatures and longer times This method should result in lower concentration gradients, but detailed measurement of the lithium distributions after such cycles showed the concentrations and gradients were not as expected

One test used two forms of silicon (CG and Lopex) and five lithium schedules, i e , 425°C for 90 min, 400°C for 90 min, 375°C for 180 min 350°C for 300 min, and 325°C for 480 min These cycles had comparable (Dt) products, the last three cycles being very closely matched

Figure 9 shows how I_{sc} and V_{oc} varied for the two silicon forms As the diffusion temperature was decreased, I_{sc} increased for both forms, whereas Voc stayed fairly steady for CG silicon and decreased for Lopex silicon Figure 10 shows the C-V plots, showing steady increase in slope and decrease in capacitance for both forms of silicon The Lopex silicon gave a wider range of variation for both these parameters

Next, probe measurements were made on typical samples Figure 11 shows the donor concentration profiles for the five schedules for CG silicon The back surface concentration of lithium

[1] All I-V values quoted are for 2 cm^2 cells, at 28°C under AMO 140 mW/cm^2 test conditions

falls steadily with temperature, as does the concentration near the front surface The same pattern is seen in Fig 12 for Lopex silicon Here, however, the back surface concentrations and the concentration in the bulk of the cells are much lower than those in CG silicon for comparable lithium diffusion conditions The donor concentrations near the PN junction were explored in more detail by capacitance methods Figures 13 and 14 show the results for the two forms of silicon The CG silicon has lower concentration ($<10^{15}$ cm^{-3}) at the junction, and larger gradients near the junction For both forms of silicon, the concentration at the junction decreased as temperature decreased Qualitatively, the measured concentrations account for the measured I_{SC} values, but it appears that, contrary to earlier results, I_{SC} may be determined more by the lithium concentration very near to the PN junction (say within 5μ) rather than by the concentration in the bulk near the junction (say in the first 50μ) The fall-off in back surface concentration for Lopex at lower temperatures to below 10^{15} cm^{-3} explains the lower V_{OC} observed as a result of the formation of an opposing Schottky barrier

These tests led to the specification of cells for JPL shipment C-11 Four groups of 60 cells are in preparation with the following parameters

(1) CG silicon, reduced BCl_3 tack-on time, lithium 325 °C for 480 min

(2) CG silicon reduced BCl_3 tack-on time, lithium 375 °C for 180 min

(3) CG silicon, BBr_3, lithium 325 °C for 480 min

(4) Lopex silicon, reduced BCl_3 tack-on time, lithium 325 °C for 480 min

Figure 15 shows the yield for the three BCl_3 groups of cells in shipment C-11 The lithium level is low, and thus the cells have high output Lopex silicon is seen to give cells of high performance with these reduced boron and lithium cycles

V OTHER TOPICS

Front surface introduction of lithium led to shelf instability for cells and was not pursued further

The oxygen layer cells described last year showed some promise in reducing the post-irradiation instability, especially for Lopex silicon The behavior of the FZ silicon with the oxygen layer was intriguing because it recovered as slowly as CG silicon This suggests that it is the movement of lithium very close to the PN junction that controls the recovery More work is scheduled on oxygen layer cells

VI SUMMARY

Lithium cells have maintained their promise Their output has been increased, partly because of improved processing methods, partly because CG silicon has been used more, and because the specified lithium concentrations have been lower By controlling the amount of lithium, cells can be made with a wide (and predictable) range of pre-irradiation power extending up to levels comparable to the best current N/P cells The CG cells have slower recovery rates, although they may still be adequate for some missions Lopex silicon has given cells of good output these should be considered when fast recovery rates are needed The redegradation problems found for Lopex silicon earlier may be reduced at the lower lithium levels, and more work on oxygen layer cells is warranted It is possible that Lopex silicon may require slightly different lithium diffusion schedules, however Figs 11 through 14 show that cycles such as 375°C for 180 min give similar distributions near the PN junction for CG and Lopex silicon

Work already done on thin cells showed that even more reduced lithium cycles may be sufficient The 8-mil cells diffused at 325°C for 480 min gave maximum powers in the range 27 5-29 5 mW

The methods currently available can give lithium cells with most of the range of properties available on N/P cells Thus, cells can be made as thin as 4 mils and as large as 2 × 8 cm with integral covers and with all degrees of solder coverage The cell appearance is comparable to N/P cells, and the cell surface has the same chance of being coated with the optimum anti-reflecting films The same range of cell contacts (Ti-Ag, Ti-Pd-Ag, Al, etc) can be used Lithium-doped cells are still superior to N/P cells when heavy particles are the cause of cell damage Lithium cells have been considered for synchronous orbits, but are worth considering also for some planetary missions They have performed well under Jupiter conditions, and although no recovery is expected at the low temperatures, the degradation differences with N/P cells may be less than for 1-AU conditions Lithium cells may also be useful for near-sun missions, since the particle radiation is mainly protons from solar flares (favorable for lithium cells) and the increased temperatures will help recovery and allow the use of CG silicon

VII PROBLEM AREAS

(1) There is still a need to understand better the silicon properties that control cell performance However, it should be remembered that millions of good N/P cells have been produced without any better understanding of these silicon properties

(2) Several methods of boron and lithium diffusion are capable of giving good cells, the best methods must be determined There is still the need to analyse the effects of lithium on cell behavior so as to find how best to specify where the lithium is needed most

(3) The contact adhesion needs improvement, especially for the front surface contacts Careful control is needed of both the boron diffusion and the surface treatment of the silicon before contact application The back surface contact adhesion has

been reduced somewhat by the lack of a sintering cycle, but adequate adhesion should still be possible

(4) More flight evaluation tests are needed, especially in mechanical and environmental areas For these tests, the range of cell designs can be restricted to a relatively few variables

(5) Real-time tests showed that the recovery under realistic dose rates did not match the degradation Thus, to predict real-time behavior, care must be exercised in extrapolating accelerated recovery rates after pulsed irradiation

(6) Shorter feedback times are needed to allow a steady delivery of larger numbers of cells One possibility is to take 5% of the cell shipments, to irradiate them with a fixed fluence, and to monitor recovery under conditions suited to the form of silicon used This would not give a comprehensive evaluation but would indicate whether the shipments showed promise

(7) Caution must be exercised in extrapolating tungsten measurements (which are useful to emphasize radiation losses) to predict AMO output Already, good lithium cells have I_{sc} ratios (AMO to tungsten 100 mW/cm^2) around 1 15 (compared to 1 20 for older cells) and our experience shows that, as the bulk response of cells is further increased, this ratio will fall to 1 10 if short wavelength response stays high

VIII CONCLUSIONS

Lithium cell work is still worth pursuing despite the fact that, in recent months the target cells (N/P) have been improved considerably, and, in general, silicon solar cell outputs have been increased As predicted in earlier years the pressure and the understanding generated in the lithium cell program have been partly responsible for N/P cell improvements

Figure 16 surveys the best output measured for various silicon cells It is clear that recoverable lithium cells are well placed to justify continued study

The breadth of the JPL program allows access to a wide range of sophisticated techniques and experts to help explain lithium cell behavior This concentrated effort can help explain the pre-irradiation properties and the defect interactions during and after irradiation It is possible that the lithium cell might be one of the best understood devices developed for practical purposes In turn, the incentive provided by the practical end-product offers a challenge to the study of basic properties and may accelerate the understanding of these properties

ACKNOWLEDGMENT

We would like to thank NASA and JPL for their support under Contract No 952546, and Mr Paul Berman for his technical guidance

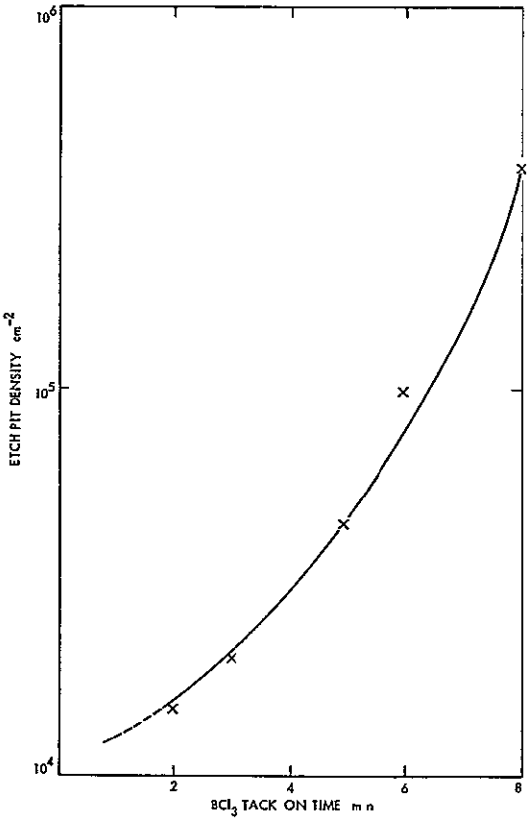

Fig 1 Etch pit density as a function of BCl_3 tack-on time

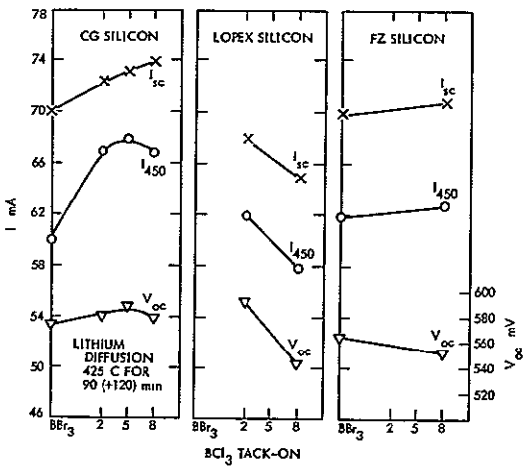

Fig 2 I-V variations for different boron conditions for three types of silicon

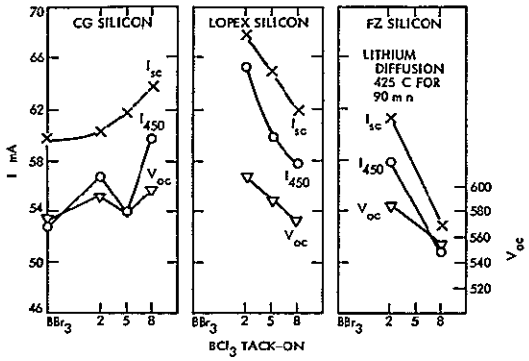

Fig 3 I-V variations for different boron conditions for three types of silicon

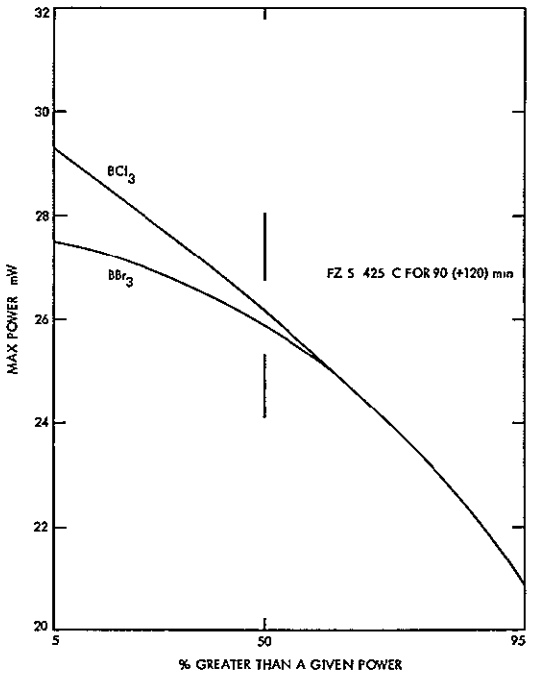

Fig 4 Yield for cells in JPL shipment C-9

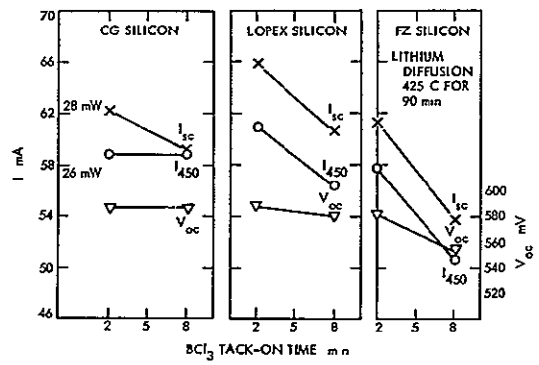

Fig 5 I-V variations for different boron conditions for three types of silicon (JPL shipment C-10)

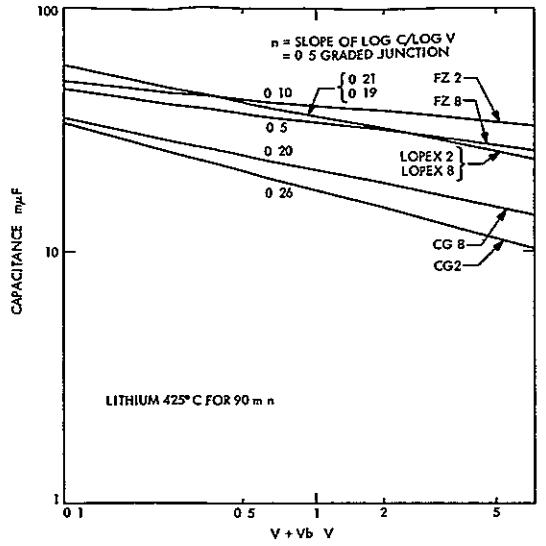

Fig 6 Capacitance vs voltage, log-log plot for three types of silicon, two BCl_3 tack-on times (cells in JPL shipment C-10)

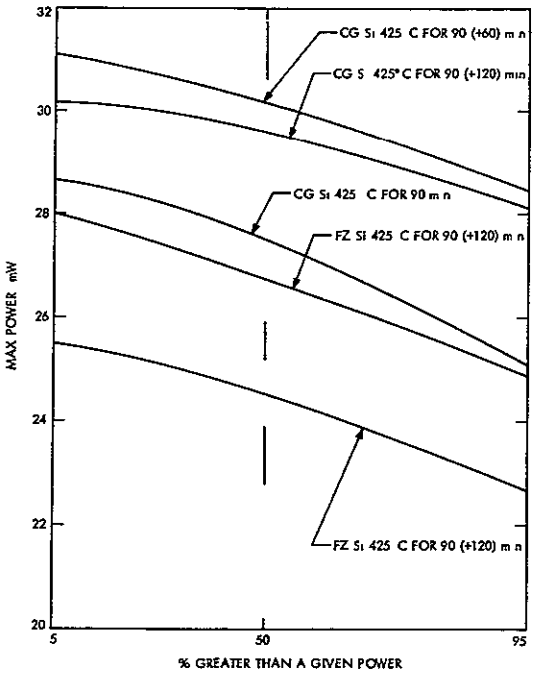

Fig 7 Yield for cells made from various ingots with reduced BCl_3 tack-on times

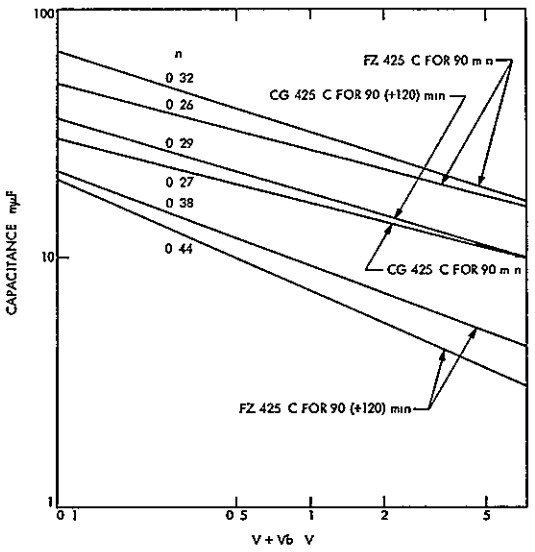

Fig 8 Capacitance vs voltage, log-log plot for various ingots with reduced BCl_3 tack-on times

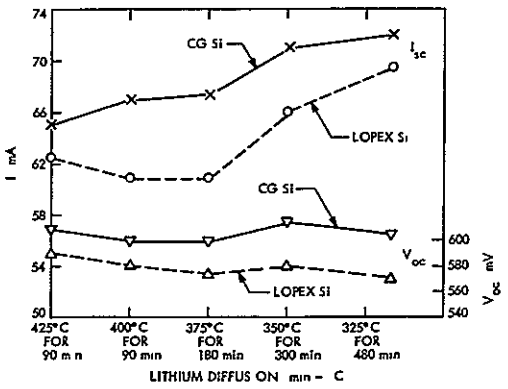

Fig 9 I_{sc} and V_{dc} for various lithium schedules for Lopex and CG silicon

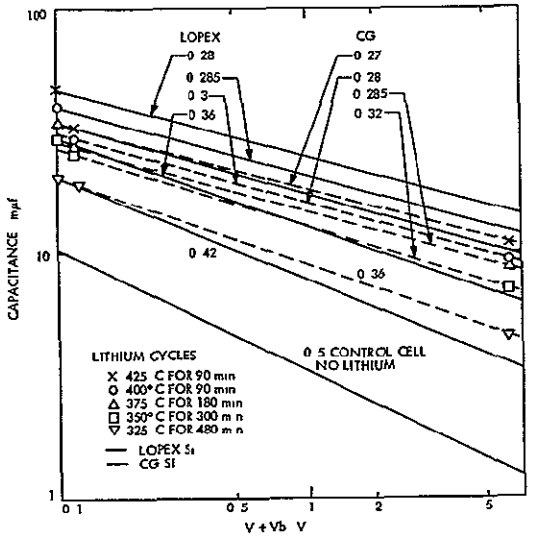

Fig 10 Capacitance vs voltage, log-log plot for various lithium schedules for Lopex and CG silicon

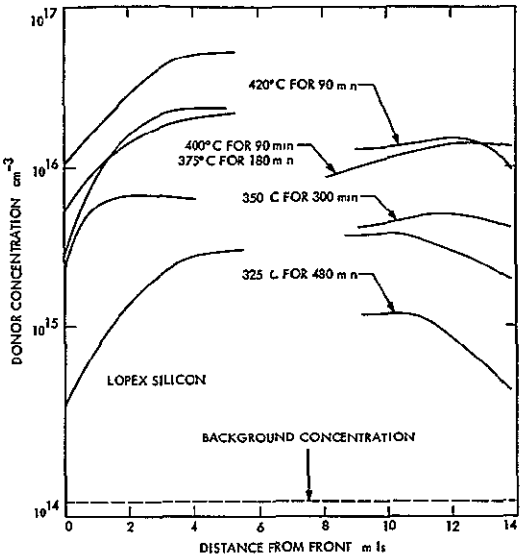

Fig 12 Donor concentration profiles for various lithium diffusion schedules, Lopex silicon

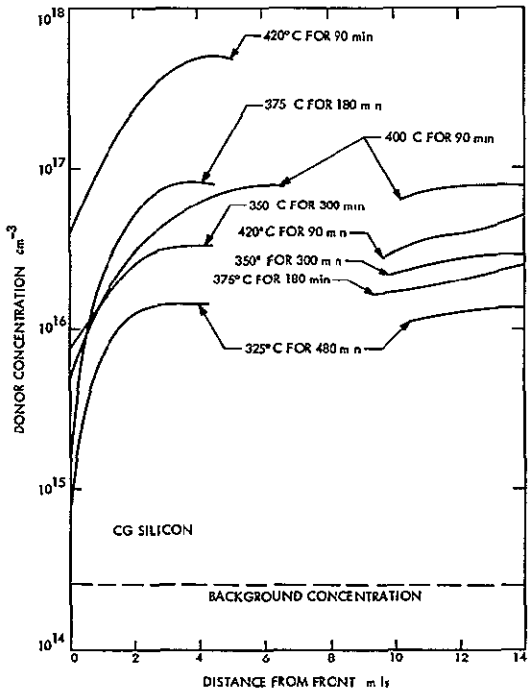

Fig 11 Donor concentration profiles for various lithium diffusion schedules, CG silicon

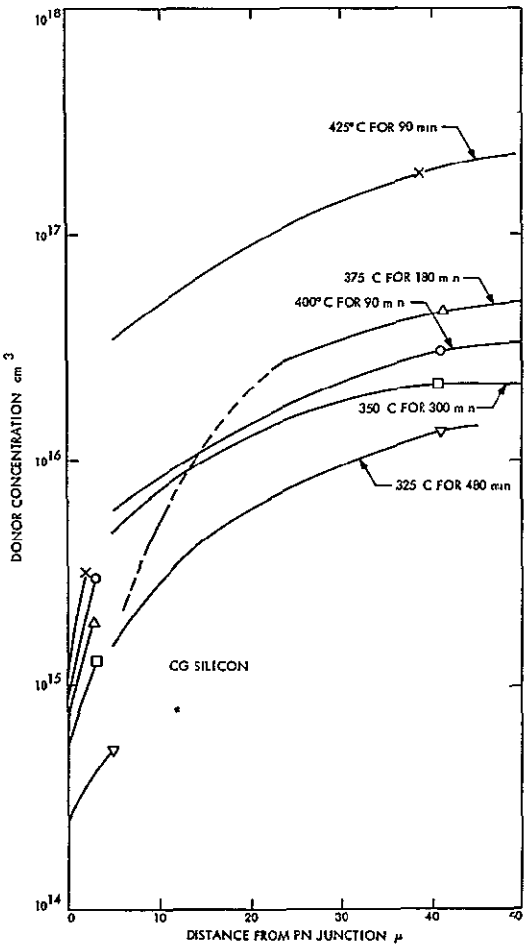

Fig 13 Donor concentration profiles for various lithium diffusion schedules, CG silicon

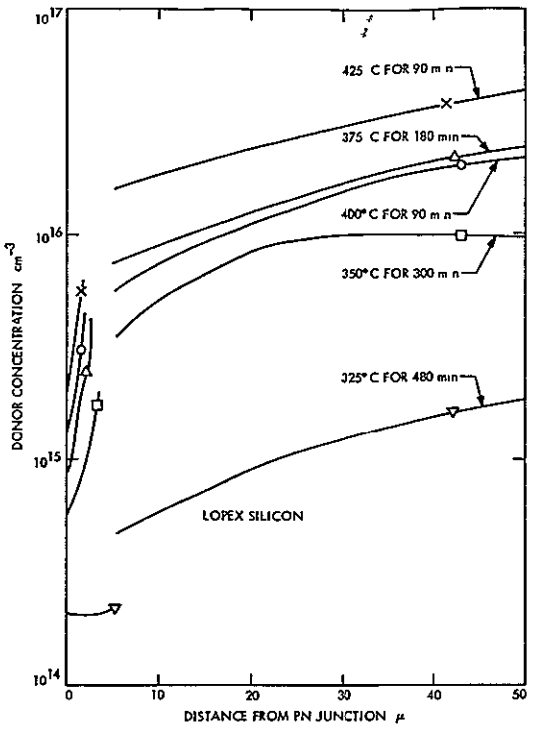

Fig 14 Donor concentration profiles for various lithium diffusion schedules, Lopex silicon

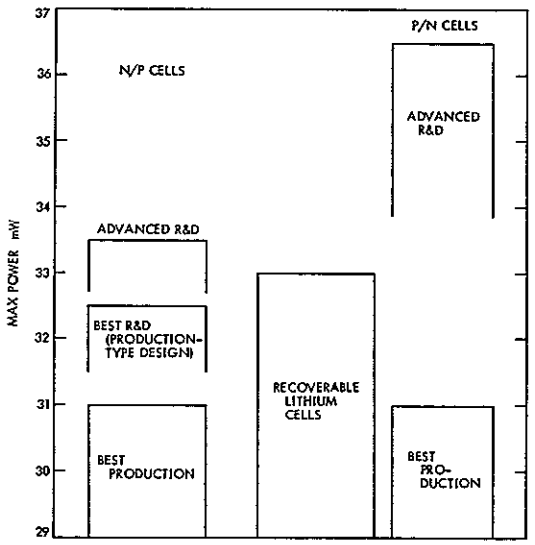

Fig 16 P maximum range for various types of silicon solar cells

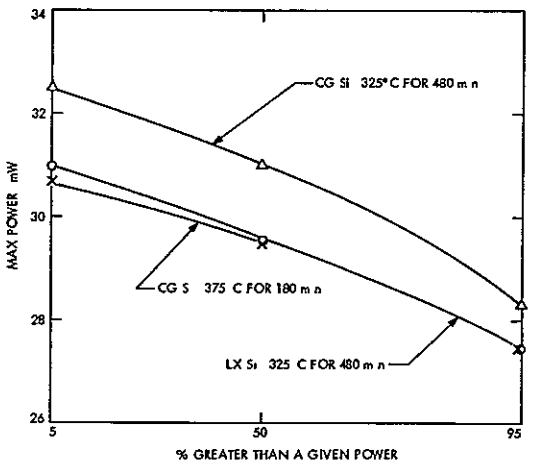

Fig 15 Yield for cells in JPL shipment C-11

DEVELOPMENT OF IMPROVED PROCESSES AND EFFICIENCIES FOR LITHIUM-DOPED SOLAR CELLS

P Payne and E L Ralph
Heliotek Division of Textron Inc
Sylmar, Calif

I INTRODUCTION

This paper summarizes the Li-doped solar cell research and development carried out over the past nine months under JPL Contract No 952547 The work performed can be separated into two basic areas (1) experimental work aimed at the improvement of cell processes and efficiencies, and (2) the fabrication and statistical analyses of a quantity of various lithium solar cell types

The essential processes used in the fabrication of Li-doped solar cells include boron diffusion using a BCl_3 source, lithium diffusion, redistribution of the lithium, evaporation of the TiAg contacts, and SiO antireflection coating Some of these procedures were altered for different groups of cells i e , BBr_3 has been utilized as the boron source, both lithium evaporation and lithium paint-on techniques have been used, and for particular lithium diffusions the lithium redistribution was eliminated however, when any of these changes were made, it is noted in the discussion

II EXPERIMENTAL STUDIES

The primary areas of investigation were lithium diffusion techniques boron diffusion source contact evaluation, and storage stability studies BCl_3 is the dopant source used for standard boron diffusions at Heliotek High output cells are obtained with this process, however, certain characteristics of this diffusion are undesirable The stresses introduced into the silicon with this diffusion are not usually a problem with small 1 × 2 cm blanks, but as the cell size is increased or the cell thickness decreased, the stresses result in a larger percentage of bowed cells

In addition, silicon is etched during this diffusion This is a drawback in fabricating special cell types such as a cell with a stable N^+ region at the junction The purpose of the N^+ region is to maintain the majority carrier concentration and, consequently, good junction characteristics as the lithium is depleted by the reaction with radiation defect sites The N^+ region is obtained with a phosphorus diffusion and then the cell is processed according to standard lithium cell fabrication techniques Use of BCl_3 as the boron diffusion source with its variable etch rate makes it impossible to fabricate this special cell with a controlled width of the phosphorus region The variable etch rate and introduction stresses were the primary reasons for investigating other sources

Previous work had included investigation of B_2H_6, BN, and Borofilm, but they were not included in present contract work

The BBr_3 has been successfully used by other manufacturers, it was the source which was investigated during the performance of this contract This diffusion is usually performed in an oxidizing atmosphere with the BBr_3 reacting with O_2 to produce B_2O_3, which deposits on the slice as a glass layer It reacts with silicon to form elemental boron, which then diffuses into the lattice The N_2 is used as the carrier gas Diffusions were performed varying the BBr_3, O_2, and N_2 flow,

diffusion time, and temperature Some sets of parameters gave better results than others, but in the best cases, the I_{sc} was 10 to 20 mA low Since none of the diffusions with O_2 gave high enough short-circuit currents the BBr_3 was used without O_2 in a diffusion process similar to the BCl_3 to ensure that the low I_{sc} were not caused by impurities in the BBr_3 The resulting short-circuit currents were high and in the expected range In addition, it was discovered that although the BBr_3 etches the cell surface and a heavy boron layer forms, the stressing (a problem with the BCl_3) is absent with the BBr_3 Large (2 × 2 cm and 2 × 6 cm) area cell blanks were diffused, there was no evidence of bowing even in the large 2 × 6 cm blanks When the 2 × 6 cm blank thickness was reduced to 0 006 in , there still was no noticeable bowing Figure 1 shows I-V curves for a 1-Ω-cm crucible-grown cell measured in both tungsten and simulator light sources using BBr_3 without O_2 The tungsten output is as good as that obtained with BCl_3-diffused cells The simulator output is low due to low Isc The ratio of the simulator I_{sc} to tungsten I_{sc} is 1 1, this is normally around 1 18 if the diffusion is optimum

The same was the case for 20-Ω-cm crucible-grown 2 × 2 cm and 2 × 6 cm cells The tungsten output was in the expected range but the simulator output was low The AMO short-circuit current for an area equivalent to a 1 × 2 cm cell was about 6-mA low 64 mA instead of the 70 mA which is normally obtained with BCl_3 diffused cells

Large area (2 × 2 cm and 2 × 6 cm) lithium cells have also been fabricated using the BBr_3 diffusion The I_{sc} (based upon 1 × 2 cm) ranged from 6 17 to 64 5 mA The curve factor on many of these cells was low due to rounded knees, however, one of the better cells had a power output of 58 0 mW which is equivalent to the efficiency of 10 9% for a 2 × 2 cm cell (see Fig 2)

Use of BBr_3 without oxygen does <u>not</u> provide for diffusion of the special cell described at the beginning of this discussion, but it does eliminate the problem of stresses encountered with the BCl_3 diffusion on large area and thin cells

Humidity and pull tests were performed to evaluate the TiAg contacts presently used on lithium cells The TiPdAg and Al contact systems on lithium cells were also included in this contact evaluation The TiAg contacts showed the least humidity resistance They were subjected to 95% relative humidity at 65°C and, periodically I-V curves were measured and tape tests performed After approximately 100 h exposure, an average of 35% of the front contact peeled and some edge peeling occurred at the back contact After 200 h the front contacts on all cells peeled completely and an average of 15% of the back contact peeled After 288 h exposure only one cell out of ten with TiPdAg contacts showed any degradation Approximately 20% of the bar peeled Two out of ten of the Al-contacted cells exhibited peeling after 288 h 30% of the bar on one cell and 80% on another Althrough the TiPdAg and Al contacts do degrade with humidity their performance is superior to the TiAg contact

The electrical measurements (performed in 100 mW/cm^2 tungsten light source) showed that the most significant loss factor was at maximum power due to an increase in series resistance and the subsequent rounding out of the knee No electrical degradation was measurable after 48 h, however, the maximum power degradation after approximately 100 and 200 h was 4 and 5% respectively The cells with Al contacts exhibited the following degradation after 244 h 0-3 3% for the I at 450 mV, 0-2 5% for the I_{sc}, and less than 1% for the V_{oc} The degradation of the lithium cells with TiPdAg contacts was about the same after 288 h

The TiPdAg-contacted P/N cells <u>without</u> lithium generally showed less than 1% electrical degradation over the same period of humidity exposure This seems to indicate that the lithium is moving around in the bulk of the cell or that it is reacting with the contact, either of which could change the output

Pull tests (i e wire-soldered or ultrasonically welded to the contact and pulled perpendicular to the cell surface until failure) were performed to determine the mechanical strength of the contacts In all cases where silicon fractures or divots did not occur pull strengths in excess of 500 g were obtained for TiAg and TiPdAg contacts The Al contacts had equivalent strengths Because of silicon fractures there was an unusually large percentage of failures at less than 500 g pull This seems to be an indication of the stresses present in P/N lithium cells, since this does not typically occur with conventional N/P cells These stresses are presumed to be primarily due to the boron diffusion since the P/N cells with no lithium that were pull-tested also failed with silicon fractures at less than 500 g

It has been suggested that the percentage of the back surface which is covered with lithium should have an effect upon the radiation recovery characteristics of lithium cells Cells fabricated by Heliotek have generally been painted with lithium so that the lithium source is always within 0 010 to 0 020 in of the cell edge This undiffused region around the perimeter of the cell, although small, could result in residual radiation damage Lithium would not be present in this region to anneal damage sites and the junction edge effects might degrade the characteristic curve An experiment was designed to evaluate the effect of varying the area of this region and the significance of this residual damage Lithium was painted on the cells as follows the first group had 100% lithium coverage, the second approximately 85% and the third, approximately 50% The undiffused regions did not affect V/I (a measure of the slice resistivity) Also no clear correlation could be drawn between lithium coverage and electrical output The cells from this experiment were submitted to JPL for radiation testing These radiation tests should indicate whether complete lithium coverage of the back cell surface is important Evaporating lithium as an alternative to painting on a lithium mineral oil suspension has been investigated Evaporating lithium is desirable because (1) it is less tedious than the paint-on technique (2) it

is adaptable to a production line, and (3) there is no problem with the uniformity of the lithium layer on different parts of the same cell and from cell to cell

Large diameter (0 125 in) lithium wire was used as the source This was handled far more easily than the lithium pellets which have previously been used in investigations of lithium evaporation Oxidation of lithium while opening the vacuum system was another problem area which had been encountered previously This problem has been reduced by using helium rather than air to open the vacuum system after the lithium evaporation The cells have been exposed to air during transfer from the vacuum system to the diffusion furnace, but with apparently little oxidation since cells have been obtained with the same V/I and lithium concentration profiles as cells with the painted-on lithium mineral oil source Many of the cells with evaporated lithium have outputs as high as cells with the painted-on lithium, however comparison of the cumulative frequency distributions for cells with painted-on versus evaporated lithium layers showed that there was more fall-off in cell output and consequently a larger percentage of lower output cells with the evaporated lithium Figure 3 shows the maximum power distribution as a function of lithium application for lots 3 and 4 At a cumulative frequency of 90%, there is a difference in output of about 1 mW for both lots

The movement of lithium in the silicon lattice at room temperature could cause electrical instability in long-term storage To evaluate this, cells fabricated in 1966 have been periodically measured After 3 1/2 years of storage at room temperature the following changes have occurred

(1) Three of the float-zone cells which exhibited approximately 10% power loss one year ago have now degraded approximately 13%

(2) These three float-zone cells had unusually large V_{oc} decreases

(3) Not all float-zone cells degraded in the above manner Some of the other float-zone cells degraded slightly in the past year, but they are still higher than they were initially

(4) The 100-Ω-cm float-zone cells diffused at 350°C, which one year ago showed a maximum of 1 84% I_{sc} degradation and 1 49% P_{max} degradation, now exhibit 2 0-3 7% total I_{sc} loss and 3 6-4 5% total loss in P_{max}

(5) The crucible-grown lithium cells have degraded slightly in the past year but their outputs are still higher than the initial outputs measured on October 1966

III CELLS DELIVERED TO JPL

Five lots of 60 Li-doped solar cells have been shipped to JPL for radiation tests in other laboratories For each lot more than 60 cells were processed and tested so that a good selection could be made Statistical analyses of the electrical output of each lot were performed

Lot 2 consisted of 60 cells fabricated from 100-Ω-cm Lopex silicon They were Li-diffused 90 min and redistributed 120 min at 425°C Eighty-seven cells are included in the maximum power distribution shown in Fig 4 The median output was 25 4 mW 5% of the cells had outputs ≥28 4 mW and 95% had outputs ≥22 8 mW These cells showed the same variations in open-circuit voltage previously observed with Lopex silicon Some of the cells with high outputs had not only high short-circuit currents but also open-circuit voltages of 570-580 mV Some of the lower output cells had open-circuit voltages as low as 540 mV The cause is still uncertain, it could be dependent to some degree on oxygen concentration which, some investigators have indicated varies considerably in Lopex silicon At any rate Lopex silicon seems to be the least predictable with respect to the lithium cells fabricated from it Eight-hour lithium diffusions at 325°C have been investigated during this contract and lots 1 3 and 4 have been processed using these diffusion parameters Cells with this type of diffusion have been known to exhibit very high output The output of lot 1, 20-Ω-cm float-zone cells is shown in Fig 5 The median output of this group of cells is 25 5 mW which is about 3 5% lower than the average output of 20-Ω-cm float-zone cells diffused 90 min and redistributed 60 min at 425°C This is not the high output which was expected

The output of lot 3 is shown in Fig 6 These cells were fabricated from 20-Ω-cm crucible-grown silicon and the high outputs expected from an 8-h diffusion at 325°C were observed The maximum power distribution includes only the 60 cells shipped to JPL since a number of the cells had poor I-V curve shapes due to contact shunting problems Some of the cells with poor curve shape exhibited a carrier removal effect in that they did not have exceptionally high dark reverse currents at 0 7V, but did pass high current at low voltages The maximum power distribution is narrow and high The median output is 30 mW with 10% of the cells having outputs ≥32 mW and 90% having outputs ≥27 mW For lot 4, 20-Ω-cm float-zone cells with an 8-h diffusion at 325°C were again fabricated The output of this lot was no higher than for lot 1 Figure 7 compares this lot of float-zone cells to the crucible-grown cells fabricated for lot 3 The median output of the crucible-grown lithium cells was 6 mW higher than the median output of the float-zone cells This corresponded to an average efficiency of 9% for the float-zone cells and 11% for the crucible-grown lithium cells It is typical for crucible-grown lithium cells to have higher outputs than float-zone lithium cells, but, usually the difference is 2-3 mW or half an efficiency group The low output of the float-zone cells could be a boron diffusion lithium diffusion or material problem

The crucible-grown lithium cells diffused 8 h at 325°C which had such high initial outputs, also had exceptionally high recovered outputs after being irradiated with 1 MeV electrons to an integrated flux of $3 \times 10^{15} e/cm^2$ Figure 8 shows a cell with an initial output of 32 6 mW and a recovered output after irradiation of 21 9 mW The cell shown in Fig 9 had a lower initial output 29 4 mW but it recovered to 23 5 mW Figure 10 compares these two cells to a 10-Ω-cm N/P cell irradiated to the same level The output

of the lithium cells is 11 to 20% higher than the output of the N/P cell This increased efficiency and radiation resistance means that the Li-doped cells would withstand about three times the radiation fluence for the same power output degradation when compared to the 10-Ω-cm N/P solar cell

In summary, the output of crucible-grown cells Li-diffused 8 h at 325°C (lot 3) have exhibited the highest efficiency for the amount of lithium present of any cells fabricated to date Efficiencies as high have only been observed for cells with low lithium concentrations The average output of lot 3 was 6% higher than the average output of the best lot of crucible-grown cells fabricated during the previous contract

ACKNOWLEDGMENTS

The authors wish to thank P Berman of JPL for his technical coordination, and JPL for the support of the program under Contract No 952547

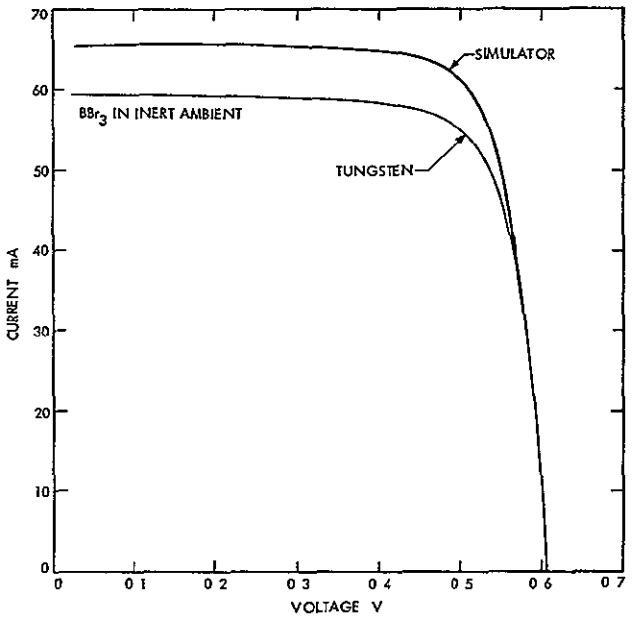

Fig 1 I-V characteristic curves of 1-Ω-cm P/N cell diffused with BBr_3 source

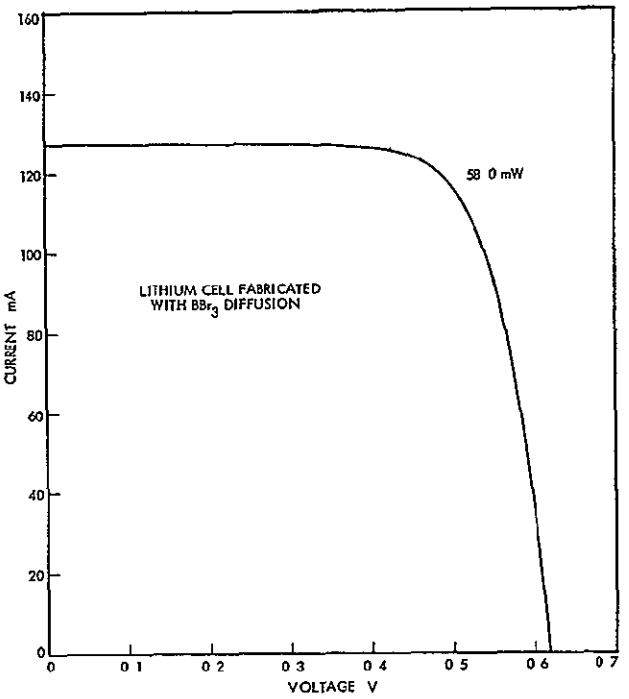

Fig 2 I-V characteristic curve of lithium cell fabricated with a BBr_3 diffusion The 20-Ω-cm crucible grown cell was lithium-diffused 90 min and redistributed 120 min at 425 °C (measured in solar simulator at 140 mW/cm^2)

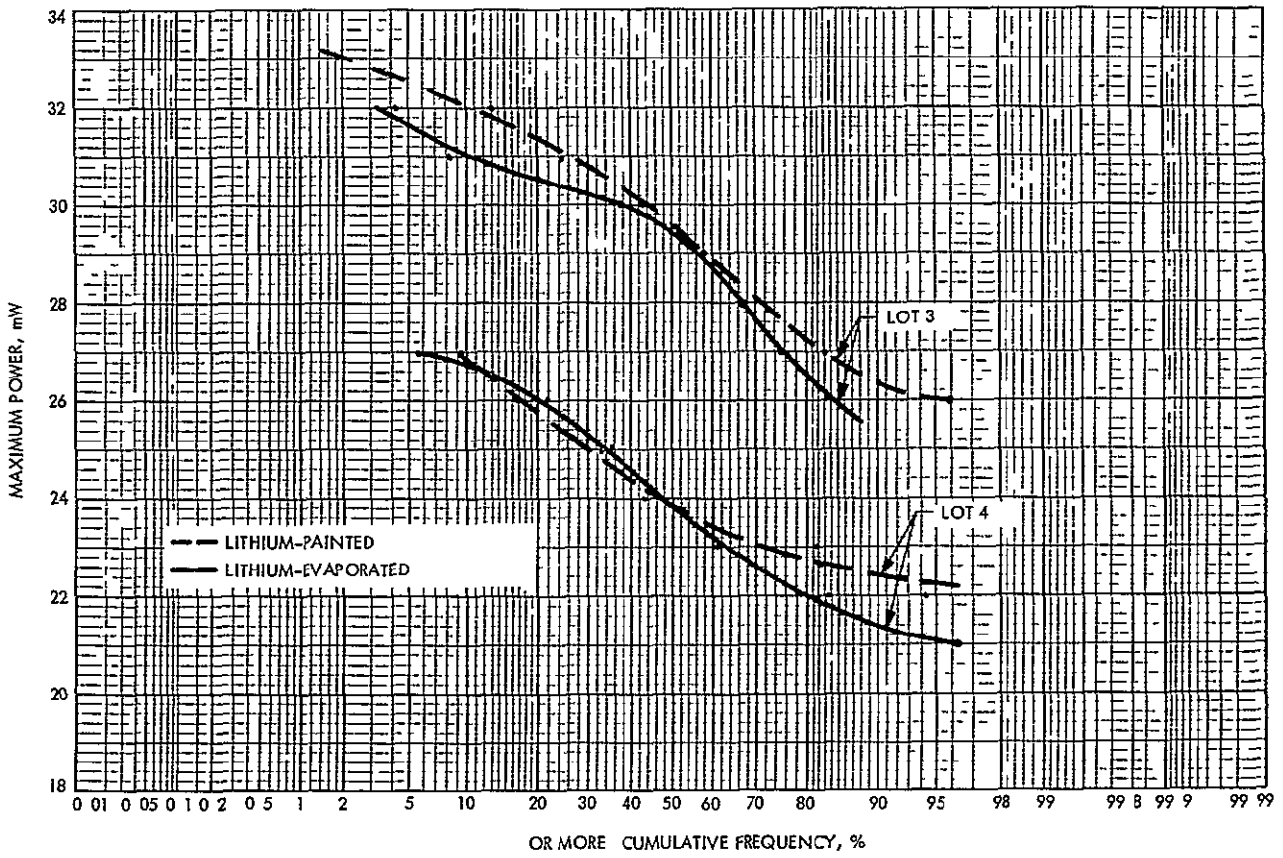

Fig 3 Maximum power distributions of lithium cells (measured in solar simulator at 140 mW/cm^2)

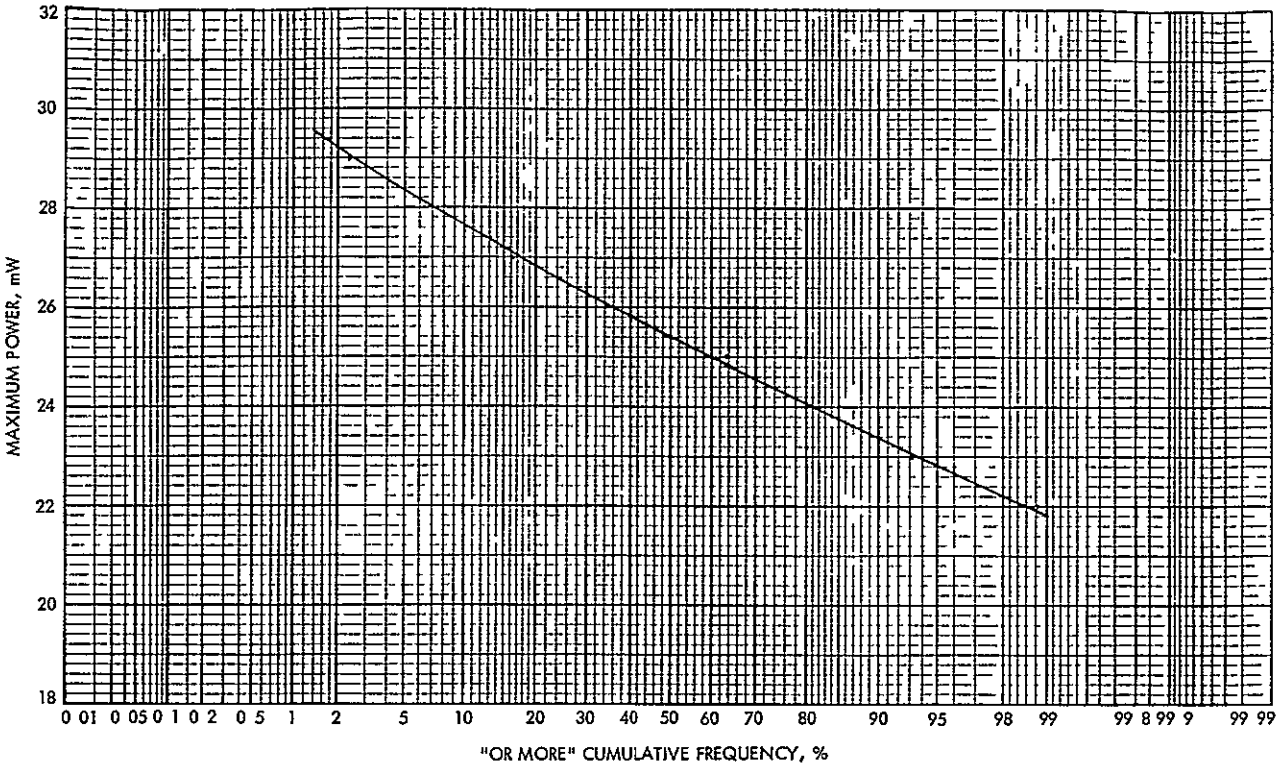

Fig 4 Maximum power distribution of lithium cells fabricated for the second lot (87 cells) of 100-Ω-cm Lopex cells Li-diffused 90 min and redistributed 120 min at 425°C (measured in solar simulator at 140 mW/cm^2)

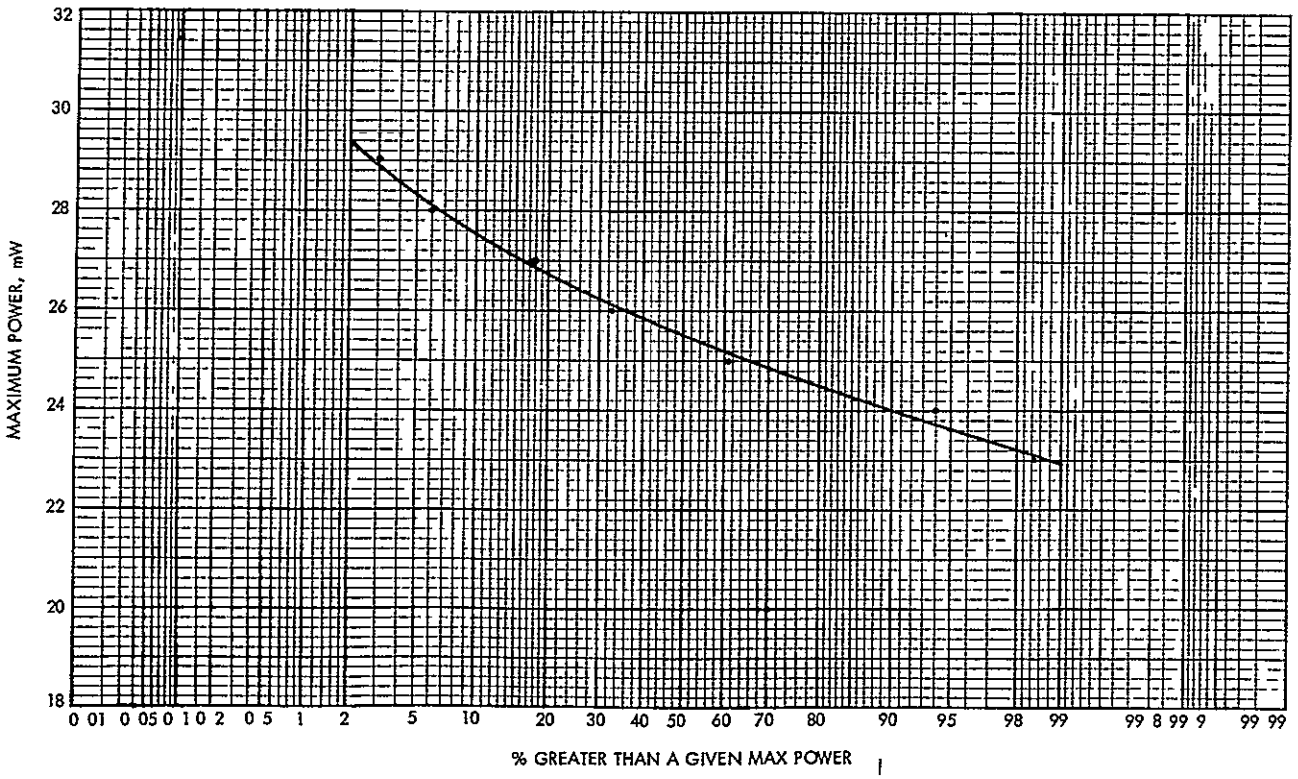

Fig 5 Maximum power distribution of lithium cells fabricated for the first lot (66 cells) of 20-Ω-cm float-zone cells Li-diffused 8 h with no redistribution at 325°C (measured in solar simulator at 140 mW/cm^2)

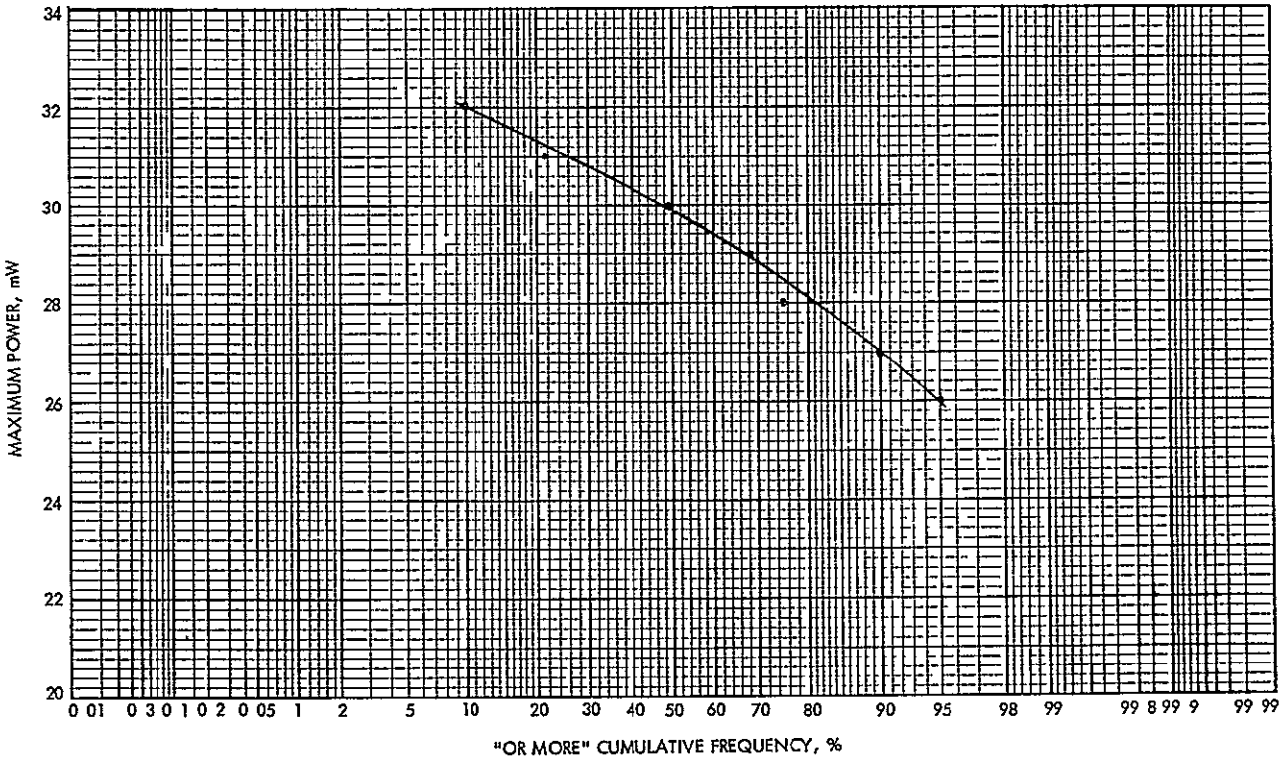

Fig 6 Maximum power distribution of high-output lithium cells Li-diffused 8 h at 325°C with no redistribution TiAg contacts (measured in solar simulator at 140 mW/cm^2)

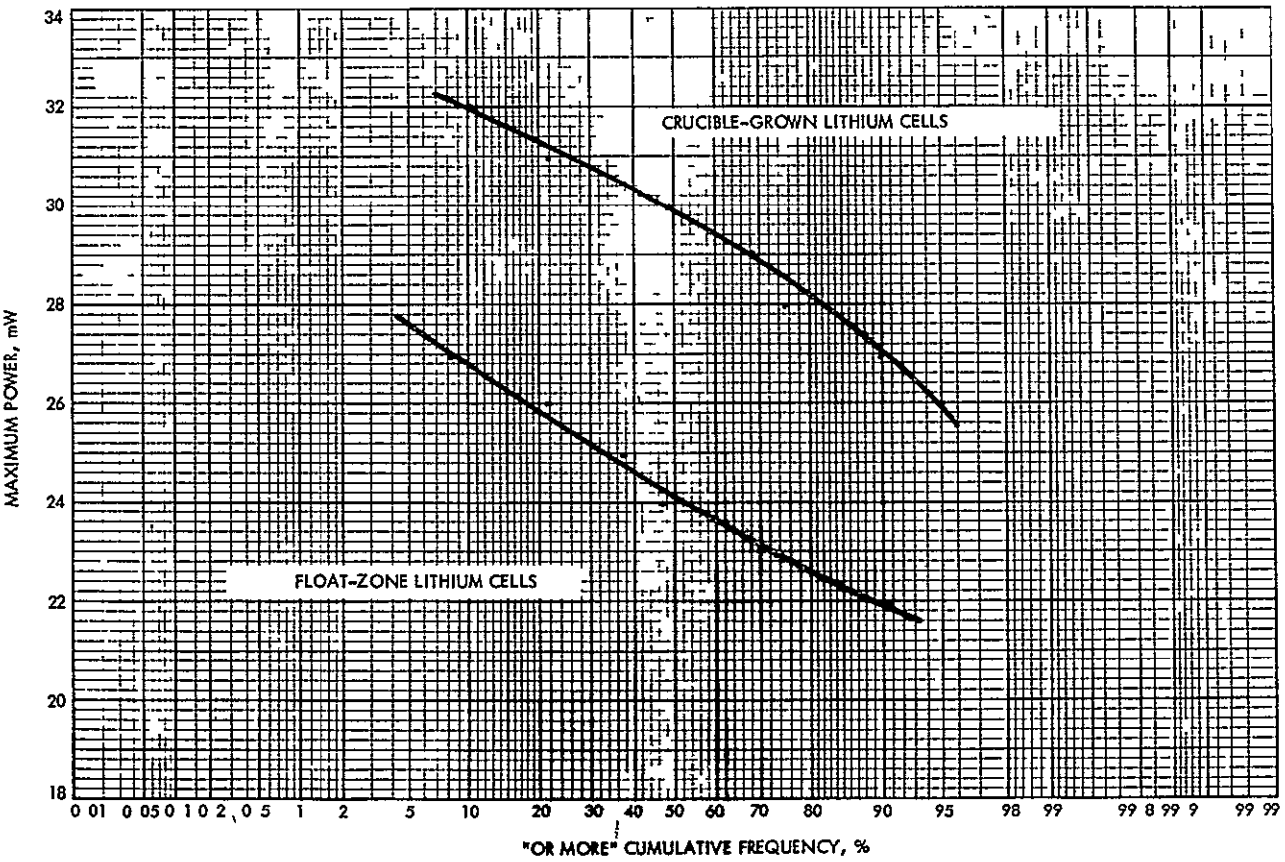

Fig 7 Comparison of float-zoned and crucible-grown lithium cells diffused 8 h at 325°C (measured in solar simulator at 140 mW/cm^2)

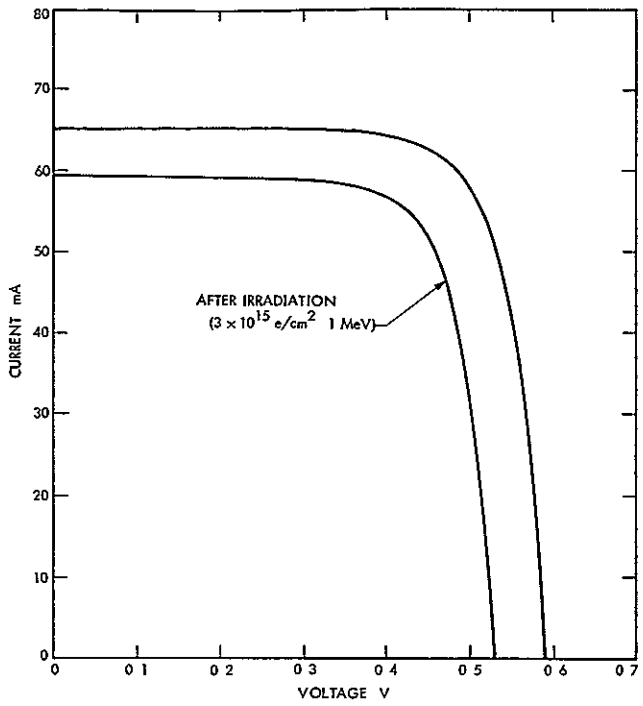

Fig 8 20-Ω-cm Czochralski-grown lithium cell before and after irradiation Cell Li-diffused 8 h at 325°C (measured in solar simulator at 140 mW/cm^2)

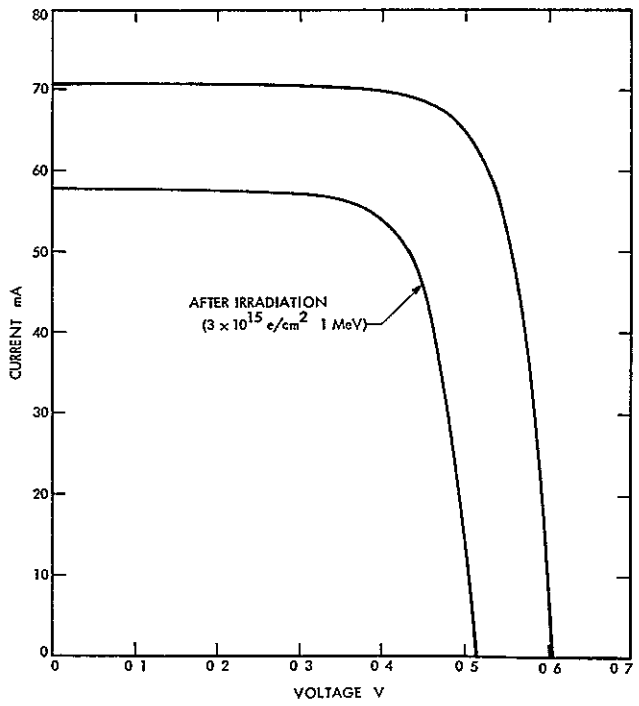

Fig 9 20-Ω-cm Czochralski-grown lithium cell before and after irradiation Cell Li-diffused 8 h at 325°C (measured in solar simulator at 140 mW/cm^2)

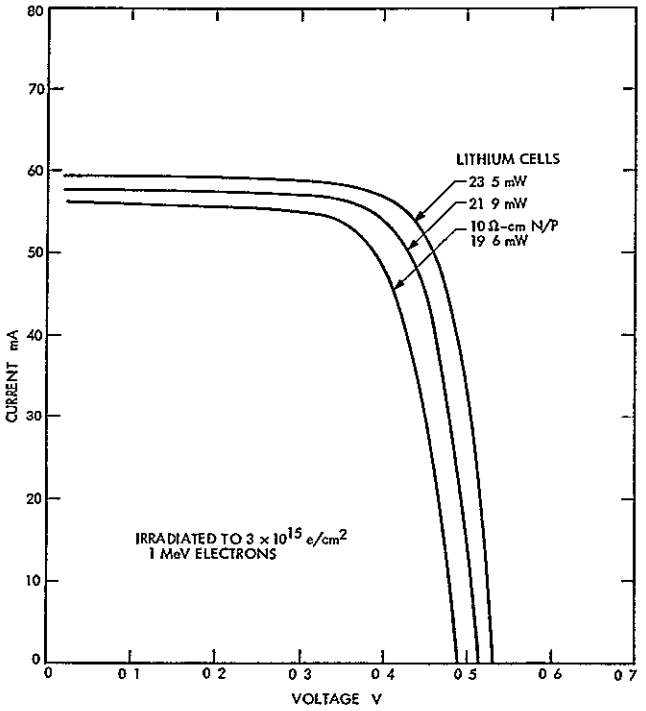

Fig 10 Lithium cells vs 10-Ω-cm N/P cell (measured in solar simulator at 140 mW/cm^2)

USE OF LITHIUM TO RADIATION-HARDEN SOLAR CELLS[1]

J R Carter, Jr , and R G Downing
TRW Systems Group
Redondo Beach, Calif 90278

I INTRODUCTION

Work to improve the radiation hardness of Li-diffused solar cells has been divided into two main efforts The first area involves basic studies of the underlying physical and chemical phenomenon of lithium behavior in irradiated silicon The second area is a direct attempt to improve the state of the art by systematic fabrication of Li-doped solar cells and their evaluation in a radiation environment The work at TRW Systems has involved basic studies and the evaluation of cells fabricated by other contractors

Hall coefficient measurements have been utilized to study the changes that occur in Li-doped silicon during irradiation and after recovery By this technique, it has been possible to identify the major defects produced during the irradiation of this material, and to monitor the changes which occur after irradiation All irradiations discussed herein were done with 1-MeV electrons Extensive capacitance measurements on Li-diffused solar cells have allowed similar studies of the changes in donor concentration which confirm and support the Hall measurements

The evaluation program consisted of time-dependent measurements of Li-doped float-zone (FZ) silicon solar cells irradiated at 3×10^{14} and 3×10^{15} e/cm^2 with 1-MeV electrons for measurements during storage at room temperature The evaluation of Li-doped quartz-crucible solar cells was by storage at storage temperature of 60, 80, and 100°C after irradiation to 3×10^{15} e/cm^2 with 1-MeV electrons Lithium concentrations near the junction were determined by capacitance and related to observed behavior

II LITHIUM REACTIONS IN IRRADIATED SILICON

The principal theoretical problem remaining in connection with the study of radiation damage in Li-doped silicon is the confirmation of a physical model for the production and annealing of damage in this material There have been four approaches to this problem to date Since two types of silicon (FZ and quartz crucible) have been used in these studies, all of the results cannot be compared The results can be summarized as follows

(1) Vavilov, et al , suggested that in quartz-crucible silicon damage results from "A" center formation and annealing results from pairing of "A" centers with lithium donors

(2) The RCA group has proposed the damage recombination centers of Li-V^- in FZ and Li-O-V^- in quartz-crucible silicon The annealing occurs by pairing of lithium donors with the respective damage center

(3) The TRW group experiments support the concept of Li-V^- formation during irradiation with annealing by reaction of one or

[1]This work was performed for the Jet Propulsion Laboratory, California Institute of Technology, as sponsored by the National Aeronautics and Space Administration under Contract No NAS 7-100

more lithium donors with the recombination centers

(4) Stannard of NRL has irradiated Li-doped FZ silicon at lower temperatures and allowed it to recover at room temperature The results indicated that the irradiation resulted in the production of an unidentified deep acceptor A similar loss of lithium donors occurred at the same time During the room temperature anneal, the deep acceptors were removed A loss of lithium also occurred during the annealing The lithium loss during annealing was roughly twice the deep acceptor loss

In general, most investigations support a view that lithium donors react with displacement products to form the dominant recombination center Annealing is caused by the reaction of one or more lithium donors with the recombination center Such a model explains most of the observations that have been reported for lithium solar cells The only major effect, which remains unexplained by this model, is the redegradation observed in heavily doped cells It must be emphasized that these conclusions are reached by indirect means and are in need of confirmation Our own work has involved very heavily Li-doped samples which are not typical of doping levels in solar cells For this reason, we are extending our observations to include silicon with less than 10^{15} Li atoms/cm^3

III HALL COEFFICIENT MEASUREMENTS

Lithium was diffused into wafers of 50-Ω-cm N-type quartz-crucible silicon to make several Hall specimens The lithium concentrations were about 7×10^{14} atoms/cm^3 This doping level is comparable with that found in Li-doped solar cells Thus, it was hoped that the results would be typical of behavior in Li-doped solar cells

Our initial results in the irradiation of this material are shown in Fig 1 The sample was irradiated with a fluence of 1×10^{16} e/cm^2 of 1-MeV electrons Figure 1 is a plot of reciprocal Hall coefficient versus reciprocal temperature for sample Q-2A This reciprocal Hall coefficient can be interpreted as conduction carrier concentration The data prior to irradiation indicated a constant electron concentration throughout the temperature range investigated Irradiation produced a small change in the room temperature electron concentration The low temperature electron concentration was greatly lowered in a manner that indicates the irradiation produced a large concentration of acceptor defects with a deep-lying level The manner in which the Hall coefficient of the irradiated specimen changes with temperature indicates that the Fermi level has become pinned to the energy level of the radiation-produced defect The defect energy level calculated from the slope shown in Fig 1 is 0 19 eV below the bottom of the conduction band This value is not properly corrected for the temperature variation of the density of states in the conduction band To properly account for the density of states, the quantity log $1/T^{3/2} R_H$ must be plotted against $1/T$ This has the effect of lowering the apparent energy level a small amount Although this analysis has not been completed it is apparent that the true energy level will lie very close to the known position of the Si-A center (0 17 eV) These data strongly suggest that one of the main defects produced during room-temperature irradiation of Li-doped quartz-crucible silicon is the Si-A center A second sample (Q-2C) was irradiated with an electron fluence of 1×10^{15} e/cm^2 The data for this sample are shown in Fig 2 It can be seen that there is evidence of a deep level after irradiation and annealing reduces the concentration of deep level defects and conduction electrons To assist in the analysis of the data, these data were normalized to the results prior to irradiation Thus the temperature variation of the Hall factor is removed from the data These results are shown in Fig 3 Several observations can be made from these data The concentration of the deep-level defects produced by irradiation is about 2×10^{14} cm^{-2} The indicated defect production rate would be 0 2 cm^{-1} The Si-A center has an energy level at 0 17 eV below conduction band If a degeneracy factor of 1/2 is assumed, the two-thirds ionization point will be reached at a temperature of 195°K (1000/T°K = 5 15) Additional calculations show the Fermi level of sample (Q-2C) at 195°K after irradiation to be at 0 17 eV below the bottom of the conduction band There also appears to be some evidence of other extremely shallow energy level defects, because the carrier concentration is again declining at 120°K After an anneal of 150 h at 100°C, the concentration of A centers was reduced to 7×10^{13} cm^{-3} During the same period, the concentration of carrier electrons or lithium donors was reduced by $3\ 3 \times 10^{14}$ cm^{-3} The loss in A centers was $1\ 4 \times 10^{14}$ cm^{-1} These results indicate that roughly two lithium donors are consumed in the anneal of one Si-A center This behavior is very similar to that reported by Vavilov (Ref 1) The defect production in this case is much greater than that reported by Vavilov for A centers

Since the Si-A center is known to be an effective recombination center, the previous results form the basis for the model of irradiation damage and recovery in Li-doped quartz-crucible silicon solar cells The behavior in cells may follow the following model

Irradiation

$$V + O \rightarrow O - V \text{ (un-ionized A center)}$$

Recovery

$$O - V + Li^+ + e^- \rightarrow Li - V - O \text{ (inactive defect)}$$

or

$$O - V + 2Li^+ 2e^- \rightarrow Li_2 - V - O \text{ (inactive defect)}$$

The apparent consumption of two lithium donors per annealing A center may be misleading The data point out the possibility of other defects with more shallow-lying energy levels It is entirely possible that some lithium donors are consumed in the annealing of such defects

Our previous Hall coefficient measurements on Li-doped float zone silicon have been concentrated on heavily doped specimens These heavy doping levels are not typical of those found in solar cells To extend the previous work, FZ specimens were prepared with lithium concentrations in the

range of 10^{14} to $10^{15}/cm^3$ The FZ silicon used for this work was originally 1000-Ω-cm N-type silicon This purity level restricts the possible defect interactions with impurities to those with lithium and possibly oxygen Sample E-4 is an example of such a specimen The Hall coefficient data relating to the irradiation and recovery of this sample is shown in Fig 4 Since the reciprocal Hall coefficient is closely related to the conduction band carrier concentration the results in Fig 4 can be interpreted as changes in carrier concentration The results of the irradiation similar samples of quartz-crucible silicon show a very small carrier concentration change at room temperature after irradiation Those results support the production of Si-A centers (oxygen-vacancy pairs) during irradiation of the Li-doped quartz-crucible silicon Two significant points can be observed regarding the postirradiation results of sample E-4 First, the carrier removal at room temperature is approximately 0 1 cm^{-1} The second point is the large inflection in the Hall coefficient at temperatures at which the Fermi level is near 0 17 eV below the bottom of the conduction band Although alternate explanations can be proposed, the simplest model would be the formation of two types of defects during the irradiation one defect being the Si-A with ionization energy of 0 17 eV and the other being a defect of undetermined structure with an ionization greater than 0 3 eV from the conduction band The second defect is probably a lithium-vacancy pair The introduction rate of the Si-A center in this sample appears to be approximately 0 2 cm^{-1} The value is in excellent agreement with that found in similar quartz-crucible silicon It should be noted that this sample contains only $3\ 7 \times 10^{14}$ lithium donors/cm^3 Since the residual oxygen concentration in float-zone silicon is believed to be in the range of $10^{15}/cm^3$ oxygen is probably the dominant impurity in a FZ specimen such as E-4 In this regard it is not unusual that the Si-A center should be produced during irradiation After irradiation, the sample was stored at room temperature to study recovery changes After 310 h at 26°C, the carrier concentration was greatly reduced during storage At this time, the decline of the reciprocal Hall coefficient at temperatures below room temperature indicates that many shallower level defects (i e Si-A centers) remain in the sample After 1500 h, the conduction electron concentration has been reduced to only a few percent of that present immediately after the irradiation It appears that the time-dependent decrease in carrier concentration is directly related to the reaction of lithium donor ion cores and their attendant electrons with radiation defects

A similar specimen, F-2, with a somewhat higher lithium concentration, was studied in the same manner The results of this study are shown in Figs 5 and 6 In this sample, the concentration of lithium donors was $1\ 5 \times 10^{15}/cm^3$ This is roughly four times the amount present in sample E-4 The FZ silicon used in samples E-4 and F-2 was purchased from the Wacker Chemical Corp , Los Angeles Figure 5 shows the reciprocal Hall coefficient versus reciprocal temperature plot for sample E-2 before irradiation, after irradiation, and 800 h after irradiation To facilitate the interpretation of these data, they were normalized to the pre-irradiation results and replotted on a linear scale in Fig 6 The features of the change produced by irradiation of this sample are very similar to those shown in Fig 4 for sample E-4 The presence of both the Si-A center and the defect with a deeper level are implied after the irradiation The introduction rate for Si-A centers in sample F-2 is approximately 0 2 cm^{-1} This is similar to that found in sample E-4 It is also similar to that found previously in a quartz-crucible sample (Q-2C) with similar lithium concentrations A significant difference between the results in sample F-2 and those in sample E-4 is that the introduction rate of defect with deeper energy is about 0 2 cm^{-1} in the former and 0 1 cm^{-1} in the latter case It would appear that increased lithium concentrations cause higher concentrations of the defect formed during irradiation Because of mass action principles, this increased introduction rate is direct evidence that lithium is involved in the structure of the defect under consideration After 800 h at room temperature, the results in Fig 6 indicate greatly reduced carrier concentration The data also indicate a very much reduced concentration of defects with energy levels less than 0 32 eV (i e , Si-A centers)

IV CARRIER REMOVAL STUDIES IN CELLS

Parallel studies of capacitance and electrical output were made on a quartz-crucible solar cell, AF 4921 The concentration of lithium donors at the junction (V_a = 0) and the short-circuit current were studied during irradiation and recovery at 100°C These data are again shown in Fig 7 In general, the results are very similar to those of FZ cells in that a large decrease of lithium concentration occurs simultaneously with a recovery of the degraded short-circuit current The point of interest is that during the irradiation of 3×10^{15} e/cm^2, only 2×10^{13} carrier electrons/cm^3 are removed This is an order of magnitude lower than that observed in FZ cells Since the lithium lost during recovery is comparable in both FZ and quartz-crucible silicon, it can be assumed that similar numbers of radiation-induced recombination centers were present in both types of cells Even if the damage centers are un-ionized, the small quantity of carriers removed during irradiation would not indicate a lithium loss adequate to allow a lithium atom in the structure of each damage center This result tends to support the need for an entirely different damage center in the case of quartz-crucible cells

A more extensive analysis of the above sample was recently completed By use of capacitance measurements, the donor concentration was determined at depths up to 5 into the N-type region These data are shown in Fig 8 The figure shows that the small "loss of donors" during irradiation is a general condition which extends deep into the N-type region The change which occurs during the 500-h recovery period, appears to vary greatly with distance into the cell To permit a closer analysis the data were converted into removal rates ($dn/d\Phi$) and plotted as a function of distance into the N-type region The removal rates during irradiation and recovery are both shown in Fig 9 as a function of distance It is readily apparent from these data that the low apparent removal rate (0 006 cm^{-1}) during irradiation extends deep into the N-type region The removal rate during recovery rises very rapidly with distance A different view of these data is shown in Fig 10, where

two removal rates are plotted as functions of the lithium donor concentration at a point in the cell where the particular removal rate was determined Two facts are apparent the removal rate during irradiation is not a function of lithium concentration and the removal rate during recovery is a very strong function of the lithium concentration

Since the result of the capacitance measurements of removal rates during irradiation of Li-doped quartz-crucible cells strongly indicates that Si-A centers are formed, it would be interesting to examine similar measurements made on conventional P on N solar cells The silicon A center is believed to be the major recombination center in the conventional P/N solar cell (quartz-crucible silicon) In Fig 11 the donor concentrations, determined by capacitance measurements, are shown for a non-lithium solar cell (CEG 112) as a function of distance into the N-type base region The measured carrier removal rate is constant throughout the distance investigated with a value of 0 013 cm^{-1} Under the conditions in this cell Si-A centers would be about 9% ionized The actual introduction rate of A centers would be 0 15 cm^{-1} This value is quite close to the value of 0 2 cm^{-1}, which is calculated from similar measurements on Li-doped quartz-crucible solar cells This result tends to support the previous conclusions that oxygen-vacancy pair (Si-A centers) play a prominent role in the degradation process of all P/N silicon solar cells

Up to this time the full potential of the capacitance measurement has not been utilized in the examination of irradiated solar cells In this section the changes in carrier concentration during and after irradiation are analyzed for three Li-doped FZ solar cells of widely varying lithium concentrations The current-voltage plot for cell C3-18 is shown for several stages of irradiation and recovery in Fig 12 In Fig 13, the donor concentration as a function of distance into the N-type region is shown for the same cell in the same stages of irradiation and recovery illustrated in Fig 12 It appears that the donor removal during irradiation is a strong function of distance into the N-type region In addition, the amount of donors removed during recovery for 200 h is much larger than that removed during irradiation After 400 h, the lithium donor concentration deep in the cell has risen somewhat, apparently from diffusion of lithium into this region The increase in lithium concentration is probably the cause of the slight redegradation in short-circuit currentwhich occurs between 200 and 400 h after irradiation The data relating to donor concentration changes are replotted in Fig 14 for various depths in the N-type region as a function of electron fluence The data in Fig 14 indicate that the removal rate appears linear with electron fluence The removal rate however, increases rapidly with distance into the N-type region The removal rate at the original edge of the space charge region (1 4 μ is only 0 04 cm^{-1} Measurements made with barrier width at 3 7 μ indicate a removal rate of 0 206 cm^{-1} A five-fold increase in removal rate has occurred in a distance of only 2 3 μ from the original unbiased space charge region

Cell C3-18 is typical of a low lithium cell The initial lithium concentration at the junction was 3 8 $\times 10^{14}$ atoms/cm^3 A similar study will now be discussed for a cell with a somewhat higher lithium concentration The solar cell current-voltage characteristic of cell AF 14-4903 is shown in Fig 15 for several stages of irradiation and recovery Figure 16 presents the results of the capacitance analysis during stages shown in Fig 15 In general the donor concentration changes in cell AF 14-4903 are very similar to those discussed for cell C3-18 After 312 h of recovery, the donor concentration is approaching that of the original phosphorus concentration (2 $\times 10^{14}$ atoms/cm^3) of the silicon To further analyze the data in Fig 16 the donor concentrations for specific widths of the space charge region (distance into the N-type region) is replotted in Fig 17 as a function of electron fluence In cell AF 14-4903 the removal rates found during irradiation are somewhat higher than those found in cell C3-18 A rapid increase in removal rate is also noted with increases in barrier width

An additional cell (T4-10) with a much higher lithium concentration was studied in the same manner The current-voltage relationships are shown for before and after irradiation and after recovery in Fig 18 The lithium concentrations as a function of barrier width for cell T4-10 are shown in Fig 19 In this cell, the lithium concentrations are large enough at all depths to allow recovery without making major changes in the lithium concentration It can be noted that the lithium loss during irradiation is exceeded by that during recovery by 50 to 100% These data are of importance in formulating a physical model for the process The removal rates during the irradiation of cell T4-10 at various distances into the N-type region are shown in Fig 20 Similar data are also shown for cells AF 14-4903 and C3-18 Figure 20 provides a graphic example of the extreme variation of removal rate (during irradiation) with depth that is possible within this type of solar cell These variations may in part, be responsible for the wide differences in removal rate reported by different investigators The exact reason for this pattern of removal rate is not clear The trend can be roughly described as a tendency for the removal rate to go to zero at the position of zero barrier width and rise rapidly from this value in some manner directly related to the lithium donor concentration To further clarify this relationship the removal rate data were replotted versus the lithium concentration at the point in the cell at which the rate was determined The data in Fig 21 show that certain lithium concentrations will not result in a specific removal rate Of particular interest in Fig 21 is that removal rate data for cell AF 14-4903 and T4-10 do show near linear behavior in respect to lithium concentration The fact that the individual curves are considerably displaced indicates the presence of some other strong factor in the determination of the removal rate It is possible that distance from the space charge region edge and lithium concentration both act to determine the removal rate during irradiation of Li-doped FZ silicon cells It is reasonable to expect the lithium concentration to affect the removal rate during irradiation Simple mass action principles suggest that areas with higher concentrations of lithium donors should capture more displacement-produced vacancies before annihilation than similar areas of lower lithium concentration It is more difficult to postulate an independent effect which would cause the apparent defect production rate to be so low adjacent to the space

charge region and increase so rapidly with distance from the barrier

These results tend to support a previously proposed model of the damage and recovery processes The model is as follows

Irradiation $V + Li^+ + 2e^- \rightarrow Li\text{-}V^-$

Recovery $Li\text{-}V^- + Li^+ \rightarrow Li\text{-}V\text{-}Li$

or

$$Li\text{-}V^- + 2Li^+ + e^- \rightarrow Li_3\text{-}V$$

The data which support this model are as follows

(1) Lithium is apparently consumed during irradiation

(2) Lithium is apparently consumed during recovery

(3) The lithium consumed during recovery is roughly equal to, or greater than, that consumed in irradiation

V DEFECT STRUCTURES IN CELLS

In our previous investigation, the possibility of using the frequency dependence of solar cell capacitance in the study of radiation defects was explored This technique has recently been used to study lithium solar cells The results of this experimentation appear to be very significant and should provide an excellent means of study in the future In this measurement, the region of the solar cell space charge region is caused to widen and contract under a high-frequency voltage When deep-lying energy levels are present under certain conditions of frequency and temperature, these defects are not able to change their charge state rapidly enough by thermal emission and capture as the space charge region passes through their position This difficulty provides a relaxation effect which can be studied to determine the energy levels of defects present This behavior is illustrated in Fig 22 In this work, Li-doped quartz-crucible silicon solar cells were studied in the unirradiated and irradiated conditions by capacitance measurements at temperatures from 27 to -190°C and frequencies of 5 to 400 kHz In the case of a typical Li-doped solar cell, the donor concentration at the edge of the space charge is related to the capacitance in the following expression

$$N_D = \frac{SVC^2}{q \epsilon}$$

All of the factors in this expression are constant before and after irradiation except S, which is related to exponent of the $k = VC^n$ relationship of the cell In this case, the S factor was observed to be unchanged by irradiation For this reason changes in donor concentration caused by irradiation can be studied by examining the changes in the square of the ratio of capacitance after irradiation to that observed before irradiation This parameter is plotted on the ordinate of Fig 22 Examination of the data indicates that at higher temperatures, no frequency dependence is observed As the sample temperature is reduced, a divergence in the data for various frequencies is observed The lower-frequency (5-kHz) capacitance values diverge first as the sample temperature is decreased, followed by those of higher frequency at still lower temperatures At -190°C (1000/T = 12), the capacitance variation with frequency again converges The behavior in general is indicative of deep-lying traps produced by the electron irradiation The point at which the transition from maximum to minimum donor population is half complete is marked for each frequency used This point is defined as the cutoff frequency at that particular temperature It can be assumed that the reciprocal of the cutoff frequency is proportional to the relaxation time of the electronic capture process dominating the process as follows

$$\tau = k\frac{1}{f_c}$$

The relaxation time of such processes can be determined from statistical considerations In a case which can be described as a net loss of donors, the expression would be

$$\tau = 1/C_n N_c \exp\left[-\Delta E/kT\right]$$

where

N_c = the effective density of state

C_n = capture constant for electrons

To facilitate the analysis, it has been assumed that the reciprocal of the cutoff frequency is equal to the relaxation time To determine the energy level of the centers involved in the relaxation (ΔE), an activation energy plot is presented in Fig 23 To construct a plot in which the slope will directly reflect the value of ΔE, the relaxation time divided by the density of states is plotted versus the reciprocal temperature The data indicate the value of ΔE to be 0 17 eV Since this value is also identified with the ionization energy of the Si-A center, these measurements add more support to previously discussed evidence indicating that the primary defect produced during irradiation of Li-doped quartz-crucible silicon solar cells is the oxygen-vacancy pair or Si-A center Certain factors such as spin degeneracy, temperature dependence of capture cross section, and width of the space charge region have been neglected in this analysis It is believed that consideration of such factors would not significantly alter the conclusions

VI LITHIUM COUNTERDOPING OF P-TYPE SILICON

The benefits of radiation hardening by lithium doping have been so far confined to N-type silicon This is an unfortunate circumstance, as N-type silicon is inherently more prone to displacement radiation damage than P-type silicon Lithium doping has made N-type silicon competitive with and, in some cases, superior to P-type silicon with regard to radiation hardness A much more desirable situation would be to further increase the radiation hardness of P-type by lithium or any other type of doping In an effort to determine if any

such advantage does exist, we have fabricated P-type silicon which is counterdoped by the diffusion of lithium The results of electrical measurements made on a few P-type lithium counterdoped samples are summarized in Table 1 Two of these samples were made with quartz-crucible silicon and the other from FZ silicon In all cases, the resistivity after lithium diffusion is much higher than the original resistivity of the crystal This is evidence that many of the boron donors originally present in the crystals have been compensated by the presence of the lithium donors This compensation was also confirmed by Hall coefficient measurements The boron and lithium concentrations shown in Table 1 were determined in this manner The Hall mobility of each specimen after the lithium diffusion is also shown It can be noted that the mobilities shown are relatively low for samples of the resistivities exhibited after lithium diffusion This is because mobility reflects the total concentration of scattering centers (i e , both boron and lithium ion cores) The mobilities shown are more typical of the original crystal, since the possible scattering center population has been increased although the net carrier concentration in the valence band has been decreased For this reason, a lithium compensation diffusion of a P-type crystal will raise the Hall coefficient and decrease the Hall mobility A large decrease in mobility may not be detected because of pairing of the lithium and boron atoms The significant point is that P-type silicon can be Li-counterdoped to achieve resistivities of interest to the device designer and lithium concentrations which could be of importance in radiation hardening

In an effort to obtain some indication as to possible hardening mechanisms, the P-type Li-doped silicon samples discussed in Table 1 were irradiated with 1-MeV electrons In this work, only the Hall coefficients and resistivity were monitored Thus, any radiation-induced reactions which affect majority carrier behavior can be detected Although this does not measure the minority carrier lifetime, similar measurements in N-type reflect the reaction of lithium with the radiation-generated defect complexes In Fig 24, the hole concentration of sample Li-P-QC-1-1 is plotted versus electron fluence After an irradiation of 3×10^{16} e/cm^3 the sample was stored at 100°C The slightly elevated temperature was used because of the known reduction of effective diffusion constant of lithium in quartz-crucible silicon As shown in Fig 24, the hole concentration was significantly increased during the storage at 100°C Since defects in P-type silicon do not normally anneal at this temperature it appears that lithium may have reacted with some of the defects generated during the irradiation to annihilate them In this P-type of sample a decrease in lithium donors causes the hole concentration to increase because of the lowered compensation These results are by no means conclusive, but do indicate that further work is warranted

The data shown in Fig 25 relate to a similar sample which was Li-counterdoped to a much higher resistivity (Li-P-QC-10-4) In the sample, the removal rate during irradiation was 0 03 cm^{-1}, which is similar to that of ordinary boron-doped silicon In this sample, the hole concentration also increased during storage at 100°C The initial increase was larger than that of the previous sample, however, after 40 h at 100°C, the hole concentration decreased to less than that observed after the irradiation The nature of this change is not clear at this time

The data in Fig 26 represent the only study to date on P-type Li-counterdoped FZ silicon (Table 1) This material is of interest, in this case, because of the lower oxygen concentration This lower oxygen concentration may allow any lithium reactions occurring to be observed in a shorter period of time at room temperature In Fig 26, the hole concentrations before and after irradiation are plotted on the ordinate of the graph The hole concentrations at various times after completion of the irradiation are shown in the figure It is apparent that, after the decrease of hole concentration caused by irradiation, a large time-dependent increase in hole concentration occurs The hole concentration reaches a maximum of 40 h after irradiation and then declines somewhat from the maximum The magnitude of the hole increase observed with time is much greater than that of the decrease which occurred during irradiation It is difficult to give a full explanation of these effects on the basis of this limited work It does appear that, in some way, irradiation of this material initiates a time-dependent reaction, probably involving lithium donors, which results in a very significant increase in the hole concentration Because of equilibrium considerations involving boron, this loss of donors cannot be explained as a simple precipitation of lithium In view of the known behavior of annihilation of recombination centers in N-type, the behavior observed in P-type Li-compensated silicon strongly suggests that similar reactions between lithium and recombination centers may also occur in P-type silicon If this is the case, the development of Li-doped N on P solar cells with a highly superior radiation resistance may be within practical achievement Further work in this area appears to be warranted

VII LARGE SUBSTITUTIONAL DOPANTS IN SILICON

We have previously evaluated silicon doped with larger substitutional atoms in regard to a possible radiation-hardening mechanism In previous work, a single crystal silicon -- 13% germanium alloy -- was grown by the quartz-crucible technique This alloy crystal was doped with boron in the usual manner to produce an 8-Ω-cm P-type crystal This material was fabricated into solar cells and evaluated for radiation resistance The cells produced from this alloy were satisfactory with regard to photo output, but proved to be more prone to radiation damage than conventional N on P cells The basis for this work was as follows The vacancies produced by the energetic particles are surrounded by a tensile strain field Substitutional atoms larger than silicon atoms are surrounded by a compressive strain field If radiation-produced vacancies could be trapped by large substitutional atoms, due to the lowering of their collective strain energy, the vacancies would be prevented from forming complexes which are recombination centers This logic is in error in the case of bismuth since a vacancy trapped next to a bismuth atom is simply a Si-E center (i e , a possible recombination center) In the case of

germanium, the strain field is limited because that atom is only 3% larger than silicon

Our current effort involved two silicon crystals doped with larger substitutional atoms Both crystals were grown from quartz-crucibles One crystal was N-type silicon doped with bismuth to a resistivity of 0 5 Ω-cm The other crystal was a P-type silicon — 0 5% tin alloy doped with boron to 20 Ω-cm

The two groups of cells[2] were evaluated by monitoring the short-circuit current with a one sun equivalent of tungsten illumination, during a 1 MeV electron irradiation The results of this work are presented in Fig 27 The behavior of typical P/N and N/P solar cells are also shown as dashed lines in Fig 27 The short-circuit currents of the bismuth cells (2, 5) are slightly higher during irradiation than that of a comparable P/N cell This difference does not appear to be of any practical significance In the case of the silicon-tin alloy cells (A4, B2), they appear to degrade under electron fluence well before the comparable N/P cells which are commonly used today Therefore, it must be concluded that little or no practical hardening advantage can be achieved by addition of large substitutional atoms to the silicon lattice In fact, the addition of the large neutral substitutional atoms to P-type silicon appears to promote the formation of more or more effective recombination centers No further work is planned in this area

VIII LITHIUM SOLAR CELL EVALUATION

In this phase of the program, Li-doped solar cells manufactured by Centralab, Heliotek, and Texas Instruments have been irradiated with electrons, and their recovery characteristics have been studied Several different processing experiments were represented in these cells, including an oxygen layer adjacent to the junction, lithium-diffused through both front and back surfaces, phosphorus n^+ layer near the junction, and cells processed from whole slices The groups evaluated are listed, along with their material and processing variables, in Table 1

All of the cells received a radiation exposure of 3×10^{15} e/cm^2 at 1 MeV Tungsten I-V characteristics and capacitance versus voltage measurements were then obtained as a function of time at either room temperature or 100°C The general radiation damage and recovery characteristics of each group of cells are summarized in Table 2 The recovered levels given in the table are the peak of the recovery curve and do not take into account any redegradation that may have occurred The one-half recovery time is the time necessary for the short-circuit current to reach a point midway between the damaged level and the peak recovery level In general, it can be observed that the higher lithium concentrations result in lower initial characteristics, higher recovered levels, and more rapid annealing rates, while with lower lithium concentrations, higher initial levels and slower recovery rates exist

In Table 3, the peak recovery levels are compared graphically with each other and with the equivalent damage level for contemporary 10-Ω-cm N/P solar cells The spread of the data and the half-recovery time are also shown It should be noted that most cell groups tested here are not only inferior in recovered level to the best groups tested previously, but are also no improvement over contemporary N/P cells

A Centralab Cells

In Centralab groups C8A through C8D the important feature is an oxygen-rich layer approximately 1 mil thick formed by diffusion in an oxidizing atmosphere prior to formation of the P^+ layer It was hoped that this oxygen layer would prevent redegradation of the recovered level without affecting the bulk-dependent rapid recovery in FZ and Lopex material However, in both the FZ cells (C8A and C8B) and the Lopex cells (C8C and C8D), the oxygen layer slowed the recovery rates by more than two orders of magnitude at room temperature This is reasonable since the capacitance data in Table 1 indicate lithium concentrations of an order of magnitude less in the oxygen layer cells than in the non-oxygen layer cells for both materials

To find out if recovered levels were stabilized, it was necessary to accelerate the recovery process for half of the cells by annealing them at 100°C No noticeable stability improvement was seen for the FZ cells, however, in the Lopex case, much less (2% versus 25%) redegradation was observed in the oxygen layer cells as compared to the non-oxygen layer cells after 1000 h

Centralab groups C8E through C8H had lithium diffused through the P^+ layer on the front of the cells as well as through the back The reasons for this experiment are to prevent excess lithium concentrations and severe lithium gradients The initial outputs of the FZ cells (C8E and C8F) were so poor, about 30 mA for C8E, that they were not included in the testing program The crucible-grown cells (C8G and C8H) had fairly good initial outputs, were irradiated, and were annealed at 100°C Lithium concentrations in the front-back diffused cells were 3 to 10 times higher than in the back-only cells and, as expected, they annealed faster However, the front-back diffused cells did not recover as far as expected with peak short-circuit currents of only 30 mA compared to 33 and 38 for the back-only cells

B Texas Instruments Cells

The Texas Instruments solar cell groups (T9 and T10) were processed from whole slices to eliminate potential edge effects due to non-uniform lithium concentrations In addition, the lithium diffusion was designed to produce half the lithium concentration of Texas Instruments standard lithium cells in the T9 group and twice the standard concentration in the T10 group. The capacitance measurements confirm this plan, indicating a factor of 4 in lithium concentration between the

[2]We are indebted to Peter Iles of Centralab Semiconductor Division who fabricated several wafers of these two crystals into solar cells for evaluation

two groups Recovered levels for both groups are disappointing, however, since neither cell group reached 35 mA, while last year's T6 group reached 40 mA As expected, the annealing rate of the T10 group is faster than that of the T9 cells however, this rapid recovery is associated with a significant redegradation about 35% after 700 h It is concluded that the reducing of edge effects does not improve recovery performance

C Heliotek Cells

Heliotek solar cell group (H8) has a phosphorus N^+ layer diffused near the junction prior to the boron P^+ diffusion Except for this additional phosphorus layer, these cells were identical to the H4 group tested in 1969 The H8 cells have recovered a few milliamperes farther (37 versus 33) than the H4 cells, but at a factor of 4 more slowly The H7 cells tested in 1969 and several other Heliotek groups are superior in recovered level, with the best between 40 and 45 mA and recovery rates similar to those for the H8 cells (Figure 28)

The recovery characteristics of the most recent groups of cells, H3A (325/480), H9 (425/90/60), and H10 (425/90/60), were determined as a function of time and temperature after irradiation with 1-MeV electrons and were compared with the best of previous cell groups A brief summary of the comparison is presented herein for the crucible and FZ base material The best prior groups of crucible cells annealed at 100°C are shown in Fig 29 Although the H14 group was not constructed specifically for this program, it represents one of Heliotek's better crucible groups and is included here for comparison purposes The two new groups, H10 and H3A, exhibited recovery levels of 38-40 and 40-41 mA respectively with half-annealing times of 1 h at 100°C In addition the H3A group exhibited higher initial outputs than any prior group of Li-doped cells tested to date that possessed annealable characteristics As indicated, the recovered short-circuit current levels are slightly lower for the latter groups compared to the best prior data which were represented by the T2 and T7 groups, however, the H3A group exhibited less curve factor degradation and, to date, less redegradation effects than the prior groups, which would indicate overall superiority in terms of preservation of maximum power output It is of interest to note that the longer-time, lower-diffusion temperature groups are continuing to exhibit characteristics competitive with, or better than, the best of the shorter-time, higher-diffusion temperature groups (see Tables 2 and 3 and Figs 28 and 29)

A similar comparison can be made for the recovery characteristics at room temperature of FZ Li-doped cells As in the previous comparison, all of the groups of cells were not directly associated with this particular contract but are included as being representative of the state of the art The best groups are shown in Fig 29 The new groups now under study are H9 (425/90/60) with maximum recovered level of 38 mA in half-annealing time of 5 h Although we have not yet tested any recent long-time, low-temperature diffused FZ lithium cells there appears to be a measurable difference, although slight in the superiority of the 120-min redistribution over the 60-min redistribution The new groups of cells have not to date exhibited any detrimental curve factor decay or redegradation (Tables 2 and 3 and Figs 28 and 29)

Several trends seem evident in the above summary of cells fabricated over the past two years First, it appears that the 325°C, 480-min diffusion consistently produces cells which are equal to the best produced with the higher-temperature, longer-time diffusion, whereas the average response over all the cells produced with the latter diffusion schedule is considerably poorer and widely variant Other variables, such as initial resistivity, paint-on versus evaporated source, inclusion of an N^+ layer, and variation of parent dopant do not seem to have measurable or significant effects on overall cell performance Finally, annealing rates of the more recent cells appear to be consistent with previous data as shown in Fig 30 for the H3A and H10 crucible cell groups The activation energies for annealing appear to be consistent with the 1 10 eV slope anticipated for oxygen-rich crucible material

D Solar Simulator Measurements

The majority of the I-V curves in the evaluation program have been obtained using tungsten illumination because of its convenience, reliability, and amplification of radiation-induced degradation In addition, most of the annealing data has been taken at the short-circuit current point Although most cell groups exhibit stable I-V characteristics allowing qualitative linear comparisons for anticipated responses, under solar simulation the quantitative magnitude of the annealing performances is difficult to extrapolate for the lithium cell For these reasons, solar simulator measurements have been performed on a selected number of cell groups which are representative of the most superior Li-doped P/N cells evaluated to date The pre-irradiation, post-irradiation, and after-annealing maximum power points have been plotted in Fig 31 The annealing rate curves shown are the same as those observed under tungsten illumination and are assumed to have been the same under solar simulation As shown in Fig 31, the pre-irradiation initial efficiencies are competitive with contemporary N/P solar cells and the annealed outputs are in every case superior to the contemporary N/P cell after 3×10^{15} e/cm^2 There is, however, a wide divergence in annealing rates which is probably due to differences in oxygen concentration among the various groups It is of interest to note that, of the three groups presented, two of them were fabricated utilizing the slower 325°C, 480-min diffusion schedule These data confirm that significant progress has been made in the last several years in the generation of a technology to manufacture high-efficiency stable Li-doped P/N cells which exhibit superior radiation resistance after annealing relative to the contemporary 10-Ω-cm N/P cell

IX SUMMARY

It is apparent from Hall and capacitance measurements that the silicon A center (oxygen-vacancy pair) is the major defect formed during irradiation of a Li-diffused quartz-crucible solar cell In the case of the irradiation of Li-diffused FZ solar cells, the silicon A center is also

formed however a second defect with a deeper-lying energy level (probably a lithium-vacancy pair) is also formed Both defects are annihilated by reactions with lithium donors during recovery

It is possible to fabricate excellent Li-diffused solar cells from either FZ or quartz-crucible silicon When Li-diffused solar cells are fabricated with an optimum diffusion schedule, they are superior in radiation resistance to contemporary N/P cells after electron irradiations of 3×10^{15} e/cm^2 Such irradiated and recovered lithium cells will produce 10 to 20% more power than a similarly irradiated contemporary N/P solar cell

Initial efforts at lithium counter-doping of P-type silicon suggest the feasibility of lithium hardening of N/P solar cells

REFERENCE

1 Vavilov V S , "The Interaction of Radiation Defects with Impurities and other Defects in Semiconductors," in Proceedings of the 7th International Conference on Physics of Semiconductors, Paris-Roy Aumont, France, July 16-18, 1964, Vol III, "Radiation Damage," Academic Press, N Y , 1964, pp 115-129

Table 1 Summary of P-type Li-counterdoped samples

Sample	Original crystal		Boron concentration, atoms/cm^3	Li-diffused crystal		Lithium concentration, atoms/cm^3	Hall mobility, cm^2/V-S
	Type	Resistivity, Ω-cm		Type	Resistivity, Ω-cm		
Li-P-QC-1-1	P	0 1	8×10^{17}	P	1 3	4×10^{17}	175
Li-P-QC-10-4	P	1 8	8×10^{15}	P	26	$7\ 5 \times 10^{15}$	290
Li-P-FZ-10-3	P	1 5	1×10^{16}	P	8	$0\ 8 \times 10^{16}$	300

Table 2 Lithium solar cell manufacturing parameters

Cell group	Base material			Lithium introduction		
	Material type	Dopant	Resistivity, Ω-cm	Diffusion schedule, °C/min/min	Lithium concentration at junction, cm^{-3}	Remarks
C8A	FZ	P	100	400/120	3×10^{14}	Oxygen layer
C8B	FZ	P	100	400/120	4×10^{15}	Without oxygen layer
C8C	Lopex		90	400/120	6×10^{14}	Oxygen layer
C8D	Lopex		90	400/120	4×10^{15}	Without oxygen layer
C8E	FZ	P	100	400/10	$>1 \times 10^{16}$	Li-diffused front and back
C8F	FZ	P	100	400/120	4×10^{15}	Li-diffused back only
C8G	Crucible	As	30	400/10	1×10^{15}	Li-diffused front and back
C8H	Crucible	As	30	400/120	$<10^{14}$ and 3×10^{14}	Li-diffused back only
H8	FZ	P	100	425/90/60	6×10^{14}	Phosphorus layer
H9	FZ	P	20	425/90/60	1 2 to 10 5 $\times 10^{14}$	
H10	Crucible	P	20	425/90/60	2 2 to 6 3 $\times 10^{14}$	
H3A	Crucible	P	20	325/480	0 to 4 1 $\times 10^{14}$	
T9	Lopex	P	>50	325/480	9×10^{14}	Processed from whole slices
T10	Lopex	P	>50	400/135	4×10^{15}	Processed from whole slices

Table 3 Lithium solar cell recovery characteristics after 3×10^{15} e/cm^2, 1 MeV

Cell group	N_{Li}, cm^{-3}	Annealing temperature, °C	Initial level, I_{sc}, mA	Damaged level, I_{sc}, mA	Recovered level, I_{sc}, mA	Time to 1/2 recovery point, h
C8A	2×10^{14}	25	50	21	Not yet peaked	
	4×10^{14}	100	47	18	36	<1
C8B	4×10^{15}	25	42	16	33	4
C8C	5×10^{14}	25	51	20	Not yet peaked	
	7×10^{14}	100	50	18	35	<0 3
C8D	4×10^{15}	25	50	18	33	1 2
C8G	1×10^{15}	100	52	16	30	<0 3
C8H	$<10^{14}$ and 3×10^{14}	100	60 and 48	25 and 17	38 and 33	7 and 0 5
H8	6×10^{14}	25	37	22	36	12
H9	9×10^{14}	25	45	22	38	5
H10	4×10^{14}	100	54-58	22-24	38-40	1
	4×10^{14}	60	49-55	22	38-40	30
H3A	3×10^{14}	100	52-64	21-27	40-41	2
	3×10^{14}	60	53-61	22-27	38-42	70
	2×10^{14}	25	59	23-25	--	--
T9	9×10^{14}	25	53	15	33	20
T10	4×10^{15}	25	47	18	30	<1

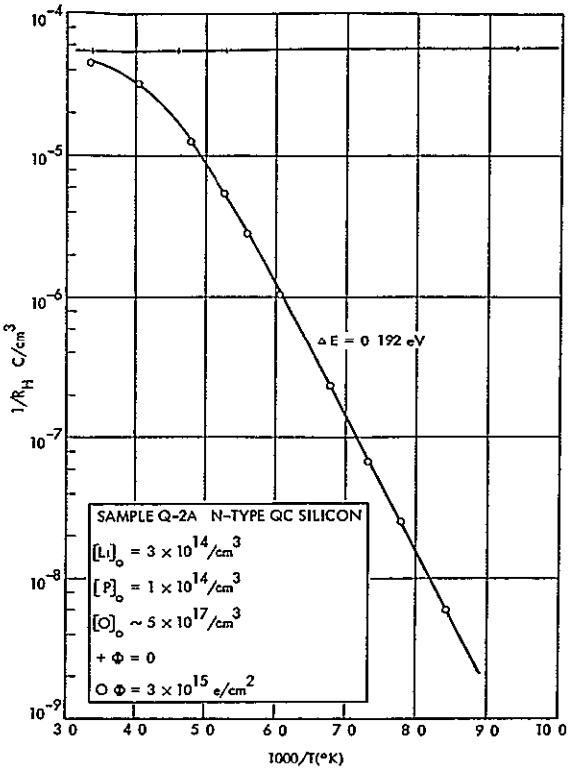

Fig 1 Hall coefficient vs temperature, irradiated Li-doped QC silicon

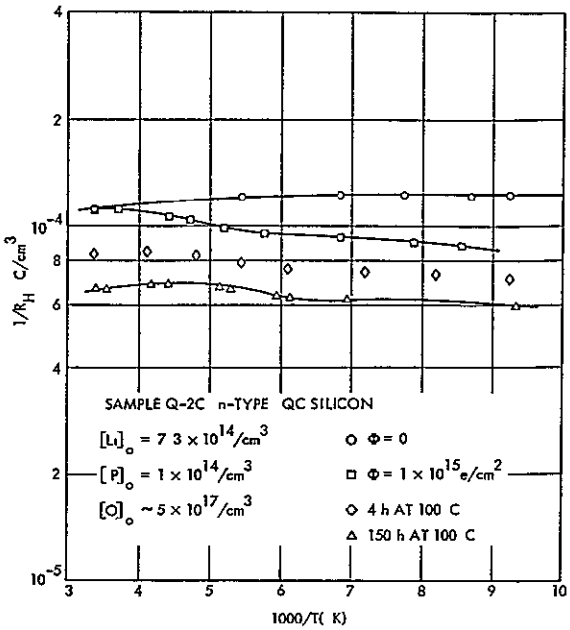

Fig 2 Hall coefficient vs temperature, irradiated Li-doped QC silicon

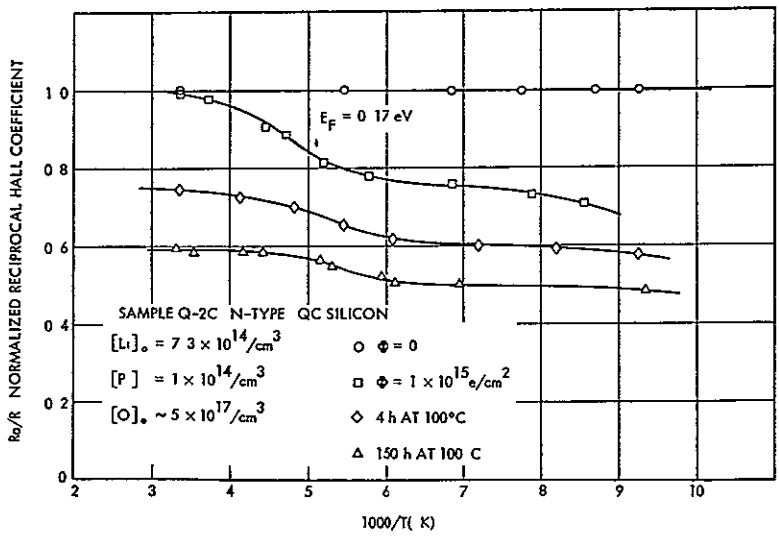

Fig 3 Normalized Hall coefficient vs temperature, irradiated Li-doped QC silicon

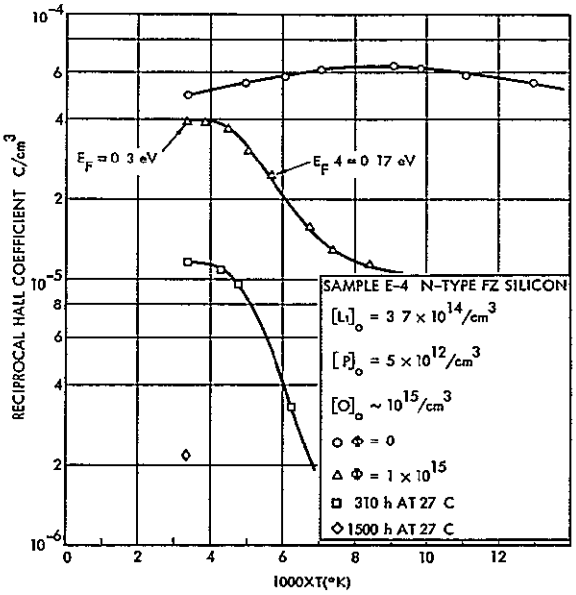

Fig 4 Hall coefficient vs temperature, irradiated Li-doped FZ silicon

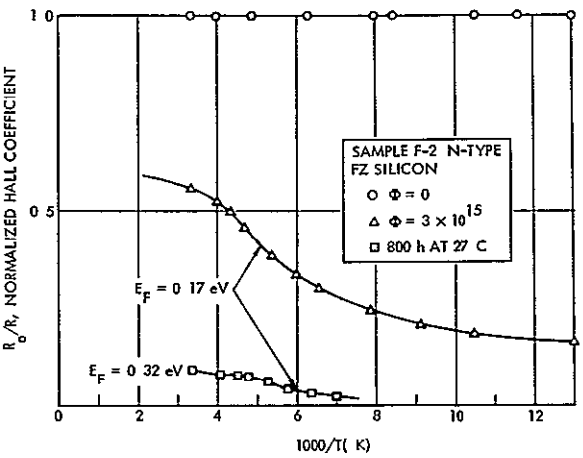

Fig 6 Normalized Hall coefficient vs temperature, irradiated Li-doped FZ silicon

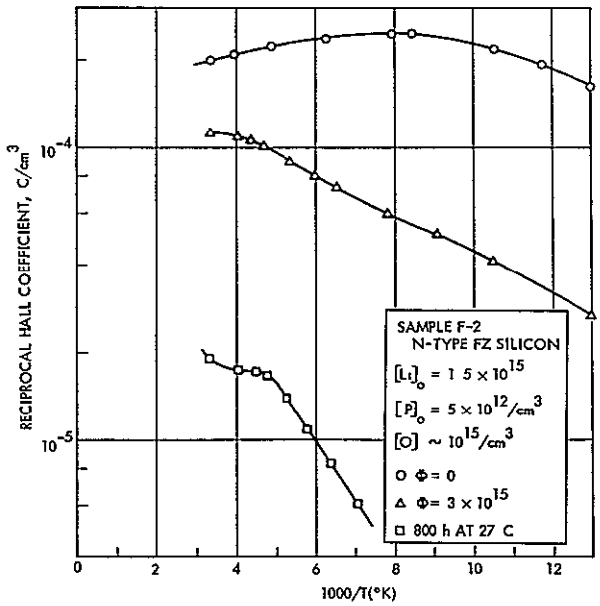

Fig 5 Hall coefficient vs temperature, irradiated Li-doped FZ silicon

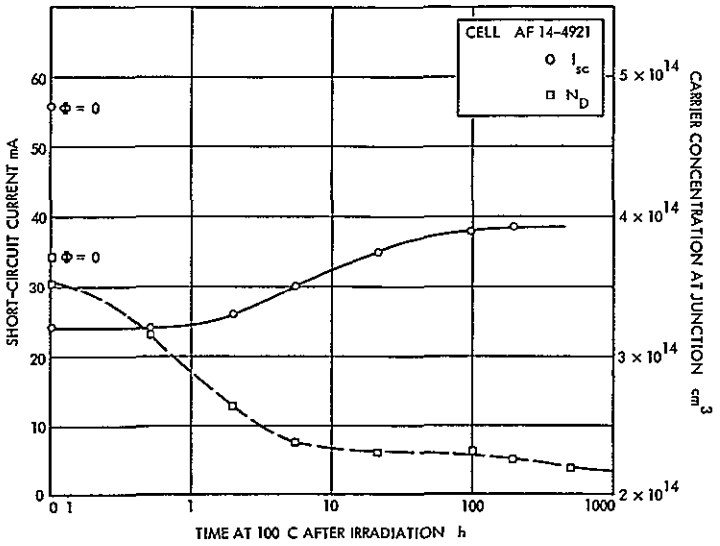

Fig 7 Recovery of Li-doped QC cell

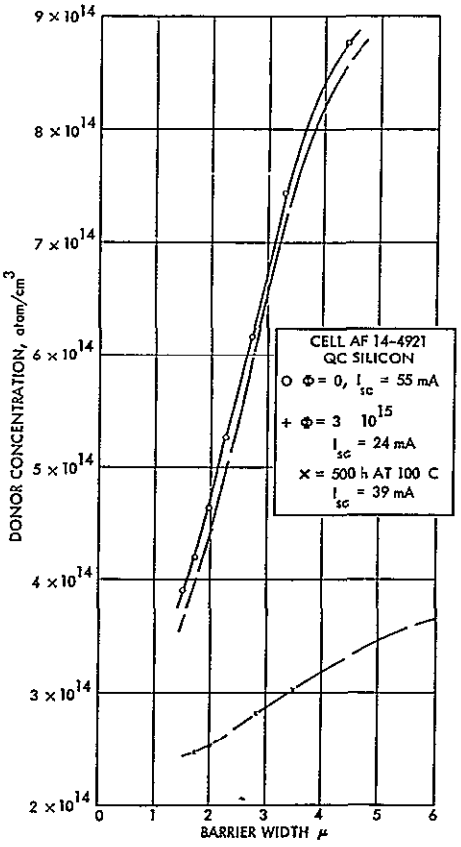

Fig 8 Donor concentration vs barrier width, cell AF 14-4921

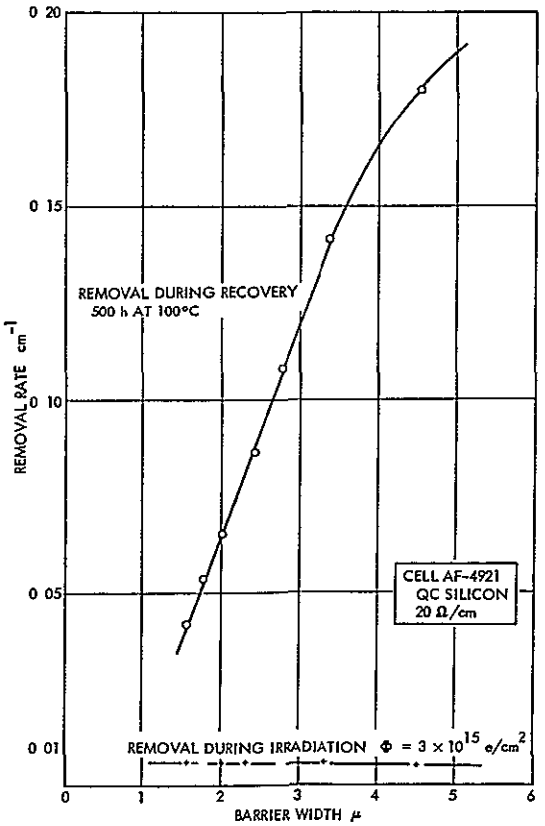

Fig 9 Removal rate vs barrier width, cell AF 14-4921

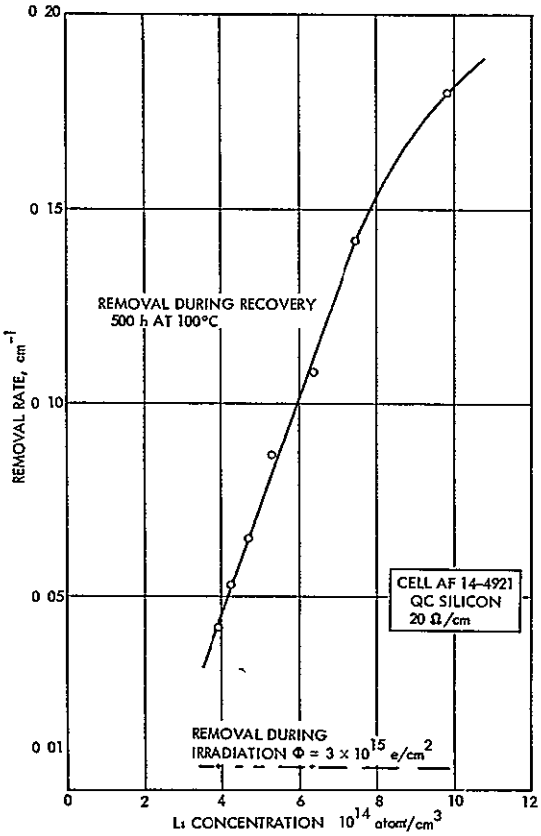

Fig 10 Removal rate vs lithium concentration, cell AF 14-4921

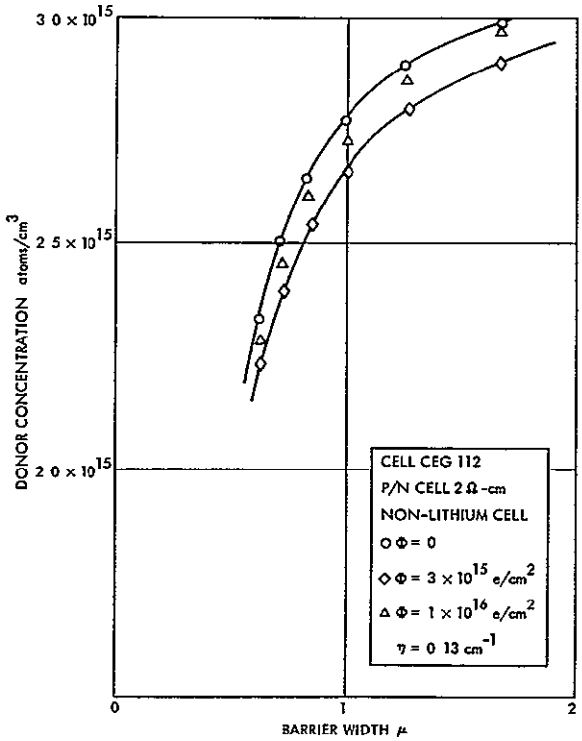

Fig 11 Donor concentration vs barrier width, conventional P/N cell

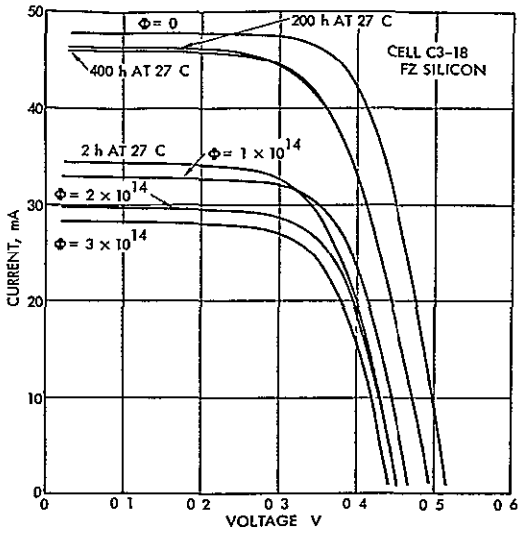

Fig 12 Solar cell characteristics, cell C3-18

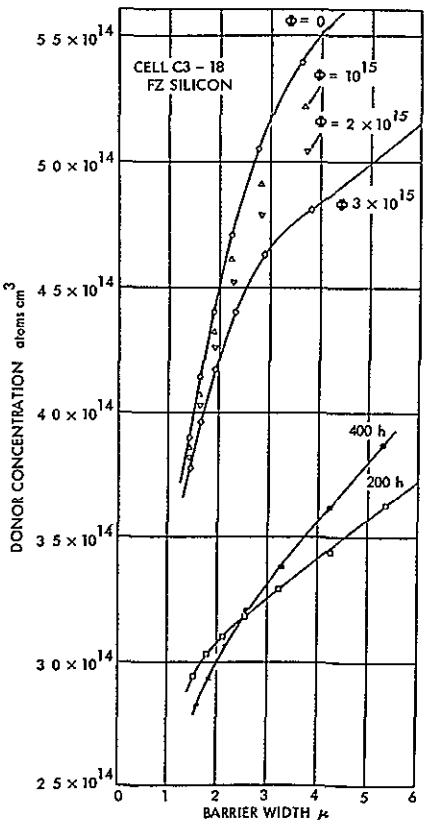

Fig 13 Donor concentration vs barrier width, cell C3-18

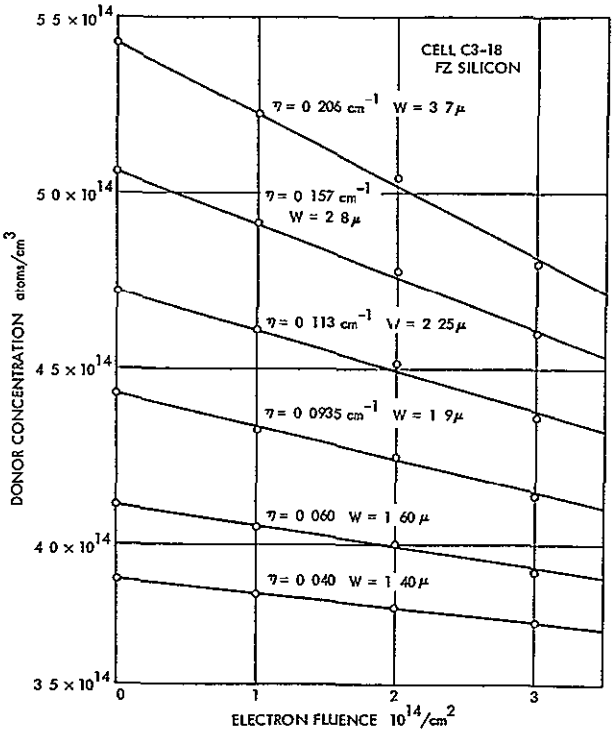

Fig 14 Donor concentration vs fluence, cell C3-18

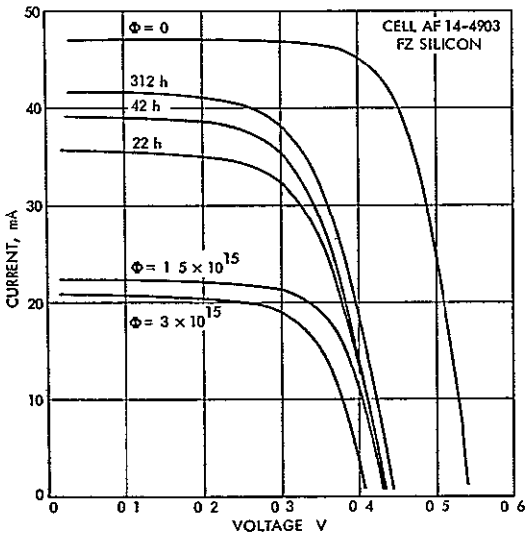

Fig 15 Solar cell characteristics, cell AF 14-4903

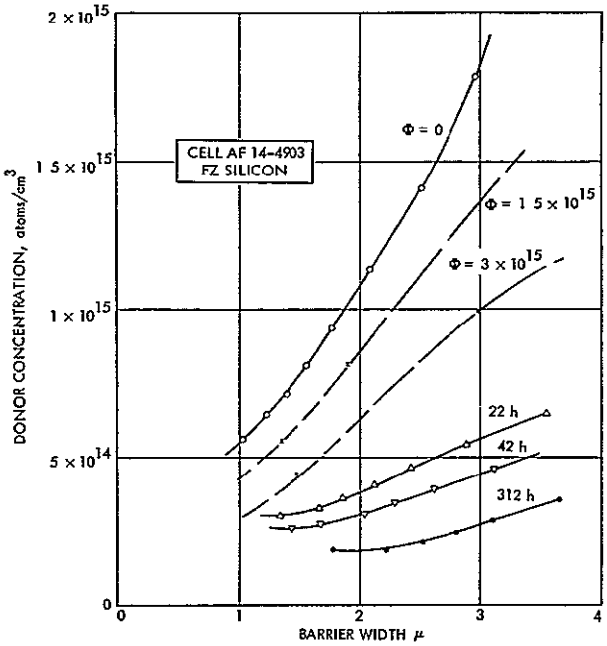

Fig 16 Donor concentration vs barrier width, cell AF 14-4903

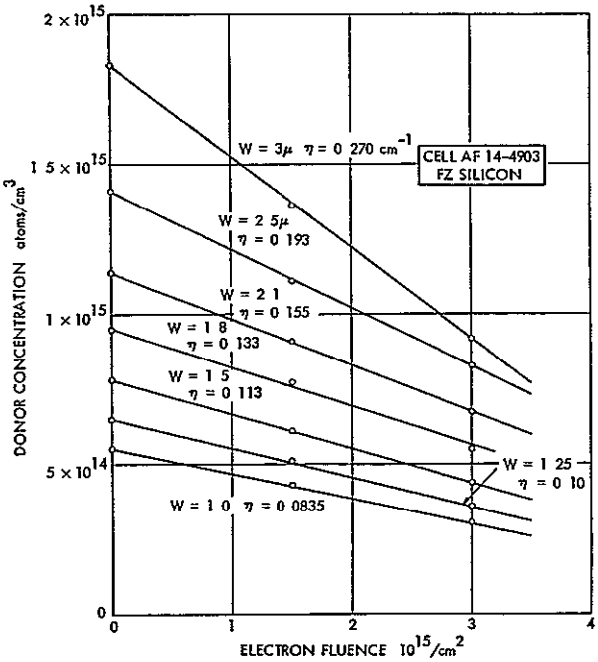

Fig 17 Donor concentration vs fluence, cell AF 14-4903

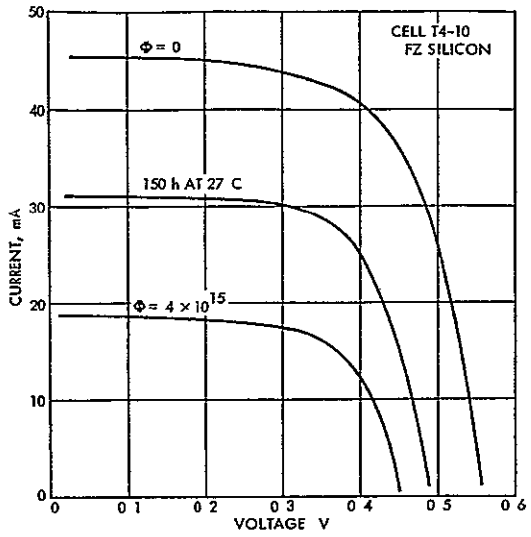

Fig 18 Solar cell characteristics, cell T4-10

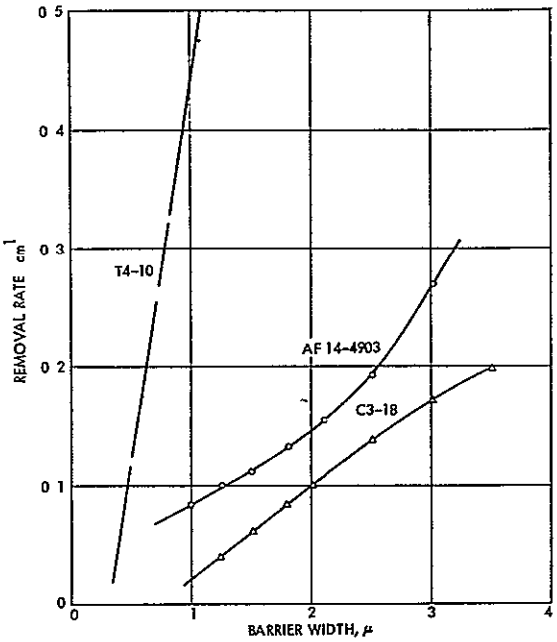

Fig 20 Removal rate vs lithium concentration, FZ cells

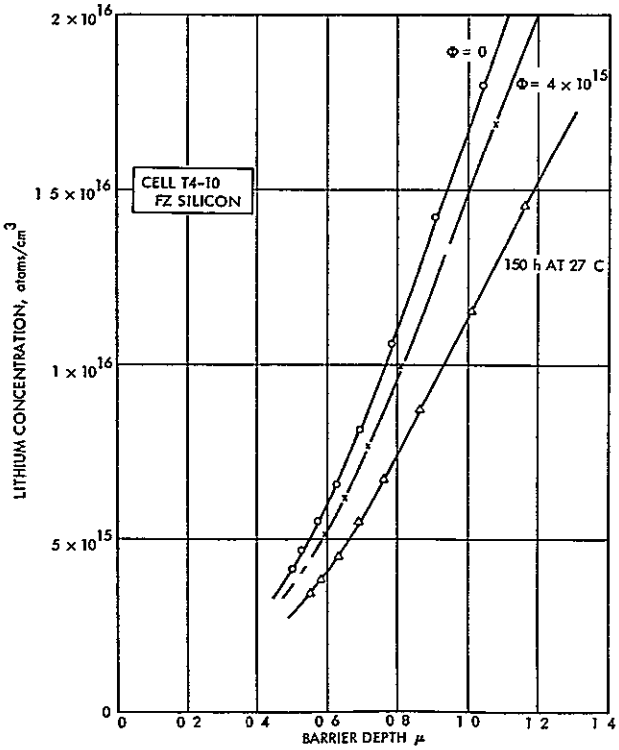

Fig 19 Donor concentration vs barrier width, cell T4-10

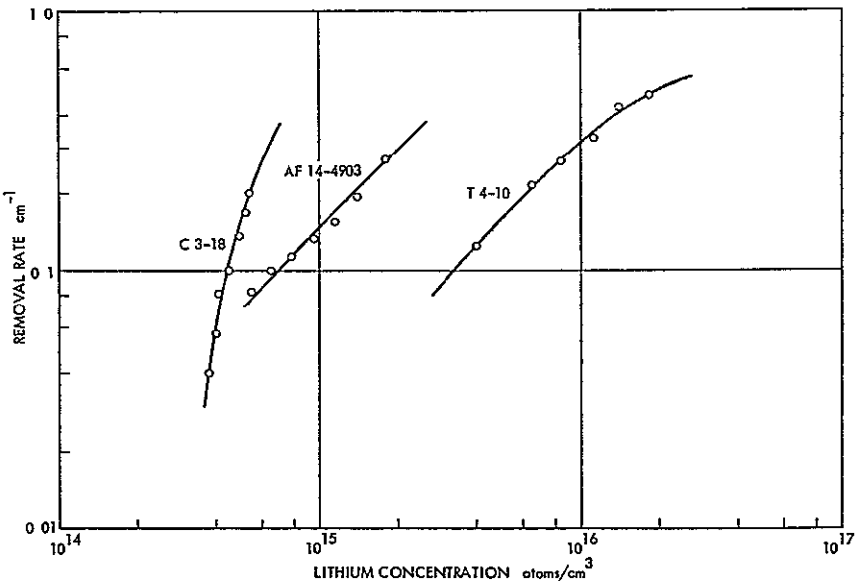

Fig 21 Removal rate vs barrier width, FZ cells

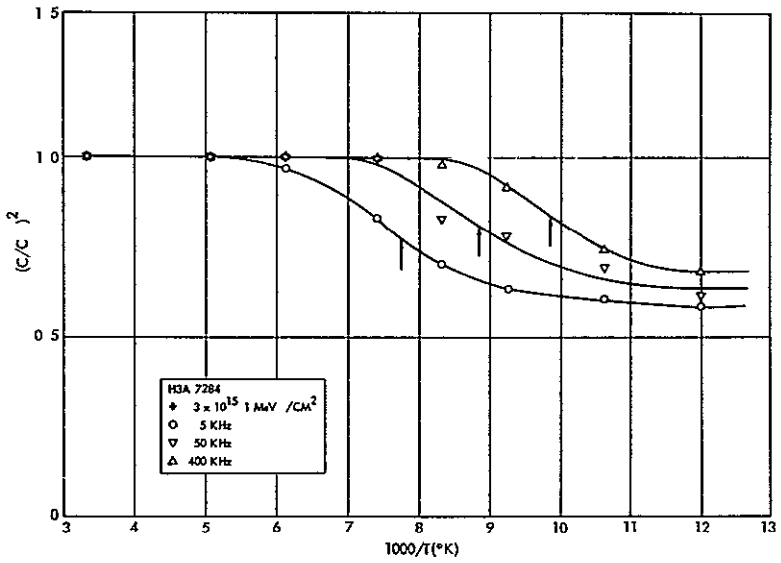

Fig 22 Capacitance vs temperature, various frequencies

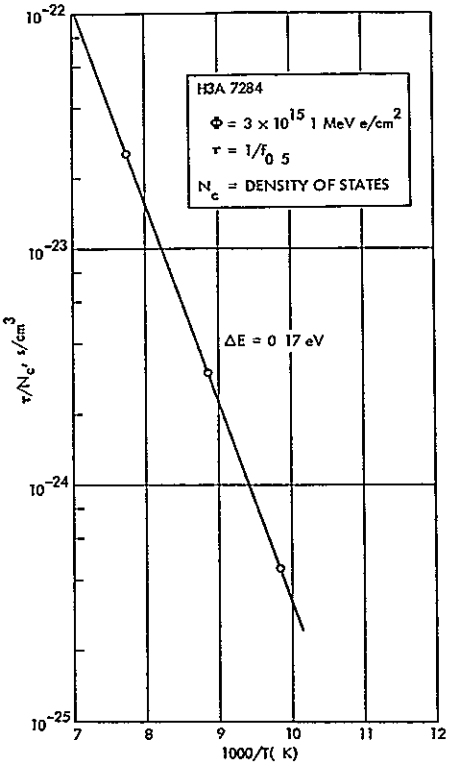

Fig 23 Activation energy plot, cell H3A 7284

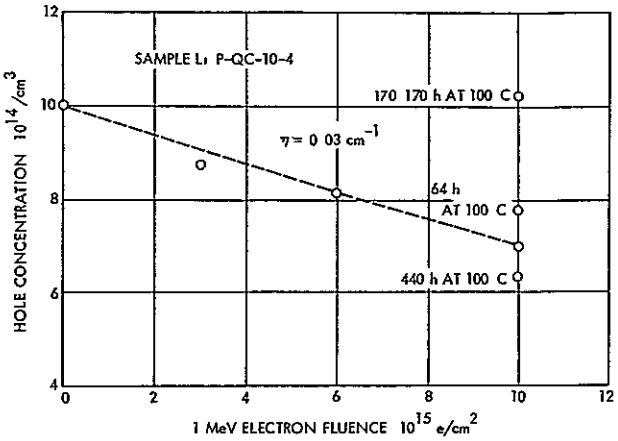

Fig 24 Li-compensated P-type silicon, QC

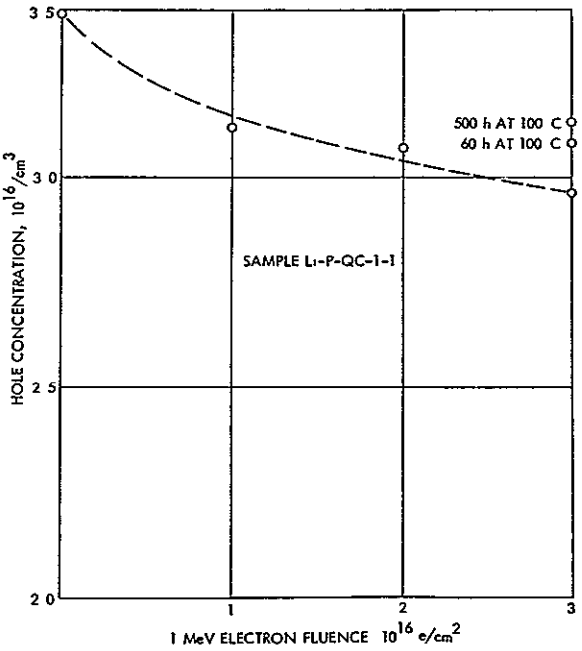

Fig 25 Li-compensated P-type silicon, QC

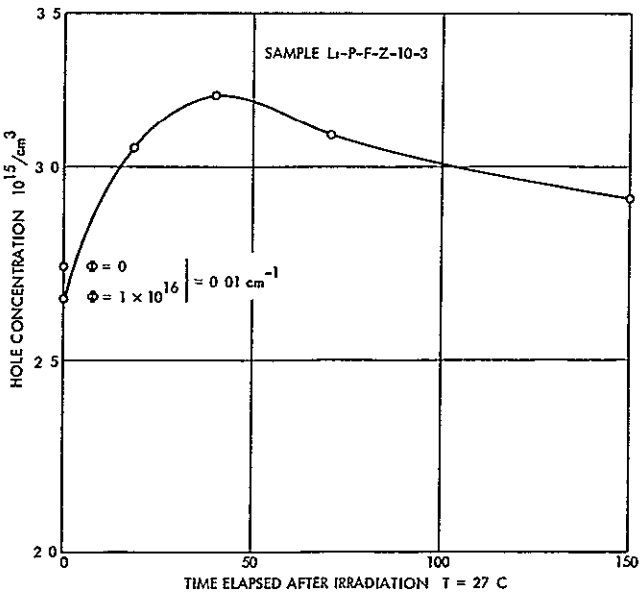

Fig 26 Li-compensated P-type silicon, FZ

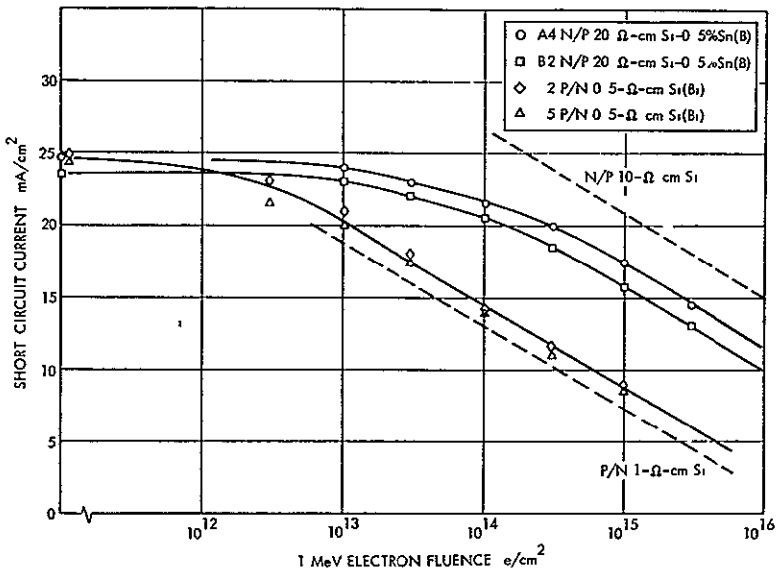

Fig 27 Solar cells with large substitutional impurity atoms

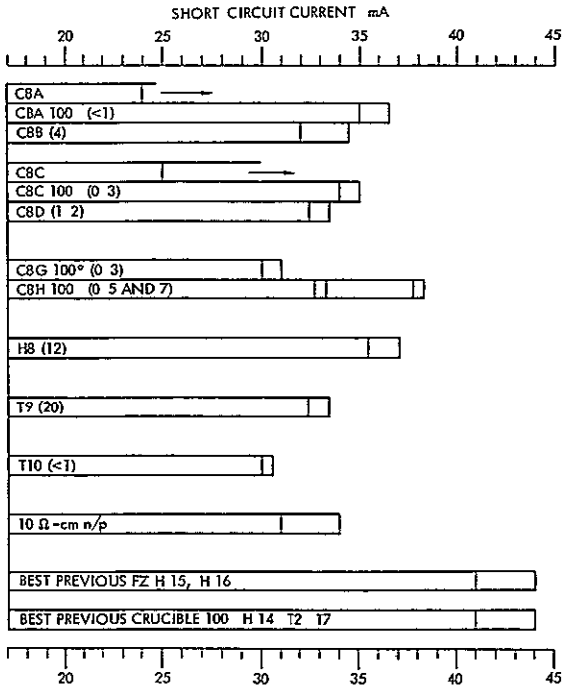

Fig 28 Recovered level and half-recovery time (hours)

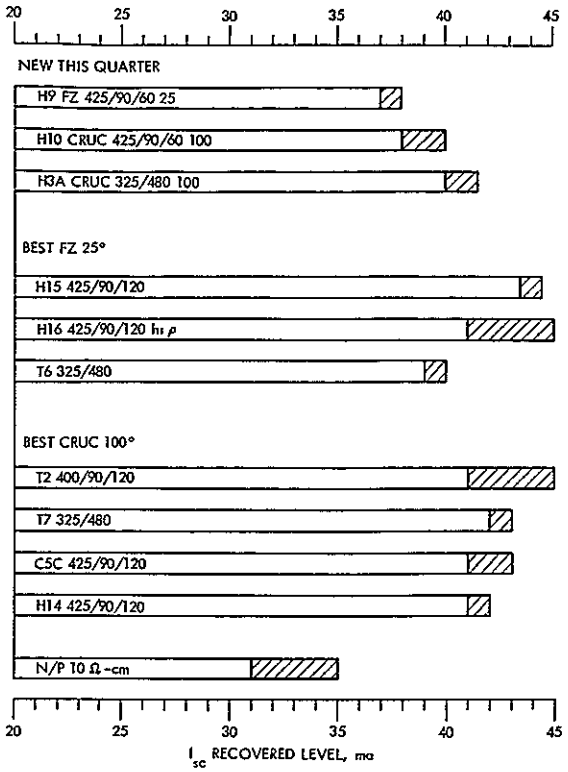

Fig 29 Comparison of peak recovered levels (I_{sc}-tungsten)

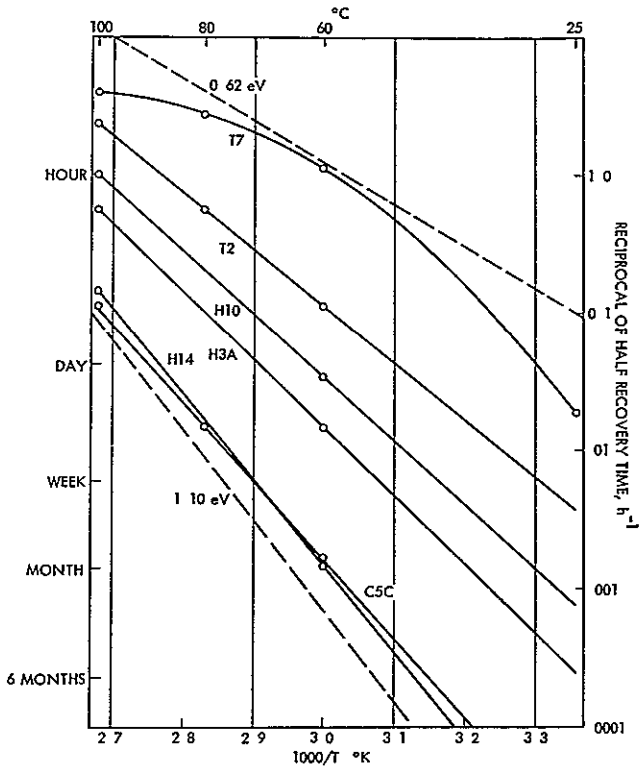

Fig 30 Annealing time vs storage temperature for crucible lithium solar cells

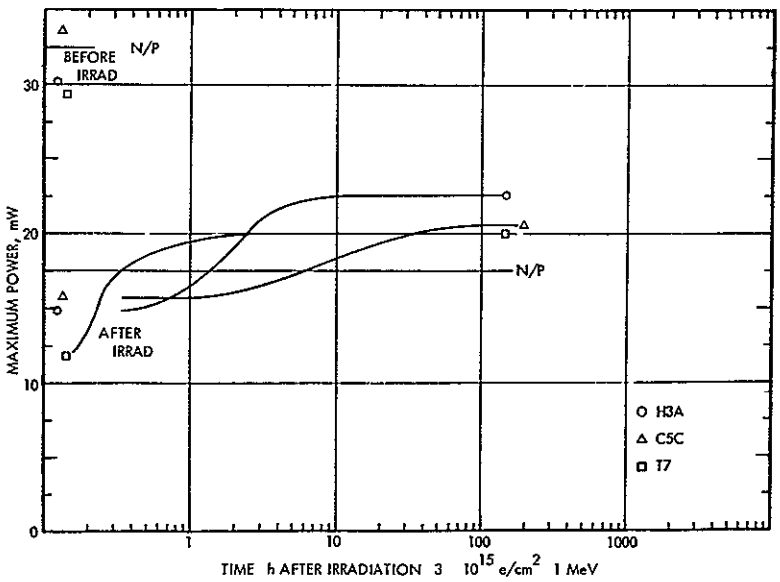

Fig 31 Recovery of maximum power point of best crucible cell at 100°C using solar simulator illumination

STUDY TO DETERMINE AND IMPROVE DESIGN FOR LITHIUM-DOPED SOLAR CELLS

G J Brucker, T J Faith, and J P Corra
RCA Corporation
Astro-Electronics Division
Princeton, N J

I INTRODUCTION

The contract effort reported herein represents an experimental investigation of the physical properties of lithium containing P on N solar cells and bulk silicon samples, and of the processes which occur in these devices and samples before and after irradiation The program objectives are to develop and reduce to practice analytical techniques to characterize the radiation resistance of Li-doped solar cells and its dependence on the materials and processes used to fabricate them The approach to the objectives was based on the irradiation and measurement of the electrical properties of bulk-silicon samples and government-furnished (GFE) solar cells Experiments on bulk samples include Hall and resistivity measurements taken as a function of (1) bombardment temperature, (2) resistivity, (3) fluence, (4) oxygen concentration, and (5) annealing time at temperatures from 300 to 373°K Diffusion length measurements on solar cells were made as a function of the same parameters as for bulk samples In addition, capacitance, I-V, and diffusion constant measurements were made on selected cells Stability studies employing I-V measurements under 140 mW of tungsten light were conducted on solar cells which were irradiated and observed for long periods under storage at room temperature

The discussion will deal with the more important results obtained in the electrical studies on bulk silicon, solar cells, the correlation of solar cell and bulk silicon results, a defect model suggested by our experimental results, and finally their implication on the optimum design of lithium solar cells

II HALL AND RESISTIVITY MEASUREMENTS ON BULK SILICON

A Objectives

The objectives of the Hall and resistivity measurements on bulk-silicon samples diffused with lithium are to determine (1) the dependence of carrier-removal on lithium concentration, oxygen concentration, and electron fluences at low- and high-bombardment temperatures, and (2) the dependence of annealing at temperatures from 300 to 373°K on the same parameters as for carrier removal To achieve these objectives, Hall and resistivity measurements were made on Hall bars fabricated from quartz-crucible (QC) grown and float-zone (FZ) refined silicon Measurements of carrier-removal rates as a function of bombardment temperatures and carrier-density and mobility changes as a function of annealing time and temperature were made on Hall samples irradiated by 1-MeV electrons

B Carrier-Removal Rates

One of the objectives of the study is to determine the dependence of carrier-removal rate in irradiated silicon on bombardment temperature and lithium concentration To achieve this objective, several Hall bars fabricated from 1500- and 5000-Ω-cm FZ refined silicon were diffused with lithium to concentrations from 2×10^{14} to 2×10^{16} Li/cm^3 and irradiated at bombardment temperatures from 79 to 200°K The rates of carrier removal were determined after each bombardment These rates, measured after annealing to a temperature of 200°K versus the reciprocal of the

bombardment temperature, are shown in Fig 1 Lithium concentrations of the samples used in the measurements are shown as a parameter These four concentrations cover approximately the range of lithium concentrations which have been measured at the junctions of solar cells furnished to date by JPL There are two important points to note in Fig 1 i e , the shift of the curves along the temperature axis towards lower temperatures as the lithium density decreased, and the progressively lower carrier-removal rates measured on the samples of decreasing lithium concentration in the high-temperature region (≈120 to 200°K) These concentrations correspond to resistivities of 0 3, 1 5, 10, and 20 Ω-cm This shift of the temperature dependence portion of the curves is in agreement with the prediction of the interstitial-vacancy-close-pair model (Refs 1 and 2) of radiation damage in silicon It should be noted in Fig 1 that the saturated value of carrier-removal rate (0 1 cm^{-1}) measured on samples of FZ silicon-doped to a lithium concentration of 2 to 5 × 10^{14} Li/cm^3 is the same as the value reported (Ref 2) for samples of QC silicon-doped to a lithium concentration of 2 × 10^{16} Li/cm^3 The dependence of this saturated value of carrier-removal rate on resistivity is weak since it decreased by a factor of 2 5 for an increase of resistivity by a factor of approximately 30

The temperature-dependence of the carrier-removal rate measured on the five Hall bar samples which were fabricated from two different sources of initially high resistivity (1500 and 5000 Ω-cm, hereafter referred to as "J" and "H" FZ silicon) was unusual, i e , the carrier-removal rate decreased to a minimum and then increased again as the bombardment temperature ranged through 95°K These data points were not shown in Fig 1 and, therefore, these curves were replotted in Fig 2 to illustrate this unusual behavior All five samples showed this effect therefore, the experimental evidence strongly supports the validity of this minimum in the temperature-dependence curve of carrier-removal rate

Obviously a defect level located at an energy corresponding to the position of the Fermi level at a bombardment temperature of 95°K would affect the measurements If this defect is being introduced by the bombardment then it was expected that an unirradiated sample initially bombarded at T_B = 95°K would not exhibit the minimum value of carrier-removal rate (0 04 cm^{-1}) To test this theory, one of the three samples of J silicon was bombarded initially at a temperature of 95°K, whereas the other two were bombarded starting at T_B = 200 and 85°K, respectively The bombardment temperature of the latter two samples was slowly decreased to 78°K and increased to 200°K As expected, the first sample bombarded at 95°K indicated a carrier-removal rate of 0 092 cm^{-1}, which is approximately twice the value measured on the two J samples and the two H samples It appears that a defect level was responsible for this minimum in the curves of Fig 2 Further evidence will be given in later sections to support this hypothesis

C Carrier Density Versus Temperature

The carrier density was measured as a function of temperature at various times during the bombardment of the samples Figure 3 shows the results obtained on one of the J samples All three J samples exhibited a similar carrier-density dependence on measuring temperature Curve I was obtained from measurements on the sample before bombardment, curve II was obtained following the completion of bombardments, and curve III was obtained following the completion of the high-temperature annealing cycles (T_A = 300 and 373°K) Curve II shows that the irradiation has introduced a defect level or system of levels covering a wide temperature range The temperature at which half of the traps are filled is $T_{1/2}$ = 146°K, as shown in Fig 3 The energy level corresponding to this temperature was calculated to be $E = E_c$ - 0 14 eV This effective defect level appears to be responsible for the minimum carrier-removal rate shown in Fig 2 at a bombardment temperature of 95°K Curve III indicates that interaction of lithium with this unknown defect and other possible lithium centers takes place during the high-temperature annealing cycles Both the trap density and the carrier density measured at low and high temperatures decreased The lithium density decreased by a factor of 1 8, whereas the carrier density measured at low temperature (78°K) decreased by a factor of 1 1

Figure 4 is particularly interesting since it shows the results of carrier density versus temperature measurements taken on the sample of unirradiated J silicon which was initially bombarded at T_B = 95°K and subsequently bombarded at lower and higher temperatures As previously stated, the $\Delta n/\Delta\phi$ measured at T_B = 95°K was 0 092 cm^{-1} rather than 0 04 cm^{-1}, indicating the absence of this unknown defect level at the beginning of the bombardment Figure 4 shows that curve II, taken immediately after bombardment at T_B = 95°K, does not indicate the presence of any defect level, but the level does appear in the measurements (curve III) made after the other bombardments were completed Thus, these results support the carrier-removal measurements Curve IV taken after annealing, shows that the defect level is reduced in density and modified in energy, but is not completely removed in agreement with the results of Fig 3 The measurements taken on the third J sample were in complete agreement with those shown in Figs 3 and 4

D Annealing

1 Dependence on resistivity One of the important properties of irradiated Li-doped silicon is the annealing of the damage at T_A = 297°K, and the dependence of annealing properties on the lithium concentration Figures 5, 6, and 7 show the dependence on lithium density of the annealing properties in irradiated FZ silicon The unannealed fraction f_n (Ref 3) of the carrier density is plotted as a function of annealing time at room temperature (T_A = 297°K) in Fig 5 Measurements of carrier density were made at a reference temperature of T_M = 80°K In contrast to the behavior of the three other samples, H9-1 did not indicate any increase in the carrier density as a function of annealing time, but rather a slight decrease at T_A = 297°K The behavior of the lithium concentration during the annealing cycle can be inferred from the behavior of the carrier density measured at a temperature of 297°K These

measurements are shown in Fig 6 where the unannealed carrier density f_n versus annealing time is presented for the same four samples In contrast to the behavior of the other samples shown in Fig 6, which were heavily doped with lithium, the carrier density of sample H9-1 decreased continuously as a function of annealing time Thus, a loss of lithium as a function of time was observed on H9-1 instead of a gain in lithium concentration as observed on the other samples of lower resistivity

Hall and resistivity measurements made during the annealing cycles enable changes to be determined in the mobility which indicate the presence or absence of charge-scattering centers introduced by the electron bombardment The results obtained on the four samples are shown in Fig 7 where the unannealed fraction of reciprocal mobility versus annealing time at an annealing temperature of 297°K is shown Obviously the behavior of the mobility measured on H9-1 is different than the behavior of the lower resistivity samples

Initially, at the start of the annealing cycle, the mobility decreased and then increased at a very slow rate for approximately 17 h of annealing at 297°K The mobility increased to its pre-irradiation value after a total annealing time of 150 h The mobility did not change significantly when the sample was annealed at a temperature of 373°K for 20 min It should be noted that the mobility measured on sample H9-1 was completely dominated by lattice scattering before bombardment The room temperature value of mobility before irradiation was 1600 $cm^2/V\text{-}s$ and the value measured at 80°K was 15,000 $cm^2/V\text{-}s$ These values of mobility are those for a sample of silicon which is very lightly doped with impurities and with no significant contribution to the total mobility from charged scattering processes

2 High-resistivity FZ silicon After completion of all irradiations, isothermal annealing of selected samples was carried out at annealing temperatures of 300 and 373°K Figure 8 shows the results obtained after annealing a J sample at room temperature (300°K) for a total of 75 min, and at 100°C for 60 min The unannealed fraction of carrier density and the reciprocal of mobility are plotted versus the annealing time The time scale of the data taken during the 100°C annealing cycle was multiplied by a factor of 150 so as to normalize these data to the results obtained during the 300°K annealing cycle An activation energy of 0 66 eV was used to determine this multiplication factor The two annealing temperatures are indicated in Fig 8 where dotted lines connect the last data point at T_A = 300°K to the first data point at T_A = 373°K The unannealed fractions increase slowly with time for T_A = 300°K, but decrease by large amounts for T_A = 373°K It appears that the higher annealing temperature initially increases the supply of free lithium and subsequent recovery of mobility occurs However, the carrier density measured at both high and low temperature decreased with time after the initial (t = 0) increase The three samples of J silicon and the two samples of H silicon displayed the same annealing properties

3 QC Compared to FZ Silicon A sample of low-resistivity (0 3 Ω-cm) QC silicon was bombarded and annealed at temperatures of 300 and 373°K The unannealed fractions versus annealing time are plotted in Fig 9 together with the results obtained at T_A = 300°K on H9-1, which is a sample of high-resistivity (10 Ω-cm) FZ silicon The time scale of the QC data taken during the 373°K anneal was multiplied by a factor of 2000 The dotted lines indicate the start of the annealing cycle at 373°K The similarity in the speed of response and in the behavior of carrier density and mobility in the two samples should be compared to the annealing properties of low-resistivity FZ samples shown in Figs 5, 6, and 7 High-resistivity FZ silicon appears to behave like low-resistivity QC silicon during annealing cycles It should be noted that the oxygen concentration in the FZ samples is $\leq 10^{14}$ cm^{-3}, which is now comparable to the lithium concentration in the J or H samples

A QC Hall bar which was irradiated approximately 1-1/2 years ago (Ref 2) was still in working condition, this sample was recently measured The results of this measurement are shown in Fig 10 where the unannealed fractions versus time are plotted There is an initial recovery in carrier-density measured at T_M = 78°K, but after longer annealing times, the carrier density decreased The carrier-density measured at T_M = 300°K, or the assumed lithium density, continuously decreased over the 540 days of the measurements However, the mobility continuously recovered for the entire time, and at the last measurement (540 days) it has approximately recovered to its pre-irradiation value

E Discussion of Results

1 Carrier removal rates The dependence on resistivity (lithium concentration) of the carrier-removal rate versus temperature characteristic was confirmed by the results obtained on samples of four resistivities In addition, the "saturation" level of carrier-removal rate (i e , the rate measured at approximately 125 to 200°K) decreased as the lithium concentration decreased This trend is in agreement with the experimental observations of other authors on phosphorus-doped silicon (Ref 4) The following mathematical model can explain this The probability of formation of vacancy-impurity defects is a function of impurity concentration Thus, the total probability, P, of defect formation can be written as the product of P_1 and P_c, where P_1 is the probability of forming a vacancy-impurity defect and P_c is the probability that the close-pair (vacancy-interstitial) dissociates so as to provide a free vacancy The probability P_1 depends on the impurity concentration and controls the saturated value of carrier-removal rate at the high-temperature limit where P_c = 1, and thus, P_1 sets the absolute upper limit of η, the carrier-removal rate Then these values of η are the absolute rates which control the introduction of carrier-removal defects in lithium-containing silicon without modification of these values by lithium ions in motion

The minimum in the carrier-removal curve of Fig 2 is a surprising result There is sufficient experimental evidence (four samples) to support the validity of the measurement In addition, the carrier density versus temperature curves indicate the resistance of a defect level of system

of levels close to the bombardment temperature where the minimum occurred Finally, supporting evidence was obtained in the experiment where one of the unirradiated J samples was initially bombarded at $T_B = 95°K$ and did not exhibit this minimum $\Delta n/\Delta\phi$ but the value of 0 092 cm^{-1}, which is more like the expected value Obviously, the existence of this unknown defect level has a strong influence on the rate of carrier-removal which occurred when the bombardment temperature located the Fermi level close to the defect energy level If the defect is an acceptor then, at best, the Fermi level could alter the net carrier density by the magnitude of the defect density All the acceptors are filled and emptied of electrons by the passage of the Fermi level through the acceptor level The defect density was not great enough to change the effective carrier density by more than a factor of 2 The value of $\Delta n/\Delta\phi$ is unaffected by a change in carrier density of this amount, therefore, it is not clear why $\Delta n/\Delta\phi$ decreased so much Further study of high-resistivity samples is necessary to resolve this question

2 Carrier density versus temperature The results shown in Figs 3 and 4 clearly indicate that a defect level was introduced during bombardment The spread of the effective energy level over such a wide temperature range makes the calculation of the level position uncertain There may be more than one energy level within the temperature range of 100 to 190°K due to this unknown defect A discrete energy level would be effective only if the Fermi level was within ±2 kT of its position This corresponds to the defect level being from 88 to 12% filled Assuming that the level is discrete, the position of the energy level was calculated using the following equation

$$E_T = kT_{1/2} \ln \frac{Nc}{N_D - N_T/2} \qquad (1)$$

where

E_T = the position of the defect energy level below the conduction band

$T_{1/2}$ = the temperature at which half of the traps are filled

N_T = the trap density

N_D = the donor density

k = Boltzman constant

N_c = the density of available states in the conduction band

The energy level E_T was calculated to be 0 14 eV with $T_{1/2} = 146°K$ The expression $E_T \pm 2$ kT is equal to 0 163 or 0 117 eV The Fermi level is located approximately at these energies for T = 170 and 124°K These limits indicate an effective temperature spread of 46°K, whereas the experimental results indicate a spread of 90°K This calculation suggests that there is more than one level A more complete expression was also used to fit curve II and to obtain a value of E_T Equation (2) is the relationship that was used

$$n^2 + n (N_T - N_D + N_C \exp E_T - E_C/kT)$$

$$- N_D N_C \exp E_T - E_C/kT \approx 0 \qquad (2)$$

All the quantities in Eq (2) were defined before, except for n, the carrier density, and E_C, the energy of the conduction band A fit to curve II of Fig 3 over a range of T = 100 to 190°K was obtained for $E_T = 0$ 115 eV, $N_T = 5\ 8 \times 10^{13}$, and $N_D = 1\ 08 \times 10^{14}$ cm^{-3} This value of E_T is closer to the value suggested by the results shown in Fig 2 Since the minimum in the carrier-removal curve occurred at 95°K, it can be concluded that the Fermi level must be close to the effective defect energy level The Fermi level was calculated to be at ≈0 085 eV ± 2 kT where 2 kT = 0 016 eV Thus, this calculation indicates the level is located near $E_T = 0$ 1 eV Whether or not lithium is involved in the formation of this defect cannot be deduced from the present experiments The defect could involve lithium, a vacancy, and/or oxygen, since the lithium concentration is comparable to the oxygen concentration ($\leq 10^{14}$ cm^{-3}) in these high-resistivity samples This defect level could have been present in the low-resistivity (0 3 Ω-cm) samples previously reported (Ref 2) but could have been undetected because of the greater density of other lithium-containing defects (e g , LiV) Since this unknown defect formed during low-temperature bombardments (78 to 90°K) as well as high temperature (90 to 250°K), it must be formed by the trapping of mobile vacancies at impurity sites The vacancy is mobile at approximately 80°K, whereas the interstitial is not mobile until T ≅ 140°K, and all impurities are frozen in the lattice for temperatures in this range Stannard (Ref 5) reported finding a defect level at $E_T = 0$ 13 eV in irradiated FZ silicon doped with lithium to a concentration of 1×10^{14} Li/cm^3 after room temperature annealing However his experiment indicated that the defect was a donor In our previous work (Ref 2) a defect level located at approximately 0 08 eV was observed in the measurements made on QC samples after room temperature annealing All of these levels may be due to the same defect The A center located at 0 186 eV is the only well-identified center that comes close to the energy of this unknown defect, but it is still outside the experimental error of the energy determination

3 Annealing results The carrier-density changes observed in sample H9-1 (5×10^{14} Li/cm^3) during the annealing cycle at $T_A = 297°K$ were not similar to those changes observed in the more heavily-doped samples There was no recovery of the carrier density as measured at low temperature, and the lithium concentration continually decreased during the annealing cycle This behavior continued until the annealing temperature was increased to 373°K, then the apparent acceptor density decreased and the free lithium concentration increased In contrast to this behavior, the mobility recovered as the apparent acceptor density increased slightly However, this slight increase is within the experimental error It should be noted that the Fermi level at

room temperature in this high-resistivity sample (H9-1) is located deep in the forbidden gap and, therefore, the number of ionized donors is larger at low temperature (80°K) than in the low-resistivity samples Approximately 96% of the lithium donors are ionized at T_M = 80°K compared to 50% in previous samples Thus, the sensitivity of the measurements to the introduction or annealing of acceptors is reduced The complete recovery of the mobility indicated that neutralization of charged scattering centers had taken place without the necessity of increasing the annealing temperature to 373°K

Comparison of low-resistivity (0 3 Ω-cm) QC silicon to high-resistivity (10 to 20 Ω-cm) FZ silicon shows that both types of silicon have similar annealing properties Mobility increases slowly at room temperature and faster at a temperature of 373°K, whereas the carrier density measured at low and high temperature decreased Dissociation of defects during room temperature annealing with an increase in carrier density measured at room temperature did not occur in the high-resistivity samples This effect has always been observed in irradiated and annealed FZ samples which varied in lithium concentration from 3×10^{15} to 2×10^{16} cm^{-3}

III SOLAR CELL EXPERIMENTS

A Objectives

The objective of these experiments is to obtain information on solar cells paralleling that obtained in the bulk sample measurements i e , (1) dependence of lifetime damage constant, K_τ, on bombardment temperature, (2) dependence of cell recovery rates and redegradation rates on annealing temperature in the temperature range from 280 to 380°K, and (3) energy levels of defects introduced during irradiation and possible changes in these during recovery and redegradation

The solar cell experiments utilize the beam from a 1-MeV Vande Graaff generator The cells are mounted on a cold-finger apparatus built during the performance of JPL contract No 952249 (Ref 3) The cold finger accommodates two devices and operates in the temperature range from ≈77 to 400°K through use of a liquid nitrogen container and ohmic heaters in thermal contact with the finger

The beam from the Vande Graaff was used for diffusion length measurements (Ref 6) as well as for cell irradiation Minority-carrier lifetime, τ was obtained from the measured diffusion length, L, through the relation $L = \sqrt{D\tau}$, where D is the minority-carrier (hole) diffusion constant, and through use of the mobility data of Morin and Maita (Ref 7) and the Einstein relation Periodic measurements of diffusion length during electron irradiation enabled the calculation of lifetime damage constant, K_τ, using the equation

$$\frac{1}{\tau} = \frac{1}{\tau_{bb}} + K_\tau \phi \qquad (3)$$

where

τ_{bb} = the lifetime prior to irradiation

ϕ = the electron fluence

Measurements were repeated for a set of bombardment temperatures to obtain the bombardment-temperature dependence of K_τ After irradiation, diffusion length measurements versus cell temperature for temperatures ranging from 80 to approximately 380°K yielded curves of lifetime-temperature (τ vs T_M) from which defect energy levels were obtained using Hall-Shockley-Read analysis (Refs 8 and 9)

A series of anneals performed at temperatures ranging from 280 to 380°K determined activation energies for the recovery process in the lithium-containing cell In some cases, annealing was continued beyond peak recovery to investigate stability and redegradation

The solar cells used in these experiments were furnished by JPL and manufactured by Centralabs (C-cells), Heliotek (H-cells) and Texas Instruments (T-cells) These cells are from the same lots as those used in the stability tests previously discussed For the cold-finger experiments, the cells were cleaved into small rectangles approximately 0 13 × 0 36 in to accommodate the size limitations of the cold finger All cold-finger cells were given pre-irradiation reverse-bias capacitance measurements from which the donor density profile in the base region near the junction was determined (Ref 10) Measurements on a large number of lithium cells showed the profile to be a reasonable approximation to a linear graded junction For the cells tested, the lithium density gradient, dN_L/dw, ranged from approximately 10^{18} to 10^{20} cm^{-4}

B Lifetime Damage Constant, K_τ

Results of carrier-removal experiments were presented in Section II Measurement of life-time damage constant over the same set of parameters was carried out on solar cells to compare the mode of formation of recombination defects in solar cells with that of carrier removal defects in bulk samples The results of these measurements are shown in Fig 11 where the measurement temperature, T_M is 200°K Since the density near the junction increases approximately linearly with distance from the junction the cells are characterized in Fig 11 by the density gradient dN_L/dw The cell diffusion length at T_M = 200°K was approximately 20 μm during the measurements, therefore, an approximate estimate for the average density in the current collection volume would be that which is approximately 10 μm from the junction or approximately 10^{-3} dN_L/dw (cm^{-3}) The figure shows both high-oxygen content (QC) and low-oxygen content (FZ and Lopex[1]) cells The QC cells have saturated values of K_τ well below (a factor of approximately 3) the FZ and L cells, in agreement with the carrier removal results on bulk samples The exponential decrease in K_τ at low temperatures and saturation at high

[1]Trademark of Texas Instruments

temperatures is also in agreement with the carrier-removal results The relative insensitivity of the saturated value of K_T to lithium density gradient is also evident In low-oxygen content silicon, the value of K_T changes by approximately 2 for a gradient change of approximately 20 The change in high-oxygen content silicon is nil (within error) for cells differing in dN_L/dw by a factor of approximately 30 The equivalent change in carrier removal rate for FZ cells as seen in Fig 1, was a factor of approximately 3 over a density factor of approximately 60

C Cell Recovery

Successive anneals at different annealing temperatures, T_a, were performed on several high-oxygen and low-oxygen content cells During the anneal, the quantity $f_r^{-1} = e^{St}$ (Ref 11), where $S = 4\pi r_o N_L D_L$ was plotted versus annealing time, where f_r^{-1} is reciprocal fraction of damage remaining S is the recovery slope, r_o is the capture radius for lithium by the defect, N_L is the lithium density, and D_L is the lithium diffusion constant The only quantity in S which is strongly temperature-dependent is D_L Thus, D_L can be calculated by finding S and inserting values for r_o and N_L Figure 12 shows an example of the experimental recovery curves The semi-log plot of f_r^{-1} versus time is a good approximation to a straight line thus, the equation $f_r^{-1} = e^{St}$, which represents a process with first order kinetics, describes the recovery process The recovery slopes in this case are $5\ 1 \times 10^{-4}\ s^{-1}$ for cell C6C - 17 (1) and $4\ 5 \times 10^{-4}\ s^{-1}$ for cell C6C - 18 (1) In Fig 13, plots of S versus inverse annealing temperature are given for QC cells with two different values of dN_L/dw The solid lines drawn through the experimental points represent an activation energy of 1 07 eV which is the activation energy reported by Pell (Ref 12) for the diffusion of lithium in QC silicon The values of D_L calculated from the data assuming $r_o = 10$ Å and $N_L = 10^{-3}\ dN_L/dw$ are compared with those found by Pell, they agree well with Pell's values for silicon containing an oxygen concentration of approximately $5 \times 10^{17}\ cm^{-3}$ The good agreement between the recovery data and that for D_L confirms that lithium diffusion to defect sites is responsible for recovery in lithium containing QC cells

The recovery curves for three groups of low-oxygen content cells are given in Fig 14 The solid lines represent the 0 66-eV activation energy obtained by Pell (Ref 13) for lithium diffusion in low-oxygen content silicon With $r_o = 10$ Å and $N_L = 10^{-3}\ dN_L/dw$ the values calculated from the data for D_L agree with Pell's within a factor of approximately 2 It is noteworthy that the ratios of the values of S at a given value of T_A are (within a factor of 2) equal to the ratios of the lithium density gradients, dN_L/dw measured in the cells This indicates that the quantity dN_L/dw is a reasonable index of recovery speed This will be further established in the photovoltaic recovery results presented in Section IV Another point worthy of note involves the T7 cells When these cells were received, they were classified as QC cells however, the photovoltaic recovery of these cells which was very fast at room temperature (see Section IV), indicated that they were low-oxygen content cells For this reason, the T7 cells were put on the cold finger to obtain the activation energy for recovery The result, $E_a =$ 0 66 eV is taken as a confirmation that these are low-oxygen content cells

Recovery characteristics at 373°K were measured on the cold finger for two QC, Sb-doped, lithium-containing cells The Sb-doped cells had shown unusually slow photovoltaic recovery at room temperature (see Section IV) Figure 15 gives the results of the 373°K anneal for cells C6A-18(2) and C6A-19(2) Minority carrier lifetime, τ, is plotted versus annealing time Both cells had equal density gradients, $dN_L/dw = 2 \times 10^{18}\ cm^{-4}$, however, C6A-19(2) had a much heavier Sb background doping level, $1\ 7 \times 10^{15}\ cm^{-3}$, than C6A-18(2), $4 \times 10^{14}\ cm^{-3}$ Figure 15 shows that C6A-18(2), with lighter background doping, recovers much faster than C6A-19(2) This gives rise to speculation concerning the possibility of Sb acting as an agent to reduce the effective lithium diffusion constant This would be surprising since Sb and Li both carry positive charge in Si and, thus, should repell each other Obviously, the data presented here are insufficient to draw any conclusions However, an agent for controlling lithium diffusion constant does hold interesting possibilities, therefore, the roll of Sb should be further studied

D Lithium Diffusion Constant

To further investigate the relationship between cell recovery and lithium diffusion, a capacitive drift technique was devised for measuring the lithium diffusion constant in the cell near the junction (Refs 3 and 14) With this technique, measurements of the lithium diffusion constant in a QC cell from lot C6C (cell C6C-20) have been made This particular cell has a density of approximately $3 \times 10^{14}\ Li/cm^3$ at the junction edge and a gradient of approximately $2 \times 10^{18}\ cm^{-4}$ with a background phosphorus density of approximately $1\ 7 \times 10^{14}\ cm^{-3}$ The diffusion constant for this cell was measured between 38 and 87°C with the results shown in Fig 16 Also shown as dashed lines in Fig 16 are the results drawn from Pell's work (Ref 12) for QC silicon The circles represent the diffusion constant measured at a distance, W, of value 1 68 μm from the junction while the crosses are those values for 2 5 μm into the base The lithium diffusion constant is shown to increase with junction depth in this crucible cell This behavior is similar to that reported previously (Refs 3 and 14) for FZ cells, and is probably due to the decrease of defects which immobilize with distance from the P-N junction in both silicon types The activation energy, E_a, obtained experimentally in Fig 16, is approximately 1 03 eV, in good agreement with the 1 07 eV obtained by Pell However, the diffusion constant measured in this cell is about one order of magnitude lower than expected from Pell's work in silicon containing an oxygen concentration of about 10^{18} atoms/cm^3 If high-oxygen content were the reason for this very low-diffusion constant, an oxygen content in this cell of the order of 10^{19} atoms/cm^3 would be required, a somewhat unlikely condition It is more likely that some additional defect or impurity may be prohibiting lithium from diffusing More information is required to resolve this question

E Defect Levels

Recombination levels can be found by obtaining lifetime-temperature (τ vs T_M) plots and applying Hall-Shockly-Read analysis (Refs 8 and 9) For N-type material, the equations are (Ref 15)

$$\tau/\tau_{p0} = (1 + n_1/n_0) \quad (4)$$

or

$$\tau/\tau_{p0} = (1 + \gamma p_1/n_0) \quad (5)$$

where

n_0 and p_0 = the thermal equilibrium electron and hole concentrations

τ_{p0} = the minority-carrier (hole) lifetime when the Fermi level is near the conduction band

γ = the ratio of the hole capture cross-section to the electron capture cross-section

n_1 and p_1 = the fictitious electron and hole concentrations that would exist if the Fermi level was located at the recombination level E_t

Thus

$$n_1 = N_c \exp\left[e(E_t - E_c)/kT\right]$$

$$p_1 = N_v \exp\left[e(E_v - E_t)/kT\right]$$

where $N_c = N_v = 4\ 82 \times 10^{15} T^{3/2}$, E_C and E_v are the energy levels at the edge of the conduction and valence band, respectively Equation (4) applies if the recombination level is in the upper half of the band gap, Eq (5) applies if the level is in the lower half The value of n_0 to be used in these equations is the donor density obtained from C-V measurements The large density gradients in lithium cells provide an uncertainty since no single value of n_0 is applicable over the current collection volume in the short-circuit current measurements (i e over a diffusion length) However the uncertainty ΔE, introduced by the variation in n_0 can be approximated by the shift in Fermi level associated with this variation, i e

$$\Delta E_F \approx \frac{kT}{e} \ln \frac{n_{02}}{n_{01}} \quad (6)$$

where n_{01} and n_{02} are the lower and upper limits of n_0 Assuming the linear grade approximation applies out to one diffusion length, n_{02}/n_{01} will range from about 3 to 5, giving an error due to nonuniform density of approximately $2T/e$ or 0 03 V

Lifetime versus temperature measurements were made on QC Sb-doped cell C6A-19(3), and control[2] (non-lithium) cell C6A-B (3) after the cells were irradiated to fluence increments of 1×10^{15} e/cm^2 at 90°K bombardment temperature and 2×10^{15} e/cm^2 at 100°K The results of these measurements are shown in Fig 17, in which $\ln(\tau/\tau_{po})$ is plotted against inverse temperature $1000/T_M$ The slope of this curve at high τ/τ_{po} gives the activation energy, E_a, of the predominant defect Figure 17 shows the curves for the lithium cell and the non-lithium cell to be virtually identical above $\tau/\tau_{po} \approx 10$ The activation energy is calculated to be 0 21 eV a value that is close to the 0 18 eV found for the A center (oxygen-vacancy), which is shown for reference in Fig 17 Similar measurements were made on lithium containing QC cells from lots C5 ($dN_L/dw = 5 \times 10^{19}$ cm^{-4}) and C6C ($dN_L/dw = 1\ 8 \times 10^{18}$ cm^{-4}), both having phosphorus as the initial dopant Curves for both the C5 cells and the C6C cells indicate the presence of a level, or a number of closely spaced levels (the latter suggested by changes in the slope of the curves) in the vicinity of 0 13 eV immediately after irradiation After recovery, only small changes in the defect activation occur although the value of the lifetime, τ, is increased This result is in agreement with those obtained in QC bulk samples (Ref 2) and in lightly Li-doped FZ silicon (Section II, Figs 3 and 4)

Recently, τ versus τ_M measurements were initiated on low-oxygen-content Lopex cells from lot T9 ($dN_L/dw = 5 \times 10^{19}$ cm^{-4}) The results of these measurements have not been fully interpreted and, therefore must be considered as preliminary However, some interesting trends were observed Immediately after a series of low-temperature irradiations, a level at approximately 0 12 eV was observed The lifetime, τ, at 250°K during this measurement was 10^{-7} s After a partial anneal, $\tau(250°K) = 4 \times 10^{-7}$ s, the level had shifted to approximately 0 09 eV After a further partial anneal, $\tau(250°K) = 6\ 5 \times 10^{-7}$ s, a further shift to approximately 0 06 eV had occurred Such shifts, if they are confirmed would suggest a basic difference in lithium-defect interactions between high- and low-oxygen content lithium-containing silicon This has already been suggested by the differences in long-term carrier annealing between low- and high-oxygen content bulk samples

F Redegradation

Cells from lot T9 had shown considerable (~10%) redegradation of photovoltaic characteristic after recovery from irradiation Therefore, they were chosen for redegradation studies on the cold finger Anneals at various temperatures were carried out beyond the point of maximum recovery The redegradation characteristic was thus observed as a function of annealing temperature The results of the experiment are shown in Fig 18 in which normalized lifetime is plotted versus annealing time for annealing temperatures of 357, 345 and 322°K Plotted on the same coordinates is an annealing curve of normalized carrier density for a FZ Hall-bar sample at an annealing temperature of 300°K Each of the curves rises to

[2]Six control cells from lot C6A were generously furnished by Peter Iles of Centralab

a peak (recovers) and then redegrade The recovery and redegradation rates increase with increasing annealing temperature, and all four redegradation curves show similar shape The last fact indicates that there may be an effective activation energy for redegradation which is close to that for lithium diffusion in silicon The significance of this is not yet fully understood

IV LONG-TERM PERFORMANCE OF JPL-FURNISHED CELLS

A total of seven cell shipments were received from JPL including (1) Centralab (C) lots 1, 2, 4, 5, 6 and 8, (2) Heliotek (H) lots 1, 2, 4, 5, 6, 7, 8, and 3a and (3) Texas Instruments (T) lots 2 3 4, 5, 6 7, 8, 9, and 10 The cells were manufactured from a wide variety of silicon stock with varying lithium introduction conditions Several competitive 10-Ω-cm N/P commercial solar cells were supplied for comparative purposes Tests performed on the cells included measurements of photovoltaic I-V characteristic under 140 mW/cm^2 tungsten illumination, P/N junction characteristics in the dark, reverse-bias capacitance characteristics and minority-carrier diffusion length in the base region Tungsten I-V characteristics were measured with a power density of 140 mW/cm^2 incident on the cell surface Cell temperature was maintained at 28°C by water and forced-air cooling These measurements have long-term reproducibility of approximately 2%

The cells were irradiated at room temperature by 1-MeV electrons at a rate of approximately 3×10^{13} e/cm^2/min to one of the following fluences 1×10^{14} 3×10^{14}, 5×10^{14} or 3×10^{15} e/cm^2 Commercial N/P cells were simultaneously irradiated and, wherever possible, a group of at least three lithium cells from a given lot was irradiated to a given fluence After irradiation, the cells were stored at room temperature and periodic measurements of photovoltaic I-V characteristic were made to investigate recovery dynamics, stability and possible redegradation From shipment 3 onward several cells from each lot were left unirradiated to test for shelf-life stability and for subsequent use in cold-finger experiments

Because of their high-oxygen content, ~10^{18} cm^{-3} crucible-grown cells have much slower dynamics than the lower oxygen content FZ and Lopex cells Therefore, the two types of cells will be discussed separately

A QC Cells

The crucible cell groups are listed in Table 1 which is divided into three parts according to fluence In each part of Table 1 the cells are listed in order of increasing speed of recovery, the group showing slowest recovery being first The performance of each lithium cell group is compared with ten Ω-cm N/P cells irradiated during the experiments to the same fluence In the cases of groups T2(2), T7(1), T2(3), and T7(2), short-circuit currents are given instead of powers since these picture frame cells were partially shorted by the light table contact block, thus invalidating power measurements

The comparison between the 8th and 10th columns in Table 1 is noteworthy The numbers in column 8, which represent the immediate post-irradiation powers of the N/P cells, are ~10% below the latest readings in column 10 Thus, very significant recovery of power has occurred in the N/P cells stored at room temperature This puzzling, but very significant recovery at room temperature, suggests further study of the recovery dynamics of such cells

Of the five lithium cell groups irradiated to 1×10^{14} e/cm^2, three cells, C1(1), T2(1), and H2(1), have recovered to powers greater than, or comparable to, those of the N/P cells Group C2(1), a slowly recovering Sb-doped group, is still recovering Only the H1(1) cells with low initial power (21 7 mW) have completed their recovery cycle at a power significantly below that of the N/P cells

Fourteen lithium cell groups, irradiated to fluences of 3 to 5×10^{14} e/cm^2, are listed in Table 1(B) The recovery times become longer with increasing fluences due to the greater loss of lithium during irradiation Consequently, none of the cell groups with density gradients below 10^{19} cm^{-4}, except T2(2), have recovered to the N/P power levels Actually, the first four groups listed have not yet recovered at all Of the cells which have recovered, groups H2(2), T2(2), T7(1), H6(1), and C5(1) are competitive with the N/P cells Group T8(1) and cell C8G-7 are not yet competitive, but are still recovering The H1(2) cells (initial power of 17 7 mW) are not competitive and recovery has been completed

Eleven cell groups irradiated to 3×10^{15} e/cm^2 are listed in Table 1(C) The first five groups with low density gradient (10^{18} cm^{-4}) have yet to show any signs of recovery Four groups, H2(3), C5(2), T2(3), and T7(2), have recovered to power levels competitive with the N/P cells Three of these four groups had high initial density gradients (>10^{19} cm^{-4}), however, T2(3) recovered well despite the low density gradient

The recovery curves for the crucible-grown cells are S-shaped when plotted versus log time after irradiation An example is shown in Fig 19, which gives plots of short-circuit current (I/I_o), open-circuit voltage (V/V_o), and maximum power (P/P_o), normalized to their pre-irradiation values versus time after irradiation for cell group C5(1) Figure 19 also shows the recovery of N/P cells which occurred at room temperature during this time period

In general, the speed of cell recovery varied directly with the lithium density gradient in the cells Figure 20 gives a logarithmic plot of time-to-half-recovery, θ, of short-circuit current versus lithium density gradient All of the cell groups from Table 1 (A) and (B), except the Sb-doped groups, are included All of the cell groups, except the T2 and T7 cells, fall along a straight line with unity slope indicating a linear relationship between recovery time and inverse density gradient The appropriate relation for cells irradiated to 3×10^{14} e/cm^2 is $\theta dN_L/dW = 6\ 5 \pm 2\ 5 \times 10^{20}$ days/cm^4 The T2 and T7 cells,

however, recover at a rate approximately three orders of magnitude faster than the other cells Recent tests on T7 cells (Section III) give strong evidence that these cells are actually low-oxygen content cells, i e , Lopex or float zone Similar tests remain to be made on T2 cells, however their speed of recovery also suggests a low-oxygen content

The crucible cells show remarkable post-recovery stability All have been free from redegradation throughout the duration of the tests Assuming these cells remain stable over the long haul, they deserve further consideration in view of their comparable performance to N/P cells under electron irradiation, and previously observed (Ref 16) superior performance under fast heavy-particle irradiation

B FZ and Lopex Cells

Table 2 presents the performance and stability of low-oxygen-content FZ and Lopex cells As the 8th and 10th columns in Table 2 indicate, redegradation is suffered by most groups of low-oxygen content cells In these columns the current, voltage, and power redegradations do not always appear to correlate, e g , in T3(3) cells the current has redegraded by 6%, whereas the power redegradation is only 1% This is because the open-circuit voltage recovery is occurring at the same time as the short-circuit current redegradation, thus reducing, and in some cases eliminating, power redegradation In general, the recovery-redegradation cycle in voltage is on a longer time scale than that of current The redegradation columns in Table 2 also indicate that there is no obvious correlation between percent redegradation in I or V and lithium density A parameter in Table 2 that correlates reasonably well with lithium doping level is the time after bombardment at which redegradation starts In general, the faster the redegradation sets in, the higher the lithium density, although there are exceptions to this rule, e g , T6(1), which in spite of a high-density gradient, $dN_L/dW \approx 3 \times 10^{19}$ cm^{-4}, shows insignificant (2%) redegradation A partial correlation is also observed with fluence in that the time after irradiation at onset of redegradation is somewhat shorter after the lower fluences than after the higher fluences This is probably because, during light irradiations, less lithium is tied up in defects thus leaving more free lithium after irradiation Cells from lot T6 (Lopex) are interesting in that they have remained essentially stable since recovery from irradiation The output of group T6(1) ($\emptyset = 3 \times 10^{14}$ e/cm^2) 200 days after irradiation matches that of the N/P controls, ~21 mW The only redegradation suffered by these cells was a 2% drop in current, which is within the experimental error of the long-term measurements The T6 cells have the high-density gradient previously mentioned and would, therefore, normally be expected to redegrade, however, unlike many of the other high-density lots they were Li-doped with a long-, low-temperature diffusion (8 h at 325°C) It is therefore possible that the T6 cells owe their good properties to this diffusion schedule, which should be tested further Only one other low-oxygen content cell group, H7(1), (Lopex, $dN_L/dW \approx 2 \times 10^{19}$ cm^{-4}) is at present competitive with its N/P control groups, approximately 200 days after irradiation to 3×10^{14} e/cm^2, both groups yield 21 mW This is the case despite approximately 6% current redegradation in the H7(1) cells spanning in time from approximately 1 to 60 days after irradiation The H7(1) cells have been stable over the last 140 days

Even though attempts to categorize instability in FZ and Lopex cells in terms of their measured physical parameters have not been fully successful, it is possible to list the modes of redegradation (or pre-irradiation degradation) observed and, in some cases, ascribe them to a measured physical change in the cells The observed modes of (re) degradation are

(1) Redegradation in short-circuit current This is usually associated with radiation-induced defects, however, in a few instances (C4 cells and cells C5 - 41 to 50), shelf degradation with no irradiation was observed

(2) Open-circuit voltage loss This occurred in both irradiated and unirradiated C4 cells with high initial density gradient It was due to a measured loss in carriers near the junction

(3) A degradation and redegradation involving loss in open-circuit voltage and curve power factor This was previously (Ref 16) shown to be caused by gross lithium motion in the junction region

C Summary

Lithium-containing crucible-grown cells which have initial powers competitive with commercial 10-Ω-cm N/P cells for a wide range of lithium densities have been tested Only a small fraction of the lithium-containing cells made from FZ and Lopex silicon have been competitive in initial output

Recovery of crucible cells in general is a slow process at room temperature, taking from several months to over a year, depending on the lithium density The recovery curve is S-shaped with the greatest recovery slope occurring approximately 1 to 10 months after irradiation Float-zone cells without exception recover rapidly at room temperature, with characteristic recovery times ranging from several hours to several days, the recovery time varying inversely with the lithium density Only cells with essentially no lithium in the region near the junction after irradiation fail to experience recovery

Over test periods ranging up to 15 months, crucible cells have been stable Most FZ cells tested show significant redegradation The redegradation starts later and is somewhat less severe in lightly Li-doped cells Redegradation occurs in open-circuit voltage as well as short-circuit current although the voltage redegradation usually occurs later Heavily irradiated cells with light lithium doping have less tendency to redegrade, however, they do have the tendency to develop series resistance

Crucible-grown cells then are the better cells at room temperature and should afford interesting possibilities at elevated temperatures From the groups of FZ and Lopex cells tested it is evident that applications for these cells would be limited to short-term use, or for use at temperatures below room temperature

V CONCLUSIONS

A Hall Bar Experiment

A defect located at approximately E_c - 0 12 eV is produced by electron bombardment of lithium-containing FZ silicon of high resistivity (2×10^{14} Li/cm^3) This defect may also be produced in low-resistivity silicon, but at a reduced rate so that it is undetectable This particular defect level would not influence the electrical characteristics of solar cells operating at room temperature However, if the lithium concentration was very high, the Fermi level could be located at an energy of 0 12 eV at room temperature, and then this defect would affect solar cell operating characteristics

There is no evidence of any dissociation of LiV damage centers during the annealing cycle at T_A = 300°K of the high-resistivity (10 to 20 Ω-cm) FZ samples The damage centers responsible for carrier-removal in high-resistivity FZ silicon are stable, i e , dissociation of damage centers does not occur This property is in agreement with the results obtained on QC samples (Ref 2) In addition, the annealing processes and the carrier-removal rates measured at high temperatures (100 to 200°K) on high-resistivity FZ samples suggest that this type of silicon behaves like QC silicon It appears that the concentration of oxygen relative to the concentration of lithium determines the annealing properties and the carrier-removal rates measured at high temperatures The Hall bar experiments suggest, in agreement with the conclusions of stability studies on solar cells, that the lithium concentration can be high (2×10^{16} Li/cm^3) in QC silicon without producing unstable defect centers and annealed-defect centers In contrast the concentration of lithium must be limited to a value less than approximately 10^{15} Li/cm^3 to achieve stability This lower concentration of lithium also produces lower carrier-removal rates in Hall samples made from this type of silicon

B Suggested Damage Model

The experimental results presented herein suggest that the previously reported (Ref 3) radiation damage and annealing model be modified to explain these results It is suggested that the dominant damage center in low-resistivity FZ silicon (10^{15} to 10^{16} Li/cm^3) is the L1 center which is described by Eq (7)

$$Li^+ + V \rightleftharpoons LiV^- \left[\text{L1 center}\right] \qquad (7)$$

One of the observed (Ref 2) annealing mechanisms is the dissociation of the L1 center thus Eq (3) is written with a double arrow indicating that an equilibrium exists between the formation of the defect center and the dissociation of this center

In addition to the dissociative mechanism of annealing, there is the mechanism of neutralization by which lithium complexes with the L1 center This process is described by Eq (8)

$$LiV^- + Li^+ \rightleftharpoons Li_2V \qquad (8)$$

Equation (8) is written with a double arrow so as to indicate that the annealed L1 center is unstable and the reaction can proceed in the reverse direction The redegradation is caused by this reverse process (Figs 5 6, and 7) The dominant damage center in low-resistivity (≤5 × 10^{14} Li/cm^3) FZ silicon appears to be the L2 center which is given by Eq (9)

$$LiO^+ + V^= \rightleftharpoons LiOV^- \left[\text{L2 center}\right] \qquad (9)$$

The annealing of the L2 center takes place by means of the mechanism of neutralization described by Eq (10)

$$LiOV^- + Li^+ \rightarrow Li_2OV \qquad (10)$$

In QC silicon the dominant center appears to be the A center for samples with lithium concentrations from 10^{15} to 2×10^{16} Li/cm^3 The formation of the A center is described by Eq (11)

$$O + V^= \rightarrow OV^- \left[\text{A center}\right] \qquad (11)$$

For the samples with higher lithium concentrations or samples bombarded by higher fluences, the production of the L1 and L2 centers will contribute to the total damage It is necessary to postulate that lithium continues to complex with annealed defect centers during the postirradiation period of annealing, since our results showed that the mobility recovered as a function of annealing time, but the carrier density continued to decrease at the same time (see Fig 10) Therefore, a possible mechanism is given by Eq (12)

$$Li^+ + OV^- \left[\text{A center}\right] \rightarrow e + LiOV \left[\text{annealed center}\right] + Li_n^+ \rightarrow Li_nOV \qquad (12)$$

where the subscript n indicates that more than one lithium ion can complex with the annealed A center This mechanism will also apply to the neutralization of the L2 center as given by Eq (13)

$$LiOV^- \left[\text{L2 center}\right] + Li^+ \rightarrow e + Li_2OV \left[\text{annealed center}\right] + Li_n^+ \rightarrow Li_nOV \qquad (13)$$

It is further conjectured that the energy level observed at an $E_C - 0.12$ eV in experiments on high-resistivity Hall bars of FZ silicon is the L2 center. It appears to have a low probability of formation except when the lithium concentration is low and comparable to the oxygen concentration.

C Solar Cell Experiments

Measurements of lifetime damage constant, K_T, in both crucible-grown and Lopex solar cells containing lithium have established that the bombardment temperature, T_B, dependence of K_T is similar to the bombardment temperature dependence of carrier removal rate measured previously in Hall-bar bulk samples. The value of K_T was shown to saturate at high temperatures and to decrease exponentially at lower temperatures, in agreement with a defect model proposed by Stein (Ref. 1). The damage constant is greater in low-oxygen content cells than in high-oxygen content cells, and is only slightly dependent on the cell density gradient, dN/dW; a factor change of approximately 2 occurs for a density gradient change of approximately 25 in low-oxygen content cells while no observable change occurs in high-oxygen content cells. Activation energy for lifetime recovery was measured by making successive isothermal anneals. In the crucible cells, the activation energy for lifetime recovery was approximately 1.1 eV, which is the activation energy for lithium diffusion in crucible silicon, in the Lopex cells the activation energy for lifetime recovery was approximately 0.65 eV, which is the activation energy for lithium in low-oxygen content silicon. This proves that, as predicted in the original model of Wysocki, lithium diffusion to defect sites is responsible for lifetime recovery in silicon of both low- and high-oxygen content. The rates of cell recovery vary approximately linearly (at a given annealing temperature) with the lithium density gradient. A measurement of lithium diffusion constant using a drift-capacitance technique yielded an activation energy for diffusion of 1.03 eV in a high-oxygen content cell. This independent measurement involving no irradiation, lends further weight to the cell recovery results and the lithium diffusion mechanism they point to.

Defect energy levels obtained from lifetime versus temperature measurements for antimony-doped and phosphorus-doped lithium-containing, crucible-grown cells and for antimony-doped non-lithium, crucible-grown cells indicate that, as expected, the oxygen vacancy (A center) is the predominant defect causing lifetime degradation in these cells. In some cases, however, the measurements indicate defect activation energies of approximately 0.13 eV, well below the 0.18 eV found for the A center. There is also the indication of several closely spaced levels, as was also indicated in bulk sample measurements.

High-temperature anneals carried out on Lopex cells resulted in a temperature-dependent redegradation rate which fitted in well with room temperature photovoltaic redegradation observed on similar cells and with room temperature carrier loss observed in FZ bulk samples. The study so far thus provides an encouraging degree of consistency between lifetime, bulk sample, and photovoltaic measurements at all temperatures tested.

D Solar Cell Performance and Stability

Lithium-containing crucible-grown solar cells which have initial powers competitive with commercial 10-Ω-cm N/P cells for a wide range of lithium densities have been tested. Only a small fraction of the lithium-containing cells made from FZ and Lopex silicon have been competitive in initial output with the QC cells.

Float-zone cells (without exception) recover rapidly at room temperature with characteristic recovery times ranging from several hours to several days, the recovery time varying inversely with the lithium density. Only cells with no measurable amounts of lithium in the region near the junction after irradiation fail to experience recovery. Recovery of crucible cells, in general, is a slow process at room temperature, taking from several months to more than a year depending on the lithium density. The recovery curve is S-shaped with the greatest recovery slope occurring approximately 1 to 10 months after irradiation.

Over test periods ranging up to 15 months crucible cells have been stable. Most FZ and Lopex cells tested have shown significant redegradation. The redegradation in lightly Li-doped cells starts later and is somewhat less severe. Redegradation occurs in open-circuit voltage as well as short-circuit current, although the voltage redegradation usually occurs later. Heavily irradiated cells with light lithium doping have less tendency to redegrade however they do have the tendency to develop series resistance. Consistent correlation between the various modes of redegradation, extent of redegradation, and the measured physical parameters of the cells has not yet been obtained for FZ and Lopex cells.

Crucible-grown cells, then, are operationally the better cells at room temperature and should afford interesting possibilities of stability at elevated temperatures. From the groups of FZ and Lopex cells tested, it is evident that applications for most of these cells would be limited to short-term use after irradiation or to use at temperatures below room temperature. A possible exception to this is suggested by a lot of Lopex cells (T6) which underwent a long low-temperature lithium diffusion cycle (8 h at 325°C). Lot T6 cells had relatively good initial power and (so far, at 200 days) stable post-recovery behavior, in spite of a high-density gradient ($\sim 3 \times 10^{19}$ cm^{-4}) which usually foreshadows redegradation. The performance of the T6 cells suggests a further study of cells using this diffusion cycle.

REFERENCES

1. Vook, F. L., and Stein, H. J., "Production of Defects in N-Type Silicon," Proc. of the Santa Fe Conference on Radiation Effects in Semiconductors, Plenum-Press, N. Y., pp. 99-114, Oct. 1967.

2. Brucker, G. J., Phys. Rev., Vol. 183, p. 712, 1969.

3. Brucker, G. J., Faith, T. J., and Holmes-Siedle, A. G., Final Report Under

JPL Contract No 952249, prepared by RCA Corp , April 21, 1969

4 Stein, H J , and Gereth, R , J Appl Phys , Vol 39, p 2890, 1968

5 Stannard, J E , Proceedings of the Conference on Effects of Lithium Doping on Silicon Solar Cells, Technical Memorandum 33-435 Jet Propulsion Laboratory, Pasadena, Calif , May 9, 1969

6 Rosenzweig, W , Bell Syst Tech J , Vol 41, p 1573, 1962

7 Morin, F J , and Maita, J P , Phys Rev , Vol 96, p 28, 1954

8 Hall, R N , Phys Rev , Vol 83, p 228, 1951, and Vol 87, p 387, 1952

9 Shockley, W and Read, W T Jr , Phys Rev , Vol 87, p 835, 1952

10 Hilibrand, J , and Gold, R D , RCA Rev , Vol 21, p 245, 1960

11 Wysocki, J J , IEEE Trans on Nuclear Sci , NS-14, December 1967

12 Pell E M , J Appl Phys Vol 32, p 6, 1961

13 Pell, E M , Phys Rev , Vol 119, p 1222 1960

14 Faith, T J , Brucker, G J , Holmes-Siedle, A G , and Neadle, R S , IEEE Trans on Nuclear Sci , NS 15, p 61, 1968

15 Baicker, J A , Phys Rev , Vol 129, p 1174, 1963

16 Faith, T J , Brucker, G J , Holmes-Siedle, A G , and Wysocki, J Conf Record of the Seventh Photovoltaic Spec Conf , IEEE Catalog No 68C63ED, p 131, 1968

Table 1 Properties and performance of crucible-grown lithium cells and comparisons with commercial 10-Ω-cm N/P cells

Cell group	No of cells	Dopant	dN_D/dw, cm^{-4}	Cell power,[a] mW						TAB,[b] days
				Initial		After irrad		Latest reading		
				Li cell	N/P	Li cell	N/P	Li cell	N/P	
(A) Low fluence, 1×10^{14} e/cm^2										
C2 (1)	5	Sb	1×10^{18}	30 3	28 1	17 9	21 3	20 8	23 3	442
C1 (1)	7	As	1×10^{18}	30 3	28 1	18 6	21 3	24 2	23 3	442
H2 (1)	5	P	1×10^{19}	26 0	28 1	17 0	21 3	23 1	23 3	442
H1 (1)	8	As	2×10^{19}	21 7	28 1	15 7	21 3	20 2	23 3	442
T2 (1)	6	P	1×10^{18}	26 8	28 1	16 5	21 3	23 4	23 3	442
(B) Intermediate fluence, 3 to 5 $\times 10^{14}$ e/cm^2										
C2 (2)	2	Sb	1×10^{18}	30 3	27 7	14 8	17 7	14 9	18 9	376
C6A (1)	3	Sb	1×10^{18}	28 2	28 2	15 1	19 5	15 3	20 9	194
C6B (1)	3	Sb	1×10^{18}	29 3	28 2	15 7	19 5	16 1	20 9	194
C6C (1)	3	P	1×10^{18}	28 1	28 2	16 0	19 5	16 3	20 9	194
C5 (5)	3	P	1×10^{18}	30 9	28 2	16 6	19 5	17 7	20 9	194
C1 (2)	2	As	1×10^{18}	31 8	28 4	13 8	16 6	16 2	18 9	376
T8 (1)	3	P	1×10^{19}	26 1	28 2	12 6	19 5	18 7	20 9	194
H2 (2)	2	P	1×10^{19}	24 3	27 7	13 5	17 7	20 0	18 9	376
H6 (1)	3	P	1×10^{19}	24 7	28 2	14 0	19 5	20 7	20 9	194
H1 (2)	2	As	2×10^{19}	17 4	28 4	10 8	16 6	15 8	18 9	376
C8G-7	1		---	27 6	28 2	11 5	19 5	18 0	20 9	98
C5 (1)	3	P	5×10^{19}	25 0	28 2	13 0	19 5	20 7	20 9	194
T2 (2)	2	P	1×10^{18}	(69 3)	(69 6)	(36 6)	(49 3)	(58 9)	(52 8)	376
T7 (1)	3	P	5×10^{19}	(70 8)	(70 1)	(35 3)	(54 0)	(56 2)	(57 3)	194
(C) High fluence, 3×10^{15} e/cm^2										
C2 (3)	2	Sb	1×10^{18}	30 1	28 4	10 7	13 9	10 9	15 6	411
C6A (2)	3	Sb	1×10^{18}	28 9	28 3	9 7	14 2	9 8	15 6	194
C6B (2)	3	Sb	1×10^{18}	28 9	28 3	10 1	14 2	10 1	15 6	194
C6C (2)	3	P	1×10^{18}	28 3	28 3	10 7	14 2	10 7	15 6	194
C5 (6)	3	P	1×10^{18}	28 4	28 3	11 0	14 2	10 9	15 6	194
T8 (2)	3	P	1×10^{19}	26 1	28 3	8 5	14 2	9 4	15 6	194
H6 (2)	3	P	1×10^{19}	20 9	28 3	9 5	14 2	11 6	15 6	194
H2 (3)	3	P	1×10^{19}	25 2	28 4	9 9	13 9	15 0	15 6	411
C5 (2)	3	P	5×10^{19}	25 1	28 3	8 2	14 2	14 8	15 6	194
T2 (3)	2	P	1×10^{18}	(68 8)	(69 1)	(31 8)	(40 4)	(49 6)	(44 7)	411
T7 (2)	3	P	5×10^{19}	(70 5)	(70 1)	(25 3)	(42 2)	(50 6)	(45 4)	194

[a]Numbers in parentheses are short-circuit currents (mA)
[b]TAB = time after bombardment at latest reading

Table 2 Stability and performance of lopex and FZ grown lithium cells received from JPL

Cell group	N_{DO}, cm^{-3}	dN_D/dW, cm^{-4}	Cell power, mW			TAB days	% Redegradation			Start of redegradation, days
			P_o	P_{AB}	P_L		I	P	V	
(A) Low fluence, 1×10^{14} e/cm^2										
C4 (9)	2×10^{14}	1×10^{18}	21 1	16 6	20 1	313	3	4	1	70
C4 (17)	3×10^{14}	1×10^{18}	19 6	16 0	18 5	313	3	5	2	>70
C4 (5)	2×10^{15}	2×10^{19}	17 7	15 3	16 0	313	5	8	3	20
C4 (13)	2×10^{15}	2×10^{19}	15 0	13 6	13 1	313	5	5	5	30
C4 (1)	3×10^{15}	5×10^{19}	15 8	14 2	14 0	313	2	8	5	10
T3 (1)	3×10^{15}	1×10^{20}	23 1	17 3	21 1	24	3	3	1	3
(B) Intermediate fluence, 3 or 5×10^{14} e/cm^2										
H5 (1)	3×10^{14}	4×10^{16}	28 4	12 3	13 5	110	0	0	0	-
C4 (10)	2×10^{14}	1×10^{18}	20 3	12 1	17 6	313	2	1	0	80
C5 (7)	2×10^{14}	1×10^{18}	21 6	10 9	17 2	110	0	0	0	-
*C4 (18)	3×10^{14}	1×10^{18}	20 8	12 7	19 1	313	4	2	0	70
C4 (6)	2×10^{15}	2×10^{19}	17 5	12 1	15 6	313	5	6	2	60
C4 (14)	2×10^{15}	2×10^{19}	15 3	12 6	13 9	313	3	5	4	60
*T6 (1)	1×10^{15}	3×10^{19}	26 8	12 1	21 0	110	2	0	0	60
C5 (3)	3×10^{15}	4×10^{19}	17 5	13 3	15 9	110	-	-	-	PBD
C4 (2)	3×10^{15}	5×10^{19}	15 8	12 2	13 8	313	4	6	4	30
T3 (2)	3×10^{15}	1×10^{20}	23 1	(I_{sc} only)		313	8	-	-	15
T4 (1)	5×10^{15}	1×10^{20}	22 9	15 3	18 1	110	7	6	0	3
T5 (1)	6×10^{15}	3×10^{20}	25 2	11 4	18 4	110	10	8	0	3
(C) High fluence, 3×10^{15} e/cm^2										
H5 (2)	3×10^{14}	2×10^{16}	25 1	(Series resistance)		110	-	-	-	-
C4 (11)	2×10^{14}	1×10^{18}	19 1	"	"	313	-	-	-	-
C5 (8)	2×10^{14}	1×10^{18}	20 8	"	"	110	-	-	-	-
C4 (19)	3×10^{14}	1×10^{18}	20 0	8 7	12 3	313	0	0	0	-
C4 (7)	2×10^{15}	2×10^{19}	17 7	8 1	14 3	313	6	0	0	60
C4 (15)	2×10^{15}	2×10^{19}	15 1	9 5	13 2	313	5	2	1	50
C5 (4)	2×10^{15}	2×10^{19}	15 8	9 7	13 6	110	-	-	-	PBD
C4 (3)	3×10^{15}	5×10^{19}	15 3	9 0	12 7	313	4	4	1	50
T3 (3)	3×10^{15}	1×10^{20}	24 4	8 2	13 9	313	6	1	0	20
T4 (2)	5×10^{15}	2×10^{20}	22 3	7 9	12 9	110	5	3	0	10
T5 (2)	6×10^{15}	3×10^{20}	23 4	7 5	12 2	110	7	6	1	5

Notes

P_o = initial power
P_{AB} = power after irradiation
P_L = latest power reading
TAB = time after bombardment as of latest reading
PBD = pre-bombardment degradation

42

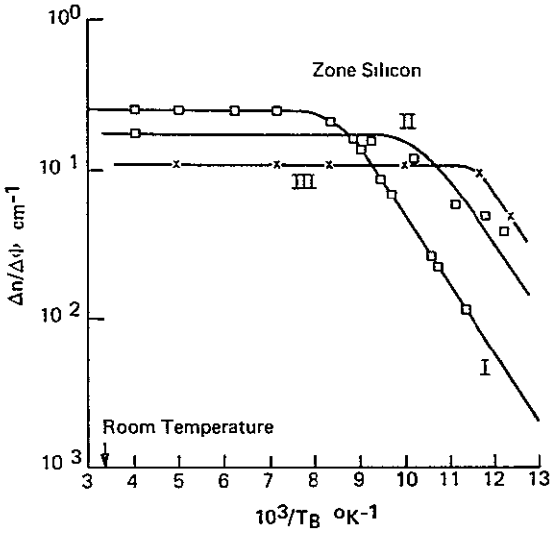

Fig 1 Carrier-removal rates vs reciprocal bombardment temperature for FZ silicon with several lithium concentrations (measurements at 79 to 81 °K after annealing to 200 °K)

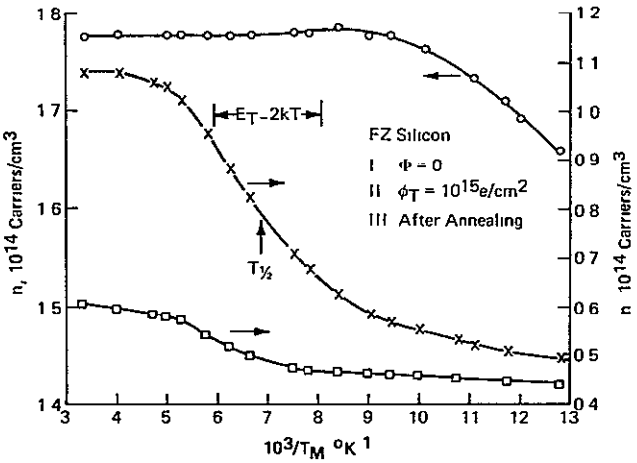

Fig 3 Carrier density vs reciprocal measurement temperature for FZ silicon (20 Ω-cm) initially bombarded at T_B = 79 °K

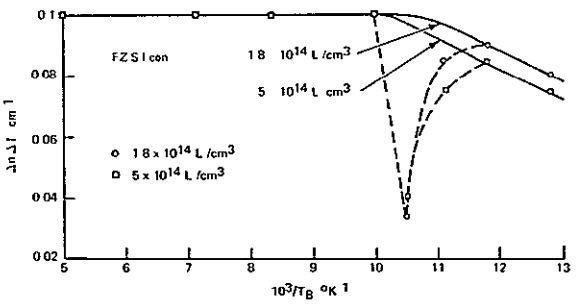

Fig 2 Carrier-removal rates vs reciprocal bombardment temperature for high-resistivity FZ silicon irradiated by 1-MeV electrons (measurements made at 78 °K)

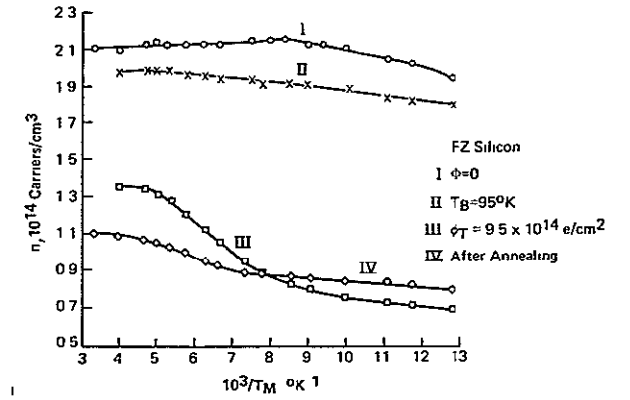

Fig 4 Carrier density vs reciprocal measurement temperature for FZ silicon (20 Ω-cm) initially bombarded at T_B = 95 °K)

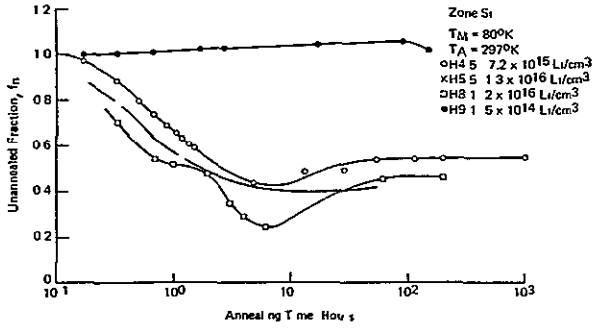

Fig 5 Unannealed fraction of carrier density vs annealing time for four samples of FZ silicon annealed at 297°K and measured at 80°K

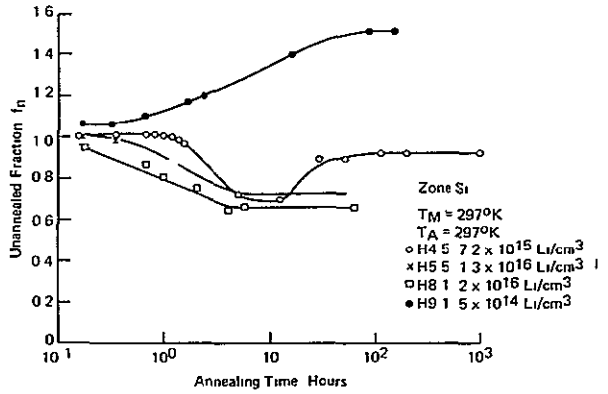

Fig 6 Unannealed fraction of carrier density vs annealing time for four samples of FZ silicon annealed and measured at 297°K

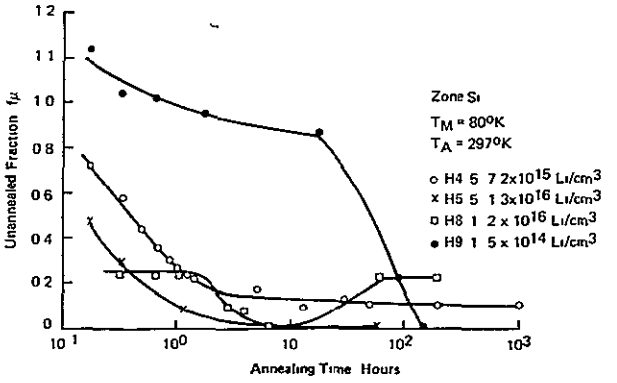

Fig 7 Unannealed fraction of reciprocal mobility vs annealing time for four samples of FZ silicon annealed at 297°K and measured at 80°K

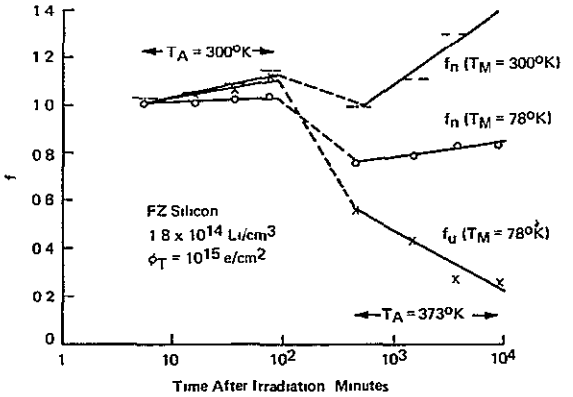

Fig 8 Unannealed fraction of carrier density and reciprocal mobility vs annealing time for 20-Ω-cm FZ silicon annealed at T_A = 300 and 373°K and measured at 78 and 300°K

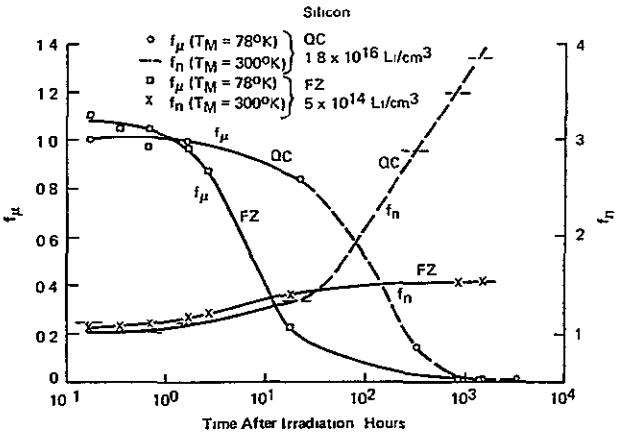

Fig 9 Unannealed fraction of carrier density and reciprocal mobility vs annealing time for 0.3-Ω-cm QC and 20-Ω-cm FZ silicon annealed at T_A = 300 and 373°K and measured at T_M = 78 and 300°K

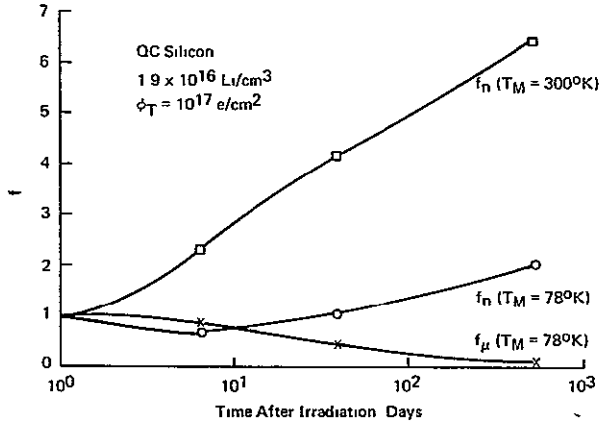

Fig 10 Unannealed fraction of carrier density and reciprocal mobility vs annealing time for 0 3-Ω-cm QC silicon annealed at T_A = 300 °K and measured at T_M = 78 and 300 °K

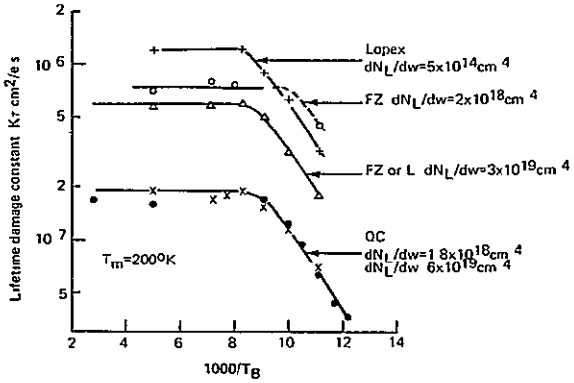

Fig 11 Lifetime damage constant, K_T, vs inverse bombardment temperature, T_B, for a measurement temperature, T_M = 200 °K

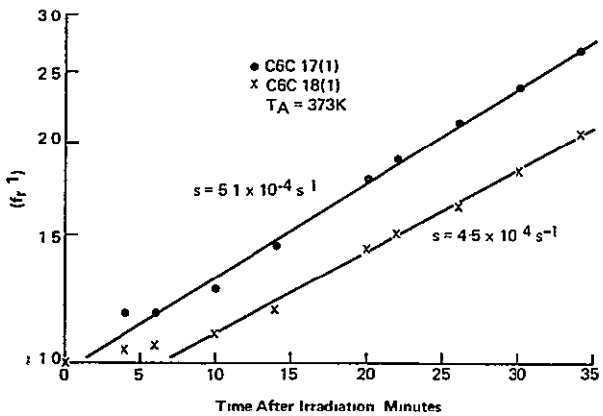

Fig 12 Reciprocal fraction of damage remaining vs time after irradiation at 373 °K

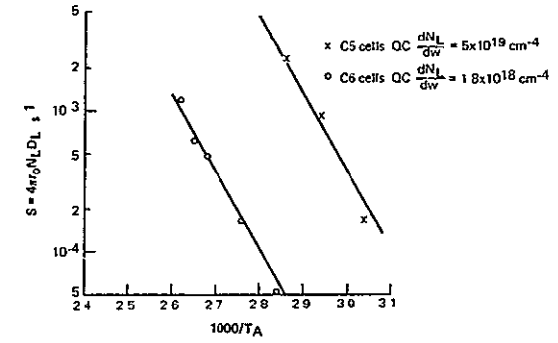

Fig 13 Recovery slope vs inverse annealing temperature (recovery activation energy for crucible-grown cells)

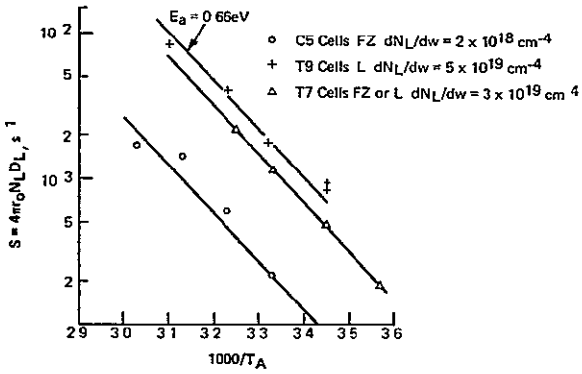

Fig 14 Recovery slope and lithium diffusion constant vs inverse annealing temperature (recovery activation energy for Lopex and FZ cells)

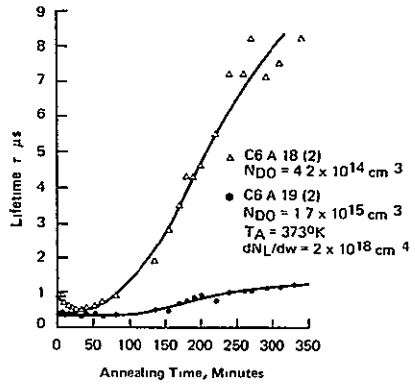

Fig 15 Lifetime at 373 °K vs annealing time at 373 °K

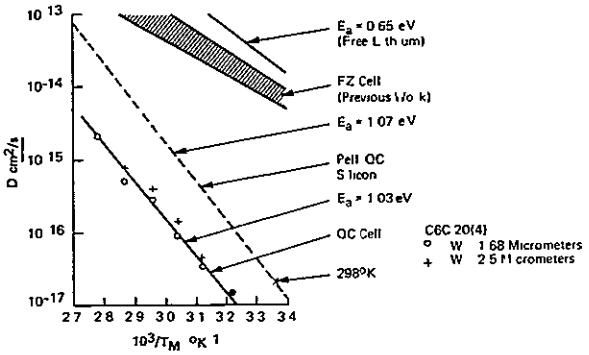

Fig 16 Diffusion constant of cell C6C-20(4) vs inverse temperature

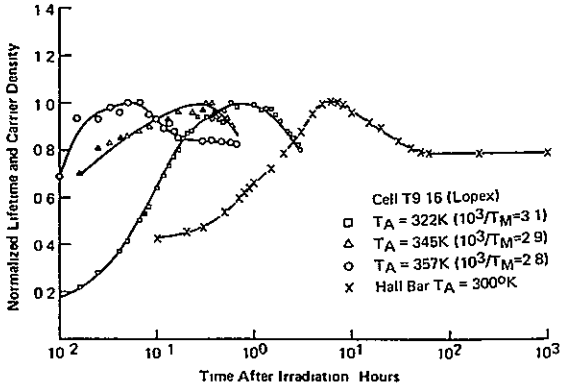

Fig 18 Normalized lifetime and carrier density vs annealing time at 357, 345, 322, and 300°K

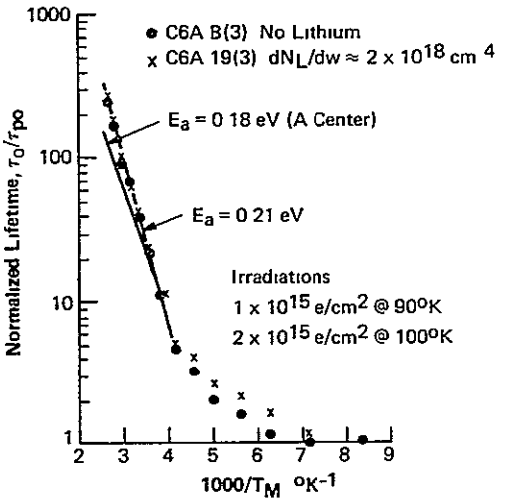

Fig 17 Lifetime vs temperature data on cells C6A-B(3) and C6A-19(3)

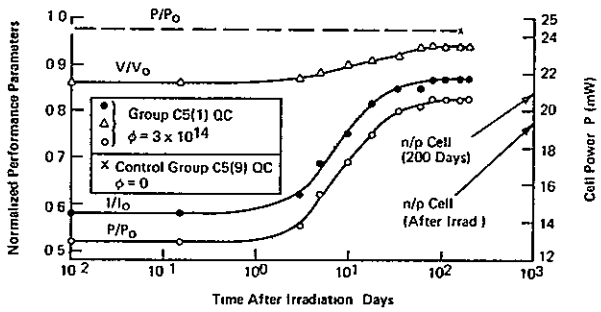

I/I_o = normalized short-circuit current

V/V_o = normalized open-circuit voltage

P/P_o = normalized maximum power

Fig 19 Normalized performance parameters vs time after irradiation for group C5(1) cells and group C5(9) cells

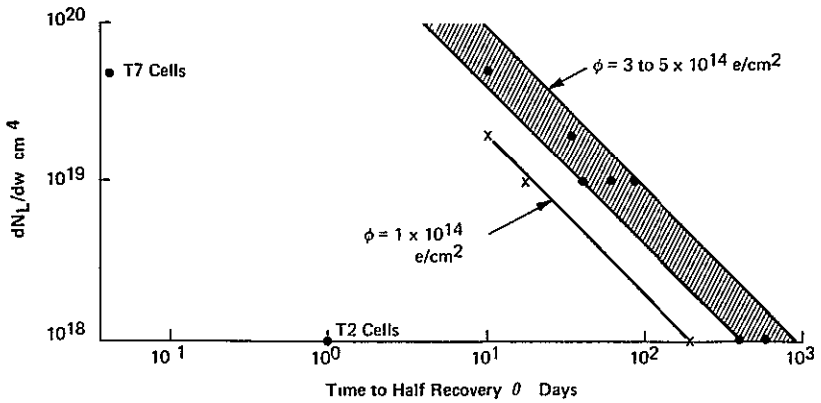

Fig 20 Time-to-half-recovery of short-circuit current vs lithium density gradient for crucible-grown cells

HALL EFFECT STUDIES OF IRRADIATED Si(Li) AT CRYOGENIC TEMPERATURES[1]

John Stannard
U S Naval Research Laboratory
Washington D C

I INTRODUCTION

This work proposes to follow the events that occur during electron damage and room temperature recovery in float-zoned (FZ) silicon doped with lithium Cryogenic Hall measurements allow the overall concentration of radiation-induced deep acceptors to be monitored along with the overall concentration of shallow donors In addition, the activation energy and concentration of levels lying between 0 06 and 0 20 eV below the conduction band may be separately measured provided that the spectrum is not too complex

II MATERIALS

During the past period, preparation and characterization of Li-doped silicon have been improved, measurement accuracy and analysis have been improved five-fold, one irradiation experiment has been completed and another has been completed through 17 h of annealing at room temperature Three problems associated with preparation of Li-doped material were treated (1) the effect of inhomogeneity on Hall measurements (2) methods of obtaining material displaying the proper activation energy for lithium, and (3) a good method of controlling lithium concentration

In this study, lithium has been introduced by diffusion from a suspension of lithium in oil A tack-on treatment of 5 min at 425°C followed by a 60-min redistribution at the same temperature have been employed The final lithium concentration can be controlled by the number of lithium atoms present in the surface layers of the sample at the start of redistribution Etching in CP-4 allows removal of a thickness controllable to within $\pm 10^{-4}$ in , thereby reducing the overall lithium content Figure 1 shows the results of a four-point probe study of samples prepared with these techniques The lithium concentration measured after redistribution is shown to decrease uniformly as the thickness etched away before redistribution is made larger The use of starting material with a resistivity greater than 100 Ω-cm would have allowed this figure to be extended to even lower values of the lithium concentration A set of six samples was made to indicate the batch reproducibility of this method Most of the scatter seen here is due to variations in the amount of lithium applied to each slice before the tack-on treatment The final lithium concentration was not dependent upon the initial thickness of the silicon wafer

Lithium diffusion from an oil suspension is known to produce an inhomogenous lithium concentration with a minimum at the surface Figure 2 shows the degree of this inhomogeneity and its effect on Hall measurements along with the degree to which this has been reduced for this work Curve I exhibits four-point probe data taken by Heliotek (Ref 1) Graphical integration of this, and other Heliotek data, indicates that a 1-h redistribution at 425°C causes the total amount of active lithium contained in a sample to decrease

[1]Work accomplished under NASA Contract WO-8050, NAS 7-100

to 30% of its initial value The magnitude of this decrease is independent of the amount of lithium introduced by the particular tack-on treatment used Curve II indicates the lithium concentration expected for the sample of Curve I, had there been no redistribution loss Outgassing, surface precipitation and distributed precipitation could all contribute to this loss Curve III is a four-point probe profile of a sample prepared in such a way as to minimize inhomogeneity Lithium was applied to both surfaces of the wafer and followed by a tack-on of 5 min at 425°C After etching to reduce the lithium content it was redistributed for 1 h at 425°C This profile shows the sample was homogenous to within about 50% The irradiation study to be described was performed on material thus prepared except for an additional 0 002-in etch after redistribution to remove possible surface precipitates

The effect of inhomogeneity on Hall measurements is indicated by results obtained from the sample of Curve IV This curve indicates the carrier concentration as determined by resistivity measurements on a Hall bridge, while the squares indicate carrier concentration as obtained from the Hall effect It is apparent that the Hall effect is strongly influenced by the high-resistivity portion of the sample near the surface due to the larger Hall voltage generated there The second square is even lower than the first and anticipates a decrease in lithium concentration on the right that is not shown Such inhomogeneity can affect more than just the apparent lithium concentration The sample of Curve IV had been redistributed with a lapped surface and showed a low temperature activation energy of 0 0374 eV, which is the energy of the LiO complex Surface damage apparently caused complete precipitation of free lithium in the region near the surface, thereby leaving the LiO complex as the shallowest active donor present This would cause the low-temperature resistivity in this region to exceed that of the Li-doped bulk by orders of magnitude As a result, the electrical properties of the sample were dominated by the high-resistivity surface region Redistribution with CP-4 etched surfaces avoids this condition In the past some samples have shown activation energies as low as 0 026 eV This was apparently due to contamination of the lithium suspension Two samples produced and measured after changing to a new suspension have shown energies of 0 0331 and 0 0332 eV Thermal and optical values of 0 033 (Ref 2) and 0 03281 eV (Ref 3) respectively are reported for more heavily doped material and would be expected to be smaller than our value because of impurity overlap effects

III ANALYSIS

Before considering irradiation experiments, it must be said that both Hall constant and resistivity have been measured as a function of temperature, thereby giving the temperature-dependence of the carrier concentration and mobility A program for the calculation of Hall mobility in silicon from first principles has not yet been written, therefore, carrier mobility will not be treated here Figure 3 shows the dependence of carrier concentration on temperature along with a diagram of the forbidden gap of silicon The states shown in the diagram would give rise to this carrier concentration From the location of the plateau at 100°K and the location of the linear "freeze out" region, the overall donor concentration can be calculated along with the number of deep acceptors The slope of the linear region gives directly the energy separation between the lithium donor and the bottom of the conduction band Analysis of the high-temperature structure can give the concentration and energy of a level lying more than 0 06 and less than 0 2 eV below the conduction band edge The difference between the plateaus at 300°K and at 100°K gives the concentration of such a level The position of the transition between the two plateaus gives the activation energy In the case of unirradiated Li-doped silicon, the data between 50 and 100°K allow the lithium and phosphorus concentrations to be determined separately with moderate success, even though their energy separation is only 0 011 eV Models including excited states however, gave poorer fits to the data for both phosphorus- and Li-doped material

For each sample, a least-squares fit to the data was obtained for temperatures below 100°K If a level of intermediate depth was present, these results were then used to aid in obtaining a separate fit to data above 100°K Table 1 presents the results of this fitting process for an unirradiated phosphorus-doped sample and an unirradiated sample containing both phosphorus and lithium The first two columns show the results of fits using four adjustable parameters The last column used a five-parameter model to allow separate determination of the lithium and phosphorus concentrations The indicated errors are 95% confidence limits, and the bottom row is the mean error between calculated and measured values of the carrier concentration In the first column, the measured value of the phosphorus ground-state degeneracy is quite close to the theoretical value of 0 50 The measured value of the activation energy agrees closely with the reported optical ionization energy of 0 0453 eV (Refs 3 and 4) Equally reliable values of the parameters are obtained for the Li-doped sample The measured activation energy of 0 0332 eV is slightly larger than the reported optical value 0 03281 eV as expected The five-parameter model, which most accurately represents this sample gives a degeneracy factor close to the expected value of 0 1 The close correspondence between calculated and theoretical values of the degeneracy factor for both lithium and phosphorus lends considerable support to the confidence that the values of the other parameters truly reflect the properties of the sample Large errors shown for the donor concentrations would have been much less had more data been taken between 50 and 100°K Since irradiation causes a noticeable worsening of the fits obtainable, only the four-parameter model was used in irradiation studies The measured donor concentration is then taken as equal to the sum of the concentrations of the individual donors A similar interpretation is given the measured acceptor concentration

IV IRRADIATION EXPERIMENTS

To separate the events associated with damage from those associated with annealing, irradiations were performed at low temperatures where lithium is immobile Two experiments will be

described here The first was designed to discover whether lithium was associated with the level of intermediate depth reported in 1969 The second experiment involves irradiation at 240°K and subsequent room temperature annealing of silicon doped with 5×10^{14} lithium/cm^3

An earlier experiment showed that a level of intermediate depth was present following 80°K bombardment and extensive room temperature annealing of silicon lightly doped with lithium In the present experiment, a sample from the same phosphorus-doped starting material was measured before and after an 80°K irradiation by 5×10^{13} 1-MeV electrons/cm^2 The sample was then studied using isochronal annealing up to a temperature of 200°K Then the temperature dependence of the carrier concentration was remeasured above 80°K Figure 4 shows an intermediate level to be present in irradiated and annealed phosphorus-doped material as well as irradiated and annealed Li-doped material The curves shown are machine-fits obtained using three adjustable parameters While a level is present in the sample containing no lithium, its energy is definitely less than that me asured in the Li-doped sample Very similar, but more complete evidence obtained from the next experiment indicates that the association of mobile lithium with the 0 12-eV level causes a shift in its activation energy

The identity of this 0 12-eV level in silicon is not clear Its energy is close to the 0 13-eV value reported by H Stein for a level formed following 80°K irradiation and 250°K annealing of pulled 10-Ω-cm silicon (Ref 5) Unfortunately that experiment also indicated the 0 13-eV level was not formed in FZ silicon This situation is further confounded by the fact that the present experiment indicates a removal rate in FZ silicon roughly equal to the removal rate reported by Stein for pulled silicon

In the last experiment two wafers were cut from a boule of 14-Ω-cm FZ silicon Lithium was diffused into one wafer to a resistivity of 6 Ω-cm using the techniques described in Section II A full set of Hall measurements was made and each sample was irradiated at 240°K by a fluence of $1\ 7 \times 10^{14}$ 1-MeV electrons/cm^2 The samples were remeasured without warming above 240°K Subsequent measurements were made after 2 h and after 17 h of annealing at room temperature At present, this experiment has not been completed Irradiation was performed at 240°K where the 0 12-eV level might not form and yet the lithium ion would still be immobile As the results will show, the 0 12-eV level was still formed even at 240°K Figure 5 shows the room temperature annealing of carrier concentration commonly observed in irradiated Li-doped silicon As expected the control sample shows no measurable annealing of the carrier concentration Indexes on the horizontal axis indicate the annealing times at which full measurements were made

Before considering results obtained after room temperature annealing we will consider the measurements made before and immediately after irradiation E centers are formed when an electrically active donor interacts with a vacancy and the complex becomes a deep acceptor In this experiment, such an event would cause the measured donor concentration to decrease by one and the acceptor concentration to increase by one As a result changes in electrically active donor concentration indicate directly the formation of E centers It should be stressed that the measured value of overall acceptor concentration includes the E center concentration If the 0 12-eV level is an acceptor, it also is included Other experimental evidence indicates that it is an acceptor Figure 6 shows the carrier removal rates associated with E centers overall acceptors and the 0 12-eV level as a result of the irradiation of these two samples No thermal annealing has occurred Carrier removal rate shown on the vertical axis equals the formation rate times the number of electronic charges a defect assumes in the material being considered For example, the carrier removal rate and formation rate of the E center are equal since the E center is a single acceptor The left side of Figure 6 is in agreement with present concepts of damage in FZ phosphorus-doped silicon Irradiation at room temperature of phosphorus-doped silicon produces about equal numbers of E centers, di-vacancies and A centers as the primary damage centers (Ref 5) It is perhaps a little surprising that no A centers were observed in these samples However no high-temperature structure with an activation energy near 0 17 eV was observed This indicated that the A center concentration was always considerably less than 5×10^{12}/cm^3 If the removal rate of the 0 12 eV center which presumably would be replaced by a deeper level in a 300°K irradiation is added to the rates shown for the two other categories, an overall carrier removal rate of 0 6 cm^{-1} is obtained The compares well with a reported value of approximately 0 8 cm^{-1}

The details of the electron damage are quite different in the case of the other slice of silicon which was doped with 4×10^{14} lithium/cm^3 While the removal rates for the 0 12-eV level are comparable in the two samples, the lithium sample shows very little E center formation and a very large acceptor formation rate There are two possible explanations for the fact that the concentration of electrically active lithium and phosphorus does not decrease as a result of the irradiation One could presume that, while vacancies still interact with and remove donors, there is another center introduced by the lithium diffusion which interacts with vacancies to form an equal number of new donors The requirement of approximate equality between these two rates weakens the plausibility of this argument

Another, perhaps more believable explanation would be as follows Diffusion of lithium into the sample introduces some initially undetectable center, i e , a neutral one, which acts as a very efficient sink, removing vacancies from the crystal before they have a chance to encounter a donor The large magnitude of the acceptor generation would seem to support this explanation

Let us presume that there is a competition for vacancies between donors and say, dislocations in the phosphorus-doped sample Let us also assume interaction with a dislocation destroys the vacancy entirely In the Li-doped sample the assumed very efficient sink for vacancies

would not only prevent vacancies from interacting with E centers, it would also trap vacancies normally destroyed at a dislocation If it is presumed that these neutral centers form an acceptor upon trapping a vacancy, an abnormally large formation rate for acceptors would be expected

While the details of this explanation may be no more than speculative, it does seem that some neutral center involving lithium is present and affecting the way damage is occurring in this sample Such neutral centers might form during redistribution and could account for part of the lithium lost during redistribution No evidence of a level due to the acceptors was found, therefore, the level must be more than 0 2 eV below the conduction band

Photoconductivity at 6 5°K was measured to 14 in these samples before and after irradiation The photoconductive response was about what would be expected for a shallow impurity in silicon Structure superimposed upon the impurity response did not correlate well with lattice absorption bands Irradiation caused only a slight change, and that occurred only in the control sample The change seemed to indicate an irradiation-induced level somewhere between 0 25 and 0 1 eV from a band edge

After 17 h of annealing at room temperature, a statistically significant portion of the acceptors had not annealed As a result no estimate can be given of the number of lithium ions required to neutralize each acceptor Preliminary measurements made at 76 h indicate such changes are occurring

Significant annealing of the 0 12 eV level has occurred and is shown in Fig 7 The measured activation energy for this level in each sample is shown in the top half of the figure, and the measured concentration in the lower half In the phosphorus-doped sample, the activation energy of this level does not change with annealing Annealing does cause an initial increase in the concentration, however after 2 h, this too becomes constant In the Li-doped sample however annealing at 300°K initially causes the 0 12-eV level to shift deeper into the gap After the initial shift the activation energy remains fairly constant This is consistent with the observations of the previous experiment While this is going on, the concentration of this level in the Li-doped sample is steadily decreasing with time It would seem that the shift must be due to the presence of lithium

It should be emphasized that the shift in the level occurs rapidly and goes to completion in a time during which few of the centers are rendered electrically inactive This would imply that neutralization occurs in two stages It is possible that one or more lithium ions are attracted to the center relatively quickly to form some sort of stable configuration The final neutralization is perhaps rate-limited by effects associated with the microscopic nature of the defect

V CONCLUSIONS

There is no established connection between radiation-induced degradation in solar cells and the concentrations of defect centers as measured here However, the results obtained agree qualitatively with solar cell experience in both the damage and recovery phases

In the damage process, the Li-doped sample showed greater damage than its phosphorus-doped control While there was an apparent reduction in E center formation due to lithium, there was also a much larger production of deep acceptors Additional samples must be measured before any firm conclusions can be reached on the basis of removal rates

During room temperature annealing, definite evidence of the effectiveness of lithium in removing electrically active centers was obtained When lithium was allowed to become mobile, a damage-induced center at E_c 0 12 eV was observed first to move deeper into the gap and then decrease in concentration as annealing proceeded Significant decreases in the deep acceptor concentration have occurred only after 70 h

REFERENCES

1 Ralph E L , Goodelle, G S , and Payne, P , Investigation of Li-Doped Hardened Solar Cells, First Quarterly Report, Contract No AF 33-615-67-C-1458, Heliotek Div of Textron, Sylmar, Calif , Aug 1967

2 Morin, F J , Maita, J P , et al , Phys Rev , Vol 96, p 833, 1953

3 Aggarwal, R L , Fisher, P , et al , Phys Rev , Vol 138, p A882, 1965

4 Aggarwal, R L , and Ramdas, A K , Phys Rev , Vol 137, p A602, 1965

5 Stein, H J , and Vook, F L , Phys Rev , Vol 163, p 790, 1967

Table 1 Parameters obtained by fitting various models to data taken from unirradiated Si(P) and Si(Li, P)

Parameter	Si (P) 4 parameters	Si (Li) 4 parameters	Si (Li P) 5 parameters
Phosphorus concentration, $\times 10^{14}$ cm^{-3}	3 26 ±0 07		2 2 ±2 0
Lithium concentration, $\times 10^{14}$ cm^{-3}		6 8 ±0 2	5 0 ±2 0
Donor ground-state deg radiation factor	0 55 ±0 04	0 063 ±0 005	0 10 ±0 04
Acceptor concentration, $\times 10^{12}$ cm^{-3}	7 9 ±0 8	5 4 ±0 6	5 5 ±0 6
Donor activation energy, eV	0 0452 ±0 0002	0 0332 ±0 0002	0 0332 ±0 0002
Standard deviation, %	1 3	1 4	1 3

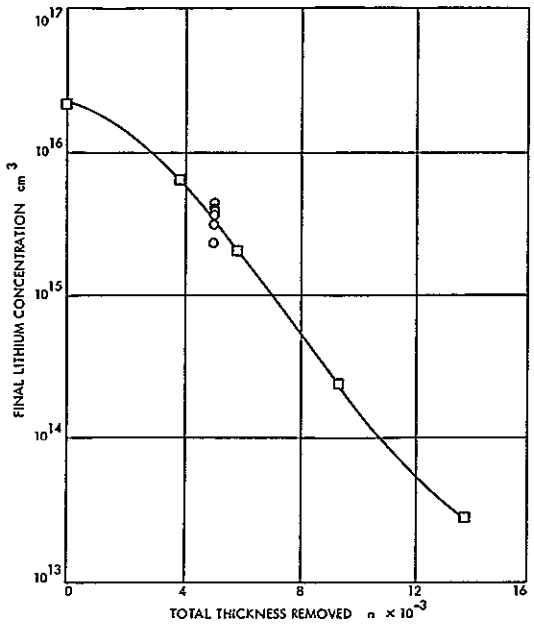

Fig 1 Reproducible control of lithium concentrations by etching prior to redistribution

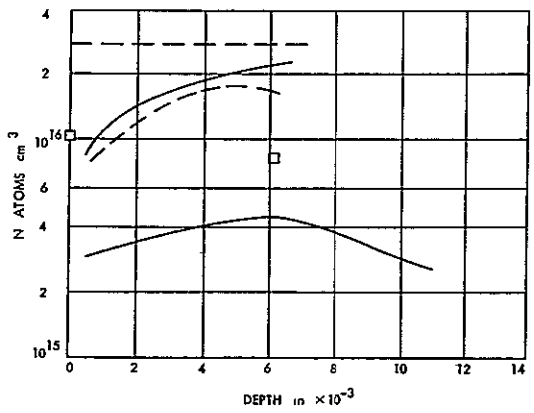

Fig 2 Inhomogeneity of lithium concentration

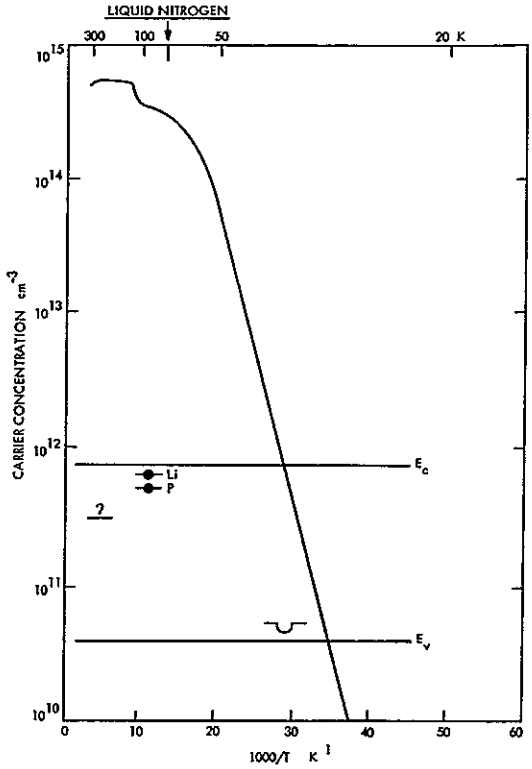

Fig 3 Information obtainable from Hall measurements as a function of temperature (The densities and ionization energies of the states shown in the forbidden gap can be determined with the restrictions explained in the text)

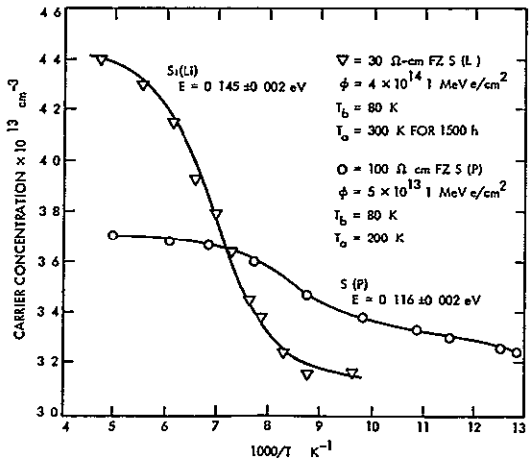

Fig 4 Radiation-induced intermediate level structure and least-squares best fits for lithium- and phosphorus-doped silicon

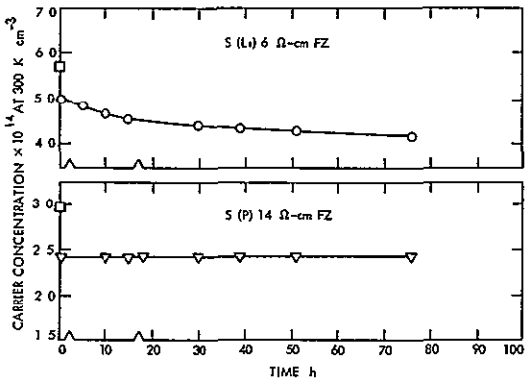

Fig 5 Annealing of room temperature carrier concentration (Both the Li-doped sample and its control were irradiated at 240 °K by 1 7 × 10^{14} 1-MeV electron/cm^2 and then allowed to anneal at room temperature)

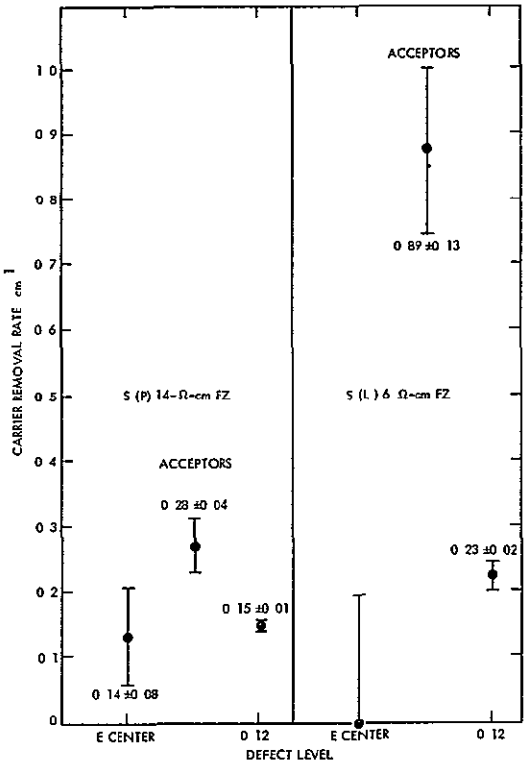

Fig 6 Radiation-induced changes in donor and acceptor concentration on Li- and phosphorus-doped silicon (The samples of Fig 4 were irradiated at 240 °K and remeasured without allowing the lithium to become mobile)

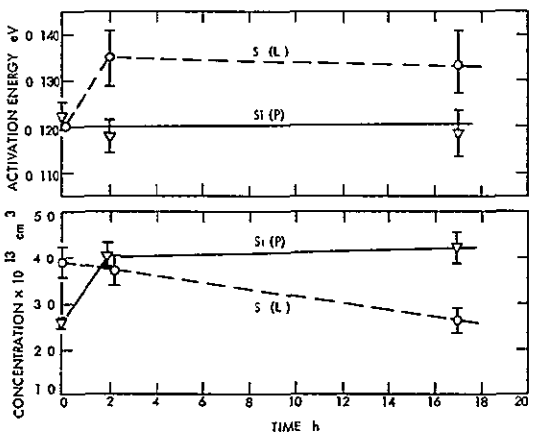

Fig 7 Effect of mobile lithium upon a radiation-induced level at E_C-0 12 eV

INTENTIONALLY

LEFT

BLANK

INTRODUCTION AND ANNEALING OF DAMAGE IN LITHIUM-DIFFUSED SILICON[1]

J A Naber, B C Passenheim, and H Horiye
Gulf General Atomic, Inc
San Diego, Calif

I INTRODUCTION

The development of a radiation-hardened solar cell is of considerable interest for space applications The advent of the Li-diffused silicon solar cell has been one of the highlights in this development However, before its hardness features can be maximized, it is necessary to understand the nature of the introduction and annealing of damage in Li-diffused silicon Furthermore, if computer codes are to be used to predict solar-cell operation on extended and varied space missions the effects of temperature, injection level time, fluence, and type of irradiating particle must be known as they pertain to bulk material

The nature of our investigations is to study the effects of space radiation on the electrical properties of Li-diffused bulk silicon In particular, neutron activation analysis, minority carrier lifetime, electrical conductivity Hall effect, electron spin resonance, and infrared absorption are used to monitor electron- and neutron-produced damage

The results described herein are a continuation of the work previously reported (Refs 1 and 2)

II SAMPLE PREPARATION

The samples used for the experiments were N-type silicon diffused with lithium by two techniques (1) lithium-oil paint-on, and (2) lithium-tin bath diffusion The lithium-oil paint-on technique was used to obtain lithium concentrations ranging from 5×10^{14} to 2×10^{17} cm^{-3}, for the lithium-tin bath diffusion, the concentrations ranged from 5×10^{14} to 5×10^{16} cm^{-3} Resistivity measurements indicated uniform distribution of the lithium in the samples

III EXPERIMENTAL RESULTS AND DISCUSSION

A Minority-Carrier Lifetime

Minority-carrier lifetime measurements have been studied for several reasons First changes in minority-carrier lifetimes due to radiation-induced defects can be observed at very low fluence levels (approximately 10^{12} e/cm^2) making these measurements some of the most sensitive measurements available Second, the temperature dependence of minority-carrier lifetime establishes the density and energy levels of recombination centers Third, the solar-cell output can be directly related to the minority-carrier lifetime

The minority-carrier lifetime was measured by both the photoconductivity-decay and steady-state photoconductivity techniques The samples used for lifetime measurements were 10^4 Ω-cm float-zone (FZ) grown, N-type silicon before diffusion, after lithium diffusion by the lithium-oil paint-on and lithium-tin-bath techniques, they had

[1]This work was performed for the Jet Propulsion Laboratory, California Institute of Technology, sponsored by the National Aeronautics and Space Administration under Contract No NAS 7-100

resistivities of 11 and 0 4 Ω-cm and carrier concentrations of 4 5 × 10^{14} cm^{-3} and 1 5 × 10^{16} cm^{-3}, respectively

1 Thirty-MeV electron irradiations—degradation and annealing

The introduction rate of recombination centers due to 30-MeV electrons at 300°K was studied for both highly Li-diffused (0 4 Ω-cm) and lightly Li-diffused (11 Ω-cm) silicon The degradation rate (K) is defined by

$$\frac{1}{\tau} = \frac{1}{\tau_O} + K\phi$$

where

τ_O = lifetime prior to irradiation

τ = the lifetime after a fluence ϕ

Figure 1 shows the lifetime degradation at 300°K as a function of electron fluence and annealing for highly Li-diffused silicon The degradation constant is 1 8 ± 0 3 × 10^{-7} cm^2/e-s for fluences up to 10^{13} e/cm^2 The degradation constant at 300°K for the lightly Li-diffused silicon is 5 0 ± 2 0 × 10^{-8} cm^2/e-s for fluences up to 10^{12} e/cm^2 (Fig 2) The degradation rate for non-Li-diffused silicon of the same resistivities is 6 ± 2 × 10^{-8} cm^2/e-s These data indicate that the degradation rate depends on the initial lithium concentration

The recombination centers produced in electron-irradiated Li-diffused silicon either contain lithium or are affected in its production by lithium The former is consistent with the defect models for recombination centers proposed previously (Refs 1 and 3)

For the isochronal annealing experiments, the unannealed fraction of the annealable damage is defined by

$$f_T = \frac{N_T - N_f}{N_O - N_f} \qquad (1)$$

where

N_T = the density of recombination centers after isochronal anneal at temperature T

N_O = the density of recombination centers immediately after irradiation and before start of isochronal anneal

N_f = the density of recombination centers when isochronal annealing is complete

Since recombination center density is inversely proportional to carrier lifetime, the unannealed fraction can be expressed in terms of minority carrier lifetime by

$$f_T = \frac{1/\tau_T - 1/\tau_f}{1/\tau_O - 1/\tau_f} \qquad (2)$$

The expression for unannealed fraction of total damage is obtained by replacing N_f and τ_f by N_B and τ_B, where N_B and τ_B are the number of defects and the corresponding lifetime before irradiation

A similar expression for the unannealed fraction of the annealable or total defects exists for isothermal annealing except that temperature (T) is replaced by time (t)

In the highly Li-diffused material Fig 1 shows that, for fluences of 10^{13} e/cm^2 and annealing at 370°K for 30 min (Ref 1), the damage completely recovered However, for fluences of 4 × 10^{14} e/cm^2, only 80% of the damage recovered with the same annealing schedule In the lightly Li-diffused material and fluences of 10^{12} e/cm^2 the annealing was only 85% complete, and at fluences of 10^{14} e/cm^2, there were no signs of annealing The greater the lithium-concentration-to-defect-density ratio the more complete the annealing

The time constant for the first-order annealing (Refs 1 and 2) also depends on lithium concentration in FZ grown material The greater the free lithium concentration, the faster the annealing Figure 3 gives a comparison of the time constants of annealing for Li-diffused FZ and quartz-crucible (QC) grown materials The activation energy for these anneals is 0 75 ± 1 eV with frequency factors ranging from 10^6 to 10^{10} s^{-1}

These results indicate that lithium is active in the annealing of recombination centers produced by electron irradiation This is consistent with our previous analysis in which we attributed the annealing to the migration of free lithium to the recombination center (Ref 1)

2 Fission neutron irradiations — degradation and annealing

Neutron irradiation of Li-diffused silicon is of interest because of the nature of defects produced by neutrons Neutrons are known to produce mainly clustered defects and the introduction of these defects is independent of the impurities present in the silicon Annealing experiments on neutron-irradiated N-type silicon containing ordinary oxygen concentrations and arsenic and phosphorus concentrations below 6 × 10^{14} have indicated insignificant impurity dependence (Ref 4)

The samples used for these irradiations were Li-diffused by the lithium-tin bath technique to resistivities of 4 Ω-cm The neutron irradiations were performed at Gulf General Atomic's APFA facility at a flux of 6 2 × 10^7 neutrons (>10 keV fission)/cm^2-s At 300°K the degradation constant was 6 4 ± 0 4 × 10^{-6} cm^2/n-s and independent of fluence up to 2 × 10^{11} n/cm^2 This degradation constant is the same as that observed in non-Li-diffused silicon (Ref 5) which is

consistent with the lack of impurity dependence for neutron damage

The isothermal annealing (Fig 4) of the neutron damage is evidence of a first-order annealing process The temperature-dependence of the isothermal annealing data indicated an activation energy of 0 66 ± 0 03 eV and an effective frequency factor of (0 4 ± 0 2) × 10^7 s^{-1} Since the nature of the annealing is first order, an analysis of the isochronal annealing data (5-min isochronal anneals) shown in Fig 5 yields an activation energy of 0 69 ± 0 02 eV and an effective frequency factor of 1 5 ± 0 8 × 10^7 s^{-1} A comparison of the isothermal and isochronal annealing kinetic constants is satisfactory

Four observations may be made about these data First the degradation constant of this Li-diffused N-type FZ silicon irradiated at 300°K is independent of the fluence to 2 × 10^{11} n/cm^2 This value of the degradation constant is nearly the same as that for silicon that contains no lithium, which is consistent with the lack of impurity dependence for neutron (clustered) damage and is to be contrasted with this laboratory's observation that the degradation constant for electron irradiated N-type silicon depends on lithium concentration Second, more than 90% of the neutron damage was annealed at temperatures between 300 and 380°K From Stein's data (Ref 5), one would expect less than 10% recovery for non-Li-diffused N-type silicon subjected to the same annealing schedule Third, the effective frequency factor of $\nu \sim 10^7$ s^{-1} for this annealing indicates a process involving long-range migration (Ref 6) Finally, the activation energies determined from isothermal and isochronal anneals agree and are very close to E = (0 66 ± 0 55) eV for the energy of lithium diffusion in silicon (Refs 7 through 9) This strongly suggests that the anneal depends on the diffusion of lithium to the neutron-produced recombination centers

B Electron Spin Resonance and Infrared Absorption

1 Historical background

Electron spin resonance (ESR) has been important in the study of radiation effects in silicon, since it is one of the few techniques (Ref 10) that provide information about the detailed nature of the defects At Gulf General Atomic, ESR has been used to investigate the production, annealing and properties of various damage centers including the Si-B1 Si-G6, Si-G7, and Si-G8 centers (Ref 1) Recently, the ESR technique has been used to study the effect of lithium in radiation damage A thorough investigation of the effect of lithium on the B-1 (oxygen-vacancy) center was previously reported (Ref 1) This study was of particular value since many investigators feel that the B-1 center is the predominant recombination center in silicon irradiated with 1-MeV electrons The results of this study provided invaluable insight into the interaction of lithium with radiation-produced entities including impurity-related defects

During the present study, the ESR technique was used to gain more fundamental information on the role of lithium in displacement damage processes The first investigation performed was an investigation of the effects of lithium on the production and annealing of the di-vacancy (Si-G7) Second, an investigation of the effects of lithium on the production and annealing of the vacancy-phosphorus (Se-G8) center was performed

2 Experimental results

A superheterodyne spectrometer was used for the ESR measurements Measurements were made at 20°K

a Si-G7 center The nature of the di-vacancy (Si-G7) and its energy levels are described in Ref 10

Lithium-diffused FZ grown samples with room-temperature carrier concentrations from 10^{16} to 10^{17} cm^{-3} were irradiated with 30-MeV electrons The irradiations were performed at room- and liquid-nitrogen temperatures Over an incremental fluence range from 1 × 10^{16} e/cm^2 to 2 0 × 10^{17} e/cm^2 it was not possible to detect the presence of di-vacancies using ESR (Ref 11) However, for non-Li-diffused N-type silicon of the same carrier concentrations and fluence ranges the di-vacancy introduction rate is 0 1 di-vacancies/e-cm

The reasons for this inability to observe di-vacancies in Li-diffused silicon may be because (1) the introduction rate of di-vacancies is lower or (2) the di-vacancies produced were in the wrong charge state

To help clarify this situation, infrared absorption measurements were performed on the same Li-diffused samples used for the ESR measurements However, the samples had been stored at room temperature for periods during which annealing, because of lithium diffusion, may have taken place The introduction rate as determined by infrared absorption, was less than 0 025 di-vacancies/e-cm This is at least a factor of 4 less than in non-Li-diffused silicon The results of these measurements can be interpreted to mean that (1) the introduction rate of di-vacancies is lower, or (2) di-vacancies are annealed because of the migration of lithium

The above experiments show that the overall effect of lithium is to decrease the number of di-vacancies present after irradiation

b Si-G8 center Samples of FZ silicon with 1 1 × 10^{16} phosphorus/cm^3 were Li-diffused to carrier concentrations of 3 6 × 10^{16} cm^{-3} The samples were irradiated with 30-MeV electrons at 78°K to fluence levels of about 10^{17} e/cm^2 All Si-G8 (phosphorus vacancy) centers produced by the irradiation are in the paramagnetic charge state A careful search for the Si-G8 center revealed nothing Its introduction rate is therefore below 0 005 cm^{-1} The introduction rate for Si-G8 centers at 78°K in non-Li-diffused silicon is about 0 1 cm^{-1} Introduction rate in Li-diffused silicon is at least 20 times lower than in non-Li-diffused silicon

The absence of the Si-G8 center for 30-MeV electron irradiations at 77°K leads to the conclusion that the presence of lithium is effective in

decreasing the number of this center Since lithium diffuses very slowly at 77°K, the decrease in the introduction rate of the Si-G8 center is not due to its annealing by lithium The reasons for the lower introduction rate may be that

(1) The vacancies produced by irradiation are preferentially attracted to the lithium instead of the phosphorus because the cross sections of the lithium are larger than those of the phosphorus for the vacancies

(2) The phosphorus is paired with the lithium and, therefore, is not free to combine with the vacancies to produce Si-G8 centers

The arguments for the decreased introduction rates of the Si-G8 centers are the same as those for Si-B1 centers (Ref 1) However, in the Si-B1 center studies, oxygen was present in the samples instead of phosphorus

IV SUMMARY

The introduction and annealing of recombination centers in 30-MeV electron-irradiated, Li-diffused silicon depend on the presence of lithium The greater the lithium concentration, the greater the introduction rate of recombination centers The annealing properties of the recombination centers depend on the amount of lithium The larger the free lithium concentration the faster the annealing rate and the more complete the annealing

These results are consistent with the damage and annealing model in which the major recombination center contains lithium (vacancy-lithium or vacancy-lithium-oxygen complex) or is affected in its production by lithium The annealing of the recombination center is due to the diffusion of free lithium to it

The neutron-irradiation data for Li-diffused silicon is consistent with the recombination center being clustered in nature, and annealing of the clusters depends on the diffusion of lithium to it

The decreased introduction rate of Si-G7 Si-G8 and Si-B1 centers in electron-irradiated Li-diffused silicon is attributed to the presence of lithium The reasons for these decreased introduction rates are either the large lithium capture cross section for the vacancy or the lithium-impurity pairing

The studies of the Si-G7, Si-G8 and Si-B1 centers help support the model that all damage centers in electron-irradiated, Li-diffused silicon contain lithium or are affected in their production by lithium Furthermore, the annealing of all damage centers in both electron- and neutron-irradiated Li-diffused silicon is due to the diffusion of lithium to these centers

REFERENCES

1 Naber J A Horiye H , and van Lint V A J Radiation Effects on Silicon, Final Report GA-8668 Gulf General Atomic Inc , Aug 20, 1968

2 Naber, J A Horiye, H , and Berger, R A , "Production and Annealing of Defects in Lithium-Diffused Silicon After 30-MeV Electron Irradiation at 300°K, " Proc of the Conference on Effects of Lithium Doping on Silicon Solar Cells, held at the Jet Propulsion Laboratory, May 9, 1969, Technical Memorandum 33-435 Jet Propulsion Laboratory, Pasadena, Calif Aug 15 1969

3 Brucker, G J , Proc of the Conference on the Effects of Lithium Doping on Silicon Solar Cells, held at the Jet Propulsion Laboratory, May 9, 1969, Technical Memorandum 33-435 Jet Propulsion Laboratory, Pasadena, Calif Aug 15, 1969

4 Curtis O L , Jr , Bass R F , and Germo, C A Impurity Effects in Neutron-Irradiated Silicon and Germanium, U S Army Materiel Command, Harry Diamond Laboratories, Report NARD-65-20R, Northrop Nortronics Applied Research, Nov 1965

5 Stein, H J , J Appl Phys , Vol 37 p 3382, 1966

6 Damask, A C , and Dienes, G J , Point Defects in Metals, Gordon and Breach New York, 1963

7 Pell, E M , J Appl Phys , Vol 31 p 291, 1960

8 Fuller, C S , and Severiens, J C , Phys Rev , Vol 96, p 21, 1960

9 Maita, J P , J Phys Chem Solids, Vol 4, p 68, 1958

10 Watkins, G D , "A Review of EPR Studies in Irradiated Silicon, " Proc of Seventh International Conference on the Physics of Semiconductors, p 97, Dunod, Paris, 1955

11 Naber, J A , Passenheim, B C , and Berger, R A , Study of Radiation Effects in Silicon Solar Cells, Report No GA-9909, Annual Report for Contract No NAS 7-100, Gulf General Atomic, Inc Jan 23, 1970

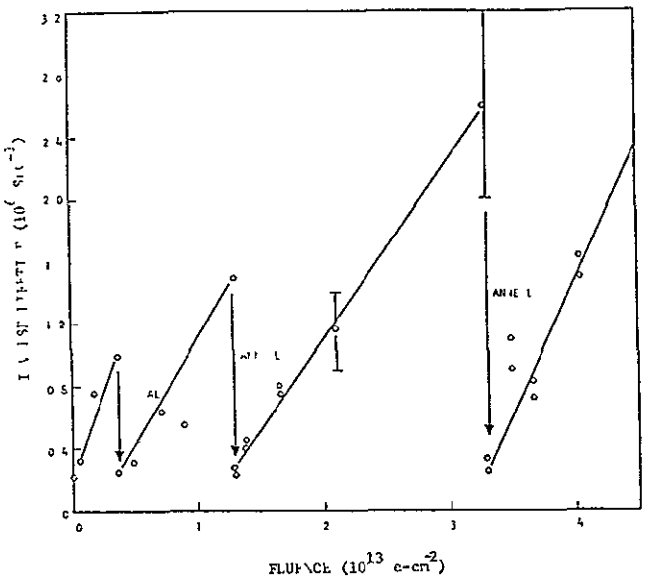

Fig 1 Inverse lifetime vs fluence for the 0 4-Ω-cm Li-diffused N-type silicon irradiated with 30-MeV electrons at room temperature

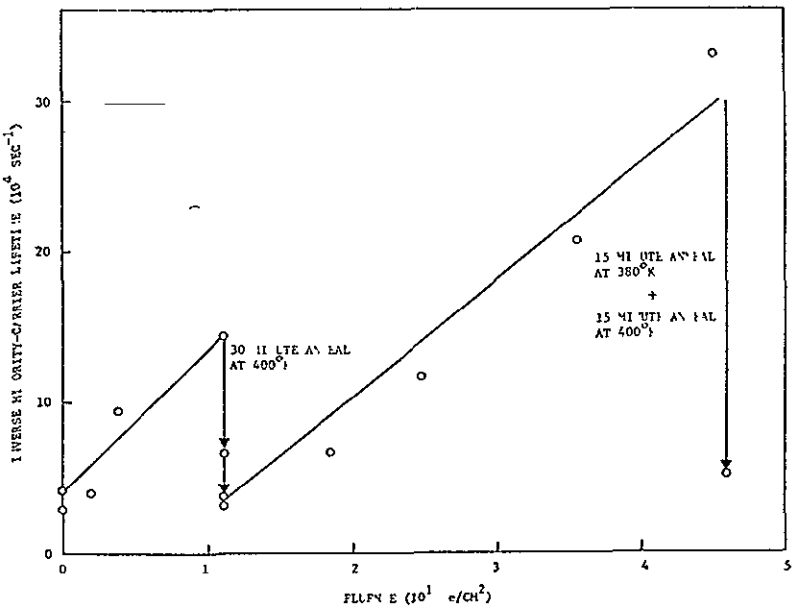

Fig 2 Degradation of lifetime vs 30-MeV electron fluence for 11-Ω-cm Li-diffused N-type silicon

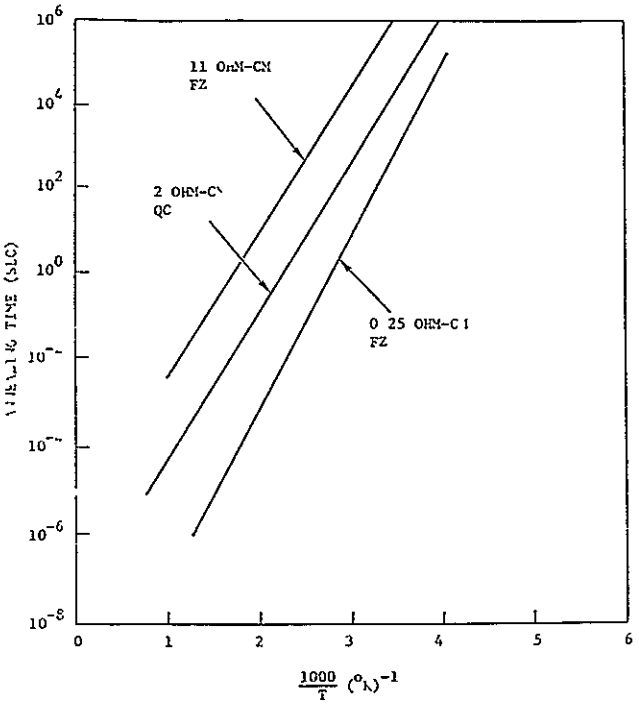

Fig 3 Annealing time of Li-diffused N-type silicon as a function of inverse temperature after 30-MeV electron irradiation

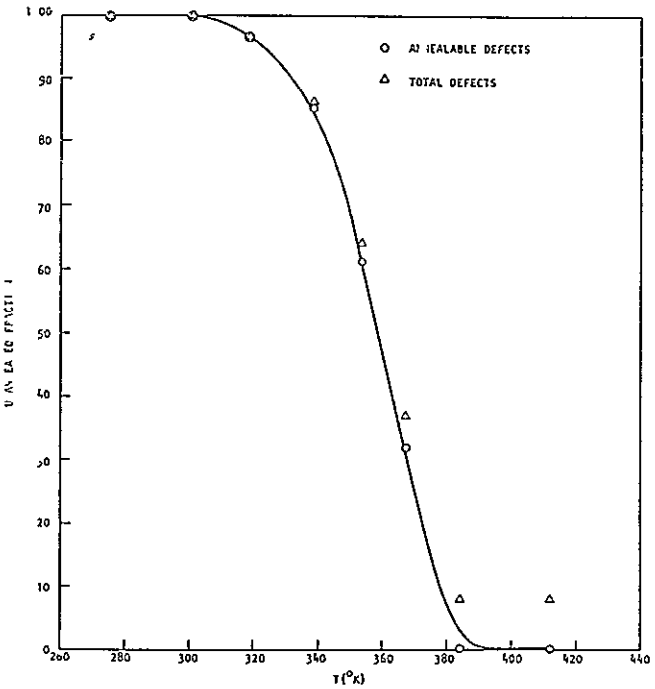

Fig 5 Unannealed fraction of defects vs isochronal anneal temperature for neutron-irradiated 3 7-Ω-cm (sample A) Li-diffused N-type silicon

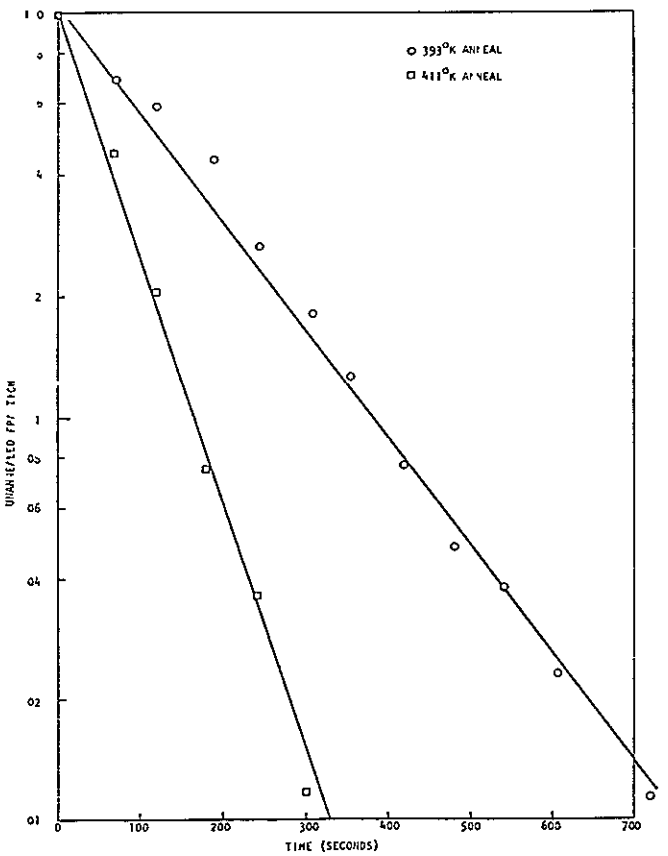

Fig 4 Isothermal anneal of sample A

RADIATION EFFECTS IN BULK LITHIUM- AND ALUMINUM-DOPED SILICON

O L Curtis, Jr , and R F Bass
Northrop Corporate Laboratories
Hawthorne, Calif

I INTRODUCTION

The work presented herein includes the observation of the effects of radiation on the electrical properties (primarily carrier lifetime) of bulk silicon which has been doped with lithium or aluminum Even though the practical interest of this conference is centered around radiation effects in solar cells, it is important that the processes associated with radiation-induced defects be understood Studies of bulk material are the logical way to study at least part of these processes, and to separate the effects that are intrinsic to silicon from those that are associated with the presence of a junction For example in the case of a mobile impurity such as lithium the impurity distribution near the junction may be extremely nonhomogeneous It is unlikely that the behavior with this nonhomogeneous distribution will be understood until an adequate understanding of the homogeneous case is obtained

A great deal of data has been accumulated on the radiation vulnerability of Li-doped solar cells Great promise has been shown for the potential use of these devices in a space radiation environment However, the obvious dependences of the observed behavior on the material from which the solar cells has been fabricated, and what appears to be inconsistencies among cells thought to be identical, point to the requirement for a better understanding of the basic processes of defect creation and subsequent annihilation

Another material of great interest, and the one upon which the most effort has been expended, is Al-doped Si In early studies of the effects of dopant impurities on neutron degradation of Si (Refs 1 and 2) it appeared possible that Al-doped material was substantially more radiation-resistant than that doped with boron or gallium Subsequent studies (Ref 3) appeared to support this result Further interest in this phenomenon was promoted by personal communication with various members of the technical community who expressed the belief that they, too had seen specific instances in which Al-doped material seemed particularly invulnerable to radiation On the other hand, there was concern that these results were not reproducible We were particularly concerned about the validity of our data because of the poor quality of the materials we had used At the time of the experiments the only Al-doped crystals available were grown by the Czocharlski technique These materials contained large concentrations of both trapping and recombination centers Because of the poor quality of the starting material, it was necessary to anneal the samples before performing experiments In the process, we observed something that had been discovered earlier (Ref 4), that the equilibrium carrier concentration was unstable to anneal in the region of 400°C and above This did not particularly concern us, and it gave a means of obtaining a range of resistivities from a single ingot

To refine the experiment, some high-quality float-zone (FZ) material was obtained later Since the lifetime was long and trapping effects small, the experimental difficulties of earlier experiments were avoided However, the experimental results were disappointing The Al-doped

material was just as sensitive to radiation as was B-doped silicon The data to be presented here concerning Al-doped material deal primarily with an effort to reconcile the experimental data and learn under what conditions, if any Al-doped material is relatively invulnerable to radiation

The type of space radiation most important to the users of solar cells is usually electrons with energies on the order of 1 MeV For the purposes of this study, we have chosen instead to use Co 60 gamma radiation Besides the obvious advantage of experimental simplicity such radiation introduces damage homogeneously into large bulk samples so that the effects of non-homogeneous damage distributions are avoided The physical nature of the defects introduced must be very similar to that obtained with electron irradiation since the damage mechanism occurs through the interaction of Compton electrons produced by the gamma rays with the silicon lattice Those electrons having energies below the threshold for displacement are unimportant, and the remainder of the spectrum is reasonably similar to that of interest

II EXPERIMENTAL TECHNIQUES

Relatively large samples were used in this study to minimize possible surface effects and thus ensure that bulk properties were being investigated Most of the samples were approximately 7 mm thick, 7 mm wide, and 30 mm long, but some samples approximately one-half as thick were also used The samples were prepared from 25 different single crystals purchased from commercial sources

The Li-doped samples were prepared in our laboratory by diffusing this impurity into sample blanks made from a P-doped Lopex crystal having an initial resistivity of approximately 160 Ω-cm These diffusions were performed in vacuum at temperatures from 400 to 450°C The source of lithium was a 4 2 molar solution of Li-Al hydride in ether which was applied to the samples using a paint-on technique Since lithium is a donor impurity the resulting samples were still N-type but had resistivities in the range from ~1 to 25 Ω-cm

Minority carrier lifetimes were determined by the photoconductivity decay technique following carrier injection by a 50-ns pulse of 150-kV X-rays To obtain exponential decays in even the best of these materials, it was necessary to perform the measurements at injection levels of approximately 10^{-4} or less

The irradiations were performed in the Northrop Co 60 gamma facility employing fluences of 1 1 × 10^{16} gammas/cm^2 As many as 22 samples were irradiated simultaneously for efficiency and to ensure that they received identical doses During the relatively long exposure (~50 h) and subsequent storage period before post-irradiation measurements were performed, the samples were kept in dry ice (-78°C) to minimize annealing

III RESULTS

A Lifetime Degradation Studies

Table 1 lists the initial and post-irradiation lifetimes and the calculated lifetime damage constants of 38 samples investigated For our purposes, we define the damage constant, K through the relationship

$$\frac{1}{\tau_\phi} = \frac{1}{\tau_o} + \frac{\phi}{K}$$

where

τ_o and τ_ϕ = the initial and post-irradiation lifetimes at 30°C, respectively,

ϕ = the gamma fluence

The damage constant thus corresponds to the fluence required to reduce the lifetime of an initially perfect sample ($\tau_o \approx \infty$) to 1 μs and is proportional to the radiation resistance or "hardness" of the material It should be noted, however, that the constant thus defined is reciprocal of that commonly used in some lifetime degradation studies and which is proportional to the damage rate

The sample designation employed in Table 1 denotes the crystal manufacturer, growth method, dopant, and the initial room temperature resistivity Manufacturers D, G, and T are the Dow Corning Corp , General Electric Co , and Texas Instruments, Inc respectively Additional Al-doped crystals were obtained from the Allegheny Electronic Chemicals Co and Electronic Space Products, Inc Samples from these crystals were not suitable for lifetime degradation studies and consequently are not listed in Table 1 However, these materials were used for annealing studies to be described later and will be denoted by the appropriate manufacturer symbol A or E

Growth techniques C, L V, and F represent the Czochralski (pulled) Lopex, vacuum-FZ, and FZ (argon atmosphere) methods, respectively

For comparative purposes samples that were prepared from the same crystal are grouped together in Table 1, Czochralski-grown crystals containing both aluminum and boron exhibited moderate to severe trapping effects which produced non-exponential photoconductivity decays and made accurate lifetime determinations extremely difficult However, due to the current world-wide shortage of bulk silicon crystals and a lengthy strike at the General Electric facilities, it was not possible to obtain more suitable materials

The various General Electric crystals were grown using research apparatus having limited capacities and were consequently smaller than those obtained from usual commercial sources A total of 14 such crystals was obtained but some, particularly pulled crystals containing aluminum

were unsuitable because they contained large resistivity gradients The gradients were presumably due to the extremely small segregation coefficient of aluminum in silicon (0 002) and were especially evident in the shorter crystals (It is often possible to offset the effects of large resistivity gradients by using only portions of large crystals however, this practice was not possible with the General Electric crystals)

Table 1 shows that the damage constants of samples prepared from the same crystal are very similar, but the values vary from crystal to crystal without any clear dependence upon the pre-irradiation characteristics Evidently, the observed differences in the damage constants of Al-doped samples from different crystals, but similar in other respects, may be due to subtle differerences in the growth processes Such differences may result in different defect species, concentrations, and/or distributions in this material (Refs 4 and 5)

With the exception of the four GFA1 samples which were prepared from the same ~10-Ω-cm crystal, all of the Al-doped samples listed appear to be more sensitive to radiation than the comparable B-doped samples This behavior is surprising because it contradicts the results of earlier studies of neutron-irradiated Al-doped silicon (Refs 1 and 2) However, more recent studies in which some of these same materials have been irradiated with neutrons show that they are also more sensitive to neutrons than are comparable B-doped materials (Ref 6)

Samples TLP 126 and TLP 130 (in Table 1) were included to compare the effects of the lithium diffusion on the properties of this material As indicated in the table, sample TLP 126 was annealed for 12 h at 400°C before it was measured This treatment was performed to determine whether any effects observed in Li-diffused samples were due to the heat treatment employed in the diffusion alone The fact that the damage constants exhibited by these two samples are identical within experimental error indicates that this treatment did not affect the radiation sensitivity of this material

The Li-doped samples listed in Table 1 exhibit a relatively large range of initial resistivities, lifetimes, and damage constants Compared to the starting material, the Li-doped material tends to have an even higher initial lifetime, in spite of its lower resistivity Evidently the introduction of lithium drastically lowers the concentration (or effectiveness) of recombination centers Although there is some scatter, the variation of damage constant with carrier concentration is close to that expected from theory, being roughly constant at higher concentrations and increasing with decreasing number of carriers Higher resistivity samples were obtained by employing shorter diffusion and/or distribution cycles and heating at 400°C Figure 1 shows the potential profile of sample TLP(Li) 12 1 which was heated for 24 h at 400°C following an 8-min diffusion at this temperature The linear profile indicates that the dopant concentration is uniform over the entire length of the sample In contrast, Fig 2 shows the potential profiles of a short test sample after two relatively long distribution heat treatments at 425°C The sample was previously diffused for 30 min at this temperature and the non-linear profiles indicate that it was not possible to distribute the resulting high concentration of lithium uniformly through the sample No sample that had been diffused longer than ~20 min at a temperature above 400°C exhibited a linear potential profile regardless of the subsequent distribution treatment Such samples were consequently not used in any studies of radiation effects

The Li-doped samples are very radiation-resistant compared to the higher-resistivity starting material Compared to P-doped samples of similar resistivity, the improvement is about an order of magnitude or greater

B Isochronal Annealing Studies

Figure 3 shows the temperature-dependence of the lifetime of TLP(Li) 12 1 before irradiation and after isochronal anneals (30 min) at the indicated temperatures Anneals were performed at several additional temperatures, however, the data have been omitted for the sake of clarity Since the radiation-induced lifetime τ_ϕ and pre-irradiation lifetime τ_o are expected to add reciprocally, or

$$\frac{1}{\tau} = \frac{1}{\tau_o} + \frac{1}{\tau_\phi}$$

it is often useful to plot the "induced reciprocal lifetime" as a function of temperature when the slopes of the initial and post-irradiation curves differ (Note that the τ_ϕ used here refers to the actual lifetime after irradiation and after annealing at various temperatures while τ is the measured value) The data of Fig 3 have thus been replotted in Fig 4 No slope value was assigned to the higher-temperature portion because of the limited data at these temperatures Figure 5 shows the recovery of the reciprocal lifetime of this sample measured at 30°C following a one-half hour anneal at each of the indicated temperatures Since the lifetime is expected to vary inversely with the recombination center concentration, the curve represents the fraction of radiation-induced centers remaining after each anneal The fraction not annealed, f, is defined as

$$f \equiv \frac{\frac{1}{\tau_T} - \frac{1}{\tau_o}}{\frac{1}{\tau_\phi} - \frac{1}{\tau_o}}$$

where

τ_o and τ_ϕ = the initial and post-irradiation lifetimes at 30°C, respectively

τ_T = the lifetime at this temperature following the anneal at temperature T

The absence of any significant recovery after the anneal at 72°C and the large reverse annealing

stage at 84°C evident in Fig 5, are surprising in view of reported self-healing of Li-doped solar cells at room temperature following 1-MeV electron irradiation (Ref 8) It is interesting to note that the approximately seven-fold decrease in lifetime damage after the anneal at 84°C was accompanied by a five-fold increase in the amount of trapping indicating the creation of both recombination and trapping centers

C Heat Treatment of Unirradiated Al-doped Silicon

Eleven Al-doped crucible-grown samples which had initial lifetimes shorter than ~10 μs and which exhibited excessive trapping were annealed for 8 h at 460°C to determine the effect of this treatment on the electrical properties and subsequent radiation response of this material In an earlier experiment, two similar samples were converted to high-resistivity N-type after heating for 24 h at this temperature However, the use of a shorter annealing period was expected to produce more moderate changes in the later samples Four of the heat-treated samples were obtained from four different General Electric crystals which had very short lifetimes Before they were annealed, the recombination behavior of these samples was dominated by a very slow trapping center with an effective lifetime of approximately 1 s at room temperature The lifetime of one of the samples was measured as a function of temperature and the results are shown in Fig 6 It should be observed that from approximately 40 to 100°C ($2\ 7 \lesssim 1000/T \lesssim 3\ 2$) the apparent lifetime of the sample decreased by more than three orders of magnitude This behavior and the apparent decrease in lifetime with increasing temperature confirm that the photoconductivity decays were associated with trapping time constants rather than recombination processes

This rendered the initial lifetimes of most of the eleven samples uncertain The sample resistivity was also monitored to determine the effects of the 8-h anneal The resistivities and lifetimes at room temperature before and after the anneal are shown in Table 2 The initial resistivity values were determined from potential profiles which were performed on each sample before the anneal The post-irradiation values were calculated from the measured resistance at room temperature Consequently, the small resistivity changes indicated for some samples may be due to differences in the measurement techniques

An examination of Table 2 shows that the resistivity of most of the samples increased as a result of the anneal However, the amount of increase varies widely and does not appear to be related to the initial value Since soldered contacts were used on the samples, it was necessary to remove them before the anneal and to replace them afterward The quality of the replaced contacts was determined by measuring the sample resistance in reverse directions at both room and dry ice temperatures With the exception of samples GCA1 5 8 and GCA1 9 1, none of the samples rectified after the anneal Additional measurements on these samples revealed that the rectification occurred at a junction in the material which was not observed before the anneal and did not involve the contacts

IV DISCUSSION

Evidently we have been quite successful in obtaining bulk samples of Li-doped material which are uniform have low resistance contacts, and are large enough to minimize surface effects Observation of radiation-induced defects in this material should be truly representative of the real defect nature without complication by device effects Comparison of the data of Fig 4 with those of Downing (Ref 9) indicates a similarity at the temperatures for which the data overlap However, our higher temperature data cannot be explained on the simple basis used by Downing It is clear that a much deeper energy level is responsible for recombination These limited data do not provide an accurate estimate of a position but several worthwhile conclusions can be drawn First, since the lifetimes associated with two levels add reciprocally, the observed slopes cannot be attributed to activation energies of two energy levels In such a case, the steeper slope would occur at the lower temperature We, therefore, conclude that the apparent activation energy at lower temperatures is from 0 06 (Ref 9) to 0 09 eV, corresponding to a variation of hole capture probability with temperature At higher temperatures, the dominant term is either $p_1/c_n nN$ or $n_1/c_p nN$ If the latter is the case, the energy level position can be determined from the intersection of the two lines through the high- and low-temperature portions of the curve At that point $n_1 = n$ This occurs at $1000/T \approx 2\ 52°K^{-1}$, yielding an energy level position at $E_c - E_r \approx 0\ 40$ eV Since the capture probability temperature variation observed at lower temperatures and the temperature dependence of the density-of-states function would affect the higher temperature slope, the observed slope should be ~0 53 eV This value is similar to that observed On the other hand, if the term containing p_1 dominates, the level would be near the center of the gap Further investigation will be required to provide more definitive information Specifically, other samples should be observed to see if the behavior is similar, and lifetime versus excess density measurements should be performed

Evidently, the factors yielding the apparent radiation resistance of Al-doped material are not understood Indeed, the absence of definitive experiments tends to promote skepticism as to whether such an effect truly exists It still appears likely that, if one begins with Al-doped material containing the proper amount of aluminum and other impurity atoms so that the net ionized acceptor concentration is sensitive to the heat treatment at ~400°C, and if the corresponding carrier concentration is reduced by $\sim 10^{15}$ carriers cm^{-3} or more, then that material is less vulnerable to radiation than normal material with the same final resistivity Although we have data in support of this viewpoint, it has not been conclusively established, primarily because of difficulties in obtaining suitable material and because of measurement difficulties associated with the high-trap concentration which appears in all materials having the mentioned instability Two approaches have been considered to solve this problem The first is to obtain better Czochralski-grown material and repeat the experiments This does not seem feasible at present because of the reticence of suppliers to expend significant efforts in this direction The

other approach is to use a bulk measurement which determines diffusion length rather than photoconductivity decay We are presently developing such a technique using a scanning electron microscope

REFERENCES

1 Curtis, O , L , Jr , "Effects of Oxygen and Dopant on Lifetime in Neutron-Irradiated Silicon," IEEE Trans Nucl Sci , NS-13, 6, p 33, 1966

2 Curtis, O L , Jr , Bass, R F , and Germano, C A , Radiation Effects in Silicon and Germanium, Report No HDL 235-3, Northrop Corporate Laboratories, Hawthorne, Calif , 1967

3 Curtis, O L , Jr , and Bass, R F , "Study of Dopants for Radiation-Resistant Silicon," Proc of the Conference on Effects of Lithium Doping on Silicon Solar Cells held at the Jet Propulsion Laboratory, May 9, 1969, Technical Memorandum 33-435 Jet Propulsion Laboratory, Pasadena, Calif , Aug 15, 1969

4 Fuller, C S , and Logan R A , "Effect of Heat Treatment Upon the Electrical Properties of Silicon Crystals," J Appl Phys , Vol 28, p 1427, 1957

5 Fuller, C S , Doleiden, F H , and Wolfstirn, K , "Reactions of Group III Acceptors With Oxygen in Silicon Crystals," J Phys Chem Solids, Vol 13, p 187, 1960

6 Curtis, O L , Jr , Srour, J R , Bass, R F , and Wikner, E G , Radiation Effects in Silicon and Germanium, Report No HDL 235-5 Northrop Corporate Laboratories, Hawthorne, Calif , to be published

7 Bass R F , and Curtis, O L , Jr , "Effects of Impurities on Carrier Lifetime in Bulk Solar-Cell Material," Report No 69-29R, Northrop Corp Laboratories, Hawthorne Calif May 1969

8 Wysocki J J , IEEE Trans Nucl Sci NS-13, p 168 1966

9 Downing R G , "The Effect of Lithium Doping on Silicon Solar Cells," Proc of the Conference on Effects of Lithium Doping on Silicon Solar Cells, held at the Jet Propulsion Laboratory, May 9, 1969, Technical Memorandum 33-435 Jet Propulsion Laboratory, Pasadena, Calif Aug 15, 1969

Table 1 Lifetime degradation of silicon irradiated with 1.1×10^{16} Co^{60} gammas/cm^2 (6.8×10^6 R)

Sample designation[a]	τ_o, μs	τ_ϕ, μs	Damage constant, K (γ/cm^{-2} μs) × 10^{17}
GCB 8 4	16 2	9 8	2 74
GCB 8 2	18 1	7 9	1 51
DCB 11 6	11 0	7 9	3 14
TLB 4 3	433	31 0	3 67
TLB 4 3	411	32 5	3 88
TLB 9 4	433	45 4	5 58
TLB 8 9	433	46 2	5 69
DVB 9 4	193	32 5	4 30
DVB 9 1	153	31 7	4 40
GCAl 6 3	17 3	7 2	1 36
GCAl 15 2	27 1	11 0	2 04
TLAl 4 4	462	12 3	1 39
TLAl 4 4	483	11 5	1 30
TLAl 6 1	115	8 4	0 99
TLAl 6 4	115	8 2	0 97
TLAl 8 9	153	10 8	1 28
TLAl 9 0	164	12 6	1 50
GFAl 4 2	60 6	8 2	1 05
GFAl 6 3	164	9 1	1 06
GFAl 6 3	274	7 9	0 90
GFAl 8 4	77 9	8 4	1 03
GFAl 8 7	77 9	9 4	1 17
GFAl 9 4	310	12 2	1 40
GFAl 10 0	382	11 9	1 35
GFAl 9 9	164	25 2	3 28
GFAl 10 0	170	26 4	3 44
GFAl 10 1	167	25 1	3 25
GFAl 10 2	173	25 1	3 23
TLP 126[a]	96 7	2 7	0 30
TLP 130	136	2 8	0 31
TLP(Li) 1 0	144	6 5	0 74
TLP(Li) 1 2	164	3 6	0 41
TLP(Li) 2 1	82 2	4 5	0 53
TLP(Li) 3 9	222	4 7	0 52
TLP(Li) 4 6	231	5 8	0 65
TLP(Li) 5 1	188	5 4	0 61
TLP(Li) 6 2	162	7 9	0 92
TLP(Li) 12 1	289	21 4	2 54

[a]Annealed 12 h at 400°C before irradiation

Table 2 Effect of heating for 8 h at 460°C on the lifetime and resistivity of Al-doped silicon

Sample designation	Crystal No	Resistivity, Ω-cm		Lifetime μs[a]	
		Initial	Final	Initial	Final
GCAl 4 0	CZ 88	4 0	333	(T)	65 (T)
GCAl 4 0	CZ 82	4 0	20	(T)	15 (T)
GCAl 5 8	CZ 87	5 8	~75	(T)	(R)
GCAl 9 1	CZ 84	9 1	~94	(T)	(R)
ACAl 1 8	6170-1	1 8	3 0	<1 0	(T)
ACAl 1 8	6170-1	1 8	1 9	<1 0	(T)
ACAl 3 7	6170-3	3 7	8 6	14 3 (T)	11 (T)
ACAl 4 9	6170-3	4 9	5 3	<1 0	1 6
ACAl 5 0	6170-3	5 0	4 9	8 7 (T)	8 1 (T)
ECAl 1 5	202	1 5	4 2	<1 0	(T)
ECAl 1 7	202	1 7	177	<1 0	(T)

[a]Lifetime value uncertain due to rectification (R) or trapping (T)

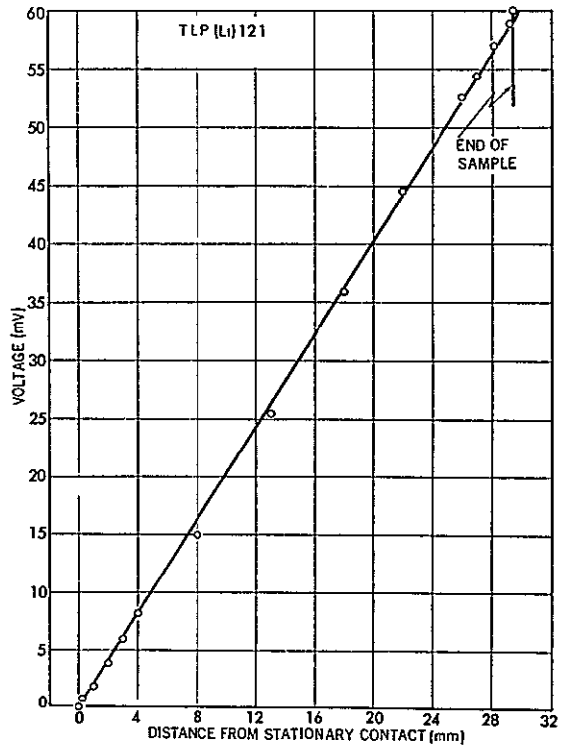

Fig 1 Potential profile of sample TLP (Li) 12 1

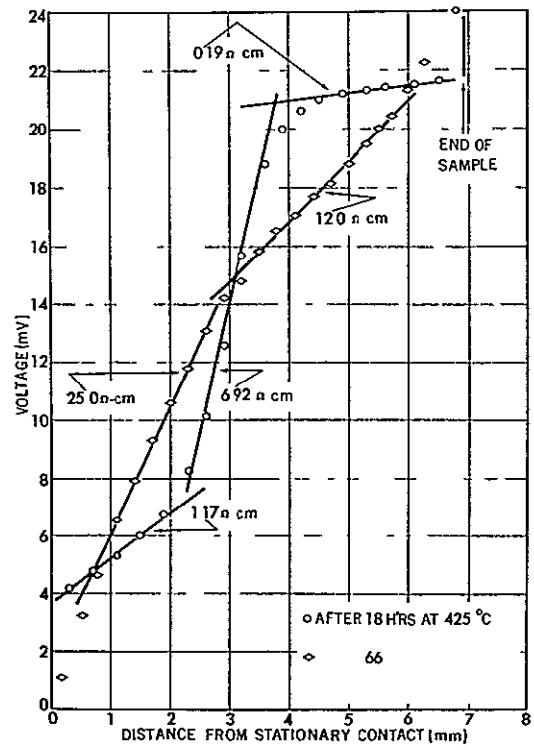

Fig 2 Potential profile of test sample showing the effect of different heat treatments on the lithium distribution

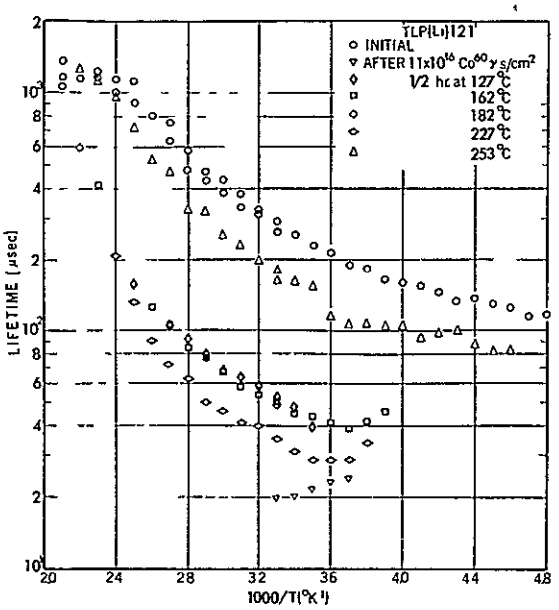

Fig 3 Temperature dependence of lifetime before and after gamma irradiation and after annealing for sample TLP (Li) 12 1

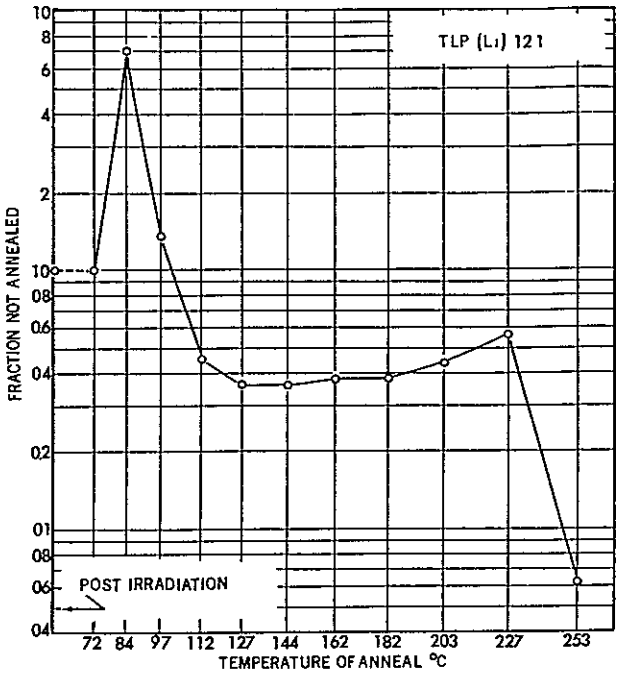

Fig 5 Isochronal annealing of reciprocal lifetime at 30 °C in a Co 60 γ-irradiated Li-diffused sample

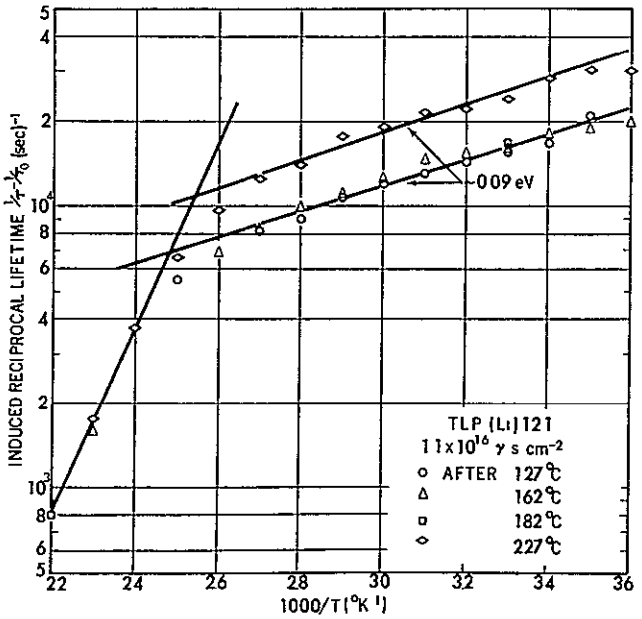

Fig 4 Induced reciprocal lifetime vs reciprocal temperature of TLP (Li) 12 1 after gamma irradiation and subsequent anneals

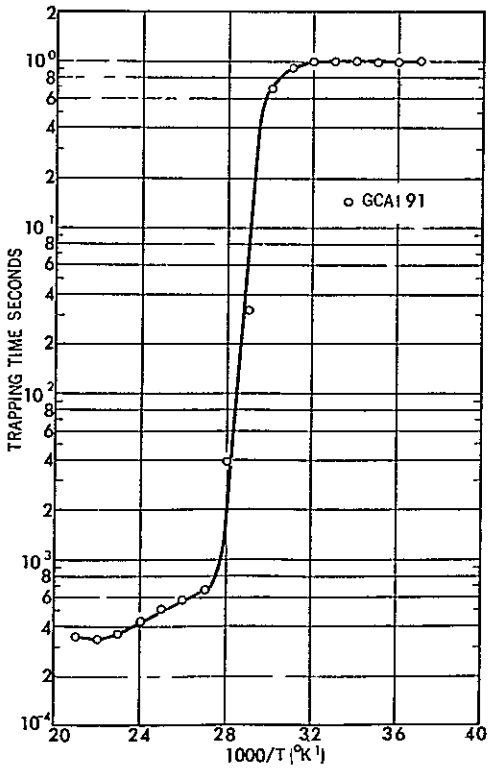

Fig 6 Recombination behavior of an Al-doped sample showing the effects of slow traps

REAL-TIME IRRADIATION OF LITHIUM-DOPED SOLAR CELLS

R L Statler
Naval Research Laboratory,
Washington, D C

I INTRODUCTION

Lithium diffused into P/N silicon solar cells as an added dopant is known to give the cell the property of self-recovery from radiation damage The amount of the recovery, and the rapidity of this process, depend largely on the concentrations of certain impurities in the silicon, the kind of radiation, the radiation dose, and the ambient temperature of the cell following irradiation Almost all radiation experiments with Li-doped solar cells have been performed with particle accelerators that generate radiation fluxes which are several magnitudes greater than space radiation flux Since no experimental evidence indicates whether the recovery of the Li-doped solar cell is dependent on the rate of radiation damage, it is important to study the damage and recovery processes at low-flux rates as well

II EXPERIMENTAL

To evaluate radiation damage in solar cells that are exposed to radiation with an intensity comparable to space radiation fluxes, the Naval Research Laboratory (NRL) Co 60 gamma pool source was utilized The intensity of the radiation at the point where the experiment is located was $4\ 8 \times 10^3$ R/h at the start of the experiment in September 1969 The strength of the source decreases about 1% per month because of the natural radioactive decay of Co 60 The damage caused by the ~1 2 MeV Co 60 gamma ray is produced by an electron in the silicon which is highly energized by a gamma photon in a Compton scattering process This energetic electron creates lattice displacements in the silicon, with the subsequent formation of defects and centers similar to those that occur in electron-irradiated silicon A first approximation for equivalency of damage in solar cells from Co 60 gammas, as compared with electrons, can be made by determining the number of gamma photons that will produce the same number of lattice displacements as a 1-MeV electron If values (Ref 1) are used for the total number of displaced Si atoms per unit of incident flux of 10^{-2} for 1-MeV gamma photons and 4 6 MeV for 1-MeV electrons, the equivalent electron dose corresponding to 1 rad (Si) which is $2\ 22 \times 10^7$ photons/cm^2 is then $4\ 35 \times 10^6$ electrons/cm^2 This equivalency factor is applicable only when the gamma environment is one of electronic equilibrium for the irradiated sample In the case of this particular experiment, where the cells are mounted on 1/8-in -thick brass plates, this condition essentially exists

The solar cells are of five types There are four groups of Heliotek Li-doped P/N cells and a group of Centralab 10-Ω-cm N/P flight-quality cells Table 1 shows the experimental matrix for this study The Li-doped cells were obtained through JPL, and the N/P cells were obtained directly from Centralab

Three stainless steel cylindrical cans about 3 in in diameter and 9 1/2 in long are used for the irradiation and environment chambers for the cells The solar cells are held against brass plates by spring clips at the main bus bar Each cell is loaded with a 10-Ω resistor, with electrical contact being made through the spring clips and brass plate

Illumination is provided by five automobile-type lamps in each can The cans are first

evacuated and then back-filled with 1 psi of argon for the environmental exposure

The cell temperatures are maintained by controlling the temperature of the brass plate by means of electrical strip heaters and water-carrying tubing soldered to the back of the plates One can is held at 30°C, and two cans at 60°C with a variation of ±1°C The cells are removed from the cans for measurement of their I-V curves under illumination from a Spectrosun X-25L solar simulator at 140 mW/cm^2 air mass zero conditions

III RESULTS

The status of the experimental results at the end of the seventh month of testing will be discussed During this time, the solar cells were removed from the source and measured five times From three to five solar cells of each group were exposed to each set of experimental parameters, so as to allow a satisfactory statistical evaluation of the results In almost all cases, this proved to be a sufficient number of samples so that the standard deviation of each set of data was less then ±0 02 The data outside this limit occurred in the H-5 and H-9 groups In the case of the H-5 cells, the low Li diffusion temperature resulted in cells which, by capacitance measurement, indicated little or no Li at the junction It is not surprising that the radiation data on these cells exhibited greater scatter than most other groups However, the unirradiated 60°C control cells in this group had self-consistent behavior In the case of the H-9 cells, the contacts on four of the five irradiated 60°C cells failed at progressive intervals over the 7-month period, so that only data for one cell at 60°C irradiation are given . Table 2 presents the results of the photovoltaic measurements comprising the initial short-circuit current, maximum power, and efficiency for each group of cells Then, the relative maximum power (also the same value for efficiency) is listed for the case of 60 and 30°C irradiation, and 60°C control cells These data were obtained following a gamma dose of 2 3 × 10^7 R, equivalent to 1 03 × 10^{14} electrons/cm^3

The absolute values of maximum power are plotted in Fig 1 for the pretest measurements and for the post-irradiation measurements after 7 months Figure 1 shows that none of the Li-doped cells have an output power as great as the conventional N/P 10-Ω-cm solar cell in this environment, suggesting that nothing is gained by diffusing Li into P/N cells fabricated at these particular diffusion schedules and temperatures The experiment will continue for at least an additional 6 months Figure 1 also reveals that the temperature of the cells during irradiation does influence the amount of observed damage, since all groups of cells irradiated at 60°C are slightly more damaged than those at 30°C There is also a certain amount of power degradation among the two groups of N/P cells and H-9 cells which are held at 60°C without irradiation The reason for this has not been determined In the case of the N/P cells, this effect may be connected with contact degradation, rather than a change in the properties of the silicon or P-N junction The cause for this deterioration in the Li float-zone (FZ) cell could be related to the increased diffusivity of Li with increased temperature, affecting either the internal properties of the cell or the contacts

IV CONCLUSIONS

The low flux Co 60 irradiation of illuminated solar cells at various temperatures has proven to be a valid, useful, and interesting experiment for comparison of both Li-doped and conventional solar cells The real-time dose rates and solar simulator measurements provide a more realistic evaluation for the performance of solar cells in environments which more nearly approximate the conditions of their utilization

No advantage has been observed for the four particular types of Li-doped solar cells over the standard N/P solar cell for the temperature region of 30 to 60°C, with a bombarding electron fluence up to 1 × 10^{14} e1/cm^2

On the other hand, this experiment has disclosed a temperature-dependence of radiation damage and the suggestion of some type of thermally induced damage in N/P cells and high Li concentration FZ cells

REFERENCE

1 Transient-Radiation Effects on Electronics Handbook, DASA 1420, edited by R K Thatcher, Battelle Memorial Institute, Aug 1967

Table 1 Co 60 experiment sample matrix

Cell group	Type	Li diffusion parameters	Number irradiated controls		
			30°C illuminated	60°C illuminated	60°C illuminated
H-2	Li P/N crucible	90 min 425°C-60 min 425°C	5	5	3
H-6	Li P/N crucible	90 min 450°C-60 min 450°C	5	5	3
H-5	Li P/N FZ	90 min 350°C-60 min 350°C	5	5	3
H-9	Li P/N FZ	90 min 425°C-60 min 425°C-	5	5	3
Centralab	N/P crucible	N A	5	5	3

NOTES

All Li-doped cells were made by Heliotek

All cells are illuminated with tungsten light and are individually loaded with a 10-Ω resistor developing a load voltage of 0 21 to 0 24 V

Table 2 Photovoltaic parameters of experimental cells

Cell group	Type	I_{sc}, mA	P_{max}, mW	Efficiency, %	Relative P_{max} after 2 3 × 10^7 r[a]		
					Control	Irradiated	
					60°C	60°C	30°C
H-2	Lo Li CG	64 5	27 8	9 9	1 01 ± 0 02	0 89 ± 0 62	0 90 ± 0 02
H-6	Hi Li CG	60 0	24 7	8 8	1 01 ± 0 01	0 92 ± 0 02	0 92 ± 0 02
H-5	Lo Li FZ	70 0	27 4	9 8	0 99 ± 0 02	0 83 ± 0 07	0 85 ± 0 03
H-9	Hi Li FZ	61 0	25 1	9 0	0 93 ± 0 01	(0 86)[b]	0 95 ± 0 02
N/P	10 Ω-cm	71 5	29 2	10 4	0 98 ± 0 01	0 89 ± 0 01	0 90 ± 0 01

[a] Equivalent to 1 03 × 10^{14} 1 MeV el/cm^2

[b] Only one cell remaining at this dose

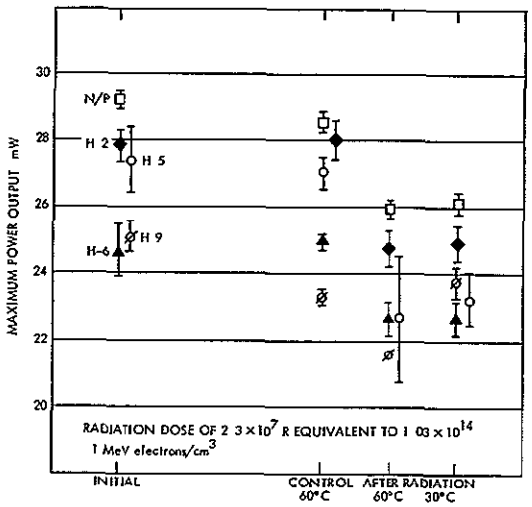

Fig 1 Output power of irradiated solar cells

OBSERVATION OF STRUCTURAL DAMAGE IN LITHIUM-DOPED SILICON SOLAR CELLS PRODUCED BY NEUTRON IRRADIATION

G A Sargent and S Ghosh
University of Kentucky
Lexington, Ky

ABSTRACT

Undoped and Li-doped silicon solar cells, of doping level 10^{15}, 10^{16}, 10^{17} lithium atoms/cm^3 were irradiated with neutrons produced by a Cockroft-Walton generator to doses of 10^{10}, 10^{11}, 10^{12}, and 10^{13} neutrons/cm^2 The cells were thinned by chemical polishing, etched and observed by surface replication and thin film transmission electron microscopy In the unirradiated and Li-doped samples, there was some evidence that lithium was present in the form of finely dispersed precipitates Damage to the cells produced by irradiation could be observed as etch pits in the form of shallow craters at the surface and as circular regions within the bulk of the sample by surface replication and transmission electron-microscopy The apparent size and distribution of the observed defects were in accord with the theories of defect clusters proposed by Gossick (Ref 1) and Crawford and Cleland (Ref 2) The density of defects produced by irradiation increased with increasing irradiation dose, however, the size of the defects seemed to decrease with the presence of lithium

I INTRODUCTION

When solar cells are exposed to the environment of space, they suffer severe degeneration due to defects caused by bombardment with a wide variety of nuclear particles

The work described herein was undertaken to investigate the form of the structural damage produced in Li-doped P/N silicon solar cells by neutron irradiation From a detailed knowledge of the structural damage produced by irradiation it is hoped to design treatments whereby the degenerative processes caused by the irradiation damage could be either reversed or prevented In this investigation, surface replication and thin-film electron microscopy of the bulk material are being used as the experimental techniques to attempt to observe the structural damage

The existence of regions of highly localized damaged in semiconductors after irradiation by fast particles (neutrons) was first predicted by Gossick (Ref 1) and Crawford and Cleland (Ref 2) Their theoretical model for the disordered regions predicts for example that N-type germanium, in the regions of highly localized damage becomes P-type, P- or N-type silicon becomes intrinsic Surrounding this region a space change region (junction) is created whose dimensions depend upon the carrier concentration of the unirradiated material Such regions would be surrounded by potential wells of sufficient depth and width as to noticeably influence the bulk

electrical properties of the material Subsequently, experimental measurements of electrical properties by Closser (Ref 3) and Stein (Ref 4) have provided additional direct evidence of the existence of these regions In the above experiments, the decrease in electrical conductivity of silicon was used as a measure of the carrier removal as a result of neutron irradiation and the carrier concentration was obtained from Hall coefficient measurements Further electrical studies of N-type silicon by Stein (Ref 5) have shown that neutron irradiation at 76°K produces light-sensitive defects at a rate that is independent of the concentration of crystal impurities Therefore, it was concluded that the defects were vacancy-liberating clusters The neutron-induced defects could thus be regarded as regions of high resistivity which were surrounded by space-charge regions Such cluster-space-change regions could be regarded as insulators in a conducting medium The light sensitivity of the irradiated silicon is believed to result from minority carrier trapping within the cluster-space-change region which effectively reduces the insulating volume

More recently Stein (Ref 6) has shown that the behavior of defects produced in P-type silicon by neutron irradiation at 76°K was independent of the method of crystal growth and found that there was an illumination dependence similar to that previously observed in irradiated N-type silicon He again attributed this effect to the presence of defect clusters He also found that annealing the samples produced several diffuse recovery stages between 150 and 550°K, with the largest stage between 150 and 240°K

To date very little work has been carried out to determine the exact structural nature of the regions of lattice disorder created by irradiation damage Fujita and Gonser (Ref 7) have attempted to determine the size of the damaged regions in irradiated germanium using an X-ray diffraction technique, but were relatively unsuccessful More recently, however, several attempts have been made to observe more directly the damaged regions in neutron-irradiated germanium and silicon using electron microscopy

The first direct observation of defect clusters was made by Parsons Balluffi, and Koehler (Ref 8) in thin-germanium films using transmission electron microscopy The number of regions which they observed was in good agreement with their theoretical estimates from electrical property measurements and a mean diameter of 53Å was measured for the defect Hemment and Gunnersen (Ref 9) have attempted to perform similar transmission electron microscopy experiments on a N-type silicon samples which were irradiated with fast neutrons at doses ranging from 5×10^{16} to 10^{19} neutrons/cm^2 however, they failed to detect the presence of any defects However, Pankratz Sprague, and Rudee (Ref 10) were successful in observing defect clusters in neutron-irradiated silicon by electron microscopy They found that the mean defect image size was dependent on the impurity content and on the annealing treatment, ranging from a maximum of about 40Å in the as-irradiated material to about 22Å in the annealed material The defect density was also proportional to neutron dose

An alternative method for observing defects in germanium and silicon semiconductors, which was tried unsuccessfully by Chang (Ref 11) and Noggle and Steigler (Ref 12) and later perfected by Bertolotti and his co-workers (Refs 13 through 15), consists of irradiating the material with fast mono-energetic neutrons, etching with suitable chemicals, and then constructing a replica of the surface for observation in the electron microscope

Bertolotti and his co-workers found that, upon etching the surface of irradiated silicon samples, craters were produced, the dimensions of which were comparable with the dimensions of the space-change regions predicted by Gossick (Ref 1) and Crawford and Cleland (Ref 2)

The work undertaken under the present contract was designed to extend these earlier experimental observations and, specifically to attempt to determine the structural nature and distribution of the damaged regions

II EXPERIMENTAL TECHNIQUE

A Material

The experimental work described herein was carried out on commercial Li-doped solar cells supplied by Heliotek, a division of Textron Inc The starting material was float-zone (FZ) refined, single crystal of phosphorus-doped N-type silicon Slices were then cut from the ingot to give a (110) crystal slice Boron was then diffused into the slice to give a junction depth of 0 5 μ Lithium was then diffused in, to produce four types of cell according to the following schedule

(1) Type 1--$0 \times 10^{\circ}$ lithium atoms/cm^3, no lithium diffusion

(2) Type 2--1×10^{15} lithium atoms/cm^3, diffusion for 5 min and redistributed 120 min at 350°C

(3) Type 3--1×10^{16} lithium atoms/cm^3, diffused 5 min and redistributed 60 min at 425°C

(4) Type 4--1×10^{17} lithium atoms/cm^3, diffused 90 min and redistributed 60 min at 425°C

B Neutron Irradiation

Samples of the un-doped and Li-doped solar cells were irradiated with neutrons produced by a Cockroft-Walton generator to doses of approximately 10^{10} 10^{11}, 10^{12} and 10^{13} neutrons/cm^2 The neutrons were produced by bombarding a tritium target with deuterium gas molecules This source of neutrons is highly mono-energetic, having an energy of approximately 14 7 MeV All the samples were irradiated simultaneously at room temperature, the dose being controlled by varying the distance of the sample from the target The relative dose was measured by placing a thin copper foil of known weight behind each cell and monitoring the decay of the Cu 62 isotope, which has a half-life of 9 9 min

After irradiation the samples were sectioned with a diamond saw for examination by surface replication and transmission electron microscopy

C Specimen Preparation for Surface Replication

The surface of the solar cells was prepared for replication by (1) mechanical grinding and polishing and (2) etching, using the CP4A etchant (15 cc acetic acid, 25 cc nitric acid, and 15 cc hydrofluoric acid) A replica was then made of the etched surface by evaporating onto it a thin layer of carbon The carbon replica was removed by means of a Mylar tape which was subsequently dissolved in acetone The replica was then observed by transmission in the electron microscope at an accelerating voltage of 75 kV

D Specimen Preparation for Thin-Film Electron Microscopy

Small samples approximately 1 mm^2 were cut from the solar cells and then chemically thinned in a solution consisting of 9 parts nitric acid and 1 part hydrofluoric acid After thinning, the sample was placed in a plastic holder which had a small hole in it, and the chemical polishing procedure was resumed until a small dimple was produced in the surface of the sample The outer edges of the sample were then painted with enamel and the chemical polishing was continued The upper surface of the specimen was observed through a microscope A light source was used to illuminate the back side of the specimen and polishing was continued until yellow-colored light could be observed through the specimen At this yellow stage, the specimen was approximately 5000Å thick Additional polishing beyond this stage resulted in complete perforation, and the thinned down section was rapidly rounded off leaving the section too thick to observe by transmission electron microscopy After thinning, the specimen was washed using a sequence of cleaning agents (distilled water, acetone, distilled water, and methanol)

Initially, some difficulty was experienced in observing the samples by transmission electron microscopy due apparently to the buildup of a charge on the surface of the sample as soon as the electron beam hit it It was found, however, that if the specimen was sandwiched between two copper grids, then the charge could be adequately grounded, and a much improved image was produced

III EXPERIMENTAL RESULTS

A thin-film electron transmission picture of the as-received solar cell material unirradiated and without lithium doping is shown in Fig 1 The figure only shows fairly broad diffraction contour lines A selected area diffraction pattern taken of this field is shown in Fig 2 (a) This diffraction pattern can be indexed as diamond cubic with a [1$\bar{1}$0] zone axis An interpretation of this diffraction pattern is shown in Fig 2 (b)

Figure 3 shows an electron transmission picture obtained from a thin foil of unirradiated solar cell doped to 10^{17} lithium atoms/cm^3 The structure here appears to contain many small defects which are distributed fairly homogeneously throughout the whole field

A selected area diffraction pattern taken from an area such as this is shown in Fig 4(a) A number of weaker diffraction spots can be observed which cannot be indexed as belonging to the silicon diamond-cubic structure They can, however, be indexed as belonging to the body-centered-cubic crystal structure From a comparison of the radius ratios of the selected area diffraction spots, and by assuming a value for the lattice parameter of silicon, it is found that the lattice parameter of the body-centered-cubic structure is approximately 3 45 Å, which agrees well with that for lithium It is possible, therefore, that fine precipitate structure, which can be observed in all of the Li-doped cells, is due to excess lithium

An interpretation of the diffraction pattern obtained from the Li-doped sample is shown in Fig 4(b) It can be seen that (110) planes of the precipitate particles are almost parallel (within about 5°) to the (110) planes of the silicon matrix

The effective macroscopic cross section for the electron diffraction was approximately 5μ^2 From such a diffraction pattern it is impossible to measure the density of the precipitates which are giving rise to the additional diffraction spots

Figure 5 shows a replica obtained from the etched surface of a sample which contained no lithium, but which was irradiated with 10^{13} neutrons/cm^2 The area shows a finely etched background structure, on the top of which craters can be observed The crater dimensions were of the order of 2000-3500 Å in diameter, and the density of these defects in the field was approximately 8×10^7/cm^2

Figure 6 shows a transmission picture obtained from an undoped cell which was irradiated to a dose of 10^{12} neutrons/cm^2 In this field of view, spherical regions approximately 2500-4000 Å in diameter can be observed with an average density of 3×10^7 defects/cm^2, together with numerous triangular-shaped images It is thought that the triangular-shaped images may be produced by etch pits in the surfaces of the thin foil or, alternatively, they may be due to diffraction fringes at stacking faults in the silicon matrix Figure 7 shows an enlargement of one of the spherical regions No additional detail is revealed, although the triangular-shaped images are all oriented in the same direction, which suggested that they bear some relation to the crystal structure in the matrix

Figure 8 shows a transmission picture obtained from a sample which was doped with 10^{16} lithium atoms/cm^3 and irradiated with 10^{10} neutrons/cm^2 Many small circular defects can be observed which have a mean diameter of approximately 2500-4000 Å and a density of about 2.0×10^7/cm^2

Figure 9 shows a replica taken from the surface of a specimen doped with 10^{17} lithium atoms/cm^3 and irradiated with 10^{13} neutrons/cm^2 Many small craters can be observed on top of the fine background structure and there appears to be some form of precipitation The average

diameter of the circular defects in this case is about 600-1000 Å with an average density of about $1.5 \times 10^9/cm^2$

IV DISCUSSION AND CONCLUSIONS

The chemical etching method appears useful to see the damage regions that are produced during high-energy neutron irradiation of silicon solar cells. It is clear that such etched structures are due to the irradiation damage because they are fairly uniformly distributed throughout the crystal volume and because such structures cannot be seen in the unirradiated material.

The size of the defects seen by etching appear to be in agreement with the size of the defects predicted by the model of Gossick (Ref. 1) and Crawford and Cleland (Ref. 2). This model was originally applied to neutron-irradiated N-type germanium. The defects in this case were described as disordered regions in the form of P-type islands with a potential barrier around them at the interface with the matrix. This assumes that the disorder regions are crystalline in nature, however, one would expect that a discontinuity in the structure could be shown by etching, because of the different etching rates in the damaged region and in the space-change region which are different from etching rates in the bulk material. As pointed out by Bertolotti (Ref. 16), it seems surprising that a junction would be produced in silicon, since one would expect that its asymptotic behavior under energetic irradiation should be intrinsic. On the other hand, a barrier could also be produced between a heavily damaged zone that becomes compensated intrinsic and the N-type undisturbed zone. The barrier height in the case of an N-i junction, should be shallow and, in fact the contours which are observed in the surface replication technique are less well-defined than those observed in the case of germanium (Ref. 13).

It is not possible from the present results to determine accurately the density of damage regions present at a given irradiation level primarily because the etched structure is very variable in its appearance, however, it does seem that the density of defects increases with increasing irradiation.

From the selected area electron diffraction studies of the Li-doped samples, it would seem that at all doping levels examined some excess lithium exists in the form of very fine precipitates.

In the Li-doped and irradiated material crater-type defects can be revealed by etching a surface replication, however, in this case, the defect regions appear to be associated with the lithium precipitates. This is particularly evident at the highest doping level and dose where the formation of some kind of precipitation network occurs.

REFERENCES

1. Gossick, B. R., J. Appl. Phys., Vol. 30, p. 1214, 1959.
2. Crawford, J. H., and Cleland, J. W., J. Appl. Phys., Vol. 30, p. 1204, 1959.
3. Closser, W. H. J. Appl. Phys., Vol. 31, p. 1693, 1960.
4. Stein, H. J., J. Appl. Phys., Vol. 737, p. 1309, 1966.
5. Stein, H. J., Phys. Rev., Vol. 163 p. 801 1967.
6. Stein, H. J. J. Appl. Phys., Vol. 39, p. 5283, 1968.
7. Fujita, F. E. and Gonser, U., J. Phys. Soc. Japan, Vol. 13, p. 1968, 1958.
8. Parsons, J. R., Balluffi, R. W., and Koehler, J. S., Appl. Phys., Letters, Vol. 1, p. 57, 1962.
9. Hemment, P. L. F., and Gunnerson, E. M., J. Appl. Phys., Vol. 37, p. 2912, 1966.
10. Pankratz, J. M., Sprague, J. A., and Ruddee, M. L., J. Appl. Phys., Vol. 39, p. 101 1968.
11. Chang, R., J. Appl. Phys., Vol. 28, p. 868, 1957.
12. Noggle, T. S., and Stiegler, D. J., J. Appl. Phys., Vol. 30, p. 1279, 1959.
13. Bertolotti, M., Papa, T., Sette, D., Crasso, V., and Vitali, G., Neuoro Cimento, Vol. 29, p. 1200, 1963.
14. Bertolotti, M., Papa, T., Sette, D., and Vitali, G., J. Appl. Phys., Vol. 36, p. 3506, 1965.
15. Bertolotti, M., Pappa, T., Sette, D., and Vitali, G., J. Appl. Phys., Vol. 38, p. 2645, 1967.
16. Bertolotti, M. Radium Effects in Semiconductors, Plenum Press, 1968, p. 311.

Fig. 1. Transmission electron micrograph from an undoped unirradiated sample (X 9000)

Fig. 2(a). Electron diffraction pattern taken from an area shown in Fig. 1

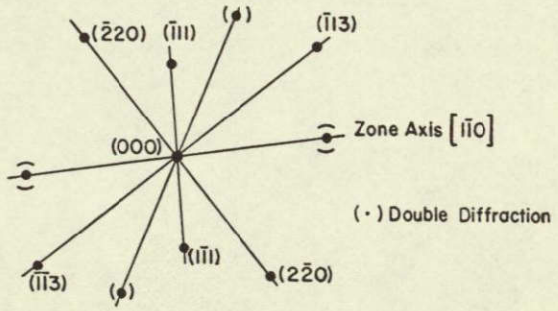

Fig. 2(b). Interpretation of diffraction pattern shown in Fig. 2(a)

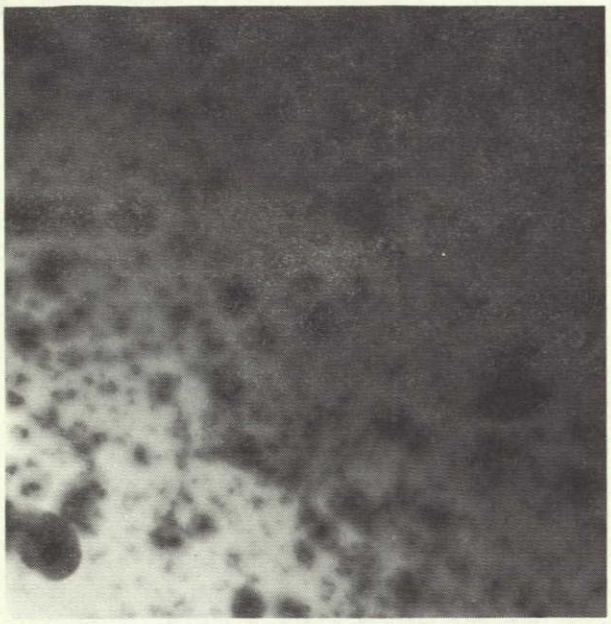

Fig. 3. Transmission photograph of unirradiated sample doped with 10^{17} lithium atoms/cm^3 (X 12,500)

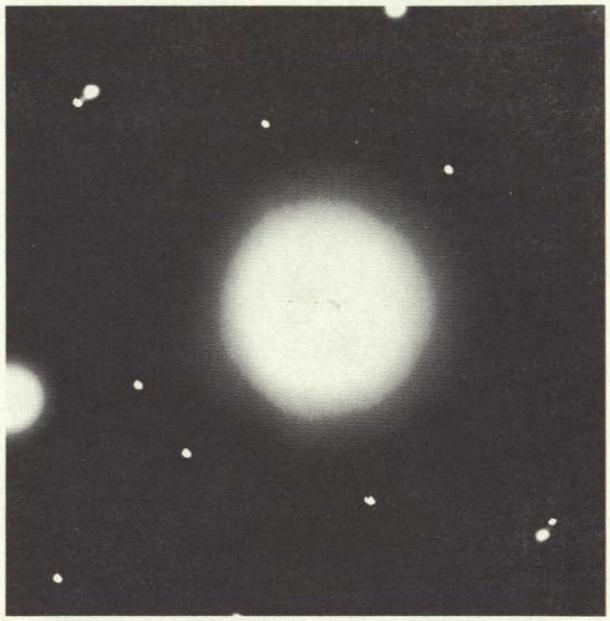

Fig. 4(a). Electron diffraction pattern taken from an area shown in Fig. 3

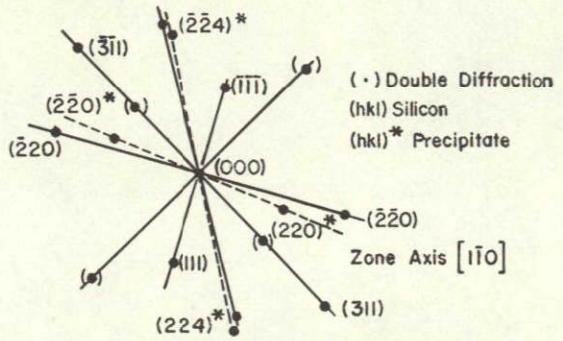

Fig. 4(b). Interpretation of diffraction pattern shown in Fig. 4(a)

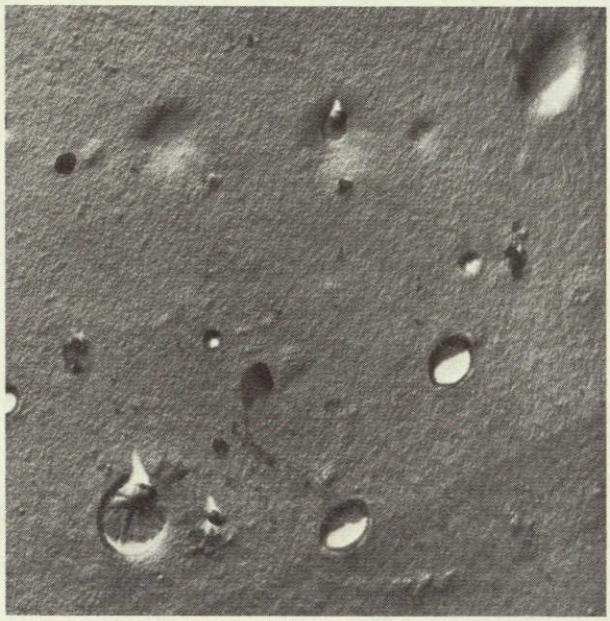

Fig. 5. Surface replica of undoped sample irradiated with 10^{13} neutrons/cm^2 (X 18,500)

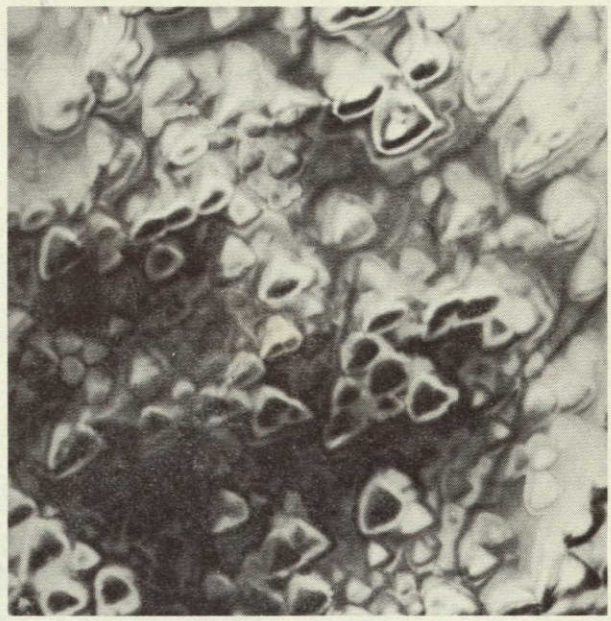

Fig. 7. Transmission photograph of undoped sample irradiated with 10^{12} neutrons/cm^2 (X 40,000)

Fig. 6. Transmission photograph of undoped sample irradiated with 10^{12} neutrons/cm^2 (X 18,500)

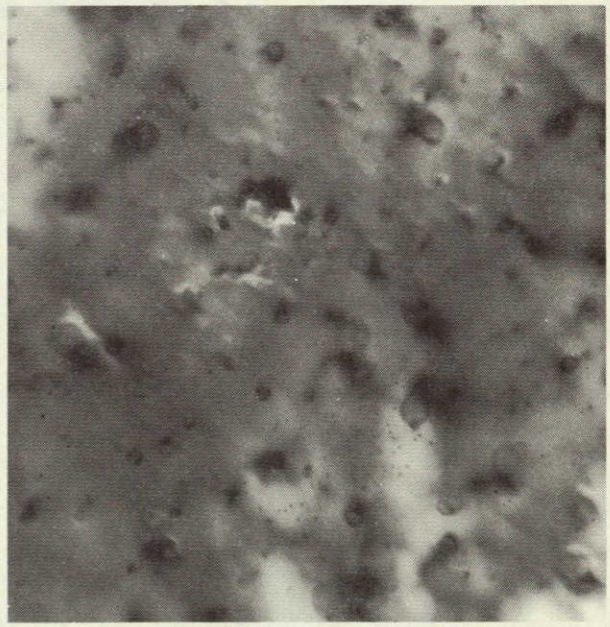

Fig. 8. Transmission photograph of sample doped with 10^{16} lithium atoms/cm^3 and irradiated with 10^{10} neutrons/cm^2 (X 5000)

Fig. 9. Surface replica from sample doped with 10^{17} lithium atoms/cm^3 and irradiated with 10^{13} neutrons/cm^2 (X 40,000)

OPTICAL PROPERTIES OF SILICON AND THE EFFECT OF IRRADIATION ON THEM

K Vedam
Materials Research Laboratory,
The Pennsylvania State University,
University Park, Pa

ABSTRACT

A new ellipsometric method for the determination of both the real and imaginary parts of the complex refractive index ($n_2 - ik_2$) of silicon will be described Measurements on cleaved samples of silicon reveal that the true values of silicon for λ5461Å are $n_2 = 4\ 14_0 \pm 0\ 02$ and $k_2 = 0\ 03_4 \pm 0\ 01$ Similar measurements on chemically polished samples yielded the values as $n_2 = 4\ 05$ and $k_2 = 0\ 028$, in agreement with the values reported in the literature These results are also corroborated by electron microprobe studies on these same specimens Optical absorption coefficient of intrinsic silicon has been determined at a number of discrete wavelengths in the spectral range 400-1000 nm at room temperature These measurements were also extended to liquid nitrogen and liquid helium temperatures Results of these measurements, in conjunction with our earlier measurements on the refractive index of silicon provide for the first time reliable data on the optical constants of intrinsic silicon, and thus form the basis for comparison with similar properties of doped and Li-diffused silicon Irradiation of silicon with 6-MeV protons to fluences of 10^{16} particles/cm^2 does not produce any noticeable change in its optical properties, as determined by techniques involving reflectivity, within the limits of experimental error

I INTRODUCTION

Precise knowledge of the effect of irradiation on the optical properties of the various silicon solar cell component materials is of extreme importance for the development of efficient, long-lasting silicon solar cells However before such measurements on actual Li-doped silicon and silicon devices are undertaken, it was felt desirable to carry out a systematic study of these properties on pure intrinsic silicon Similarly, the influence of the oxide film, which is always present on the surface of silicon, either by deliberate oxidation or by self-contamination, should also be investigated

During the course of these studies a new ellipsometric method was developed so that the true values of both the real and imaginary components of the optical dielectric constant of silicon could be determined directly (Ref 1), without making any assumptions about the nature of the surface film It may be mentioned that these results were also independently confirmed (Ref 2) by electron microprobe studies on the same $Si\text{-}SiO_2$ system A brief description of this

ellipsometric method is given below in Section II along with the results obtained on freshly cleaved samples of silicon Similar measurements on chemically polished samples yield values which differ by some 2% from those obtained on cleaved samples, but are in very good agreement with the values generally used in the literature Sections III and IV describe respectively the results obtained on optical absorption coefficient of intrinsic silicon and the effect of irradiation with 6-MeV protons on the optical properties of silicon

II OPTICAL CONSTANTS OF SILICON

The potentialities of ellipsometry for the determination of the optical constants of an optically absorbing material such as silicon have been known for a long time The exact theoretical expressions involved in ellipsometry were derived by Drude (Ref 3) nearly 80 years ago, but they could not be used until recently because the equations involved are rather complex and could not be solved in a closed form Hence numerous approximations have been tried, however, as Saxena (Ref 4) has shown, all these approximations are either of doubtful validity or valid in very narrow ranges of film thickness With the advent of modern computers, it is now possible (Refs 1, 5, and 6) to make use of the exact equations, and recourse to the various approximations is no longer necessary

Further, until now, the optical constants (n_2-ik_2) of any absorbing material could be determined by ellipsometry only if the values of the refractive index n_1 and the thickness d_1 of the film on the surface were known, even though the thickness of the film may have been as small as 10-50 Å (Refs 7 and 8) Since there is a surface film present on all surfaces exposed to the normal atmosphere the direct determination of the optical constants of the substrate from the measured ellipticity parameters Δ and ψ, without any assumption about the nature of the surface film, has in the past been rather unsuccessful Hence, attempts were usually made to apply suitable corrections and extrapolations to the measured values to obtain the optical constants of the substrate Further, the refractive index n_1 of the thin surface film is usually either not known precisely or the validity of using the refractive index of the bulk material for thin films is questionable (Ref 9)

Perhaps a greater degree of uncertainty is introduced when an a priori choice has to be made on the exact crystalline phase of the film material to arrive at an assumed value of n_1 For example in the case of very thin SiO_2 film on silicon, a choice has to be made on the exact polymorphic phase of SiO_2 i e whether it is of vitreous silica form or of α-quartz, or cristoballite, etc

Of course, all these difficulties encountered because of the presence of the film can be completely circumvented by carrying out measurements on truly "clean" surfaces in ultrahigh vacuum of the order 10^{-10} mmHg In this case it is possible to preserve the clean surface, obtained either by cleaving or after special treatment for several hours without essential contamination (Ref 10) This method is far from being used in practice, since other difficulties complicate the measurement such as, for example the problem of cleavage of the sample in a vacuum or the treatment of the surface leading to the removal of the surface film or the damaged surface layer Another major difficulty is the presence of the glass or silica windows in the high-vacuum system and their unavoidable strain bi-refringence in the optical path

The newly developed ellipsometric method can be used for the unique determination of all the four optical parameters n_2, k_2, n_1, and d_1 characterizing the system (absorbing substrate + nonabsorbing surface film) without making any assumptions about the nature of the substrate or the film This method utilizes the fact that the normal incidence reflectance of such a system, as computed from the pseudo-optical constants ($\bar{n}_2$-$i\bar{k}_2$) derived from ellipsometric measurements data (Δ and ψ), remains essentially constant at the true value for a small but finite range of film thicknesses This is demonstrated in Table 1 and Fig 1 for the case of silicon It may be recalled that these pseudo-optical constants are evaluated from the values of Δ and ψ, making use of the exact equations which are valid for "clean" surfaces i e , for the case $d_1 = 0$

Thus, by carrying out ellipsometric measurements on a freshly prepared sample as a function of time, a plot can be obtained of the variation of the normal incidence reflectance versus time (and hence versus film thickness in some arbitrary scale) By extrapolating this graph to zero time or film thickness, it is easy to obtain a value of normal incidence reflectance that will be close to the true value The exact value itself is obtained by a computer searching process to yield minimum disagreement between the various experimental ellipsometric parameters obtained on the same sample but with a number of different film thicknesses or with those obtained on the sample but with two or more different ambient atmospheres

Once the true value of the normal incidence reflectance R of the substrate material is known, n_2 and k_2 can have only certain mutually related values, given by the relation

$$R = \frac{[(n_2 - n_o)^2 + k_2^2]}{[(n_2 + n_o)^2 + k_2^2]} \qquad (1)$$

where n_o is the refractive index of the ambient medium In other words, once the time value of R is known, the number of unknown parameters is thus reduced from four (n_2 k_2, n_1, and d_1) to three

The next step is to scan with the help of a computer from all possible combinations of the various values of (1) n_1 (within the range of reasonable values) (2) d_1 (which in optical path retardation terms would be periodic and, hence, necessary to compute within only one cycle) and (3) n_2 (hence k_2 as well, since they are mutually related by Eq 1) to finally obtain the one unique combination of the values of n_1, d_1, and n_2 which

yields, on computation with the Drude's exact equations the ellipticity values Δ and ψ, which are in agreement with the experimentally observed values

This technique has been successfully applied at the Materials Research Laboratory to the case of silicon single crystals The final optical parameters obtained on cleaved samples of silicon for λ5461 Å are $n_2 = 4\ 14_0 \pm 0\ 02$ and $k_2 = 0\ 03_4 \pm 0\ 01$, as compared to the best reported values in the literature (Ref 7), $n_2 = 4\ 050$ and $k_2 = 0\ 028$ These latter values it should be mentioned, were obtained for the chemically polished samples and our own measurements on such chemically polished samples with the new technique yielded values $n_2 = 4\ 05_2$ and $k_2 = 0\ 02_9$ This indicates that optical studies on chemically polished samples cannot give values which are truly representative of the intrinsic material It should be pointed out in this connection that Fainshtein and Fistul (Ref 11) have shown that chemically polished samples usually have some trapped etchant materials on the surface

These ellipsometric studies of SiO_2 film on silicon were also corroborated (Ref 2) with studies on these same films by the electron microprobe technique By this procedure it was possible to characterize the surface film as SiO_2 and not silicon monoxide, SiO Further, a perfect linear relation was obtained between the intensity of the oxygen Kα radiation and the SiO_2 film thickness as determined by ellipsometry using the newly determined values of the optical constants of silicon, thereby indicating the reliability as well as the accuracy of the ellipsometric measurements

When the film thickness is very small (say less than 50 Å), the validity or justification of using the same value of the refractive index as that of the bulk SiO_2 is questionable An answer to this problem is provided by the variation of the ellipticity parameters Δ and ψ, as a function of thickness, in the early stages of formation of the film

In Fig 2, successive values of the experimentally determined values of Δ and ψ on a typical freshly cleaved sample of silicon are indicated by triangles marked 1 through 8 This observed positive slope can be explained only if the SiO_2 film is considered optically absorbing This will become evident from Fig 3 where computed values of Δ and ψ are plotted as a function of film thickness for different values of the optical constants of the film and substrate Such a positive slope of Δ-ψ curve was also noticed by Meyer and Bootsma (Ref 12), but these authors could not arrive at a satisfactory explanation of this behavior since they were using the erroneous values of the optical constants of the substrate silicon

Thus, from Figs 2 and 3, it can be concluded that very thin films (<50 Å) of SiO_2 on Si do exhibit pronounced optical absorption in the visible region of the spectrum — in fact, the absorption coefficient of the SiO_2 film can even be larger than that of silicon itself by almost an order of magnitude

III STUDIES ON OPTICAL ABSORPTION COEFFICIENT OF SILICON

With the ellipsometric method previously described, the real part n_2 of the complex refractive index of silicon could be determined with great precision by measurements on freshly cleaved samples However, the same studies showed that the corresponding results on the imaginary part of the refractive index, k_2 are far from satisfactory For example if the value of n_2 is altered from 4 1401 to 4 1402, then the value of k_2 must also be altered from 0 020 to 0 009 to satisfy a criterion of constancy of the reflectivity R In other words, in a weakly absorbing material like silicon, it is advisable to use the ellipsometric method only for determining the value of n_2 to determine the value of k_2, it is better to use the conventional direct method of optical absorption technique

A literature search revealed that the optical absorption of silicon has been studied by Dash and Newman (Ref 13) Braunstein, et al (Ref 14), and Runyan (Ref 15) However there is considerable disparity between the results obtained by these workers as will become evident later Since the principles and the technique involved in the direct measurement of optical absorption coefficients are well known, they will not be described in detail here Particular care and attention were devoted to avoid or minimize the errors due to nonuniformity of thickness scratches, pinholes, and other flaws in the specimen, noise in the optical and the detector electronic systems etc Significant improvement in the signal-to-noise ratio was also obtained by (1) the use of a phase-sensitive lock-in amplifier system and (2) by using two Bausch and Lomb grating monochromators in tandem to suppress the background level due to scattering After applying the various corrections for reflections at the various interfaces, the final results obtained are plotted in Fig 4

The room temperature data agree very well with those of Dash and Newman (Ref 13) The values obtained by Runyan (Ref 15) are slightly lower than ours At liquid nitrogen temperature (90°K) the agreement with the results of Dash and Newman (Ref 13) is good in the region 400-500 nm for larger wavelength, our values are higher Also, we did not observe the weak dip in K close to 2 4 eV (510 nm) at liquid nitrogen temperature as reported by Dash and Newman In the literature, this structure has not been observed by other workers as well, e g , the reflectance measurement at different angles of incidence (Ref 16) and high-sensitivity electroreflectance (Ref 17) The data of Braunstein et al (Ref 14), at room temperature are very close to ours and at liquid nitrogen temperature between the data of Dash and Newman (Ref 13) and ours These results (Ref 14) also do not show the dip close to the 2 4 eV, but since their last measurement is at 2 5 eV, this argument cannot have much weight

Further, the measurement at liquid helium temperature (about 9°K) does not show any

anomalous behavior of K at 2 4 eV The relative shift of K curves with temperature is the same as the shift of the indirect energy gap (at 1 1 eV) as reported by McFarlane, et al (Ref 18), within the experimental error at 700 nm

IV STUDIES ON RADIATION DAMAGE

The effect of irradiation of 6-MeV protons on the optical properties of intrinsic silicon was studied by two different methods (1) ellipsometry to measure any changes in the real and imaginary components of the refractive index of silicon and (2) direct measurement of the change in reflectivity of silicon by a sensitive modulation technique The results obtained on both these studies are given below

A Ellipsometric Studies

Five samples of intrinsic Si were cleaved along the (111) plane by the Gobeli-Allen technique (Ref 19) to give optically plane areas of several square millimeters each Each sample was then thermally oxidized for a different length of time at 950°C to yield a range of SiO_2 surface film thicknesses from 34 to 3840 Å

The ellipsometric parameters Δ and ψ of each sample were measured prior to the insertion of the sample into a custom-fitted holder for proton irradiation The ellipsometric parameters were again measured after exposure to 6-MeV protons at a fluence of 10^{16} particles/cm^2 This maximum specified fluence and energy were chosen for this series to first determine the maximum effect on the optical constants During irradiation, particular care was taken to prevent excessive heating of the specimen by irradiating them at low dosage rate as well as to have the specimen holder cooled by running water during irradiation The results of this series of measurements are presented in Table 2 The ellipsometric parameters Δ and ψ are determined by the index of refraction and thickness of the surface film and by the optical constants of the substrate material No change in Δ and ψ was observed which could have been caused by a change in the optical constants of the substrate The only observable change was due to a change in SiO_2 film thickness the magnitude of which is dependent on the degree of heating during irradiation

Therefore, it can be concluded that 6-MeV protons of fluence 10^{16} particles/cm^2 are not sufficient to cause a change in the substrate optical constants as determined by reflection-type optical measurements

B Reflectivity Measurements

For the measurement of small changes of reflectivity R caused by radiation damage, a simple experiment based on modulation technique was designed A sample of Si of circular cross section was first mechanically and later chemically polished by the standard procedure Later during irradiation, two diagonally opposite quadrants of the sample were masked off with absorbers For the measurement of the change in R, the sample was mounted in a rotating holder (ω = 26 Hz) and a narrow pencil of light reflected from a quadrant of the sample was detected by a photomultiplier coupled appropriately to a lock-in amplifier The experimental arrangement was similar to that used for the measurement of absorption The ac signal was proportional to the difference in the reflectance of irradiated and unirradiated parts of the sample The limiting sensitivity of the method was determined by the mechanical vibrations which caused moving of the light spot on the inhomogeneous photocathode, this spurious signal was about 0 1% The energy of protons was 6 MeV, fluence 10^{16} proton/cm^2 The measurement of reflectance in the energy interval 1-5 eV gave only negative results — the change in reflectivity was smaller than 10^{-3}, which is the limit of this method and experimental arrangement

V CONCLUSIONS

Reliable values of both the real and imaginary parts of the complex refractive index of intrinsic silicon have now been obtained Irradiation with 6-MeV protons to fluences of 10^{16} particles/cm^2 does not produce any noticeable changes in the optical properties of silicon within the limits of experimental error, as can be detected by techniques based on reflection

These studies form the basis for comparison with similar studies that should be carried out on highly doped silicon of the type used in silicon solar cell fabrication Again, the effect of lithium diffusion, which is known to affect the reflectivity of the material, should be investigated along similar lines Effect of irradiation with electrons on the optical properties of silicon and doped silicon, though not carried out in the present work for want of irradiation facilities, should be studied Only then will we be able to understand the origin of the degradation properties of silicon solar cells on irradiation and possibly develop ways and means to overcome them

ACKNOWLEDGMENTS

This research work was supported partly by JPL under Contract No 952385 and by NASA under Grant No NGR-39-009-042 The author wishes to express his sincere thanks to his colleagues, F Lukes, E Schmidt, W H Knausenberger, and S So for carrying out some of the measurements and for many useful discussions

REFERENCES

1 Vedam, K Knausenberger, W H , and Lukes, F , J Opt Soc Am , Vol 59, p 64, 1969

2 Knausenberger, W H , Vedam, K , White, E W , and Zeigler, W , Appl Phys Let , Vol 14, p 43, 1969

3 Drude, P , Ann Physik , Vol 272, pp 532, 865, 1889, Vol 275, p 481, 1890

4 Saxena, A N , J Opt Soc Am , Vol 55, p 1061, 1965

5 Lukes, F , Knausenberger, W H , and Vedam, K , Surface Sci , Vol 16, p 112, 1969

6 McCrackin, F L , and Colson, J P , Proc Symposium on Ellipsometry in the Measurement of Surfaces and Thin Films, ed Passaglia, E Stromberg, R R , and Kruger, J , NBS Misc Pub No 256, 1964, p 61

7 Archer R J J Opt Soc Am , Vol 52, p 970, 1962

8 Burge D K , and Bennett, H E , J Opt Soc Am , Vol 54, p 1428, 1964

9 Vedam, K , Rai R , Lukes, F , and Srinivasan R J Opt Soc Am Vol 58, p 528, 1968

10 Archer, R J , Proc Symposium on Ellipsometry in the Measurement of Surfaces and Thin Films, ed Passaglia, E , Stromberg, R R , and Kruger, J , NBS Misc Pub No 256 1964, p 255

11 Fainshtein, S M , and Fistul, V I , Sov Phys -Tech Phys , Vol 1, p 2009, 1957

12 Meyer, F , and Bootsma G , Surf Sci , Vol 16, p 221, 1969

13 Dash, W C , and Newman R Phys Rev , Vol 99, p 1151, 1955

14 Braunstein, R Moore A R , and Herman, F , Phys Rev Vol 109 p 695, 1958

15 Runyan, W R , Final Report, NASA Grant NGR 44-007-016, Materials Research Laboratory The Pennsylvania State University, University Park Pa

16 Schmidt, E , J Opt Soc Am , Vol 58 p 1561, 1968

17 Seraphin, B O , "Electroreflectance," to be published in Semiconductors and Semimetals, ed Willardson, R K , and Beer, A , Vol VI, Academic Press N Y

18 McFarlane, G G , McLean, T P , Quarrington, J E , and Roberts, V , Phys Rev , Vol 111, p 1245, 1958

19 Gobeli, G W , and Allen F G , J Phys Chem Sol , Vol 14, p 23, 1960, Phys Rev Vol 127 p 149, 1962

Table 1 $Si - SiO_2$ system[a]

d_1, Å	δ, °	Δ, °	ψ, °	$\bar{n}_2$	$\bar{k}_2$	$\bar{R}$
0 0	0 0	179 04	11 763	4 0500	0 0280	0 36479
1 00	0 07	178 73	11 764	4 0498	0 0370	0 36479
2 00	0 15	178 42	11 765	4 0496	0 461	0 36479
5 00	0 37	177 49	11 769	4 0488	0 0731	0 36478
10 00	0 74	175 94	11 781	4 0465	0 1182	0 36478
15 00	1 11	174 40	11 798	4 0431	0 1632	0 36478
20 00	1 47	172 86	11 821	4 0387	0 2080	0 36478
25 00	1 84	171 32	11 850	4 0332	0 2526	0 36478
35 00	2 58	168 28	11 923	4 0192	0 3413	0 36477
50 00	3 68	163 79	12 073	3 9905	0 4721	0 36477
75 00	5 53	156 57	12 424	3 9235	0 6823	0 36478
100 00	7 37	149 76	12 889	3 8347	0 8795	0 36480
125 00	9 21	143 43	13 453	3 7274	1 0611	0 36485
150 00	11 05	137 58	14 099	3 6050	1 2250	0 36494
200 00	14 73	127 30	15 580	3 3292	1 4965	0 36531
250 00	18 42	118 69	17 226	3 0336	1 6946	0 36607
300 00	22 10	111 47	18 961	2 7385	1 8280	0 36747
400 00	29 46	100 17	22 516	2 1951	1 9517	0 37362
500 00	36 83	91 99	26 063	1 7366	1 9653	0 38806
1000 00	73 66	85 12	52 853	0 7023	2 1052	0 61673

[a]Calculated values of Δ and ψ for various thicknesses of film of refractive index 1 460 on a substrate of refractive index n_2 = 4 050 and k_2 = 0 028 The value $\bar{n}_2$, $\bar{k}_2$, and R computed from these Δ and ψ are also given

Table 2 Ellipsometric parameters before and after irradiation

Sample No	Before irradiation		After irradiation		Changes observed as result of irradiation
	Δ, °	ψ, °	Δ °	ψ, °	
RD-1	165 39	12 24	161 02	12 32	Film thickness increased from 53 to 62 Å, no observable change in the optical constants
RD-2	169 12	11 86	168 47	11 96	Film thickness increased from 34 to 36 Å, no change in the optical constants was observed
RD-4	272 54	57 95	274 16	54 79	Film thickness increased from 3840 to 3865 Å, again no observable change in the Si substrate optical constants
RD-5	113 78	18 23	107 85	19 84	Film thickness increased from 278 to 323 Å, no observable change in the substrate optical constants
RD-6	88 00	28 48	87 00	29 13	SiO_2 film increased in thickness from 566 to 585 Å, no change observed in substrate optical constants

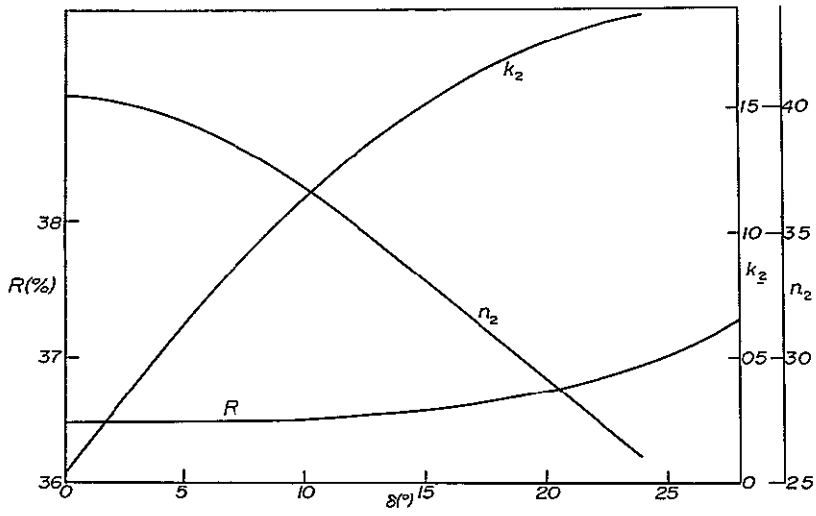

Fig 1 Si-SiO_2 system--variation of the pseudo-optical constants $\bar{n}_2$ and $\bar{k}_2$ of silicon and normal incidence reflectivity R as a function of δ (and hence the film thickness d_1) The initial parameters assumed are n_2 = 4 050, k_2 = 0 028, n_1 = 1 460, ϕ = 70°, and λ = 5461 Å

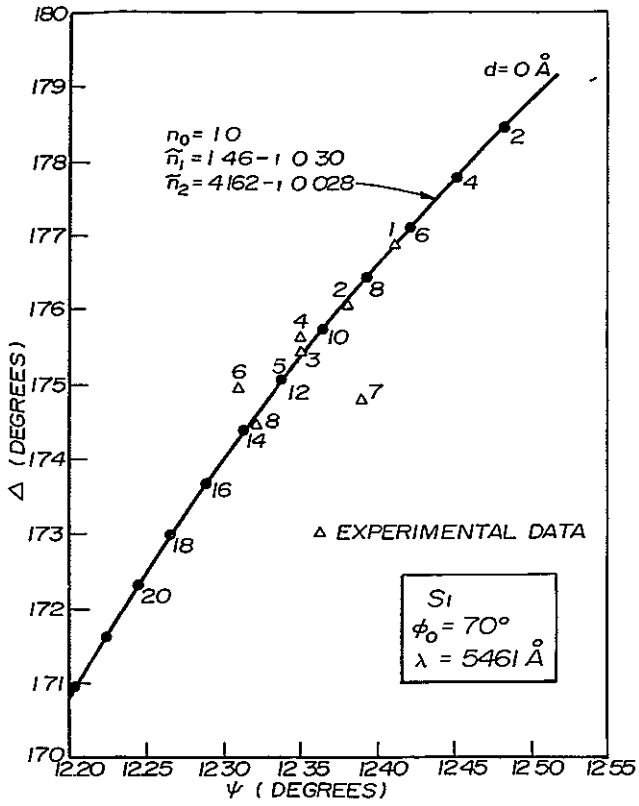

Fig 2 $Si-SiO_2$ system--variation of the ellipticity parameters Δ and ψ as a function of film thickness

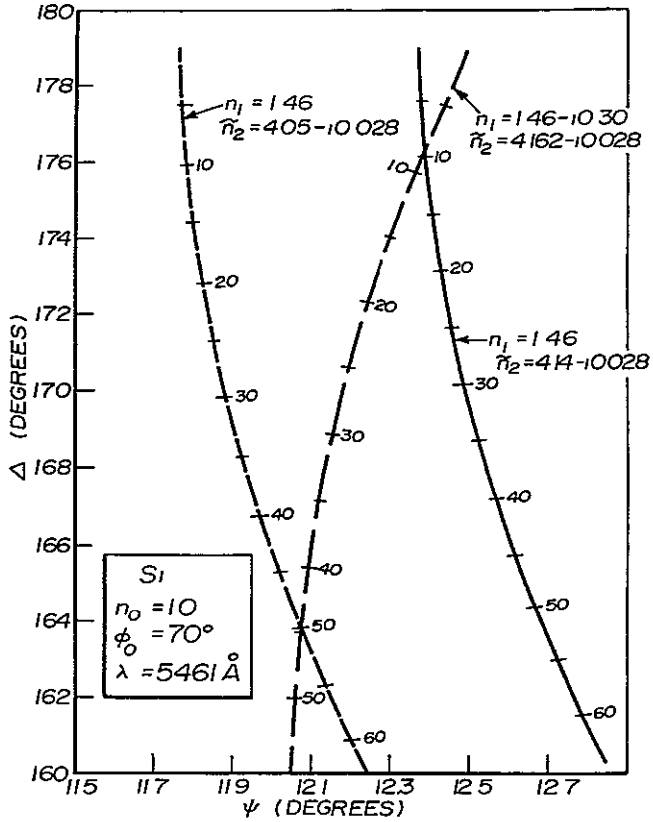

Fig 3 $Si-SiO_2$ system--variation of Δ and ψ as a function of film thickness for various possible values of the optical constants of the substrate and film

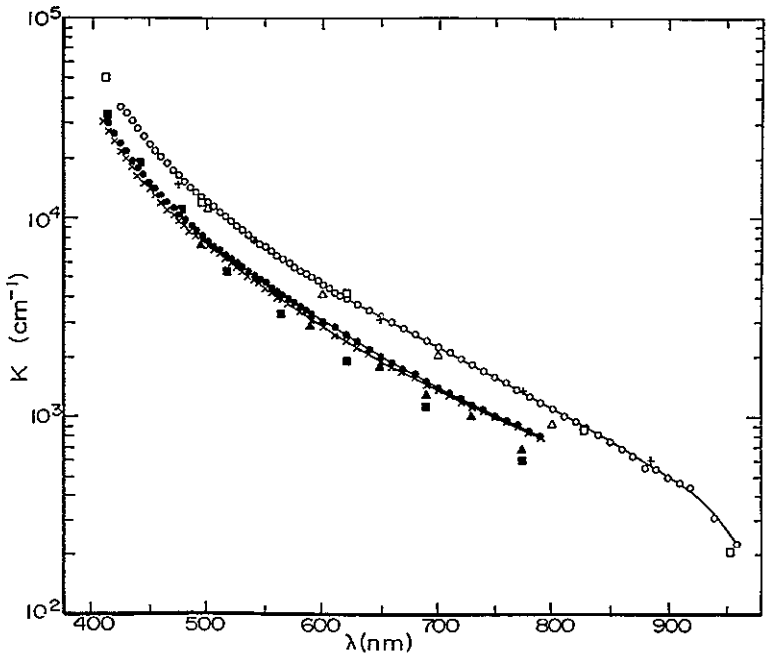

Fig 4 Absorption coefficient of silicon vs wavelength

EFFECTS OF SUB-THRESHOLD HIGH-ENERGY ELECTRONS ON THE PROPERTIES OF SILICON PHOTOVOLTAIC CELLS

E E Crisman and J J Loferski
Division of Engineering, Brown University,
Providence, RI

ABSTRACT

The possible effects on the electronic properties of Li-doped Si photovoltaic cells of irradiation by electrons whose energy is below that required to displace Si atoms are considered Such electron irradiation can produce changes in surface recombination velocity s They can also displace Li atoms because the atomic weights of Li atoms are 6 and 7, while those of Si are 28 and 29 Experimental procedures for observing the surface and bulk effects are described The results of the experiments designed to determine whether bulk effects are associated with Li atom displacements are presented It is concluded that Li atom displacement effects have been observed and that the displacement leads to a reduction in bulk lifetime It is suggested that the electron irradiation is dislodging Li from complexes in which Li had neutralized a defect existing in Si as a natural result of events involved in the fabrication of Li-doped Si solar cells

I INTRODUCTION

The purpose of this investigation was to study the effects of sub-threshold energy electrons on the properties of silicon photovoltaic cells, especially silicon cells doped with lithium Sub-threshold electrons are defined as electrons whose energies are below the minimum or threshold energy E_{th} required to produce observable changes in the electronic properties of photovoltaic cells by displacement of the host lattice (Si) atoms It is commonly assumed that E_{th} in Si is 145 keV

The changes in electronic properties produced in silicon photovoltaic cells by irradiation with electrons whose energies exceed E_{th} are always deleterious They lead to a reduction of power output capability of photovoltaic cells As is well known, these changes can be directly related to the displacement of Si atoms and the subsequent formation of complexes involving the vacancy and traces of impurity atoms present in the Si crystal

II SURFACE EFFECTS AND SUB-THRESHOLD ENERGY ELECTRONS

In addition to displacing Si atoms, electrons with energy in excess of E_{th} can also produce changes in the state of the surface which, in turn, can lead to changes in the surface recombination velocity, s, and properties related to s Similar changes can be produced by sub-threshold electrons and, therefore, the surface effects can be studied independently of the bulk effects by concentrating on the effects of sub-threshold energy electrons on the electronic properties of Si cells

The changes produced in surface recombination velocity can be transient or permanent By transient changes we mean that a new value of s is maintained only during the time of irradiation By permanent effects we mean changes in s which persist for long periods (days or weeks) after irradiation

A change in s can be attributed to changes in the populations of fast or slow states in the surface region of the Si cell (see Fig 1) Slow states are associated with the atoms adsorbed on the outer surface of the oxide layer on the Si surface or with atoms, or trapped charges, within this oxide layer The slow states determine the value of the surface potential ϕ_S The value of ϕ_S establishes the position of the Fermi level at the surface which, in turn determines the occupancy of the fast states The fast states are physically located at the interface between the silicon and its oxide These fast states are analogous to bulk recombination centers and are characterized by a minority carrier capture cross section and by the energy difference between the fast state energy and the edge of the conduction band

Electron irradiation can change s in a number of ways It can change the surface potential by changing the nature or number of atoms adsorbed on the oxide surface The electron-irradiation-produced ionization could lead to changes in the density of charges trapped in the oxide layer Electron irradiation can also cause displacements in the oxide layer and this would alter the population of oxide trapping centers Such changes in ϕ_S could be either transient or permanent

Electron irradiation can produce permanent changes in the surface recombination velocity s by changing the population of fast states at the Si-oxide interface This could result from displacements and/or rearrangements of atoms at the oxide-silicon interface

One of the purposes of this investigation was to explore the nature of electron radiation-induced changes in surface recombination properties for silicon solar cells containing lithium and for lithium-free cells

III BULK EFFECTS OF SUB-THRESHOLD ENERGY ELECTRONS

It can be shown that if an atom is bound to its site in the lattice with a minimum energy T_m then an electron experiencing an elastic collision with such an atom can displace it, provided the electron's energy exceeds a threshold value E_{th} given by the relation

$$T_m = \frac{2\left(E_{th} + 2\,mc^2\right)E_{th}}{Mc^2} \qquad (1)$$

where

m = the electron mass

M = the mass of the displaced atom

c = the velocity of light

The threshold energy for displacement of Si is 13.5 keV (Ref 1)

If a Li atom were bound to a site in the lattice with the same T_m as Si (~13 eV), then substitution in Eq (1) leads to the conclusion that it could be displaced by an electron with energy E_{th} = ~30 keV The Li atom may be bound more weakly than a Si atom at a lattice site and, therefore, it would be displaced by electrons of even lower energy

It should, however, be quite difficult to observe changes in bulk properties caused by displacement of Li ions because the concentration of Li is small compared to the concentration of host lattice Si atoms In Li-doped solar cell, the Li concentration in the base is such that there is one Li ion for 10^5 to 10^7 Si atoms The technique employed to measure changes in solar cell properties would have to be extremely sensitive if the effects of Li displacements are to be observed

If effects associated with Li displacement could be observed, they would elucidate the self-annealing mechanism of radiation damage in Li-doped silicon

IV EXPERIMENTAL PROCEDURES

A Surface Effects

In earlier work at Brown University (Ref 2), a method for studying surface effects of electron irradiation was developed and used to study the effects of electron irradiation on silicon surfaces The basic idea underlying the experiment is that the short-circuit current I_{sc} of an illuminated photovoltaic cell is a function of the surface recombination velocity s For the particular case when the cell is illuminated by very strongly absorbed light, i e , when $\alpha\ell >> 1$ where α is the optical absorption constant and ℓ is the distance between the surface on which the light is incident and the junction, and when the minority carrier diffusion length L is much greater than ℓ, it can be shown (Ref 2) that

$$\frac{1}{I_{sc}} = As + B \qquad (2)$$

where both A and B are constants for a given cell In these previously described experiments, very substantial changes occurred in the values of s of Si photovoltaic cells Figure 3 shows how the normalized value of I_{sc} (for illumination with light for which $\alpha\ell >> 1$) changes with fluence in the case of an N/P cell while Fig 4 shows similar data for a P/N cell Based on such data it has been estimated that the changes in s required to explain data such as those shown in Figs 3 and 4 would result in a change of as much as 10% in I_{sc} if illumination were AMO sunlight It should be noted that the surface effect causes an increase in I_{sc} of an N/P cell

The experiments, such as those which yielded the results shown in Figs 3 and 4, were performed with the cell in a vacuum produced by the oil diffusion pumps and nitrogen traps of the Van de Graaff accelerator which served as the

electron source These experiments left open the possibility that the effects shown in Figs 3 and 4 resulted from the interaction of the electrons residual organic vapors from the vacuum system and the silicon surface Elimination of this possibility requires that the experiments be repeated in an organic vapor-free high vacuum

With this goal in mind, an organic vapor-free high-vacuum chamber was designed and constructed for pumping by sorption and ion pumps The chamber is fitted with a 0 00015-in -thick Ni foil window that will admit electrons to the irradiations chamber and with a quartz window to allow illumination of the cell in the high-vacuum chamber The samples are mounted on the cold finger of a liquid nitrogen container so that the experiments can be conducted at low temperatures The system has been vacuum-tested, it attained a vacuum better than 10^{-8} torr on first pumpdown

B Bulk Effects

The short-circuit current produced by the absorption of penetrating ionizing radiation is a very strong function of the minority carrier diffusion length in the bulk material In our experiments the electrons bombarding the specimen served as such ionizing radiation If the beam energy (and, therefore, the range of the electrons) is kept constant, the short-circuit current I_{SC} will be proportional to the electron beam current I_B If a way to measure the ratio I_{SC}/I_B very accurately were devised, then even if I_B were to change (as can happen in any Van de Graaf machine) it becomes possible to follow very small changes in the diffusion length L and I_{SC} This goal was achieved by devising a circuit that allows the measurement of parts in a thousand changes in the ratio I_{SC}/I_B This system was used for all subsequent bulk effect experiments

In these experiments, the samples were standard Li-doped silicon photovoltaic cells (H1-31 through H1-40) manufactured by Heliotek and supplied by JPL The cells were made from crucible-grown silicon, had initial resistivity greater than 200 Ω-cm, were diffused 90 min at 425°C, were redistributed for 60 min at 425°C and were made with a paint-on Li source

The experiments were performed on samples mounted on a cold finger attached to a liquid nitrogen reservoir Because the experiments were performed at this low temperature, the displaced Li atoms could not diffuse around the Si lattice and, therefore, no self-annealing could occur nor could the Li return to the site from which it had been ejected

The cells were Cd-soldered to Al_2O_3 wafers which, in turn, were cemented with GE cement to the copper cold finger The cell was isolated from the ground of the irradiation chamber A precision resistor of a few ohms resistance was connected across the cell, the drop across this resistor was then proportional to I_{SC} One side of the sample was grounded through a resistor in series with an Elcor dc amplifier and integrator which provided an accurate measure of the total fluence delivered to the sample

The electron beam of Van de Graaf was scattered by electrostatic deflection plates so that the beam would cover an area at least as large as a cell (1 × 2 cm)

The experiments proceeded as follows The samples were exposed to electrons of a given energy until some pre-set fluence was attained Changes in the I_{SC}/I_B ratio were recorded throughout the irradiation period The values of I_{SC} and I_B were also monitored

The results of irradiations of three samples are presented in Table 1 Sample C1210B is an ordinary P/N solar cell, it does not contain Li This cell and one other ordinary P/N cell were studied to establish the sensitivity of the measurement system and to provide a basis for comparison with Li-doped cells The ordinary P/N cells were also supplied by Heliotek they were made from Si wafers whose initial resistivity was 1 Ω-cm

The following comments can be made regarding Table 1

(1) No changes have been observed in the I_{SC}/I_B ratio of ordinary P/N cells for electron beam energies less than 150 keV Slight changes have been observed in Li-doped Si cells at 100 and 125 keV

(2) For a given fluence at a specified energy, the fractional change in the I_{SC}/I_B ratio of the Li-doped cells was always larger than the fractional change in this ratio of an ordinary Si cell

From these data, it is hypothesized that the difference in behavior of Li-doped and Li-free Si irradiated by electrons whose energies are in the vicinity of the radiation damage, threshold energy results from the displacement of Li atoms Furthermore, it appears that the displacement of Li causes a reduction in I_{SC} and, therefore, in minority carrier diffusion length L A possible explanation for this behavior is that the displaced Li was part of a complex which had been neutralized by Li These complexes could be oxygen-vacancy pairs or phosphorus-vacancy pairs The vacancies are present in the Si as a natural result of the crystal growth process and also of the past annealing history of the specimen Lithium introduced into the Si lattice would neutralize such a complex for the same reason that it neutralizes the complexes produced by high-energy particle irradiation According to this hypothesis, subthreshold bulk effects involving Li atom displacements would depend strongly on the past thermal history of the cell and on its trace impurity content

V SUMMARY AND CONCLUSIONS

Radiation-induced changes in four P/N cells, three of which had a Li-doped base, were compared at energies in the vicinity of the radiation damage threshold The Li-doped cells experienced larger degradations per incident photon than the ordinary cell at all energies involved in this experiment (from 100 to 225 keV)

Electrons of 100 and 125 keV energy produced observable changes of this ratio in Li-doped cells,

whereas no change was observed at these energies in ordinary Si cells

An organic vapor-free, high-vacuum irradiation chamber has been designed, constructed, and tested The chamber is fitted with a thin metal window through which 100-keV electrons can enter the chamber and with a quartz window which allows sample illumination under high-vacuum conditions during irradiation This chamber was pumped with sorption and ion pumps and has attained a vacuum of 10^{-8} torr

REFERENCES

1 Flicker, H , Loferski, J J , and Scott-Monck, J Phys Rev , Vol 128, pp 2557-63, 1962

2 Loierski, J J , Giriat, W , Kasai, I , and Flicker, H , Proc Symposium on Effects of Radiation on Semiconductor Devices, Toulouse (France), June 1967

3 Kasai, I , M S Thesis, Brown University, Aug 1966 (This work was reported under NASA Grant NGR-40-002-026)

Table 1 Effects of electron irradiation on I_{sc}/I_B ratio for Li-doped and Li-free silicon solar cells

Sample No	Beam energy, E_B(keV)	Fluence el/cm^2 × 10^{-16}	Ratio I_{sc}/I_B		Fractional change, %
			Initial ×10^{-4}	Final, ×10^{-4}	
C1210B (No Li)	150	10 0	2 62	2 60	0 76
	175	2 0	3 01	2 97	1 32
	200	1 0	2 97	2 92	1 68
	225	0 5	2 92	2 33	20 20
H1-37 (Li-doped)	150	1 0	3 31	3 28	0 90
	150	10 0	3 54	3 42	3 38
	175	1 0	3 32	3 24	2 40
	200	0 7	2 71	2 42	10 70
	225	0 2	2 09	1 89	9 60
H1-34 (Li-doped)	125	9 0	5 53	5 46	1 26
	100	10 0	5 81	5 78	0 52
	100	10 0	5 15	5 15	0 00
	150[a]	10 0	4 96	4 90	1 20
	125[a]	7 0	5 01	4 98	0 59
	125[a]	10 0	4 99	4 93	1 20
	150[a]	10 0	4 99	4 78	4 20
	125[a]	8 0	5 02	4 87	2 98

[a]Showed initial improvement, then degraded Initial values are nearest maximum

Note These are successive runs in order of exposure to electrons Samples H1-34 and C1210B were both kept cold at liquid-N_2 temperature for all irradiations shown in the table No annealing was allowed to occur

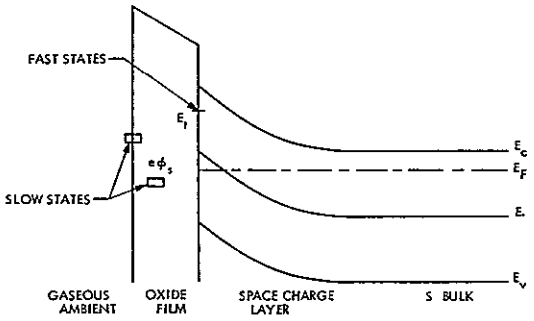

Fig 1 Energy band diagram for N-type Si surface

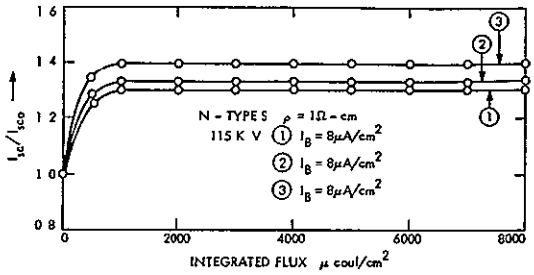

Fig 3 Normalized ratio I_{sc}/I_{sco} vs fluence of 115-keV electrons for 1-Ω-cm N-type Si surface N/P cell (after Kasai, Ref 3)

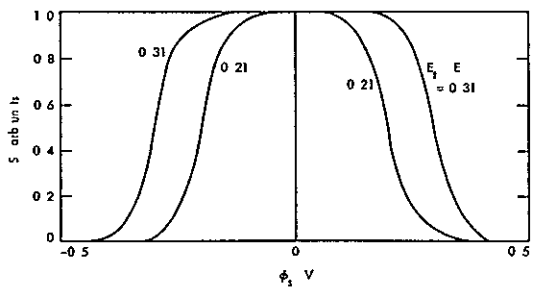

Fig 2 Surface recombination velocity s as a function of surface potential ϕ_S for two different values of the energy level associated with the fast states

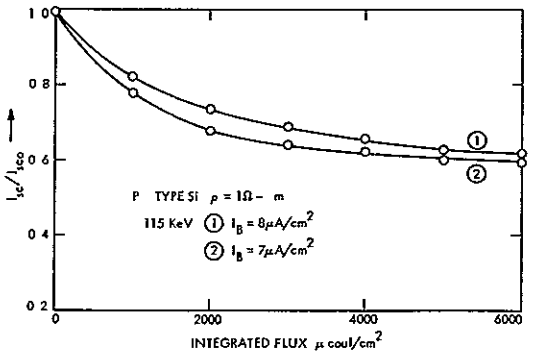

Fig 4 Normalized ratio I_{sc}/I_{sco} vs fluence of 115-keV electrons for 1-Ω-cm P-type Si (after Kasai, Ref 3)

STUDY OF RADIATION EFFECTS IN LITHIUM-DOPED SI USING INFRARED SPECTROSCOPY (1 - 50 μ) AND PHOTOCONDUCTIVITY (1 - 10 μ)

T Mortka and J C Corelli,
Rensselaer Polytechnic Institute, Troy, N Y

ABSTRACT

In this study, radiation defects were introduced by electrons of energy 1 5 and 5 MeV with some of the results obtained using 45-MeV electrons During irradiation, the sample temperature was kept at $\lesssim 320°K$ Infrared (IR) spectroscopy and photoconductivity (PC) measurements served as the probes to study the defects which had long-time stability since the measurements were made many hours after cessation of the irradiation The samples were cut from ingots that were either oxygen-lean [floating zone (FZ) $\lesssim 10^{16}$ oxygen/cm^3] or oxygen rich [crucible grown (CG) $\gtrsim 10^{17}$ oxygen/cm^3] The starting material was phosphorus-doped to resistivities $\gtrsim 10\ \Omega$-cm The lithium was diffused into varying concentrations in the 10^{15} cm^{-3} to 10^{17} cm^{-3} range The PC measurements reveal the presence of a localized energy level at E_c 0 62 eV which acts as an electron trap and is produced by radiation in all samples irrespective of oxygen content Lack of time has precluded detailed experiments on the dependence of the 0 62-eV level on electron energy, fluence, and Li impurity concentration Other levels which give rise to extrinsic PC due to defects are produced with predominant concentration and importance attributed to those levels greater than $\approx$0 20 eV below the conduction band edge The PC spectrum does not exhibit the presence of energy levels at E_c-0 54 eV and E_c-0 39 eV, which we have previously (Ref 1) shown to be identified with the di-vacancy defect in Si Additionally, strong effects of Li impurity atoms were observed on the 1 8-μ di-vacancy associated defect absorption band in which less of the 1 8-μ band is produced as the Li concentration is increased Detailed measurements of this effect have been reported recently (Ref 2) Thus, one obvious conclusion of this work is that both the PC and IR measurements show that the Li atoms act as efficient sinks for vacancies and di-vacancies by becoming attached to these defects and producing new complexes An absorption band at 9 9 μ, found only in oxygen-rich Li-doped Si, was also found in both irradiated and unirradiated material and changed with heat treatment after a 48-MeV electron irradiation to a fluence of 10^{18} e/cm^2 Recent results and improvements made to the experimental methods will be discussed herein

I INTRODUCTION

The program under discussion was a survey of electron radiation damage in Li-doped silicon in which the following parameters were varied

(1) The energy of the bombarding electrons (1 5, 5, and 45 MeV)

(2) The total electron fluence (10^{14}, 10^{15}, 10^{16} electrons/cm^2)

(3) The lithium concentration (10^{15}, 10^{16}, 10^{17} Li/cm^3)

(4) The type of silicon starting material (both FZ and CG, with phosphorus doping to both 1 Ω-cm and 10 Ω-cm)

The probes used were IR spectroscopy and IR PC

II EXPERIMENTAL METHODS

The lithium was diffused by the paint-on technique and the lithium concentration was monitored by four point-probe resistivity measurements Contacts for PC were put on with a miniature soldering iron

For the IR spectroscopy, three machines were used, a Perkin-Elmer Model 21 and a Spex grating monochromator for the 1 to 2 5-μ region, and a Perkin-Elmer Model 621 for the 2 5- to 50-μ region For the PC measurements, a modified Perkin-Elmer Model 12 and the apparatus shown in Fig 1 were used

Several serious problems were encountered The low total fluences specified did not damage the samples sufficiently to produce good PC signal-to-noise ratios with standard shielding techniques This necessitated construction of the solid shielding shown in Fig 1 The solid shielding was successful in decreasing the noise level

Another major problem was rectification after irradiation of contacts that were ohmic prior to irradiation Insufficient doping of the gold contact material was probably responsible for this problem, the problem was rectified by using a contact method developed by Dr Brucker and Mr Liebowitz at RCA

Another major problem encountered was mechanical difficulty with the fiduciary marker on the monochromator This made alignment of the sample response spectrum with the source spectrum difficult in some cases and impossible in others This defect has also been corrected

In addition to correcting the above defects, we have recently made our optical system purgeable, thereby eliminating regions of steep slope (water bands) where point-to-point alignment of sample and source spectra is extremely critical This has a significant effect on the magnitude of uncertainty in a measurement

III RESULTS

The IR results will be discussed first Figure 2 shows the presence of two new Li-associated bands at 1 4 and 1 7 μ as well as the diminution of the 1 8-μ di-vacancy band The 1 8-μ band can be clearly seen in the sample without lithium This indicates formation of the 1 4- and 1 7-μ bands at the expense of the 1 8-μ band

Figure 3 shows the effects of 15-min isochronal anneals at different temperatures First, the A-center band does not appear until after the 100°C anneal Secondly, the 9 9-μ band is completely annealed after the 130°C anneal The drastic effect of radiation upon this band is shown in Fig 4

Figure 4 shows that the annealing behavior of the 9 9-μ band is totally fluence- and energy-dependent

Figures 5, 6, and 7 indicate the type of results obtained before the previously mentioned corrections were made The following figures all show PC results

Figure 5 shows a sample spectrum which was not normalized with respect to source intensity However, knowledge of source spectrum shape allowed the identification of two levels, one at 0 61 eV and one at 0 45 eV The spectrum ends near 4 μ because, at this point, the signal-to-noise ratio equaled 1 The presence of signal out to this wavelength indicates a shallow level

Figure 6 shows a normalized spectrum with a structure (peak) found previously in P-type silicon A shallow level is indicated by the existence of signal past 6 μ

Figure 7 indicates a 0 61-eV level and a shallow level

Figures 8 and 9 show the results obtained after correcting the experimental difficulties These samples were given a total fluence sufficient to raise their 78°K resistance to approximately 10^7 Ω

Figure 8 shows many more levels than were indicated previously There is only a hint of a level at 0 61 eV and a level in the neighborhood of 0 2 eV is indicated

Figure 9 shows many levels and, again, there is an indication of a level around 0 2 eV

IV SUMMARY

Figure 10 summarizes the PC results JPL-11 and JPL-69 are the two samples for which experimental problems were solved The figure shows correlation with the IR bands at 1 4 μ (0 89 eV) and 1 7 μ (0 73 eV), as well as the absence of the 1 8-μ (0 42 eV) di-vacancy band in JPL-11 However, JPL-69 had less Li, and the presence of a 0 42-eV level in this sample does not contradict the infrared findings The 0 61-eV level occurs very frequently and it is intended to run a non-irradiated sample to see if this band is radiation-produced

No systematic variation of radiation damage with variation of experimental parameters was found This was probably due to the mobility of Li at the sample storage temperature and to the

delay between irradiation and measurement Lack of time prevented annealing studies

V CONCLUSIONS

There is a very drastic effect of radiation energy and total fluence upon the annealing behavior of the 9 9-μ band and the strength of the 1 8-μ di-vacancy band varies inversely with the lithium concentration, with 1 4- and 1 7-μ bands replacing the 1 8-μ band

In the future it is intended to do annealing studies of JPL-11 and JPL-69 as well as run an unirradiated sample to check the origin of the levels that have been found In addition, some 78°K irradiation is planned with subsequent annealing studies

REFERENCES

1 Kalma, A H , and Corelli, J C , Phys Rev , Vol 173, p 734, 1968

2 Young, R C , Westhead, J W , and Corelli, J C , J Appl Phys , Vol 40, p 271, 1968

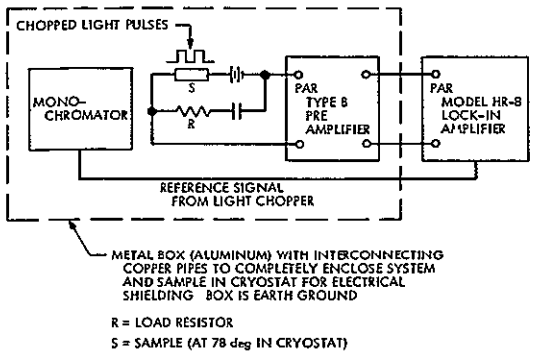

Fig 1 Block diagram of PC apparatus

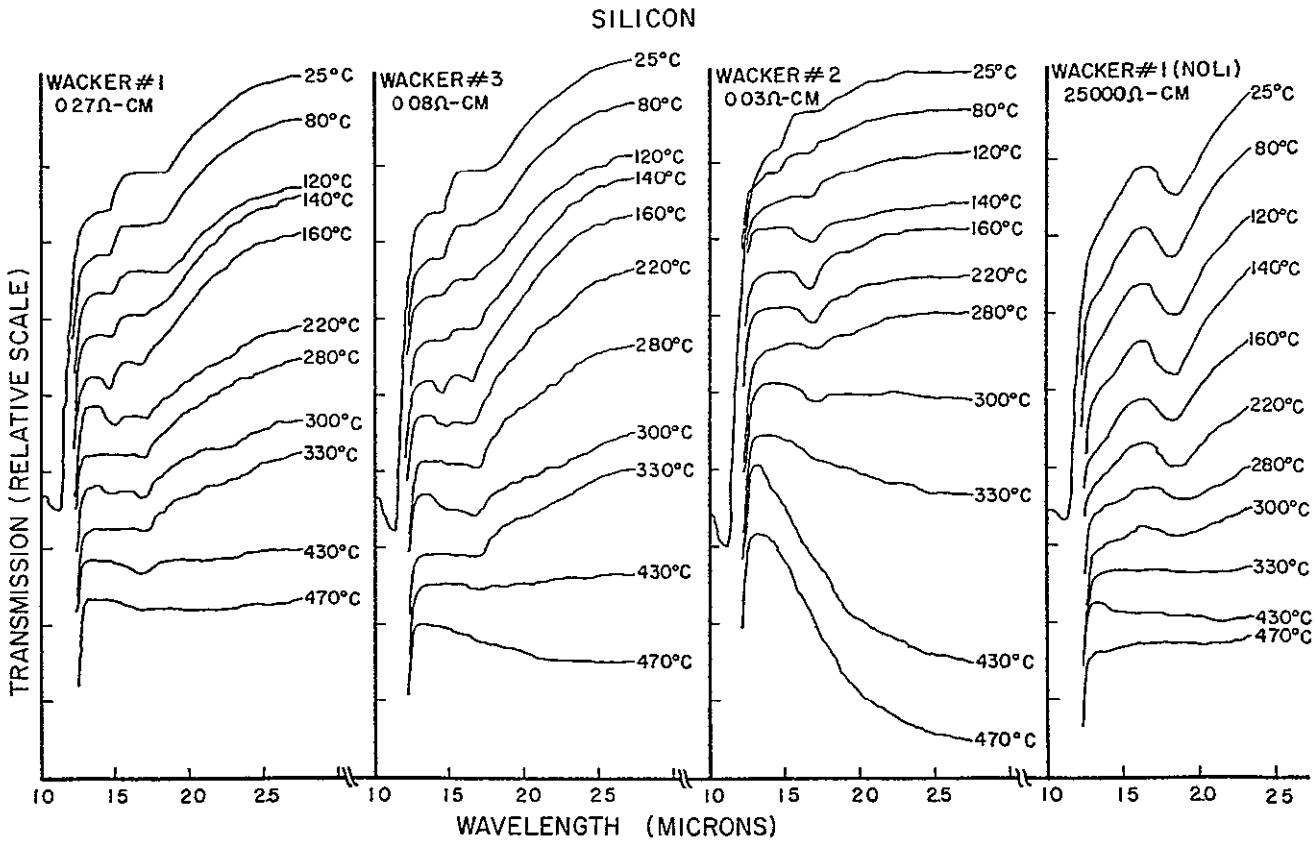

Fig 2 Wavelength vs transmission

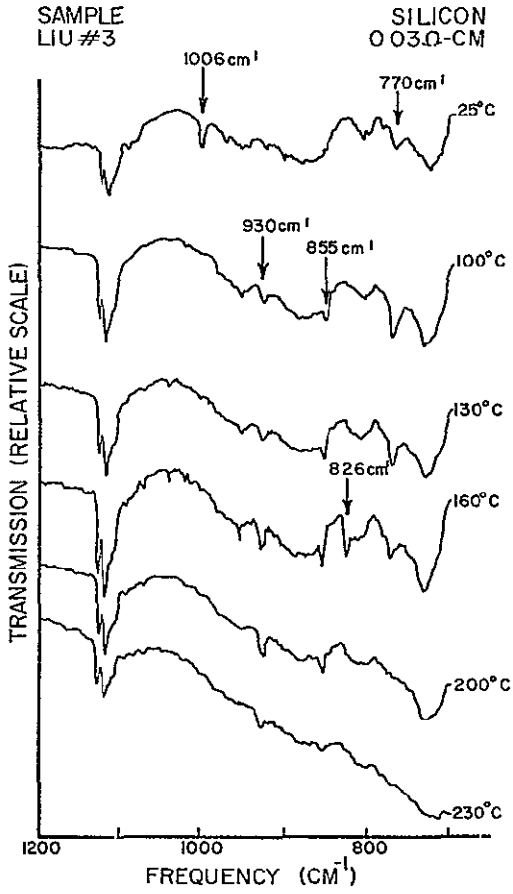

Fig 3 Effects of 15-min isochronal anneals

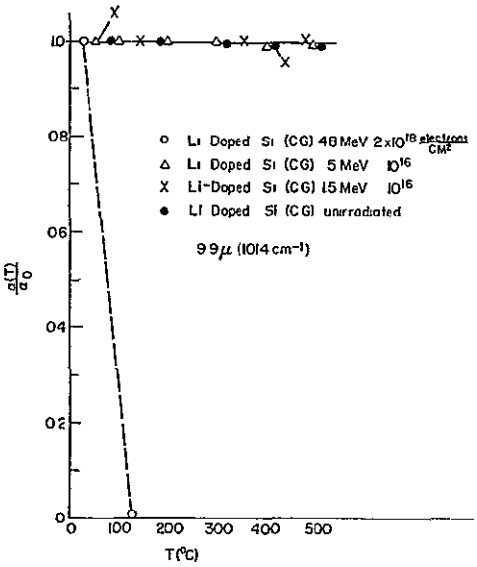

Fig 4 Effect of radiation on A center band

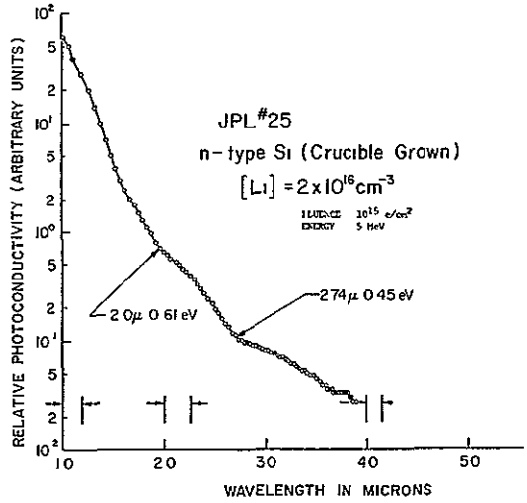

Fig 5 Wavelength vs relative PC, JPL 25 N-type Si (CG)

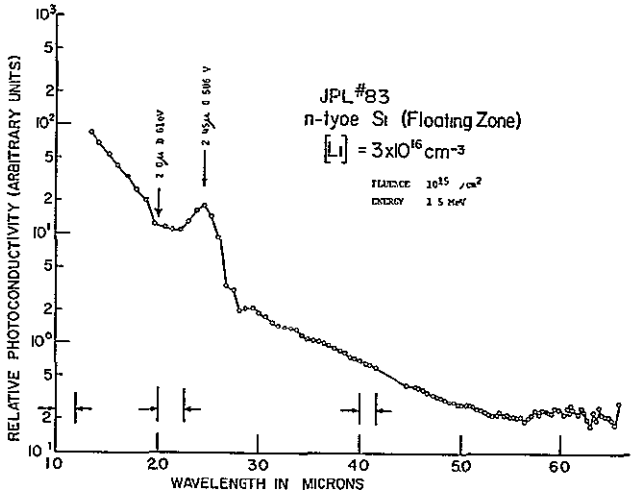

Fig 6 Wavelength vs relative PC, JPL 83, N-type Si (FZ)

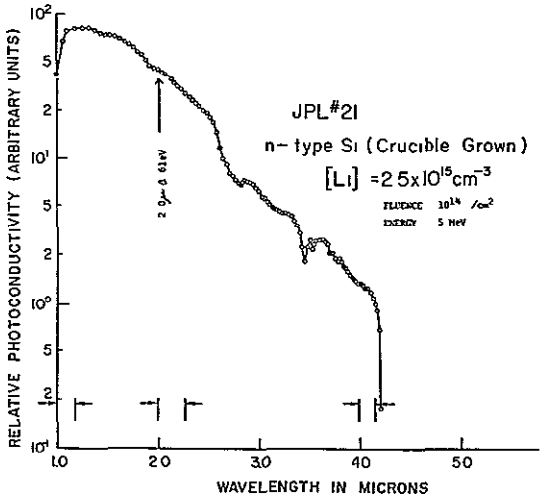

Fig 7 Wavelength vs relative PC, JPL 21 N-type Si (CG)

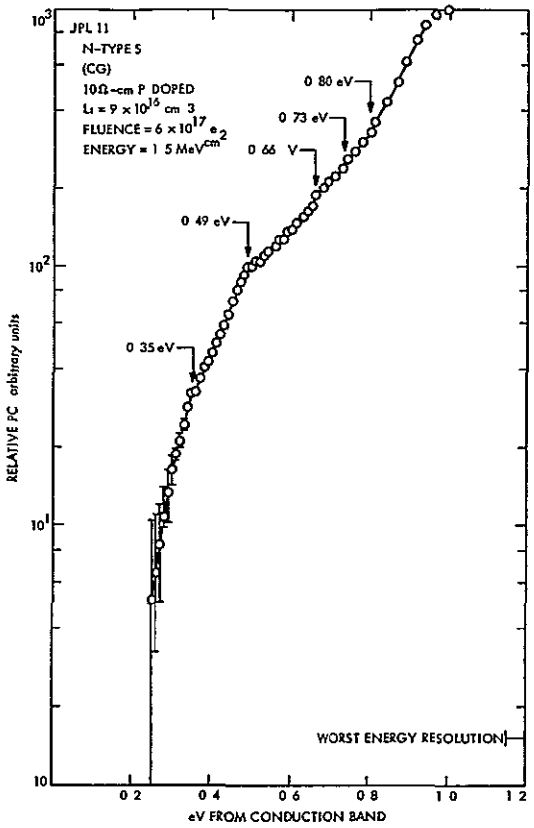

Fig 8 eV from conduction band vs relative PC, JPL 11 N-type Si (CG)

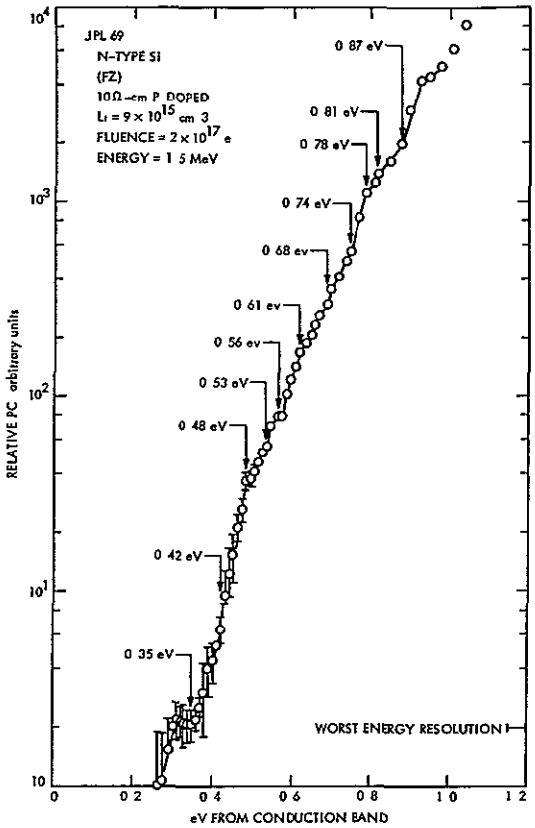

Fig 9 eV from conduction band vs relative PC, JPL 69 N-type Si (FZ)

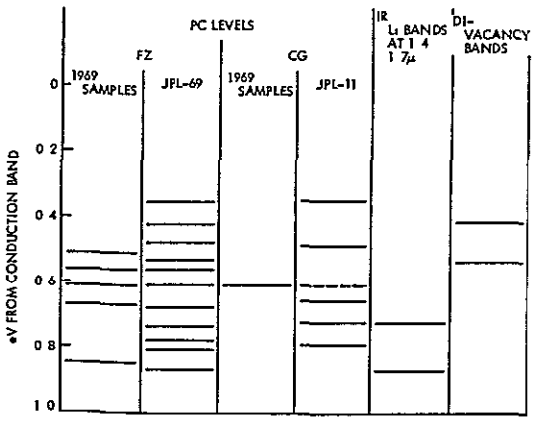

Fig 10 Summary of PC results

KINETICS IN SOLAR CELL DAMAGE

A Sosin
University of Utah

I INTRODUCTION

The degradation of minority carrier lifetime in Li-doped solar cells irradiated in a space environment is an important problem in aerospace technology It is also an interesting physics and materials problem to account for the manner of degradation, recovery, and redegradation

A complete understanding of these problems, with the technological goal of optimizing solar cell performance, requires investigation and appreciation at three levels The first level is the microscopic level in which, typically, the physical properties of irradiated Li-doped silicon are monitored This includes, among others, such measurements as carrier concentration or spin resonance, with varying parameters lithium concentration, oxygen concentration, temperature, fluence, etc At the other end of the line lies the macroscopic level — device investigations in which solar cells are used, rather than model materials Here, lifetime and diode characteristics are the major measurements, once again with some variation in the parameters listed above and, hopefully, with attention to diode fabrication procedures

Located between these extreme levels and overlapping both is the area of kinetics — the modeling and analysis of information required to weld observations at both the microscopic and macroscopic levels into a coherent unity Our work has its main thrust here

II DISCUSSION

Attention to kinetics by individual investigators has been increasing, but the earliest work in this area was performed by P H Fang and colleagues Probably the most notable example is the observation of solar cells irradiated by 1-MeV electrons at a common rate (3×10^{12} electrons $cm^{-2}\ s^{-1}$) to varying fluences 5×10^{13} to 1×10^{16} electrons cm^{-2} Short-circuit current, i, was measured at room temperature in these cells The time of irradiation was small or negligible compared to the annealing times Fang analyzed these data in two ways First he analyzed the initial rates of recovery which were apparently exponential

$$i_o - i_a \approx \exp(-t/\tau) \tag{1}$$

where

i_o = the initial short circuit before irradiation

i_a = the current at a time t during the anneal

The measure of annealing speed lies in τ Fang found τ to <u>increase</u> with fluence by an order in magnitude between 1×10^{14} and 3×10^{15} electrons/cm^{-2} If Eq (1) were a valid form to describe the entire recovery, its origin would probably be in first-order kinetics and one would expect τ to be independent of fluence, a pre-exponential factor might depend slightly on fluence, reflecting a varying number of jumps for process completion

Fang plotted these data in a more general manner, f versus $\ln t$ Here, the ordinate is the fraction of annealed defects defined as

$$f = \frac{i_a^{-2} - i_o^{-2}}{i_\Phi^{-2} - i_o^{-2}} \tag{2}$$

This definition follows if the usual assumptions are made that the minority carrier lifetime is proportional to the defect concentration, that the defect diffusion coefficient, diffusion length, and lifetime are given by

$$L^2 = Dt \tag{3}$$

and that the short-circuit current is proportional to L The term i_Φ is the short-circuit current following irradiation The conclusions from the more restricted approach are borne out in this latter method, too — the heavier the fluence, the later the recovery, even when measured on a normalized plot

Fang attempted to collect most common modes of recovery, treated on the basis of chemical rate theory, together with the expression

$$f = (1 + \lambda n_\Phi t)^{-1} \qquad (4)$$

Here n_Φ is the concentration of defects following irradiation and λ is a positive constant The latter is the case only for second-order reactions Equation (4) is either invalid for other situations or λ must be considered to be dependent on defect concentration, a course which limits the usefulness of such an expression However Fang found that such a dependence indeed obtains The dependence is started by a relation of the form

$$t(f = 0\ 5) = 74\ 5 \exp(2\ 86 \times 10^{-5} \Phi^{1/3}) \qquad (5)$$

A somewhat different equation was found to apply for the case of f = 0 1 — the pre-exponential changed from 74 5 to 5 06 × 10^{-2} and the number in the exponent changed from 2 86 to 2 73

In still another analysis, Fang introduced the concept of an activation energy which depends on defect concentration These concepts were suggested by Fang with the realization that they may have mainly empirical value, the physical meaning is difficult to comprehend since the defect concentrations involved in such experiments are so shallow that one would expect no sensible concentration dependences to enter

But the data of Fang et al , are so striking that we were asked to investigate the basis of these data and related kinetic data from a more physical basis In our work, we sought kinetic models that would be based on assumptions that seemed more realistic and would yield results which could be compared directly with experiment It has not been our intention, however to oversimplify the situation In fact we have been directed to the possibility that models based purely on chemical rate equations, with no regard for spatial dependences, may be seriously flawed from the beginning

Since this work did not include any experimental effort we were forced to use the available data obtained by other investigators The result of Fang and colleagues appeared to be the most appropriate for our purpose, at least until recently Accordingly we sought to accommodate these findings in a reaction rate model which appeared to be more physically real even though the formulation might involve a more complex initial point of departure (e g , a set of coupled differential equations) At the same time, we hoped to avoid the need to resort to highly complex, overly general treatments

Our attempts have not been successful, i e , we have not found a model which would account for Fang's observations, particularly the substantial decrease in annealing speed with increasing fluence

We have, therefore concluded that it is necessary to put aside the data of Fang and colleagues in deference to more recent observations In doing so, we are implicitly adopting a position that we will be able to explain Fang's data eventually, starting at a different origin, or that some inconsistency in these data will be discovered or reported in the future

The importance of a feasible model cannot be overemphasized We have assembled analytical-computer capabilities which we can bring to bear in chemical rate or diffusional problems which would permit a full exploration in an optimal manner By optimal, we mean that analysis could be placed at the disposal of all NASA investigators with access to computer processing Examples, which show the substantial capabilities of the use of these techniques in a parallel problem in metals, were shown in our oral presentation

In our opinion the central problem to the unraveling of kinetics in solar cells lies in the assembly of a body of experimental data derived in studies directed specifically to this problem Studies of damage and annealing in appropriately doped silicon are needed first A range of parameters — dopant concentration, defect concentration or fluence temperature of irradiation and anneal, etc — are needed The use of ~1-MeV electrons for bombardment is probably best, a range of electron energies might be useful Those properties which can be measured sensitively and essentially continuously, such as Hall coefficient and conductivity, are best for kinetics studies (but the information from ESR, for example, is most instructive for broad guidance)

A parallel effort in solar cell configuration is, of course, in order These cells should be characterized as well as possible Short-circuit current is generally an excellent monitor for kinetic studies, although the dependence on injection level and the effects of strain fields and fabrication variables lend a degree of uncertainty Collateral capacitance studies are recommended

III CONCLUSION

It is proposed that a substantial effort in kinetics — directed particularly to kinetics — should be initiated Without such an effort, the solution of kinetics may be impossible or, certainly, difficult Without an understanding of kinetics, a firm understanding of radiation effects in Li-diffused solar cells will probably not be achieved

30

DESCRIPTION OF LOW-RATE SPECTRAL ELECTRON IRRADIATION PROGRAM

D L Reynard
Philco-Ford Corporation,
Western Development Laboratories,
Palo Alto, Calif

I INTRODUCTION

Silicon solar cells diffused with lithium have the unique property of spontaneously recovering from radiation-induced damage This recovery phenomenon is primarily dependent upon temperature and the amount of lithium available within the bulk material (Ref 1) Furthermore the rate of recovery is independent of the damage rate (Ref 2) Irradiation experiments (Refs 3 and 4) with lithium cells have typically involved the use of a Van de Graaff accelerator (at flux rates as much as five orders of magnitude higher than those expected in space) and a post-irradiation period of observation of the annealing phenomena The results of such experiments are subject to much interpretation and skepticism because the attendant lithium atom availability is not the same as it would be with a slower damage introduction rate Because of these limitations, it is desirable to conduct an experimental program to irradiate lithium cells at the same rate as is expected in a typical space environment so that a direct observation of net damage can be obtained

Several years ago, it was observed that Sr 90 possessed spectral characteristics which closely approximated the trapped electron spectrum in earth orbital situations (Ref 5) Furthermore, the electron flux rate emitted by Sr 90 was such that small amounts of the isotope could be conveniently used to irradiate a fairly large sample area at typical earth orbit average rates Early experiments (Ref 5) used Sr 90 to evaluate the thermal/optical properties of spacecraft thermal control materials optical surfaces, and conventional solar cell/cover composites Therefore, Sr 90 appeared attractive for the irradiation of lithium solar cells at real-time rates so that time-dependent uncertainties were eliminated Also, Sr 90 produces a realistic spectrum of electrons which could conceivably yield results different from those obtained with a monoenergetic (accelerator) source of electrons

The NASA's Goddard Space Flight Center sponsored two programs (1967 and 1968) for the Sr 90 irradiation of lithium solar cells These programs (Refs 6 and 7), performed by Philco-Ford and Lockheed-Georgia, provided the first real-time degradation data for lithium cells as well as the first direct comparison of different lithium cell types While many qualitative conclusions (Ref 8) were reached as a result of these programs, the data produced were less than desirable for several reasons Sample characteristics (manufacturing processes, materials, etc) were not adequately defined or recorded For the most part, only one sample of each cell type was irradiated at each temperature Diffusion pump vacuum systems were used with the attendant uncertainty of contamination effects Solar cell characteristics measurements were made primarily with tungsten light sources employing questionable calibration techniques

II OBJECTIVES AND REQUIREMENTS

The program described herein has the general objective of updating knowledge of lithium cell

degradation characteristics with a substantial improvement of experimental technique over those of previous efforts Specifically the objectives of the program are

(1) Evaluate lithium cells which represent the most recent state of development of such cells

(2) Expose approximately 100 of these cells to a 6-month period of Sr 90 irradiation in a combined vacuum-temperature-illumination environment

(3) The irradiation is to represent a typical earth orbital average flux rate and electron spectrum

(4) A high-quality solar simulator is to be used for all cell measurements

(5) An ion pump vacuum system will be used for the environmental chamber

(6) The equivalence of 1-MeV accelerator data to real-time data will be studied

(7) Cell temperatures will be -50, 20, 50 and 80°C These represent a typical range of operating temperatures (+20 to +80°C) and a temperature where lithium atom mobility is extremely low (-50°C)

(8) All cells (with the exception of one group) will be illuminated during the exposure and loaded to a point near the maximum power point One group will be kept shaded during the irradiation and will be left in the open-circuit condition

III ISOTOPE CHARACTERISTICS AND SOURCE CONTAINER

Strontium 90 was selected for simulation of the trapped electron environment because the smoothed composite spectrum of Sr 90 and its daughter Y 90, closely approximates the spectrum of the trapped electron belt to approximately 2 MeV Thus Sr 90 serves as a close approximation to the natural environment at those altitudes where the electron species are dominant in terms of producing solar cell damage This tends to be valid for most orbital altitudes with the exception of those from approximately 1500 to 3000 nm where the trapped high-energy proton belt is more effective in producing cell damage than are trapped electrons The radioisotope spectrum is shown in comparison with the 18, 000-nm trapped electron spectrum in Fig 1 Curves for other orbital altitudes have an equivalent degree of similarity

The curve in the right portion of Fig 1 shows the anticipated range of electron flux rates as a function of orbital altitude Measured data are shown for a period of relative solar quiet (1964) and calculated data for a period of relatively high solar activity (1968) The increase in electron flux rate in the 6000- to 12, 000-nm range during the 1968 period is due to a compression of the trapped electron belt at these altitudes because of the influence of higher solar activity on the fringes of the earth's magnetosphere

The isotope source used for this experiment produces a spectrum which is equivalent to 10^{12} electrons/cm^2/day in terms of 1-MeV electron damage to conventional N/P solar cells This level of activity was chosen because it represents an upper bound on typical earth orbit damage rates This rate results in a loss of approximately 20% of maximum power in 1 year, which is slightly higher than rates observed in synchronous orbit flight data (Ref 9)

The source geometry was selected as an optimum shape consistent with ease of packaging and desired spectral characteristics The isotope rod and canister are shown in Fig 2 The canister serves as a shielded container to house the isotope rod during storage and transportation The canister is mated to the chamber for irradiation purposes and the rod is then inserted into the chamber after the lead-filled door is opened

Flux measurements using dosimetry techniques will be performed at the conclusion of the 6-month run for the purpose of determining the actual uniformity

IV CHAMBER DESIGN

To meet the desired objectives and requirements the environmental chamber was configured as shown in Fig 3 It was determined that, with a concentrated radioisotope source, a spherical sample arrangement was desirable to minimize $1/R^2$ effects Monoenergetic electron uniformity (solar cell equivalent) over the sample area is calculated to be within ±2%

Of greater concern was the illumination of the solar cells with the solar simulator output It was decided that taking of measurements at some angle of incidence fixed throughout the experiment was an acceptable compromise to normal illumination measurements Thus, the sample blocks have incidence angles as high as 27° from the normal Each sample block represents a given temperature condition, and all cells on that block are mounted on a plane surface Comparative data can, therefore, be obtained with no corrections Absolute data are obtained using a simple cosine correction back to the normal incidence condition

The irradiation of the solar cells is conducted in an evacuated chamber The selected chamber design is a stainless steel cylinder with a diameter of 14 in and a length of 22 in The solar cells are attached to a plate providing closure to one end of the cylinder A flanged window provides closure at the other end The vacuum-pumping system is located beneath the chamber and is attached to the lower side of the horizontally oriented cylinder Two access ports are also located in the side of the cylinder, one being used for the insertion of the isotope and the other being a spare Figure 4 shows the irradiation chamber and vacuum system enclosure

The window permitting illumination of the solar cells is Corning 7940 fused silica (optical grade) and is 15 in in diameter and 1-in thick The plane surfaces of the window were specified to be parallel within 1 min of angle to minimize distortion of the solar simulator illumination The window is mounted in a flange allowing a

13 5-in -diam clear opening A Viton O-ring between the window and the chamber provides the vacuum seal The high-purity fused silica was specified so that color center formation and the resulting decrease in transmission are minimized Corning 7940 is a proven material currently being used for most solar cell cover glass applications

The solar cells are located at the end of the cylinder opposite from the window There are six groups of cells, one group at each of the following test conditions -50 20 (dark) 20 (two groups) 50 and 80°C The 20, 50 and 80°C groups are mounted on temperature control blocks using a water-cooled heat sink The -50°C block is attached to a liquid nitrogen (LN_2) cooled heat sink The surface of each block is at an angle such that the central cell on the block is normal to a line from the isotope center and 8 in from the isotope center The cells are consequently located at angles as high as 27 deg from normal to the illumination This is well within the range of demonstrated cosine dependence (Ref 10) The water-cooled heat sink and the LN_2-cooled heat sink are attached to the door of the chamber The door seals the chamber using a Viton O-ring

The cells were mounted to aluminum plates which in turn, were attached to the temperature control blocks Dow Corning Sylgard 184, typically used as a cover glass adhesive, was selected to adhere the cells to the plate To ensure adequate heat transfer the adhesive was filled with zinc oxide to increase thermal conductance Figure 5 shows the installed cells (through the window) as well as the residual gas analyzer probe extending from the side of the chamber

A shade is attached to one of the 20°C blocks to prevent cell illumination other than when performance is being measured The shade is made of an aluminum frame hinged to the block The frame is covered with 1-mil aluminized Mylar which permits the electron spectrum to pass through essentially unaltered The shade can be opened or closed by actuating a rod through a push-pull feedthrough located on the chamber door

V AUXILIARY EQUIPMENT

The vacuum system is located directly beneath the irradiation chamber and connected to it through a 6-in opening A Varian 140-l/s ion pump provides primary pumping with a normal operating pressure of 10^{-6} torr, or lower The ion pump was selected because of its long-term operating reliability and inherent cleanliness This pumping method eliminates the possible presence of contaminants usually associated with oil diffusion pumps Any possible glow discharge in the chamber due to the pump has been eliminated by proper system design and through the use of a neutral grid placed at the throat of the pump Roughing is provided by two adsorption pumps and an aspirator

Two illumination systems are being used for this program One is a high-quality solar simulator and the other a general-purpose, quartz-iodide illuminator The Spectrolab X-25 Mark II solar simulator with close spectral filtering to match air mass zero solar characteristics is used for all electrical performahce measurements

When cell measurements are not being made, the cells are loaded near the maximum power point and will be illuminated at one-sun equivalent intensity with the quartz-iodide source This source consists of a Colortran 1 000-W lamp with a parabolic reflector With this approach to illumination, the solar simulator will not be subjected to long-term operation The quartz-iodide system has proved in other experimental programs to have long-term stability and reliability at a minimum cost

Calibration and standardization of the solar simulator is required for the correlation of I-V data over the long duration of the test To facilitate standardization, a fixture has been designed and fabricated which incorporates solar cells to measure the primary characteristics of the light beam The intensity uniformity and spectral content of the simulator beam are checked before every data cycle

Each cell mounting plate is combined with a heater and thermal resistance block The thermal resistance block was designed such that, under one-sun illumination, the desired sample temperature will be maintained with a minimum of additional heat from the heater The assembly is mounted to a heat sink cooled by water for the 20, 50, and 80°C blocks and a heat sink cooled by LN_2 for the -50°C block Cartridge-type heaters are used (200 W 3/8 in in diameter) they are inserted in the center of each sample block

The solar cell performance is determined by measuring the I-V curve of each cell using the data acquisition system This system consists of (1) four wire cell leads, (2) automatic cell switching system, (3) Spectrolab D-550 electronic load unit, (4) Moseley X-Y recorder, and (5) precision voltmeter and ammeter This apparatus coupled with high-quality solar simulation and well-defined standardization procedures, results in data with an optimum degree of accuracy and repeatability

VI RADIATION FACILITY

The Philco-Ford Radiation Facility was established to allow safe advanced research involving radioisotopes and to allow safe storage of all radioactive sources The Radiation Facility contains the irradiation chamber with the vacuum system and the illumination systems All ancillary electronic equipment used for performance measurements and environmental control is located in an adjacent room The principal items of equipment in the Radiation Facility are arranged as shown in Fig 6 The solar simulator is positioned on a platform attached with linear bearings to cylindrical rails accurately positioned in the floor When data are to be taken the solar simulator is aligned with the calibration panel and standardized, then immediately re-positioned in front of the chamber window for data acquisition The control electronics vacuum system power supply, and data acquisition system are located in the room adjacent to the Radiation Facility All wires pass through the wall behind the chamber allowing test personnel to perform all measurements in a radiation-free area

VII SAMPLE COMPARISONS AND MATRIX

Prior to contract award, it was assumed that the program should evaluate types of lithium cells that would be most immediately suitable for spacecraft use Thus only cells developed by the two commercial solar cell suppliers, Centralab and Heliotek, were considered Both companies were briefed on the intent of this program and were asked to recommend lithium cell types (from those they had developed) which should be included in such an evaluation Based partly upon these recommendations and partly upon other expressed desires a table of the basic comparisons to be performed in the program was established and is presented in Table 1 The trade-offs considered in formulating these comparisons were (1) number of cells per type, (2) number of cell types, (3) number of temperatures, and (4) available sample area within the chamber

A direct comparison of lithium and N/P cells is made primarily at +20°C Additional comparative data will be obtained at -50 and +80°C The comparison between lithium cells made from crucible-grown silicon and those made from float zone refined silicon is fundamental to the program and is, therefore made at all four sample temperatures

At the time that the sample matrix was established it was thought that appreciable differences in embrittlement characteristics would be observed in cells with junctions formed from a B Br_3 diffusion as compared to B Cl_3 It was subsequently discovered that little or no observable difference could be detected in the two types of cell[1] Therefore, the two types of boron diffusion represented in this experiment are variations of the basic B Cl_3 process normally used for P/N cell manufacture The difference between the two types is in terms of boron "tack-on" time

Another comparison involves bare versus covered lithium cells It was thought that surface characteristics might prove to be of importance in lithium cell performance degradation [2] A direct comparison has thus been provided to permit an observation of any gross differences due to covering

The effect of depletion layer width upon observable damage in lithium cells was considered potentially important in early studies of lithium cell characteristics It was felt that radiation damage (as measured in terms of power degradation) would be different if a cell were biased than if it were not biased [3] To date no observable difference has been noted in at least one early study (Ref 6) This program has an objective of again attempting to demonstrate the effect (if any) of biasing on solar cell damage

It should be of interest to note any apparent difference between lithium cells made by each of the two commercial solar cell manufacturers It is possible that differences in the manufacturing process could conceivably contribute to a different net rate of damage For this reason, comparable cells from both suppliers are included in this experiment

Degradation data will be obtained for cells from the same batches being irradiated in the chamber (with the low rate Sr 90 irradiation), using a 1-MeV electron Van de Graaff accelerator It will thus be possible to observe the relationship between damage caused by the two sources An analysis of 1-MeV equivalence will be performed in an attempt to demonstrate the value of 1-MeV electron irradiations of lithium cells

The selected sample matrix is presented in Table 2 While it was impossible to completely fill the matrix due to chamber limitations a substantial amount of comparative data for a large number of cell types will be obtained over a variety of test conditions In the final sample configuration, 128 cells will be irradiated in the chamber and 36 with the 1-MeV accelerator These numbers are significantly higher than required by the original contract matrix Current 10-Ω-cm N/P cells from both manufacturers are included, as are 1964 N/P cells from a batch used in earlier irradiation programs It will thus be possible to relate the results of this experiment with those of earlier definitive efforts

VIII PROGRAM STATUS AND PLAN

At the time of this presentation, the experimental part of the program was about to be initiated All solar cell samples have been received and evaluated All experimental equipment has been assembled and successfully checked out The 6-month irradiation will be initiated after review of the initial cell evaluation and test data with JPL

The degradation characteristics of the cells are being determined by sequentially acquiring accurate I-V measurements The cells were measured as received under one-sun illumination at 28°C Three cells of each group were also measured at 20, 30, and 40°C to determine their temperature coefficients The cells will be again measured after installation in the irradiation chamber and before the isotope is installed The chamber measurements made at vacuum and temperature test conditions are, therefore, used as the baseline measurements Prior to test initiation and three times during the exposure, measurements of the reverse illuminated characteristics and dark forward/reverse characteristics will be made

Extra cell samples are being used as test controls to determine the effect, if any, of maintaining the solar cells at 80°C for 6 months These cells will be measured periodically and stored in the vacuum oven the remainder of the time Those samples, to be used for the 1-MeV electron irradiation, are being stored at room temperature in vacuum until the tests are performed

The 1-MeV electron irradiation will be performed in September 1970 Cells for this irradiation will be evaluated prior to the irradiation to

[1] Iles, P , personal conversation, July 1969
[2] de Wys, E C , personal conversation Dec 1968
[3] Fang, P personal conversation Dec 1967

determine whether any shelf life degradation has occurred since their receipt The cells will be irradiated in air to a fluence level approximating that expected for the chamber samples after exposure for 6 months After irradiation the cells will be immediately placed in a container cooled with dry ice and returned to Philco-Ford for post-irradiation data acquisition Cell characteristics will be obtained at room temperature Repeated room temperature measurements will be made to determine the annealing characteristics of the cells

REFERENCES

1 Wysocki J J , "Self-Healing Radiation Resistant Silicon Solar Cells," in Conference Record of the Sixth Photovoltaic Specialists Conference, IEEE, Cocoa Beach Florida March 28-30, 1967

2 Fang, P H , "Present Status of Lithium-Diffused Silicon Solar Cells," in Conference Record of the Sixth Photovoltaic Specialists Conference, IEEE, Cocoa Beach Florida, March 28-30, 1967

3 Downing, R G , Carter, J R , and Van Atta, W K , Study and Determination of an Optimum Design for Space Utilized Lithium-Doped Solar Cells, Third Quarterly Report No 13154-6009-R0-00, JPL Contract No 952554, TRW Systems Group, Redondo Beach, Calif , April 15, 1970

4 Brucker G , Faith, T , Corra, J , and Holmes-Siedle, A , Study to Determine and Improve Design for Lithium-Doped Solar Cells Third Quarterly Report No AEC R-3562F JPL Contract No 952555, RCA Corp , Astro Electronics Division, Princeton N J April 10, 1970

5 Newell, D M , Investigation of the Use of Radioisotope for Space Environment Simulation, Final Report No SRS-TR150, NASA Ames Research Center Contract NAS2-3506, Philco-Ford Corp , Space and Re-entry Systems Division, Palo Alto, Calif , March 19 1967

6 Philco-Ford Corporation, Space and Re-entry Systems Division, Evaluation of the Effect of Space Radiation on Lithium P-on-N Solar Cells Report No TR-DA1875 NASA GSFC Contract NAS5-10429, Philco-Ford Corp , Space and Re-entry Systems Division, Palo Alto, Calif , August 1968

7 Radiation Effects on Lithium P-on-N Solar Cells, Report No ER 9357, NASA GSFC Contract NAS5-10415 Lockheed-Georgia Co Dawsonville, Ga

8 Reynard, D L , and Orvis, D B , "Beta Irradiation of Lithium-Doped Solar Cells " in Conference Record of the Seventh Photovoltaic Specialists Conference, IEEE, Pasadena, Calif Nov 19-21 1968

9 Picciano, W T and Reitman, R A , Flight Data Analysis of Power Subsystem Degradation at Near Synchronous Altitude, Final Report No WDL-TR4223, NASA Headquarters Contract NASW-1876 Philco-Ford Corp , Western Development Laboratories Division, Palo Alto, Calif July 15, 1970

10 Briggs, D C , Experimental Study of Solar Cell Performance at High Solar Intensities Report No TR-DA1636 NASA Ames Contract No NAS2-4248, Philco-Ford Corp , Space and Re-entry Systems Division, Palo Alto, Calif , Nov 25, 1967

Table 1 Sample comparisons

Comparison		Temperature °C
Bare lithium cells	Bare N/P cells	+20
Crucible lithium cells 425-90-60 450-20-0	Float-zone lithium cells 425 – 90 – 120 350 – 90 – 60 2 boron diffusions	-50, +20 +50, +80
Boron diffusion No 1 (float zone)	Boron diffusion No 2 (float zone)	-50, +20, +80
Bare lithium cells (425-90-60)	Integral covered lithium cells (425 – 90 – 60)	+20
Illuminated and loaded lithium cells	Dark and unloaded lithium cells	+20
Heliotek lithium cells Crucible Float zone	Centralab lithium cells Crucible Float zone	-50, +20 +80
Low-rate spectral source $\sim 10^{12}$ el/cm^2/day	High-rate monoenergetic source $\sim 2 \times 10^{17}$ el/cm^2/day	+20

Table 2 Sample matrix

Type	Diffusion characteristics	Manufacturer	Radioisotope/vacuum					1-MeV accelerator	
			Illuminated and loaded					Dark and unloaded	
			-50°C	+20°C	+50°C	+80°C	+20°C	+20°C	+20°C
Lithium P/N Crucible	425-90-60	Heliotek	4	4	4	4		4	4
	425-90-60	Centralab	4	4		4			4
	425-20-0	Centralab	4	4		4			4
	425-90-60 1-mil cover	Heliotek		4					4
Lithium P/N Float Zone	425-90-120	Heliotek	4	4	4	4		4	4
	350-90-60	Heliotek	4	4		4			4
	Boron No 1 425-90-120	Centralab	4	4		4			4
	Boron No 2 425-90-120	Centralab	4	4		4			4
10-Ω-cm N/P	Current	Centralab	4				4	4	4
	Current	Heliotek				4	4		
	1964	Hoffman Electronics, El Monte, Calif					4		

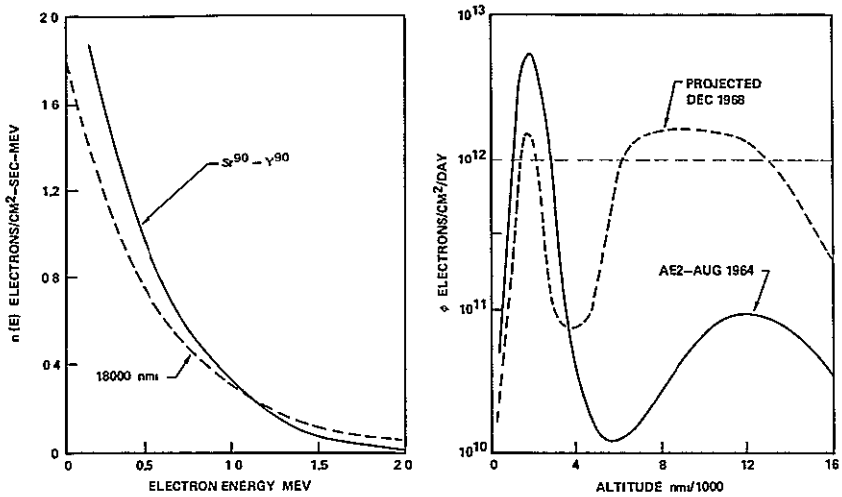

Fig 1 Isotope characteristics, range of trapped electron flux in space

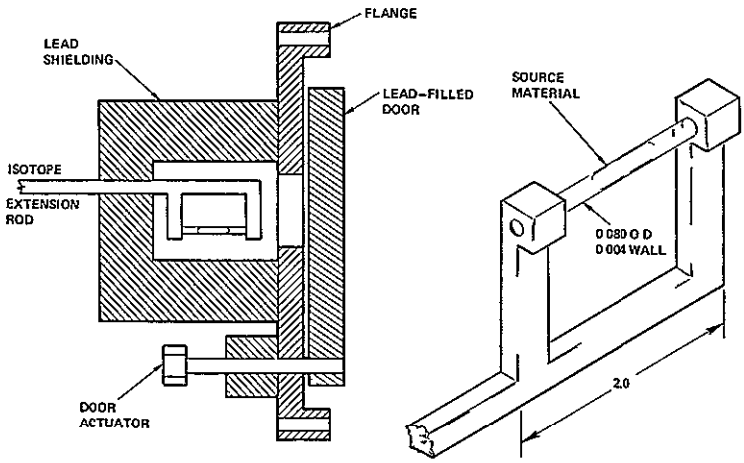

Fig 2 Isotope rod and canister

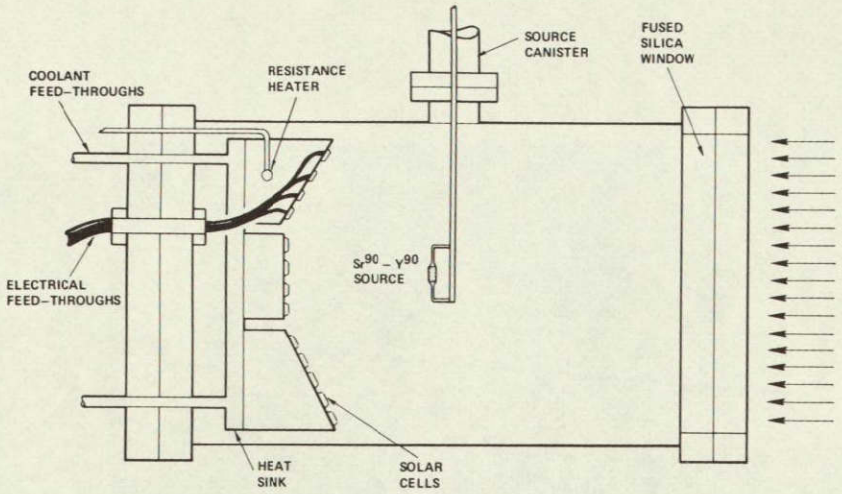

Fig. 3. Chamber design

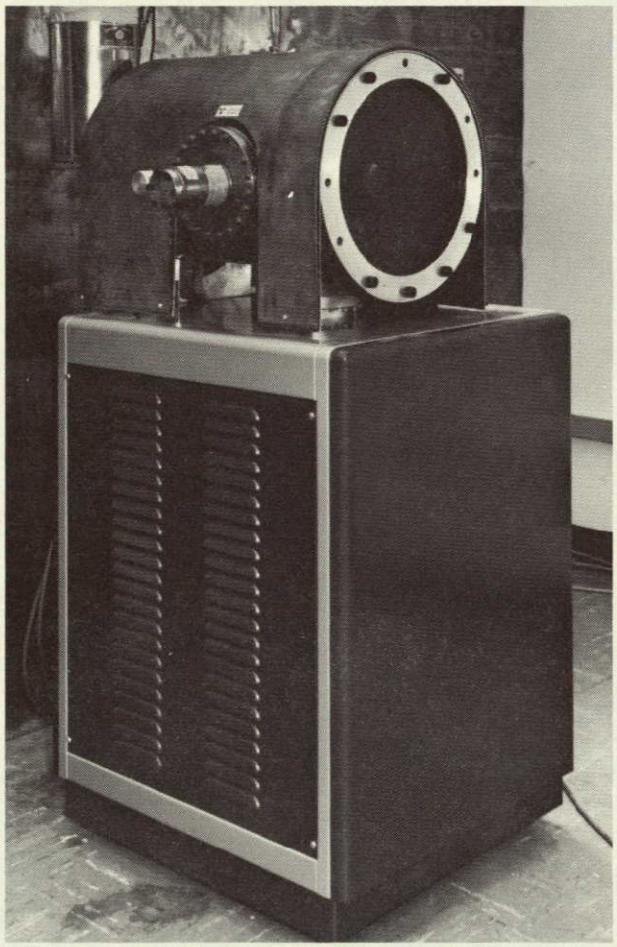

Fig. 4. Irradiation chamber and vacuum system

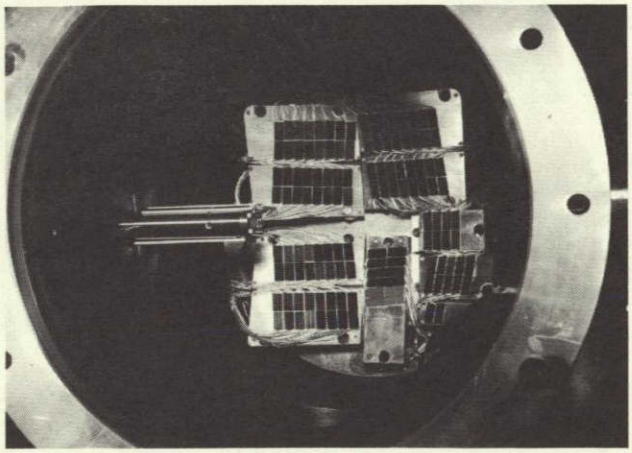

Fig. 5. Solar cell samples installed in chamber

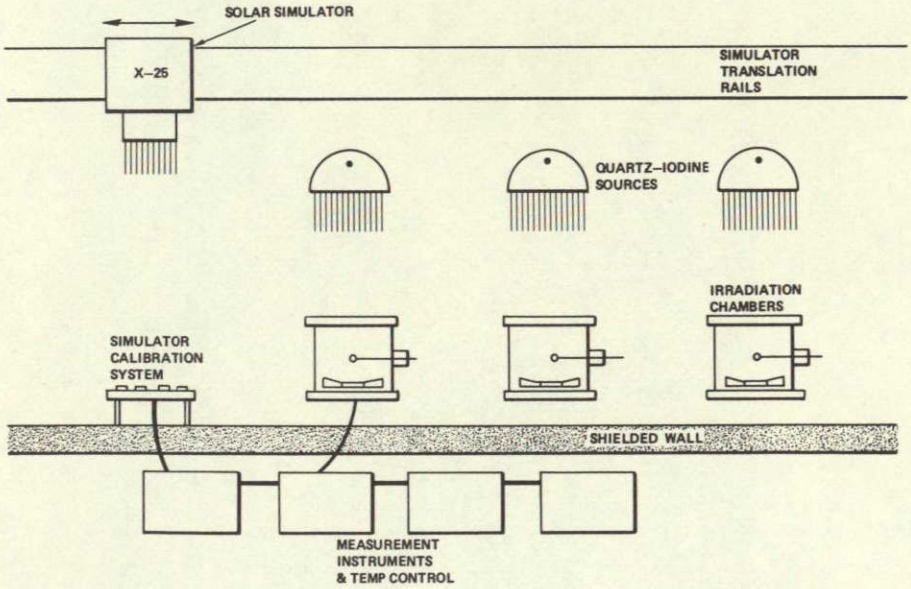

Fig. 6. Philco-Ford radiation facility

A REAL-TIME STUDY OF THE EFFECT OF ELECTRON RADIATION ON LITHIUM P/N SOLAR CELLS

R R Dayton
Lockheed-Georgia Co ,
Lockheed Research Laboratory,
Marietta, Ga

ABSTRACT

This paper describes work being performed at the Lockheed-Georgia Nuclear Laboratory under JPL Contract 95286 The primary objective is to perform a real-time study to determine the effects of electron radiation on lithium P/N solar cells A total of 144 solar cells divided among four temperatures (-50, 30 60, and 80°C) are to be exposed to the Sr 90 beta spectrum in vacuum The flux will be approximately 10^{12} electrons/cm^2/day The duration of the test will be 100 days This paper is primarily devoted to a description of the test facilities The environmental chamber is made of stainless steel and may be divided into three sections The main body of the chamber contains the test solar cells and a large fused silica window through which the light will be projected To the right of the main body is the source handling and storage area and on the left is the vacuum pumping station Data is collected in-situ by an automatic data collection system The potential drop across a series of calibrated resistors as measured by a digital voltmeter is used to derive the I-V characteristic The maximum power and maximum power point are computer-calculated The beta source to solar cell geometry required to deliver the desired flux was determined by comparative analysis The beta spectrum is shown

I INTRODUCTION

Lockheed is performing a real-time study to determine the effects of electron radiation on lithium P/N solar cells The majority of this paper will be concerned with the facilities to be utilized in the performance of the test No test data will be presented at this time because the test is just getting under way Since this is a long-term test, the facilities and techniques involved in the performance of the test become very important

II DISCUSSION

Figure 1 shows the experiment design matrix The test will be performed in vacuum with a pressure of less than 10^{-6} torr All data will be taken in-situ and at approximately the fluences indicated It is anticipated that data will be taken between 12 and 15 times during the test The data will be computer-processed immediately after collection and, if anything unusual is observed, then the data collection schedule may be revised to collect more information The exposure rate will be approximately 10^{12} electrons/cm^2/day

Data will be collected by an automatic data acquisition system The heart of the data acquisition system is a digital voltmeter The potential drop across a series of 15 calibrated resistors spanning the solar cell characteristic curve is measured Potential leads are connected to each solar cell to minimize the measurement error The digital voltmeter drives a flexowriter which provides a printed and punched paper tape presentation of the data The paper tape is then transferred to cards and fed into the computer The computer will first calculate the current that corresponds to each of the measured voltage points A least-squares fit of the data to the solar cell equation will then be performed The maximum power value and the maximum power point will also be determined The computer will output the current and voltage data for each load point, the maximum power value and its associated pair of data points, and the solar cell equation fitting parameters I_g, I_o, R_s, and n

The chamber may be divided into three separate sections In the center is the main body of the chamber This portion contains the test specimens, a vacuum gage, and the window through which the light source will be projected On the right is the source-handling and storage area and on the left is the vacuum pumping station At those times during the test when it is necessary to enter the room, Sr 90 source can be stored within this lead-shielded area to minimize the radiation hazard in the room The lead shield is cast in sections so that it is easily removable The pushrods extend through the lead shield and are magnetically coupled to the source plaque which is mounted on guides inside the chamber Two separate source tubes are used to minimize the chamber volume

One side of the chamber is the vacuum pumping station This pumping station consists of two vacion pumps and three vacsorb pumps The smaller vacion pump has a capacity of 25 l/s A titanium sublimation pump is an integral part of the smaller vacion pump This titanium pump has a capacity of approximately 550 l/s The larger vacion pump has a capacity of 110 l/s and is of the straight-through type (i e , there are flanged outlets on each side of the pump) The vacsorb pumps are connected to the main vacuum chamber through this pump The vacsorb pumps are individually valved into the cross section and the cross section may be valved off from the main part of the system once the rough down is accomplished Pressure control of the system is accomplished by cycling the vacion pumps on and off The pressure is sensed by the cold cathode gage and, once a lower limit is set, the gage will cause the ion pump or pumps to be turned on as required

A Corning Code 7940 fused silica window is mounted on one end of the chamber This window is 14 3/4 in in diameter and 1-in thick Fused silica was selected because of its high radiation resistance A window of some lesser quality than this may darken with time and exposure to the radiation and cause changes in the transmission characteristics Changes in transmission characteristics could easily be mistaken for changes in the solar cell output The fused silica window is sealed to the vacuum chamber by a Viton O-ring This is the only polymeric seal in the entire vacuum chamber All other seals are of the crushable metal type

The solar cells are mounted on a Wheeler flange at the opposite end of the test chamber The major heat sinks are massive copper bars vacuum-oven brazed into a 1/4-in -thick stainless steel plate The temperature of these copper bars is controlled and monitored Twenty-eight solar cells will be controlled at 80°C 54 solar cells at 60°C, 44 cells at 30°C, and the 18 solar cells at -50°C Five-watt power resistors are uniformly mounted along the air side of each of the 80 60 and 30°C sinks The -50°C sink is used as the evaporator of a two-stage mechanical refrigeration system The major path for heat flow is from the 80°C sink toward the -50°C sink where any heat removal required is accomplished The temperature control system for the 30 60, and 80°C sinks is relatively simple For example, eleven 5-W resistors are thermally attached to the back of the 60°C heat sink bar There are three significant sources of heat input to this bar and one output The three inputs are (1) from the light source, (2) from the 80°C sink and (3) from the power resistors The one output is the heat transfer to the 30°C sink Radiation losses are negligible The temperature of the sink is controlled by the on-off action of the power resistors The power resistors are connected in parallel with one side connected through a pair of microswitches mounted on an expanded range L&N recorder to a Variac The L&N recorder is driven by thermocouples mounted on the air side of the 60°C sink Cam action within the recorder then turns the power on or off as required The frequency or period of operation of the temperature-limiting microswitches can be adjusted by either decreasing or increasing the voltage setting of the Variac Control of the -50°C sink is considerably more complicated and will not be discussed here

The minor heat sink assemblies and solar cell mounting pads are simply 1/8-in -thick copper T sections The top of the T is just large enough to accommodate two solar cells The pre-tinned solar cells are positioned on top of these pre-tinned T sections and heat applied The re-flow solder process was performed in an inert atmosphere and a total heat time cycle of approximately 2 min was required These T sections are then securely bolted to the major heat sink assemblies and the power lead attached

As indicated previously, some of the solar cells will be irradiated while in the dark The shield that allows this to be accomplished is 5-mil aluminum foil stretched between a stainless steel framework The shield is magnetically operated from outside the chamber

A viewport has also been provided on this test item flange The solar cell is mounted to this viewport and provides an additional means for checking the light source

III Sr 90 - Y 90 SOURCE

The source/solar cell geometry required to deliver the desired flux (10^{12} e/cm^2/day) has been determined The source is composed of two

groups of five stainless steel tubes oriented in such a manner as to deliver a flat flux distribution to the plane of the solar cells Each 0 010-in wall stainless steel tube has an active length of 20 in and contains 10 curies of Sr activity

An experimental procedure was used to develop the source/solar cell geometry This procedure yielded the electron flux and energy spectrum Ten source tubes identical to those that will be used in the radiation test, but containing much less activity, were used Each of these tubes contains 13 microcuries of Sr 90 An anthracene detector and multichannel analyzer (MCA) were used to make flux and spectral measurements on these diluted source tubes System calibration was performed using a weak Co 60 source

The primary method of energy deposition in the scintillation detector under consideration is by single Compton scatter The Compton process is the dominant method of interaction between gamma rays and organic scintillators in the energy range 20 keV — 30 MeV The total energy of the incoming photon may be deposited in the scintillator only after multiple Compton scatters terminating in photoelectric absorption The dimensions of the anthracene detector (1 5-in diameter × 1-in thick) are too small to allow for the multiple scatter process, therefore the response of the detector to the Co 60 source is quite similar to the response to the Sr 90 source

An expression for the degraded photon arising from a Compton collision is

$$E_2 = \frac{E_1}{1 + \frac{E_1}{mc^2}(1\text{-COS }\phi)}$$

where E_1 and E_2 represent the energy of the incident and scattered photons respectively Setting ϕ equal to 180° and subtracting E_2 from E_1 yields the familiar expression for the kinetic energy of the Compton electron

$$E_c = \frac{E_1}{1 + \frac{0\ 51}{2E_1}}$$

In the case of Co 60, where there are two primary photons, the value for E_c is based on the average photon energy (1 25 MeV) Setting E_1 equal to 1 25 MeV, we find E_2 equals 0 21 MeV and E_c equals 1 04 MeV , The peak of the Compton distribution collected by the 512 channel MCA will be at 1 04 MeV The spectrum is shown in Fig 2 Spectral and flux measurements of the Sr 90 — Y 90 source were made after the calibration procedures were completed Figure 3 shows the beta spectrum The electron flux emitted by the diluted source tubes was determined by a simple arithmetic summation of the counts under the curve The flux obtained from the full strength source tubes was determined by a linear extrapolation The extrapolation technique has been used in previous tests incorporating the Sr source The extrapolated results agreed within 1% with vacuum Farraday Cup measurements

Spectral measurements were made with the source and detector in a minimum scatter geometry, and then the source and detector were placed inside a heavy-walled aluminum tube to simulate the scatter geometry of the actual test No significant spectral change was observed

TEMPERATURE			50°C				30°C				60 C				80 C			
SOLAR SOURCE			LIGHT		DARK		LIGHT		DARK		LIGHT		DARK		LIGHT		DARK	
FLUENCE e/cm^2			10^{12}	10^{14}	10^{12}	10^{14}	10^{12}	10^{14}	10^{12}	10^{14}	10^{12}	10^{14}	10^{12}	10^{14}	10^{12}	10^{14}	10^{12}	10^{14}
WITHOUT COVER GLASS	FLOAT-ZONE SILICON	LOW DOPE					5 SPEC				5 SPEC				5 SPEC			
		HIGH DOPE	5 SPEC				5 SPEC				5 SPEC	5 SPEC			5 SPEC			
	PULLED SILICON	LOW DOPE					5 SPEC	5 SPEC			5 SPEC	5 SPEC			5 SPEC			
		HIGH DOPE	5 SPEC				5 SPEC	5 SPEC			5 SPEC	5 SPEC			5 SPEC			
	STANDARD N/P CELL		3 SPEC				3 SPEC	1 SPEC			3 SPEC	1 SPEC			3 SPEC			
WITH COVER GLASS	FLOAT ZONE SILICON	LOW DOPE																
		HIGH DOPE									5 SPEC							
	PULLED SILICON	LOW DOPE									5 SPEC							
		HIGH DOPE	5 SPEC				5 SPEC	5 SPEC			5 SPEC				5 SPEC			

ALL TESTS PERFORMED IN VACUUM OF $<10^{-6}$ torr
DATA TAKEN IN SITU AT FLUENCES OF 10^{12} 2×10^{12} 5×10^{12} 10^{13} 2×10^{13} 5×10^{13} AND 10^{14} e/cm^2
RADIATION RATE OF 10^{12} e/cm^2/day

Fig 1 Experiment design matrix[a]

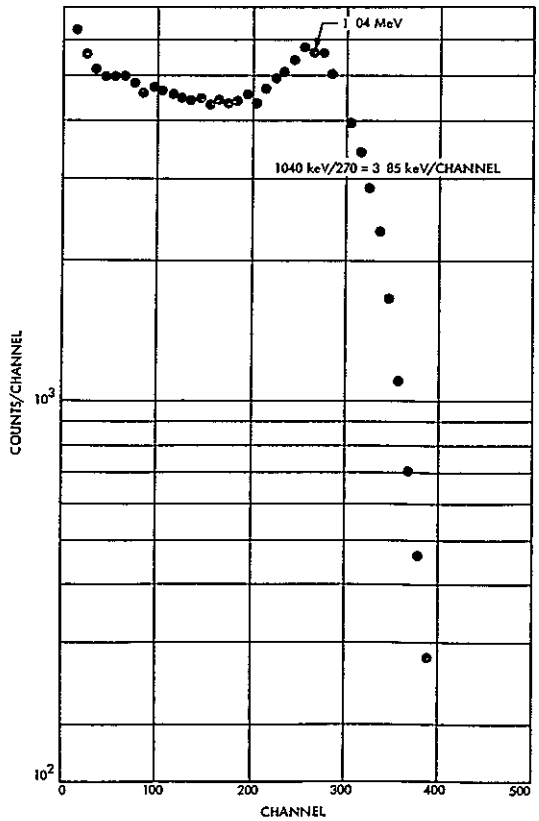

Fig 2 Compton spectrum of Co 60

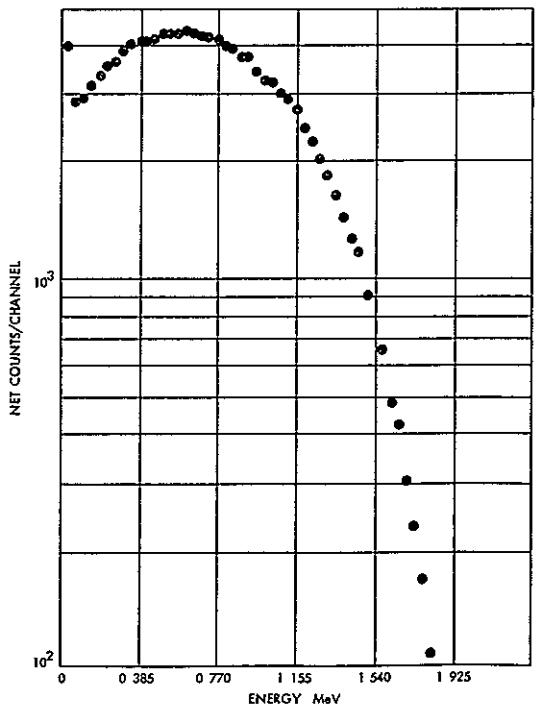

Fig 3 Sr 90 – Y 90 spectrum